Università degli Studi di Padova
Department of Industrial Engineering

Aarhus University
Department of Civil and Architectural Engineering

Master's Degree in Mechanical Engineering

Fatigue analysis of as-welded and HFMI-treated steel joints by local approaches

Supervisor: Professor Giovanni Meneghetti

Co-supervisors: Professor Halid Can Yildirim
Professor Alberto Campagnolo

Graduate Student: Francesco Belluzzo
Serial number: 1177947

Academic Year 2019/2020

Summary

Abstract (English)

In the structural design of welded joints field, the fatigue endurance is usually expressed in terms of nominal stress, based on recommended S-N curves, available in several official codes and guidelines [1-2]. However, this approach presents some relevant drawbacks, mostly due to the necessity of various fatigue classes in order to account for welded geometries of different size and shape. Along with this, the experimental reality shows that for these particular components failures predominantly originate from the regions of material discontinuity, identified by welds themselves. Consequently, the fatigue strength reveals to be a local phenomenon. The size and shape effects can be addressed with the employment of the local approaches, arisen thanks to the increasing use of the Finite Element analysis in the industry. Among the large variety of available approaches, the hot-spot stress extrapolation available in the IIW guideline [1] and the 1-mm stress by Xiao and Yamada [3] are cited. Despite the reliability offered by these methods, some of them are not able to fully account of the influence of the service-life-affecting parameters, such as the size effect [30, 31]. To overcome this issue, the Linear Elastic Fracture Mechanics has been non-conventionally extended to the structural design of welded joints, describing the concept of V-notch (i.e. weld toe, root). To quantify the linear elastic stress distribution occurring in the V-notch region, on the basis of Kihara and Yoshii's work [4], at the University of Padova the Notch Stress Intensity Factors (NSIFs) [5] approach has been proposed by Lazzarin and Tovo, aiming to correlate the asymptotic stress concentration with the crack initiation. More recently, two other finite element FE methods have been developed, capable of giving reliable results in terms of fatigue life, contemporarily speeding up the modelling and simulation times: the Strain Energy Density (SED), proposed by Lazzarin and Zambardi in 2001 [6], and the Peak Stress Method (PSM) by Meneghetti and Lazzarin in 2007 [7], deriving from the SED approach. Since coarse meshes are required, this characteristic makes these methods easily applicable in the industry. Over the years, the methods have been calibrated for 2D and 3D models, different elements types as well as FE software [8]. However, the they have always been adopted in case of post-weld tensile (as-welded) or null (stress-relieved) residual stresses at the weld toe, while no research has ever been conducted in case of compressive residual stresses, induced by specific treatments. In this context, the High Frequency Mechanical Impact (HFMI) treatment, a post-weld technique for the fatigue strength enhancement of welded joints, makes use of apposite indenters to impact and plastically deform the weld toe, consequently inducing beneficial compressive residual stresses near the treated area, at the same time improving the local geometry. The HFMI treatment has proven its effectiveness in many fields; however, the benefits in case of high stress ratios, overloads and variable amplitude loading conditions are still under investigation [9].

This elaborate can be divided in two parts: the first involves Chapters 1, 2 and 3 and deals with joints in as-welded conditions; Chapters 4, 5 and 6 deal with HFMI-treated steel joints.

Chapter 1 aims to introduce the reader to the basics and the principles of the local approaches which are going to be employed in this thesis. The first two aforementioned methods are taken from the IIW guidelines, while the remaining three have been developed at the University of Padova. Besides this, each method advantages and disadvantages are described.

Chapter 2 may be seen as a training for the thesis student, involving the application of the NSIFs, SED and PSM approaches for the fatigue assessment of specific 2D and 3D welded joints. A collection of the re-elaborated dataset is performed for the subsequent comparison in terms of statistical scatter with respect to the reference design fatigue curves proposed in the literature.

Chapter 3 deals with the fatigue assessment of specific as-welded geometries in terms of nominal stress, equivalent peak stress (PSM), strain energy density (SED), structural hot-spot stress and 1-mm stress. As done in Chapter 2, the re-elaborated datasets are entered in their respective design curves along with a fatigue life comparison, in order to quantify the grade of effectiveness and conservativeness provided by each method.

Chapter 4 aims to introduce the reader to the basics, the principles and the benefits of the HFMI treatment on steel welded joints.

Chapter 5 illustrates the fatigue assessment of specific HFMI-treated geometries in terms of structural hot-spot stress, referring to the IIW [9] indications, along with the use of PSM combined with the SED approach. The aim is to investigate the effectiveness of the PSM in combination with the SED method for blunt notches [10], currently valid only for as-welded and stress-relieved welded joints, for the analysis of HFMI-treated joints. The re-elaborated datasets are entered in their respective design curves in order to quantify the grade of effectiveness and conservativeness provided by the two local approaches.

Chapter 6 concludes with the final objective of this thesis, it is to say the feasibility of the proposal of a $\Delta\sigma_{eq,peak}$ - N_f design curve for HFMI-treated welded joints, under constant amplitude loading, able to reliably account of the size effect, as well as the fatigue-life-affecting parameters typical of post-weld HFMI treatment.

Abstract (Italiano)

All'interno della progettazione strutturale delle giunzioni saldate, la resistenza a fatica è solita essere espressa in termini di tensione nominale, sulla base delle curve di progettazione a fatica S-N, disponibili nei codici o analogamente nella normativa. Questa tipologia di approccio però presenta diversi svantaggi, dovuti principalmente alla necessità di definire diverse classi di fatica che tengano conto delle diverse geometrie e dimensioni di giunti. In parallelo a questo fatto, la realtà sperimentale dimostra che la rottura per innesco di cricca si sviluppa prevalentemente dalle regioni in cui è presente la discontinuità di materiale, ossia dalla saldatura. Di conseguenza, la vita a fatica si rivela essere un fenomeno locale. Il problema della dimensione e della forma possono essere risolti con l'impiego degli approcci locali, sviluppati grazie all'uso sempre più consistente dei software di analisi agli Elementi Finiti. Tra i numerosi metodi previsti, vengono citati l'estrapolazione della tensione di hot-spot, reperibile nella guida IIW, e la tensione a 1 mm di distanza dall'apice del piede cordone, proposto dagli autori Xiao e Yamada. Nonostante l'affidabilità di questi metodi, alcuni di questi non sono in grado di considerare importanti parametri che abbattono la resistenza a fatica di questi componenti, tra cui si menziona l'effetto scala. Per superare questo problema, i concetti della Meccanica della Frattura Lineare Elastica sono stati estesi alla progettazione strutturale dei giunti saldati, con l'identificazione del concetto di V-notch (piede cordone, radice). Per quantificare la distribuzione del campo di tensione lineare elastico che si sviluppa lungo il V-notch, sulla base del lavoro svolto da Kihara e Yoshii, presso l'Università degli Studi di Padova è stato proposto da Lazzarin e Tovo l'approccio Notch Stress Intensity Factor, che si prefigge lo scopo di correlare il campo di tensioni locale asintotico e l'innesco della cricca. Più recentemente, due ulteriori metodi agli Elementi Finiti sono stati sviluppati, in grado di fornire risultati affidabili in termini di vita a fatica, allo stesso tempo velocizzando i tempi di modellazione e simulazione: lo Strain Energy Density (SED), proposto da Lazzarin e Zambardi nel 2001, e il Peak Stress Method, sviluppato da Meneghetti e Lazzarin nel 2007, derivante dal primo. Dal momento che vengono richieste mesh grossolane, questi approcci possono essere facilmente adoperati in campo industriale. Col passare degli anni, i due metodi sono stati calibrati per geometrie 2D e 3D, per software agli elementi finiti diversi, per tipologie di elementi differenti. Un aspetto importante è dato dal fatto che questi metodi sono sempre stati utilizzati in caso di tensioni residue post-saldatura di forte trazione (as-welded) o nulle (stress-relieved), mentre nessuno studio è stato compiuto nel caso di tensioni di forte compressione, indotte da specifici trattamenti. In questo contesto, il trattamento post-salatura High Frequency Mechanical Impact (HFMI) prevede un incremento della vita a fatica dei giunti as-welded mediante l'utilizzo di appositi indentatori per impattare sul materiale saldato, deformandolo plasticamente; di conseguenza, delle benefiche tensioni residue di forte compressione vengono indotte al piede cordone della saldatura, migliorandone inoltre la geometria locale. Il trattamento HFMI ha dimostrato in svariati campi la sua efficacia; all'attuale stato dell'arte, bisogna però affermare che questi benefici nel caso di rapporti di ciclo elevati, di carichi variabili o di sovraccarichi non sono ancora stati completamente investigati.

Questo elaborato può essere diviso in due parti: la prima parte riguarda i capitoli 1,2 e 3, in cui si discute di giunti in condizioni as-welded, mentre gli ultimi tre capitoli indagano su giunti trattati con trattamenti HFMI.

Il Capitolo 1 ha il compito di introdurre il lettore alle basi e principi degli approcci locali che sono stati impiegati in questa tesi. Due metodi sono stati scelti dalla normativa IIW, i restanti tre invece sono stati sviluppati presso l'Università di Padova, come riportato precedentemente. Vengono inoltre descritti i vantaggi e gli svantaggi previsti da ciascun metodo.

Il Capitolo 2 può essere visto come un addestramento per il tesista, riguardante l'applicazione degli approcci NSIFs, SED e PSM per la verifica a fatica di specifiche strutture 2D e 3D. I dati rielaborati vengono poi raccolti per una successiva comparazione in termini di dispersione statistica rispetto alle curve proposte nella letteratura di riferimento.

Il Capitolo 3 si focalizza sulla verifica a fatica di specifiche geometrie di giunti as-welded in termini di tensione nominale, tensione equivalente di picco (PSM), densità di energia di deformazione (SED), tensione di hot-spot e tensione a 1-mm di distanza dall'apice del piede cordone. Analogamente al Capitolo 2, i dati rielaborati vengono successivamente inseriti nelle curve di riferimento, e viene effettuata una comparazione in termini di numero di cicli previsto, in modo da poter quantificare il grado di efficacia e di sicurezza previsto da ciascun metodo.

Il Capitolo 4 introduce il lettore alle basi, ai principi e ai benefici del trattamento HFMI sui giunti saldati.

Il Capitolo 5 si concentra sulla verifica a fatica di specifiche geometrie di giunti trattati HFMI in termini di tensione di hot-spot, seguendo le indicazioni fornite dall'apposita normativa IIW, e con l'utilizzo del PSM combinato al SED per intagli smussati. Lo scopo è quello di investigare l'efficacia di quest'ultimo approccio, attualmente validato per giunti in condizioni as-welded o stress-relieved, nell'analisi a fatica di giunti trattati HFMI. I dati rielaborati vengono successivamente inseriti nelle curve di riferimento in modo da poter quantificare il grado di efficacia e di sicurezza previsto da entrambi i metodi.

Il Capitolo 6 conclude con l'obiettivo finale di questa tesi, ossia la fattibilità della creazione di un'unica curva di progettazione $\Delta\sigma_{eq,peak}$ - N_f per giunti trattati HFMI, ampiezza di carico costante, in grado di sintetizzare dati di diversi modelli, di geometrie del piede cordone, contemporaneamente considerando l'effetto scala e i parametri di riduzione della vita a fatica (tra cui rapporto di ciclo e materiale) conseguenti ai trattamenti HFMI.

Chapter 1: principles of global and local approaches for the fatigue assessment of welded joints

The objectives of this in this elaborate consist in the execution of several fatigue assessment on welded joints, presented in as-welded and HFMI-treated conditions. The assessments are performed with the employment of both global and local approaches, with the use of the finite element FE software Ansys® Mechanical APDL, license from University of Padova. All the methods need the assumption of linear elastic material behaviour. Hence, the objective of this Chapter is that of describing the principles, the fundamentals, the methodologies, the advantages as well as the drawbacks each method presents.

The reference guidelines [1] and [11] can be consulted in the Bibliography section.

1.1 Global approaches (IIW guideline)

The most common type of fatigue assessment of welded joints and components is based on the nominal stress range calculated in a sectional area remote from local stress raising locations such as notches or cracks. This type of approach is generally called global (or nominal) approach because it proceeds directly from the external loads, with the assumption of a constant or linearized stress distribution in the area under investigation [11]. The fatigue strength of welded joints is given in terms of a large variety of double logarithmic S-N curves, better known as S-N curves, where S refers to the applied nominal stress range $\Delta\sigma_{nom}$ and N (or Nf) refers the number of cycles to failure of the component. In the literature, several definitions of fatigue life are available: overall, as Hobbacher affirms, small welded specimen failures refer to complete fracture; on the contrary, for large structural details, Nf is related to the observation of a through-the-thickness crack [1].

The IIW recommendations [1] describe the S-N curves with equation (1.1):

$$N = \frac{C}{\Delta\sigma^m} \tag{1.1}$$

where:

- m indicates the inverse slope of the curve; its value varies according to the range of possible fatigue strength, from the high-stress low-cycles to the low-stress high-cycle region;
- C is a constant.

The S-N curves, unless specifically stated, refer to structural details in as-welded conditions, for which, regardless of the yielding strength of the material and the stress ratio $R = \frac{\sigma_{min}}{\sigma_{max}}$, the fatigue life is mostly depending on the external applied stress range $\Delta\sigma$. As a consequence, the analysed specimens are assessed on the observation of the maximum principal stress range $\Delta\sigma_{11}$ in the section where the crack is more likely to develop. If the maximum shear stress range $\Delta\tau_{11}$ is concerned, different S-N curves are proposed [1].

In *Figure 1.1 and 1.2*, the fatigue S-N curves are displayed in terms of nominal stress $\Delta\sigma_{nom}$, under constant amplitude loading CAL, respectively for steel and aluminium alloys:

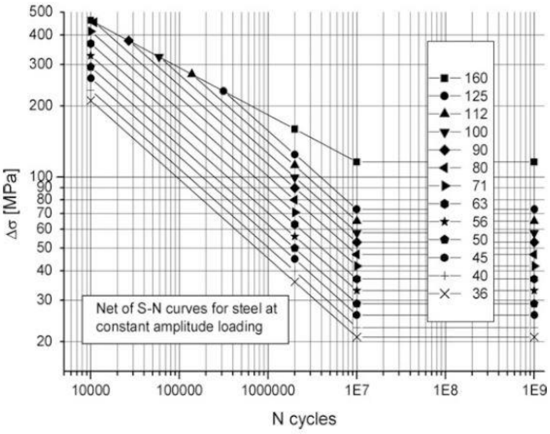

Figure 1. 1: fatigue strength S-N curves for steel, normal stress, CAL [1].

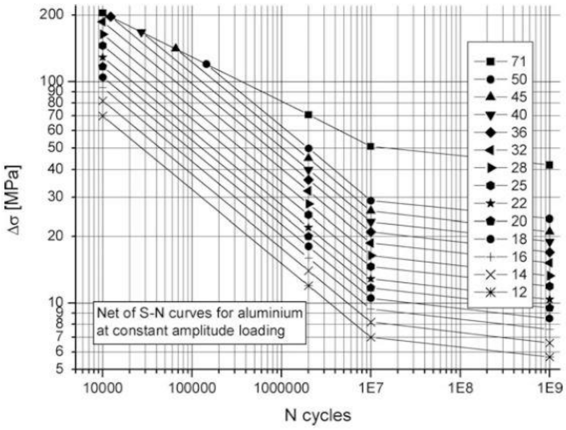

Figure 1. 2: fatigue strength S-N curves for aluminium, normal stress, CAL [1].

Each S-N curve is equated by the typical fatigue strength of the component, expressed in MPa, at 2 million cycles, called fatigue class, or FAT class. The assumed slope of the S-N curves in terms of $\Delta\sigma_{nom}$ is equal to m=3, while in terms of $\Delta\tau_{nom}$ m=5. The S-N curves slope conventionally ends at a "knee point", the constant amplitude fatigue limit CAFL, below which the fatigue life is assumed infinite: from the "knee point" onwards, the curve should be thus traced horizontally. However, recent studies brought to life the fact that the CAFL does not exist; in fact, the slope after the knee point should be modified to m = 22. In terms of normal stress $\Delta\sigma_{nom}$, the CAFL is located at $N = 10^7$ cycles, while, in terms of shear loads $\Delta\tau_{nom}$, it is placed at $N = 10^8$ cycles.

As Hobbacher [1] asserts, the S-N curves are the result of rigorous and consistent research and they include the effects of:

- Structural hot-spot stress concentrations due to the detail shown;
- Local stress concentrations due to the weld geometry;
- Weld imperfections consistent with normal fabrication standards;
- Direction of loading;
- High residual stresses;
- Metallurgical conditions;
- Welding process (fusion welding, unless otherwise stated);
- Inspection procedure (NDT), if specified;
- Post weld treatment, if specified.

The global approach, despite among the most widespread in engineering applications, presents some major disadvantages, clearly described by Sonsino, Radaj and Fricke [11]:

1. From *Figure 1.1* and *Figure 1.2*, it can be observed that the scatter band amplitude integrating all the FAT classes is very large. This significant data loss is due to the fact that the fatigue assessment of structural details in terms of global approaches does not include the shape and size effects [30, 31] which can strongly affect the service life of structural details;
2. There still is the need of satisfying code-related engineering state of art in those areas related to variable amplitude loading *(VAL)* or where $\Delta\sigma_{nom}$ is not immediate to detect.

1.2 Local approaches (IIW guideline)

With the employment of the local approaches, the analysis tends to focus on the local stress raising effects due to the change in the geometry and the weld profile itself.

Two among the numerous local approaches are employed in this thesis: the first one is the "Structural Hot-Spot Stress" type "a", available in the IIW guideline [1], the second is the "1-mm stress" by Xiao and Yamada (2004) [3]. One of the characteristics of these two methods, is that in a FE environment, in linear elastic hypothesis, the stress increment due to the weld profile is strongly dependent on the mesh size [47], therefore the idea is to consider these second stress-raising effects as secondary, so that to analyse only the stress raise due to the joint geometry modification [48].

1.2.1 Structural Hot-Spot Stress

The structural stress at the hot-spot SHSS describes the macrostructural behaviour of a structural detail, including all the stress raising effects but the non-linear peak stress σ_{nl} caused by the weld profile itself. The SHSS value varies according to the type of geometry and loading of the structural detail in the proximity of the welded joint. The SHSS method is suitable in cases where the geometry complexity, given for example by structural discontinuities, makes it challenging to detect a nominal stress comparable to that of the classified structural details. The SHSS method is performed along the exterior surface of the joint, where the non-linear peak stress is eliminated by linearization of the stress through the plate thickness, or by extrapolation of the stress at the surface to the weld toe [1].

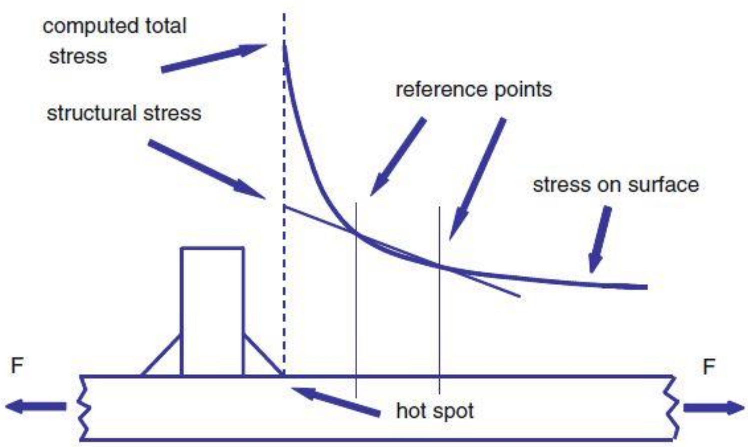

Figure 1. 3: SHSS, linear extrapolation [1].

The SHSS procedure is clearly described in the IIW guideline [1]: starting from the weld profile, two or three reference points must be specified for the subsequent stress extrapolation on them. The choice of the number of reference points depends on the employed hot-spot typology, in *Figure 1.6*. The reference point closest to the weld toe must avoid any non-linear effect caused by the weld profile itself; for this reason, a minimum distance of 0.4 t (t = main plate thickness) from the weld toe is recommended. Once the stress values are known, a linear (two reference points) or a quadratic (three reference points) extrapolation is performed to obtain the hot-spot stress at the weld toe, as illustrated in *Figure 1.3*.

The method can prove its potential for crack initiations at weld toe, which examples are displayed in *Figure 1.4* below:

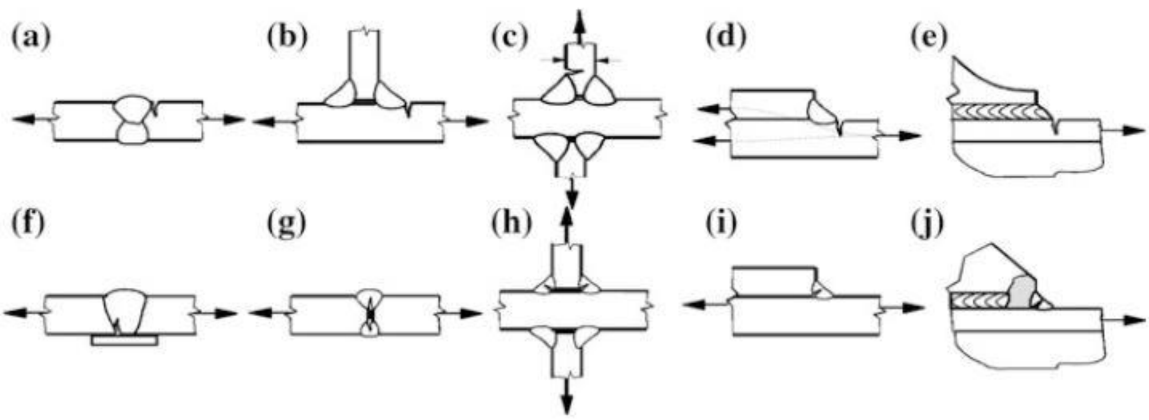

Figure 1. 4: different crack initiation points in welded joints; a–e refers to weld toe cracks, where the SHSS method can be applied f–j refers to weld root cracks, where the SHSS method cannot be applied [1].

Two different hot-spots definitions are available according to their location on the plate and their orientation with respect to the weld toe, i.e. plate surface and edge, represented in *Figure 1.5*:

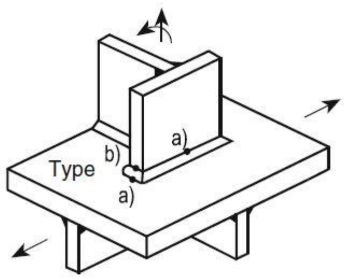

Table 2.2 : Types of hot spots

Type	Description	Determination
a	Weld toe on plate surface	FEA or measurement and extrapolation
b	Weld toe at plate edge	FEA or measurement and extrapolation

Figure 1. 5: types of hot-spot. In this elaborate, the type of hot-spot under investigation is the first one, i.e. "a" [1].

Poutiainen, Tanskanen and Marquis [12] give some useful modelling advices:

- The extrapolation can be performed with the adoption of both fine and coarse meshes;
- The first principal stress σ_{11} has to be detected in the reference points;
- In regard to the modelling of 2D structures, a mapped mesh algorithm should be used along with four-node linear plane elements;
- In regard to the modelling of 3D structures, eight-node or twenty-node linear hexahedral elements should be employed. More specifically, in case of 20-node hexahedral elements, only one element layer along the main plate thickness should be introduced to avoid any influence of the singularity; moreover, the stress closest to the hot-spot has to be evaluated at the first nodal point, which means that the element length at the hot-spot must correspond to its distance from the first reference node. In case 8-node hexahedral are used, several element layers are allowed; if finer meshes are used, the refinement should be introduced in every direction.

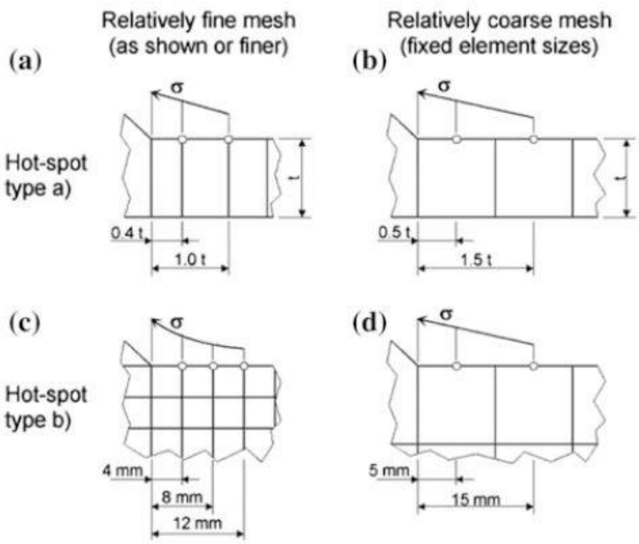

Figure 1. 6: reference points at different types of meshing [1].

According to *Figure 1.6*, the IIW recommendations [1] provide two “type a” hot-spot extrapolation formulae, function of the joint main plate thickness:

1. Linear extrapolation at two reference points given by equation (1.2):

$$\sigma_{hs} = 1.67 \cdot \sigma_{0.4t} - 0.67 \cdot \sigma_{1.0t} \tag{1.2}$$

2. Alternatively, in cases of pronounced non-linear stress increment at the hot-spot, a quadratic extrapolation at three reference points is performed with expression (1.3):

$$\sigma_{hs} = 2.52 \cdot \sigma_{0.4t} - 2.24 \cdot \sigma_{0.9t} + 0.72 \cdot \sigma_{1.4t} \tag{1.3}$$

The various nominal FAT classes are so collapsing in two SHSS FAT classes: FAT 90 and FAT 100, displayed in *Figure 1.7*, presenting the following characteristics:

- They are referred to as-welded conditions, with some exceptions made;
- The influence of high tensile residual stresses is already considered;
- Only small misalignments are taken into account. In case of consistent misalignment, a stress magnification factor k_m, accessible in the IIW guideline [1], has to be considered;
- The evaluated SHSS has to be minor to $2 \cdot f_y$, to avoid plastic yielding.

Since it does not consider the stress gradient around the weld toe, the thickness correction factor, available in [1] and adopted for the nominal approach, has also to be accounted for the SHSS method, to affirm that the SHSS cannot predict the thickness effect.

No.	Structural detail	Description	Requirements	FAT Steel	FAT Alu.
1	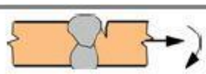	Butt joint	As welded, NDT	100	40
2	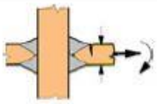	Cruciform or T-joint with full penetration K-butt welds	K-butt welds, no lamellar tearing	100	40
3	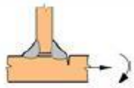	Non load-carrying fillet welds	Transverse non-load carrying attachment, not thicker than main plate, as welded	100	40
4	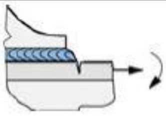	Bracket ends, ends of longitudinal stiffeners	Fillet welds welded around or not, as welded	100	40
5	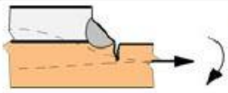	Cover plate ends and similar joints	As welded	100	40
6	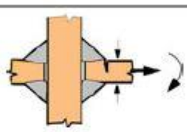	Cruciform joints with load-carrying fillet welds	Fillet welds, as welded	90	36
7	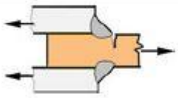	Lap joint with load carrying fillt welds	Fillet welds, as welded	90	36
8	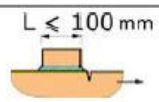	Type "b" joint with short attachment	Fillet or full penetration weld, as welded	100	40
9	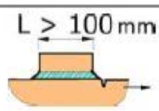	Type "b" joint with long attachment	Fillet or full penetration weld, as welded	90	36

Figure 1. 7: SHSS FAT classes according to the IIW guideline [1].

1.2.2 1-mm Stress

In 2004, Xiao and Yamada [3] proposed an alternative FE method for the fatigue assessment of welded structures. The approach is commonly known as "1-mm stress", since it is based on the computed stress value located 1-mm below the weld toe tip, normal to the exterior surface, along the theoretical direction of propagation of the defect.

As it was affirmed before, the total stress occurring at the weld toe, synthesised by the factor k_t, is caused by the structural geometry change along with the non-linear stress raise due to the weld profile itself:

$$k_t = k_s \cdot k_w \tag{1.4}$$

where:

- k_t is the whole stress concentration at weld toe;
- k_s is the stress concentration due to structural geometry change;
- k_w is the non-linear stress concentration due to weld profile.

According to the authors, k_w is thought to be equivalent to the whole stress felt by the "reference detail", described by a non-load carrying NLC transverse joint, with main plate thickness equal to 10 mm, displayed in *Figure 1.8*. Therefore, the correlation between the fatigue strength of the "object detail" and the "reference detail" lies is the k_s value, taken as critical parameter for the fatigue life of welded components.

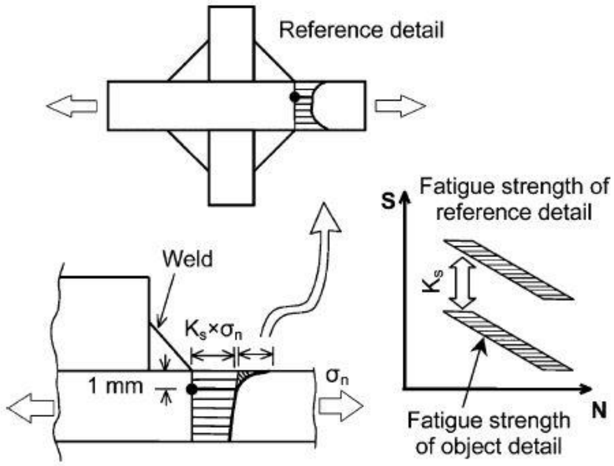

Figure 1. 8: 1-mm stress method, reference detail [3].

With respect to the type "a" SHSS, where the output hot-spot stress is function of the main plate thickness, the 1-mm stress method has the additional advantage of accounting of the size effect [3]. Hence, in terms of 1-mm stress, it is unique the proposed fatigue design curve.

The method is suitable for potential crack initiations at weld toe. Furthermore, it has proven to be valid for [3]:

- In-plane attachments;
- Out-of-plane attachments;
- T and H-attachments;
- Steel post structures.

However, this local approach also presents some limits, indicated by Xiao and Yamada:

- The mesh element size cannot exceed 1 mm;
- Different specimen geometries, such as load carrying LC cruciform joints or one-sided attachments, have to be investigated yet;
- Only axial loading cases have been considered;
- The bending stress cannot predominate over the membrane stress.

1.3 Local approaches (University of Padova)

In the classical mechanics, the structural resistance of the components is determined with the adoption of a point criterion, for which the stress calculated at the most stressed point of the specimen must be lower than a reference value (generally, the yield strength f_y). In case of cracks, as well as sharp notches, a linear elastic analysis would show that the stress at the defect tip would tend to infinite. Conversely, the experimental reality demonstrates that this phenomenon is prevented by the local material yielding near the crack tip region. The development of the linear elastic fracture mechanics LEFM bases the fatigue life of defective components on a field criterion, abandoning thus the point criterion.

After the non-conventional extension of the LEFM concept to the fatigue design of welded joints, the fatigue assessment of the latter is treated essentially as a notch effect problem: the theory of the notch stress intensity factors NSIFs, defined by Gross and Mendelson in 1972 [13], assumes that the weld toe profile is a sharp V-notch having a tip radius equal to zero (the worst case), while the root side is a pre-crack in the structure. With these assumptions, it is shown that the medium-cycle and high-cycle fatigue strength are function of the intensity of the linear elastic local stress distributions [7].

The thus-defined V-notch can be solicited in three alternative ways, better known as fracture modes, illustrated in *Figure 1.9*, each one related to a particular stress component:

1. Mode I: tensile opening;
2. Mode II: in-plane shear or sliding;
3. Mode III: out-of-plane shear or tearing.

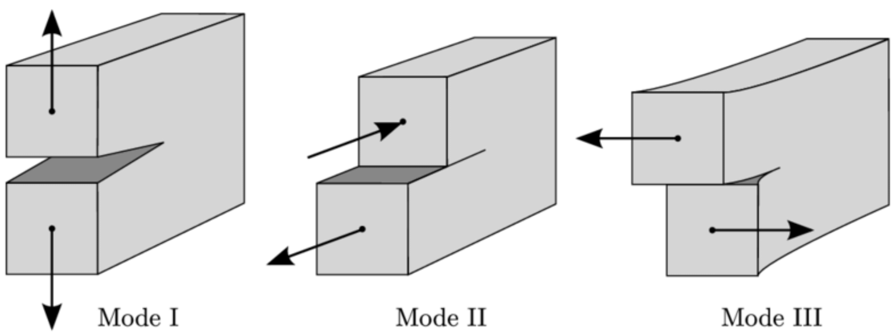

Figure 1. 9: three fracture modes which can occur at cracks as well as V-notches [14].

1.3.1 Analytical Notch Stress Intensity Factors (NSIFs)

In plane problems, the analytical expression of the stress field related to mode I and II loadings at V-notches is described by equation (1.5):

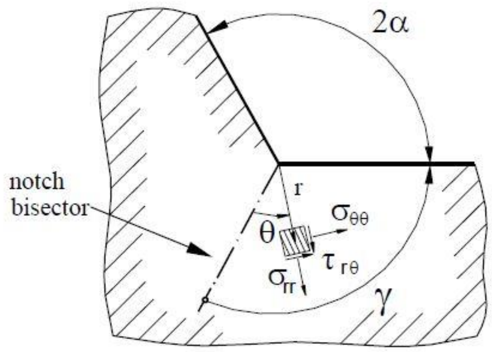

Figure 1. 10: local cylindrical system of reference for a V-notch [15].

$$\begin{Bmatrix} \sigma_{\theta\theta} \\ \sigma_{rr} \\ \tau_{r\theta} \end{Bmatrix} = \frac{K_1}{r^{1-\lambda_1}} \begin{Bmatrix} \tilde{\sigma}_{\theta\theta}(\theta) \\ \tilde{\sigma}_{rr}(\theta) \\ \tilde{\tau}_{r\theta}(\theta) \end{Bmatrix}_I + \frac{K_2}{r^{1-\lambda_2}} \begin{Bmatrix} \tilde{\sigma}_{\theta\theta}(\theta) \\ \tilde{\sigma}_{rr}(\theta) \\ \tilde{\tau}_{r\theta}(\theta) \end{Bmatrix}_{II} \tag{1.5}$$

where:

- $\sigma_{\theta\theta}, \sigma_{rr}, \tau_{r\theta}$ are the plane stress state components expressed in the cylindrical system of reference in *Figure 1.10*;
- $\tilde{\sigma}_{\theta\theta}(\theta), \tilde{\sigma}_{rr}(\theta), \tilde{\tau}_{r\theta}(\theta)$ are trigonometric functions depending on θ and the fracture mode;
- λ_1, λ_2 are the Williams' eigenvalues (1952) [16], depending on the V-notch opening angle 2α, which express the "power" of the field singularity. The table below reports their values in function of 2α:

2α [°]	**Mode I λ_1**	**Mode II λ_2**
0	*0.5*	*0.5*
30	*0.501*	*0.598*
45	*0.505*	*0.660*
60	*0.512*	*0.731*
90	*0.544*	*0.909*
120	*0.616*	*1.149*
135	*0.674*	*1.302*
150	*0.752*	*1.486*

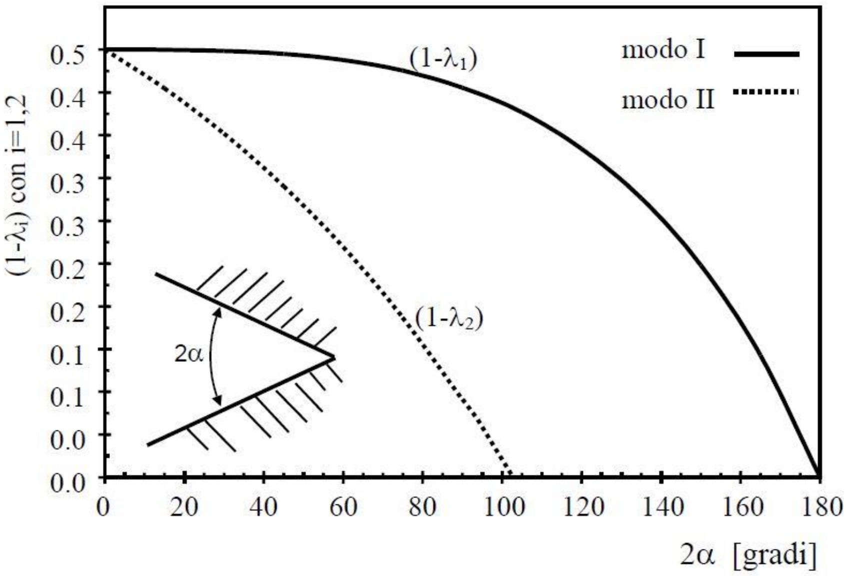

Figure 1. 11: Williams' eigenvalues related to fracture mode I and II. For opening angles higher that 102.5°, mode II singularity is null [15].

- K_1 and K_2 are the Notch Stress Intensity Factors NSIFs associated to mode I and II, which aim to quantify the intensity of the local stress field components in the V-notch region.

Subsequently, in 1997, Qian and Hasebe [17] determined the local stress distributions for mode III, defining K_3 as well as $\lambda_3 = \frac{\pi}{2\gamma}$ for axisymmetric structures.

With reference to *Figure 1.12* and *Figure 1.13*, the $K_{i,i=1,2,3}$ definitions are given in equations (1.6)-(1.8):

$$K_1 = \sqrt{2\pi} \cdot \lim_{r\to 0^+} \left[\sigma_{\theta\theta_{r,\theta=0}} \cdot r^{1-\lambda_1} \right] \tag{1.6}$$

$$K_2 = \sqrt{2\pi} \cdot \lim_{r\to 0^+} \left[\tau_{r\theta_{r,\theta=0}} \cdot r^{1-\lambda_2} \right] \tag{1.7}$$

$$K_3 = \sqrt{2\pi} \cdot \lim_{r\to 0^+} \left[\tau_{\theta z_{r,\theta=0}} \cdot r^{1-\lambda_3} \right] \tag{1.8}$$

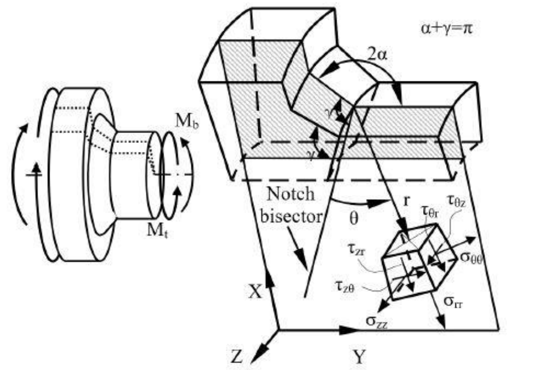

Figure 1. 12: example of polar reference system centred at the V-notch tip, and definition of the stress components related to their fracture modes [18].

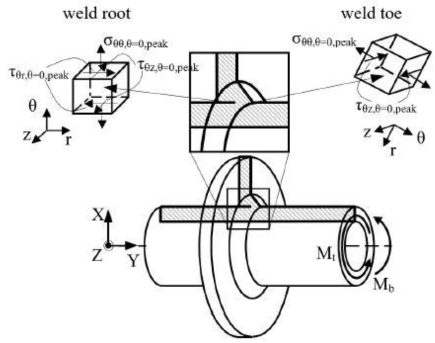

Figure 1. 13: another example of frame of reference centred at the weld toe [18].

The NSIFs approach for the fatigue assessment of sharp notched components was first proposed by Kihara and Yoshii in 1991 [4]. Subsequently, Lazzarin and Tovo in 1998 [5], Atzori in 2001 [19] and Lazzarin in 2004 [20] extended the method to monoaxially and multiaxially loaded joints. The analytical calculation of the NSIFs requires the employment of a finite element FE software.

Figure 1.14 illustrates Lazzarin and Tovo's fatigue design curve, expressing the fatigue strength of welded joints in terms of mode I NSIF K_1. As seen, the scatter band amplitude T_{K1}=1.90 is much more limited with respect to the global approach T_σ: in fact, since the fatigue is a local phenomenon which focus on the crack initiation an propagation near the V-notch region, it is unique the K_1-N_f design curve able to synthesize a large variety of experimental data coming from different welded geometries, simultaneously accounting of the size and shape effects.

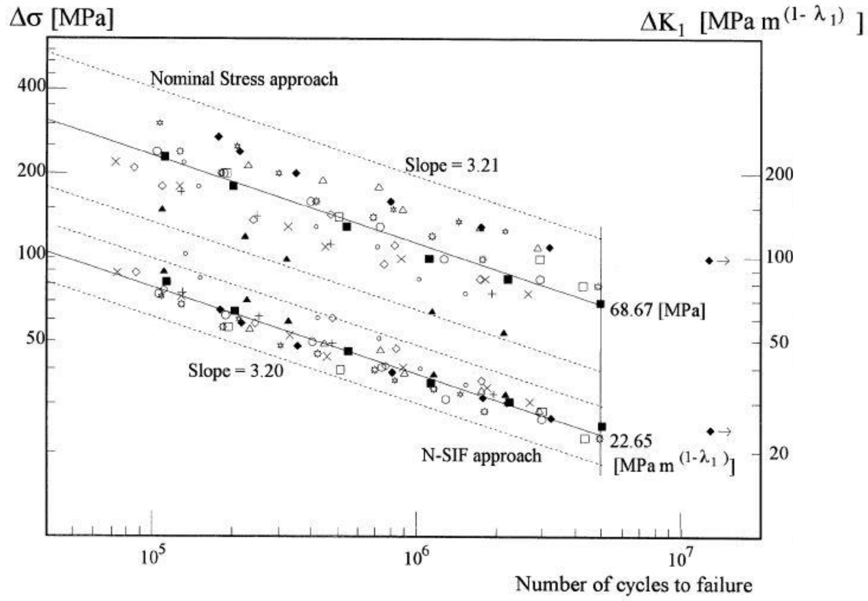

Figure 1. 14: fatigue strength in terms of nominal stress and N-SIF ranges [5].

However, as Campagnolo [18] clearly reports in his research, the analytical NSIFs detection is affected by two relevant drawbacks in engineering applications:

1. Very refined meshes are required (element size $\cong 10^{-5}\ mm$), resulting in a time-consuming modelling and simulation;
2. A number of *stress-distance* values, starting from the V-notch tip, are required to obtain K_i;
3. The $K_{i,i=1,2,3}$ unit of measurement is expressed in $[MPam^{1-\lambda_{i,i=1,2,3}}]$, therefore the singularity of the stress distribution varies according to the V-notch opening angle, impeding the comparison of the stress field intensities between V-notches with different opening angles;

1.3.2 Strain Energy Density (SED)

The proposal of the Strain Energy Density approach, an energetic criterion introduced by Lazzarin and Zambardi in 2001 [6] aims to overcome the abovementioned NSIFs limits. The method derives from Neuber's idea of a structural volume governing the fatigue life of notched structural details. In fact, at the basis of this method, the fatigue strength of welded joints is thought to depend on the strain energy density SED averaged over a circular sector of radius R_0, centred at the V-notch tip. R_0, the fatigue life critical parameter, has the characteristic of being material property: more precisely, $R_0 = 0.28$ mm for steel structures, while $R_0 = 0.12$ mm for aluminium alloys.

First calibrated under mode I [6], the method was secondly extended under combined fracture modes I+II+III [20].

In plane strain hypothesis, starting from the NSIFs values, the strain energy density can be analytically calculated with equation (1.9):

$$\overline{W} = \frac{1}{E} \cdot \left(c_{w1} \cdot e_1 \cdot \frac{K_1^2}{R_0^{2(1-\lambda_1)}} + c_{w2} \cdot e_2 \cdot \frac{K_2^2}{R_0^{2(1-\lambda_2)}} + c_{w3} \cdot e_3 \cdot \frac{K_3^2}{R_0^{2(1-\lambda_3)}} \right) \tag{1.9}$$

where:

- $K_{i,i=1,2,3}$ are respectively mode I, II and III NSIFs;
- R_0 is the structural volume radius;
- E is the Young modulus;
- $c_{wi,i=1,2,3}$ are the coefficient depending on the stress ratio $R = \frac{\sigma_{min}}{\sigma_{max}}$; they are used in case of stress relieved SR joints [20]:

$$c_w(R) = \begin{cases} \dfrac{1+R^2}{(1-R)^2} \ for -1 \le R < 0 \\ \dfrac{1-R^2}{(1-R)^2} \ for\ 0 \le R \le 1 \end{cases}$$

- $e_{i,i=1,2,3}$ are three parameters summarising the dependence on the V-notch opening angle 2α, as well as on the Poisson's ratio ν [21]. The e_i values are listed in the table below, for a set ν = 0.3, function of 2α:

2α [°]	e_1	e_2	e_3 [21]
0	*0.133*	*0.340*	*0.414*
30	*0.147*	*0.274*	-
45	*0.150*	*0.244*	-
60	*0.151*	*0.217*	-
90	*0.145*	*0.168*	*0.310*
120	*0.129*	*0.128*	*0.276*
135	*0.118*	*0.111*	*0.259*
150	*0.104*	*0.096*	-

In a FE environment, the average SED ($\Delta\overline{W}_{FEM}$) can be detected with the adoption of the so-called "direct approach", by summation of the energy contained inside each element, divided by the area of the circular sector:

$$\Delta\overline{W}_{FEM} = \frac{\sum_{V(R_0)} W_{FEM,i}}{V(R_0)} \tag{1.10}$$

The average strain energy density $\overline{W}$ is commonly expressed in $\left[\frac{MJ}{m^3}\right]$ or alternatively in $\left[\frac{J}{mm^3}\right]$.

The SED approach presents several advantages:

- The fatigue resistance expressed in terms of energy allows the comparison among different V-notches opening angles 2α;
- Deriving from the NSIF approach, the design fatigue curve is still unique;
- If calculated with a FE software, the strain energy density does not necessarily require fine meshes [22].

Figure 1.15 illustrates Lazzarin and Zambardi's design curve, which express the fatigue strength of welded joints in terms of Strain Energy Density:

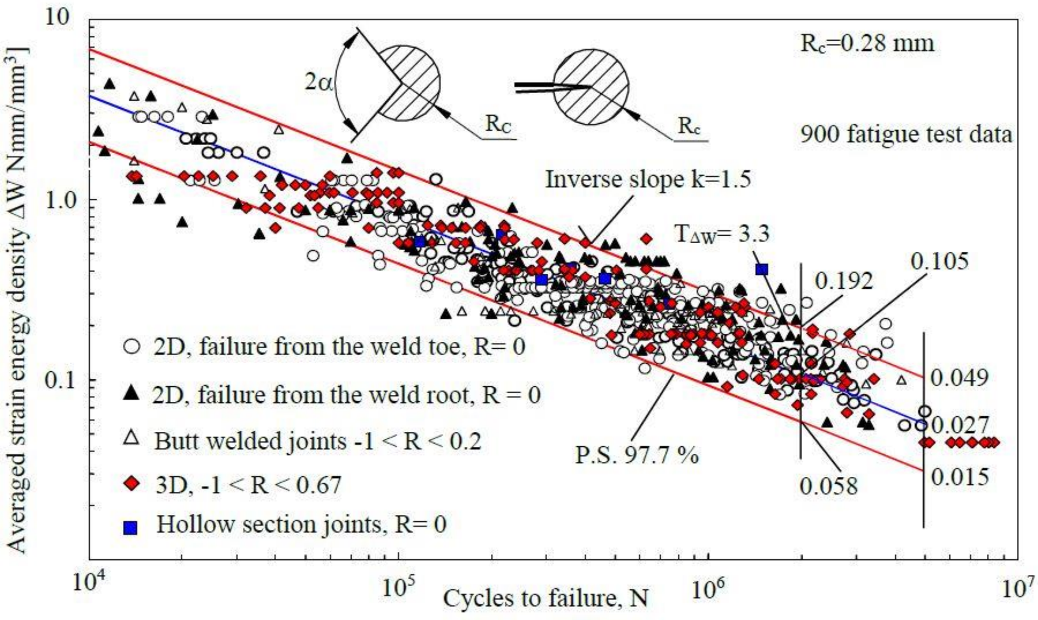

Figure 1. 15: fatigue endurance expressed in terms of averaged strain energy density [6].

In 2016, Fischer, Fricke and Rizzo [23-24] proposed a slightly different value for the structural volume size, R_0=0.32 mm, able to account for welding-induced misalignments. However, for safety advantage reasons, in this elaborate the radius is left to R_0=0.28 mm, so that the strain energy density is averaged inside a smaller circular sector.

1.3.3 Peak Stress Method (PSM)

The PSM is a rapid engineering application of the NSIFs detection for the fatigue strength assessment of welded joints. It employs the singular linear elastic peak stresses, calculated by a finite element analysis, in correspondence of the singularity under investigation without the necessity of refined meshes. The analytical NSIFs approach for the fatigue endurance assessment is thus redrafted by the PSM leverage [25]. In parallel to the SED method, the PSM aims to overcome the abovementioned NSIFs drawback. The method is applicable to steel structures as well as aluminium alloys.
According to the PSM, the correlation between mode I, II and III NSIFs and the corresponding peak stress components is respectively expressed in formulae (1.10) and (1.12):

$$K_1 \cong K_{FE}^{*} \cdot \sigma_{\theta\theta,\theta=0,peak} \cdot d^{1-\lambda_1} \tag{1.11}$$

$$K_2 \cong K_{FE}^{**} \cdot \tau_{r\theta,\theta=0,peak} \cdot d^{1-\lambda_2} \tag{1.12}$$

$$K_3 \cong K_{FE}^{***} \cdot \tau_{\theta z,\theta=0,peak} \cdot d^{1-\lambda_3} \tag{1.13}$$

where:

- K_{FE}^{*}, K_{FE}^{**}, K_{FE}^{***} are the PSM calibration constants related to mode I,II, III which depend on the element type, the element formulation, the adopted mesh pattern and the nodal stress evaluation procedure;

- $\sigma_{\theta\theta,\theta=0,peak}$, $\tau_{r\theta,\theta=0,peak}$, $\tau_{\theta z,\theta=0,peak}$ are the peak nodal stresses evaluated at the V-notch profiles, which significant examples are displayed in *Figure 1.16*;

- d is the mesh global element size;

- λ_1, λ_2, λ_3 are the abovementioned William's eigenvalues [16].

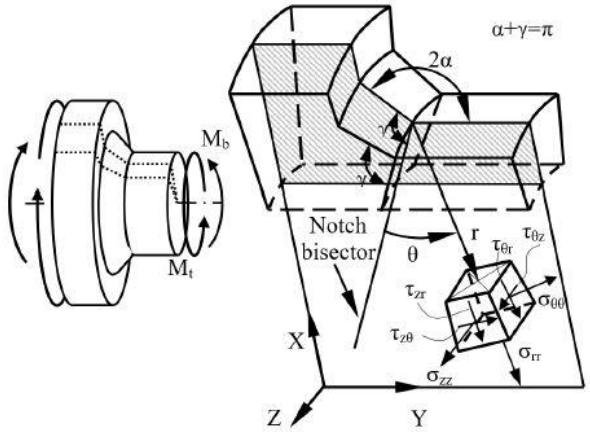

Figure 1. 16: example of polar reference system centred at the V-notch tip, and definition of the stress components related to their fracture modes [18].

In plane strain hypothesis, taking advantage of (1.11) – (1.13), the equation (1.9) can be rewritten as function of the peak stresses $\sigma_{\theta\theta,\theta=0,peak}$, $\tau_{r\theta,\theta=0,peak}$, $\tau_{\theta z,\theta=0,peak}$ by imposing the following equality:

$$\bar{W} = (1-\nu^2)\cdot\frac{\sigma_{eq,peak}^2}{2E} \tag{1.14}$$

from which, after due arrangements, an equivalent peak stress is extracted:

$$\sigma_{eq,peak} = \sqrt{f_{w1}^2\cdot\sigma_{\theta\theta,\theta=0,peak}^2 + f_{w2}^2\cdot\tau_{r\theta,\theta=0,peak}^2 + f_{w3}^2\cdot\tau_{\theta z,\theta=0,peak}^2} \tag{1.15}$$

where:

- $f_{wi,i=1,2,3}$ are the peak stresses corrective factors, described in the expression (1.16):

$$f_{wi} = K_{FE}^{j}\cdot\sqrt{\frac{2e_i}{1-\nu^2}}\cdot\left(\frac{d}{R_0}\right)^{1-\lambda_i}\Bigg|_{\substack{i=1,2,3\\ j=*,**,***}} \tag{1.16}$$

where, in their turn:

  - $e_{i,i=1,2,3}$ are the parameters summarising the dependence on the V-notch opening angle 2α, as well as on the Poisson's ratio ν;
  - R_0 is the radius of the circular sector;
  - K_{FE}^{j} are the PSM calibration constants;
  - d is the mesh global element size.

The PSM presents several advantages:

- The equivalent peak stress allows the comparison between welds presenting different V-notch opening angles 2α;
- FE analyses require coarser meshes with respect to those necessary for the analytical NSIFs calculation;
- Only one nodal peak stress is required instead of a number of *stress-distance* values;
- Deriving from the NSIF approach, the design fatigue curve is still unique;

2D PSM, linear plane elements

The PSM was first proposed to 2D geometries under mode I by Meneghetti and Lazzarin in 2007 [7], under mode II by Meneghetti in 2012 [26], under mode III by Meneghetti in 2013 [27].

The PSM calibration constants depend on several factors:

- The FE software: the original is Ansys® Mechanical APDL, even though over the years the PSM has been calibrated for six other commercial FE packages [8];
- Four-node linear plane elements, with *Simple Enhanced Strain* and *Plane Strain* as Key Options;
- Concerning the mesh pattern, a free mesh algorithm has to be generated; moreover, for V-notches opening angle 2α > 90°, two adjacent elements must share the same node at the V-notch tip, while for 2α < 90°, four elements must share the same node at the V-notch tip, as exemplified in *Figure 1.17*:

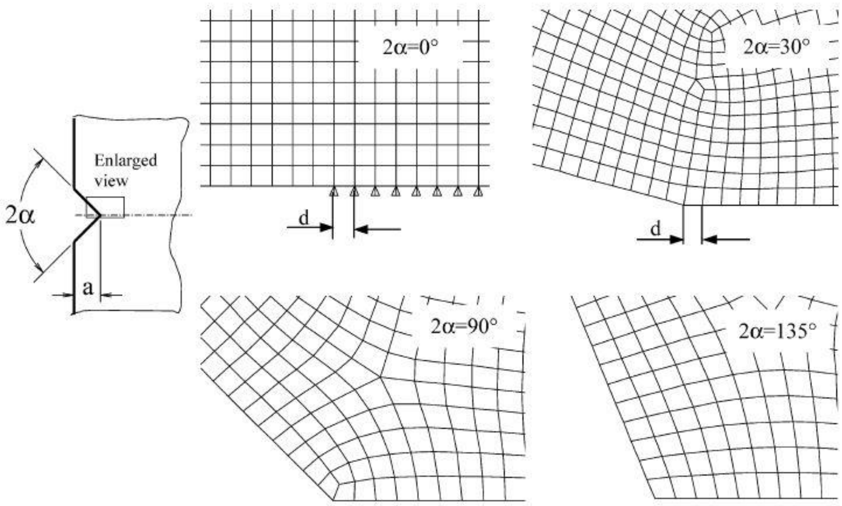

Figure 1. 17: mesh patterns which must be adopted in the numerical analyses [7].

2α	**Mode I**	**Mode II**	**Mode III**
	***a/d** min*	***a/d** min*	***a/d** min*
0° < 2α < 135°	3	14	/
0° (root) 135° (weld toe)	/	/	12 (root) 3 (weld toe)

d = finite element size   a = component's reference dimension

In respect of these requirements, the PSM calibration constants assume the following values:

K_{FE}^{*}	K_{FE}^{**}	K_{FE}^{***}
$1.38\ \pm 3\%$	$3.38\ \pm 3\%$	$1.93 \pm 3\%$

Figure 1.18 and *Figure 1.19* respectively illustrate Meneghetti and Lazzarin's design curves, which express the fatigue strength of welded joints in terms of mode I NSIF K_1 as well as $\Delta\sigma_{eq,peak}$, under prevailing mode I. The curves are valid for as-welded joints, yield strength ranging between 360 and 670 MPa, main plate thickness ranging from 6 to 100 mm, V-notch opening angle varying from 0° to 135°, stress ratio ≅0.

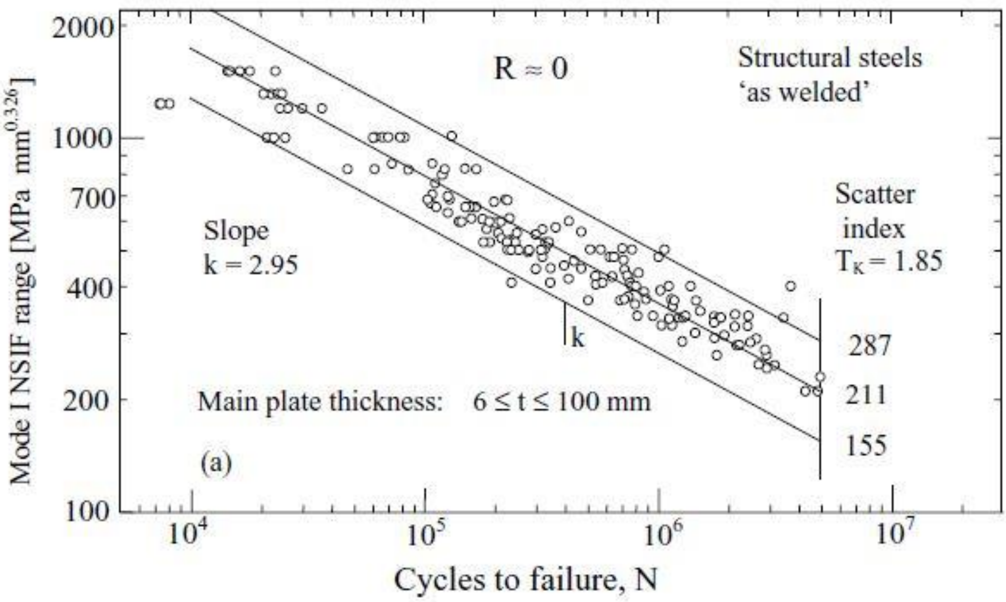

Figure 1. 18: fatigue strength in terms of NSIF K_1 mode I esteemed with the PSM, steel structures, weld toe failures [7].

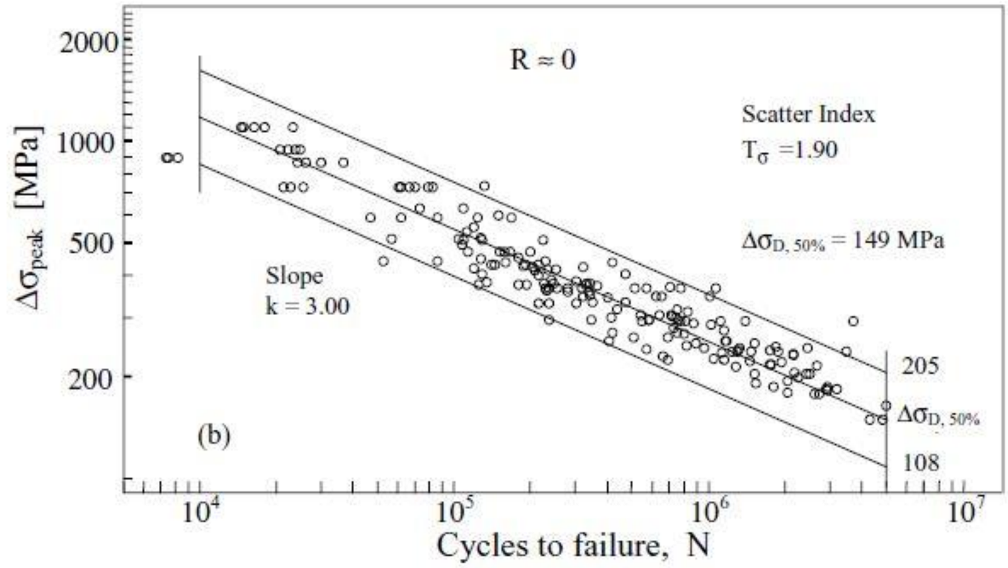

Figure 1. 19: fatigue strength in terms of equivalent peak stress, steel structures, weld toe and root failures [7].

<u>3D PSM, linear hexahedral elements</u>

In 2014, Meneghetti, Guzzella and Atzori combined the 2D Peak Stress Method with 3D numerical models to assess the fatigue strength of steel welded joints having complex geometry and characterised both by toe and root cracking [28]. As the authors report, the 3D PSM with the adoption of linear hexahedral elements requires the submodelling technique: briefly, the main model of the structure is created, meshed with ten-node quadratic elements; subsequently, a smaller submodel is extracted from it, meshed with eight-node linear elements. This technique allows to obtain very accurate results in a restricted area of interest, i.e. the fracture region. The submodel is delimited by a cut boundary region, which has to be pre-defined in the main model with a convergence analysis. The nodal displacements belonging to the cut-boundary are extrapolated for then being applied to the submodel areas. This method is based on De Saint-Venant's principle affirming that the effects of loading with the same magnitude, but different distributions, dissipate quickly as the distance increases. Consequently, if the cut boundary is sufficiently far from the local stress raising region, the final results will be accurate [29].

The 3D PSM calibration constants depend on several factors:

- The FE software: the original is Ansys® Mechanical APDL;
- Eight-node linear hexahedral elements, with *Simple Enhanced Strain* as Key Option K1;
- The mesh pattern of the submodel follows the same dispositions as the 2D case.

Conclusively, in both plain stress and plain strain conditions and in respect of the PSM 3D requirements, the PSM calibration constants previously proposed for 2D structures are still valid:

K_{FE}^{*}	K_{FE}^{**}
$1.38\ \pm 3\%$	$3.38\ \pm 3\%$

It is the authors' opinion that $K_{FE}^{***} = 1.93 \pm 3\%$ is valid even for mode III, despite lack of validation;

Figure 1.20 illustrates Meneghetti, Guzzella and Atzori's fatigue design curve in terms $\Delta\sigma_{eq,peak}$ for 3D structures. The curve, which characteristic values are equal to the ones of 2D structures, was determined for as-welded joints, yield strength ranging between 360 and 670 MPa, main plate thickness ranging from 6 to 100 mm, V-notch opening angle varying from 0° to 135°, stress ratio ranging between -0.36 and 0.7, both weld toe and root failures:

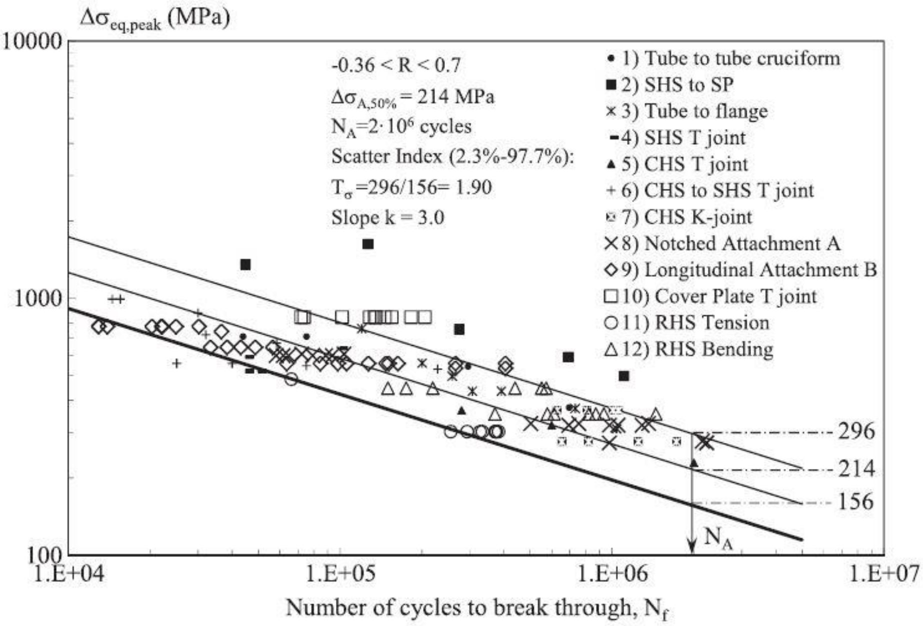

Figure 1. 20: fatigue strength in terms of equivalent peak stress, 3D steel structures, weld toe and root failures, prevailing mode I [28].

<u>3D PSM, quadratic tetrahedral elements</u>

The 3D modelling of large-scale structures is increasingly adopted in industrial applications, thanks to the growing spread of high-performance computing HPC. Following this trend, in 2018 Campagnolo and Meneghetti [18] extended the PSM to the ten-node tetra elements employment under mode I, II and III, consistently speeding up the modelling and simulation times.
Subsequently, in 2019 Campagnolo, Roveda and Meneghetti [25] updated the PSM calibration constants for ten-node tetra elements; in addition, they calibrated the PSM under mode I, II, III with four-node tetra elements.

The 3D PSM calibration constants depend on several factors:

- The FE software: the original is Ansys® Mechanical APDL;
- Ten-node quadratic tetrahedral elements, with *Pure Displacement* as Key Option K1;
- The mesh pattern obtained by the free mesh generation algorithm is not regular, so that a node belonging to the notch tip could be shared by a different number of elements having significantly different shape. Consequently, the peak stress could vary along the notch tip profile even in the case of a constant applied NSIF. To reduce the variability of the peak stress

along the notch tip profile, an average peak stress value has been introduced, defined at the generic node n=k as the moving average on three adjacent vertex nodes, i.e. n= k-1, k and k+1:

$$\bar{\sigma}_{ij,peak,n=k} = \left. \frac{\sigma_{ij,peak,n=k-1} + \sigma_{ij,peak,n=k} + \sigma_{ij,peak,n=k+1}}{3} \right|_{n=node} \tag{1.17}$$

Only peak stress values calculated at vertex nodes of the quadratic elements have to be input in (1.17). Thus, stress values at mid-side nodes located at the notch tip profile must be neglected [18].

In respect of these requirements, the PSM calibration constants assume the following values:

2α [°]	Mode I				Mode II				Mode III			
	Tetra 4		Tetra 10		Tetra 4		Tetra 10		Tetra 4		Tetra 10	
	K^{*}_{FE}	$(a/d)_{min}$	K^{*}_{FE}	$(a/d)_{min}$	K^{**}_{FE}	$(a/d)_{min}$	K^{**}_{FE}	$(a/d)_{min}$	K^{***}_{FE}	$(a/d)_{min}$	K^{***}_{FE}	$(a/d)_{min}$
0	1.75 ± 22%	3	1.05 ± 15%	3	2.65 ± 15%	3	1.63 ± 20%	1	2.50 ± 15%	5	1.37 ± 15%	3
90					-	-	-	-				
120											1.70 ± 10%	3
135			1.21 ± 10%	1								

Figure 1. 21: table containing the values of K^{*}_{FE}, K^{**}_{FE} K^{***}_{FE}, ten/four-node tetra elements, Ansys® software [25].

The advantages of the ten-node tetrahedral elements adoption with respect to the eight-node are the following:

- The calibration is valid for mode I, II and III;
- Complex 3D structures can be discretized without the need of the submodelling technique;
- Only a free mesh generation algorithm is required, instead of a mapped algorithm.

On the other hand, some disadvantages:

- The PSM calibration constants show a major dependency on the V-notch opening angle 2α;
- The error band of the PSM constants is $\pm 10-15\%$ against the $\pm 3\%$ of the previous linear elements.

1.3.4 PSM precautions

Some precautions concerning the current Peak Stress Method state of the art are described below:

- The PSM is not calibrated for V-notch opening angles higher than 135°. In cases like this, the available K_{FE} related to $2\alpha = 135°$ are non-rigorously extended;
- The PSM does not take into account several factors affecting the crack initiation point previsions, such as highly non uniform residual stresses superimposed to external loads, as well as the real weld geometry;
- The PSM is not valid yet for variable amplitude loadings VAL;
- Concerning the stress ratio, the PSM is validated for $-0.36 < R < 0.7$. Since in as-welded specimens the influence of R does not affect the fatigue life, it is conceivable to think that the stress range ratio can be extended up to $R=-1$.
- Concerning the weld toe radius ρ, the following considerations are followed:
  - If $\rho < 1.5$-1.8 mm, ρ is usually brought to 0 mm, so as to have a V-notch (worst case);
  - If $1.8 < \rho < 4$ mm, it is the case of a blunt notch, and the PSM is employed in combination with the SED approach;
  - If $\rho > 4$ mm, the classical mechanics point criterion can be adopted for the fatigue assessment;
- Whenever the PSM foresees the crack initiation in a singularity which differs from the experimental one, the $\Delta\sigma_{eq,peak}$ related to the effective region is taken.

Chapter 2: numerical elaboration of experimental data for the detection of the NSIFs and SED parameters

In this Chapter, the fatigue assessment of four different experimental datasets of welded joints is performed in terms of nominal stress, mode I Notch Stress Intensity Factor K_1, Strain Energy Density SED and Equivalent Peak Stress. The re-elaborated data are then collected together to be compared in terms of statistical scatter with respect to the reference design fatigue curves proposed in the literature. Mode I K_1 is calculated analytically, using its definition, as well as with the Peak Stress Method.

Re-elaborated datasets consist of four transverse attachments that Maddox [30] and Gurney [31], respectively in 1987 and 1991, modelled in two dimensions, plus a square chord with circular brace, analysed by Gandhi in 1998 [32], modelled in three dimensions.

The assessments are effectuated with the employment of the Finite Element FE software Ansys® Mechanical APDL 19.0, license from University of Padova; the simulations are achieved with the adoption of four-node linear element Plane182, *Simple Enhanced Strain* and *Plane strain* as Key Options K1 and K3, in case of 2D FE models; on the other hand, eight-node linear element Brick 185, *Simple Enhanced Strain* as Key Option K1, and ten-node quadratic element Tetra 187, *Pure Displacement* as Key Option K1, are chosen for the analysis of 3D structures. The elements are available in the Ansys® element library.

Maddox and Gurney's geometries are created inside SOLIDWORKS 2018 *Student Edition*, for then being imported in Ansys® APDL with the .IGS extension. Gandhi's structure is instead modelled inside the Ansys® CAD environment.

All the following joints are presented in as-welded condition. In compliance with the non-conventional LEFM extension to welded joints, the weld toe profile is assumed as a sharp V-notch, with tip radius equal to zero (the worst case), while the root is considered as a pre-crack in the structure.

2.1 Transverse attachment geometries

The first four typologies of welded joint to be investigated are transverse stiffeners, fatigue class FAT 80, tested by Maddox [30] and Gurney [31] respectively in 1987 and 1991 under constant amplitude loading CAL.

Specific information on the components is reported below:

Weld condition	**Fracture location**	**Load application**	**V-notch opening angle 2α**
As-welded, non-load carrying, full penetration	*Weld toe*	*Main plate, parent material*	*135°*

The mechanical properties of each specimen are typical of structural steel:

Material model	**Yield strength f_y**	**Young modulus**	**Poisson's ratio ν**
Linear elastic, isotropic	*360 - 670 MPa*	*206000 MPa*	*0.3*

The transverse attachments are presented with a transverse NLC geometry, schematised in *Figure 2.1*, as well as with a T-shape profile, in *Figure 2.2*:

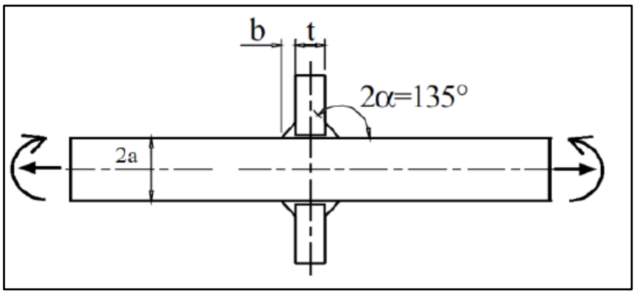

Figure 2. 1: general sketch of a transverse NLC joint, axially and bending loaded [7].

Geometrical parameters:

- Main plate thickness = *2a*
- Stiffener thickness = *t*
- Weld leg = *b*
- V-notch opening angle = 2α

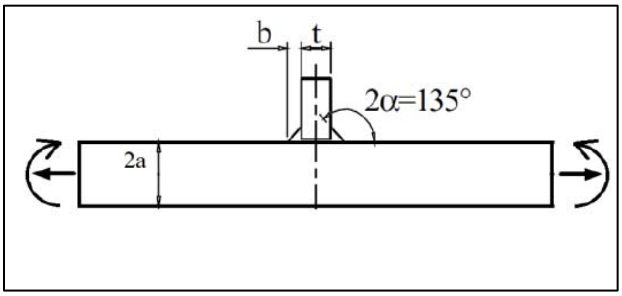

Figure 2. 2: general sketch of a T-joint, axially and bending loaded [7].

Lack of information on the main plate is justified since it has to be sufficiently long to represent the stress flowing from the "infinite". Similarly, the attachment length should be wisely chosen to be distant enough from the weld profile.

2.1.1 Maddox (1987), specimen #1

The first joint under investigation refers to a transverse NLC joint, initially assessed by Maddox in 1987. Its dimensions are reported below:

2a [mm]	**t [mm]**	**b [mm]**
13	*10*	*8*

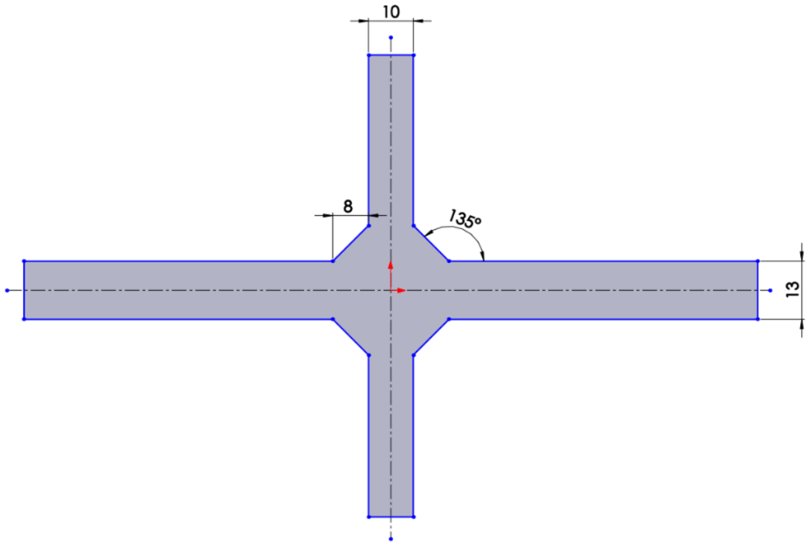

Figure 2. 3: Maddox #1, geometry. The quotes are expressed in [mm].

The experimental fatigue data are reported in terms of nominal stress $\Delta\sigma_{nom}$:

R	$\Delta\sigma_{nom}$ [MPa]	N_f [cycles]
	200	192 000
	140	507 000
0	100	2 937 000
	80	4 297 000

Inside Ansys® APDL environment, the modelling procedure is briefly described and shown in *Fig 2.4*:

- <u>Symmetries</u>: due to the double symmetry of the transverse NLC joint, only ¼ of the geometry is created, allowing to consistently speed up the computational time;
- <u>Loading</u>: specimen #1 is axially loaded, and the load is applied on the main plate as a constant pressure equal to $p = -\Delta\sigma_{nom}$, on Line 12;
- <u>Constraints</u>: symmetry boundary conditions are applied on Lines 14 and 16.

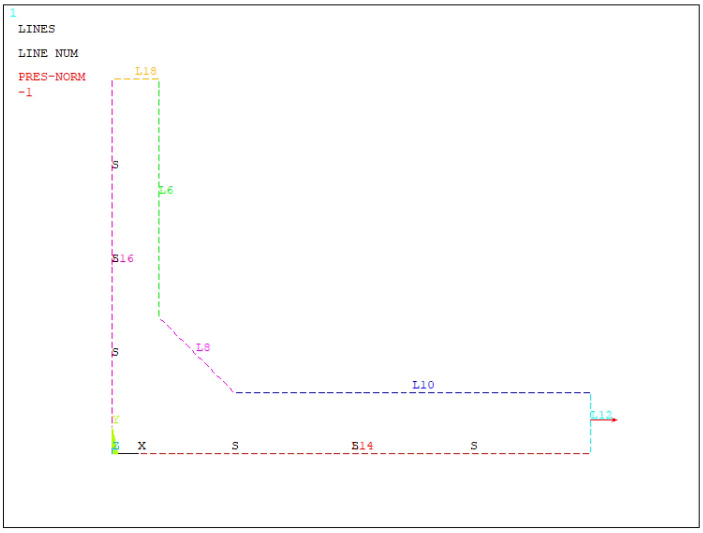

Figure 2. 4: loads and constraints to Maddox #1 joint. The letter S refers to a Symmetry BC, while the red arrow on Line 12 represents the external pressure.

2.1.2 Gurney (1991), specimen #2

The second joint under investigation refers to a transverse NLC joint, initially assessed by Gurney in 1991. Its dimensions are reported below:

2a [mm]	t [mm]	b [mm]
100	*220*	*15*

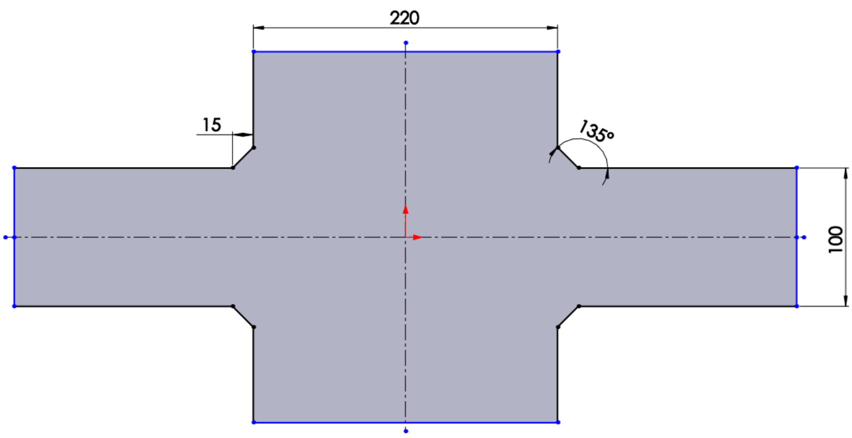

Figure 2. 5: Gurney #2, geometry. The quotes are expressed in [mm].

The experimental fatigue data are reported in terms of nominal stress $\Delta\sigma_{nom}$:

R	$\Delta\sigma_{nom}$ [MPa]	N_f [cycles]
	150	109 000
	120	224 000
0	100	322 000
	65	1 153 000
	55	2 147 000

Inside Ansys® environment, the modelling procedure is briefly described and shown in *Fig 2.6*:

- Symmetries: due to the double symmetry of the transverse NLC joint, only ¼ of the geometry is created, allowing to consistently speed up the simulation process;
- Loading: specimen #2 is axially loaded, and the load is applied on the main plate as a constant pressure equal to $p = -\Delta\sigma_{nom}$ on Line 14;
- Constraints: symmetry boundary conditions are applied to Lines 10 and 12.

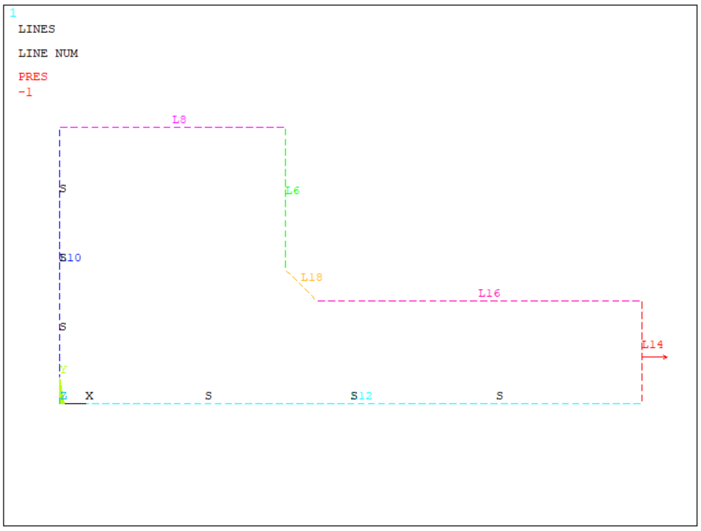

Figure 2. 6: loads and constraints to Gurney #2 joint. The letter S refers to a Symmetry BC, while the red arrow on Line 14 represents the external pressure.

2.1.3 Gurney (1991), specimen #3

The third joint under investigation refers to a transverse NLC joint, initially assessed by Gurney in 1991. Its dimensions are reported below:

2a [mm]	t [mm]	b [mm]
100	*13*	*8*

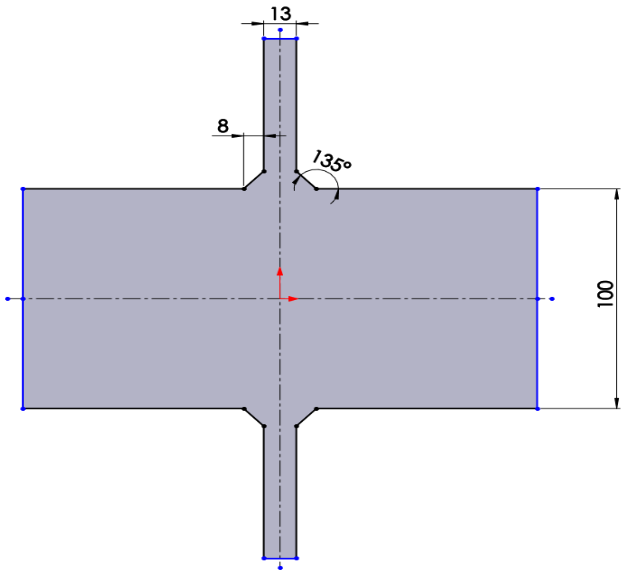

Figure 2. 7: Gurney #3, geometry. The quotes are expressed in [mm].

The experimental fatigue data are reported in terms of nominal stress $\Delta\sigma_{nom}$:

R	$\Delta\sigma_{nom}$ [MPa]	N_f [cycles]
	260	120 000
	220	200 000
	180	302 000
0	140	744 000
	120	1 180 000
	110	2 158 000

Inside Ansys® environment, the modelling procedure is briefly described and shown in *Fig 2.10*:

- Symmetries: thanks to the double symmetry of the transverse NLC joint, only ¼ of the geometry is modelled, allowing to consistently speed up the computational times;
- Loading: specimen #3 is bending loaded and the load is applied on the main plate as a linear pressure. The bending solicitation brings to a Navier's linear stress distribution, hence the nominal stresses reported in the table above refer to the maximum stress reached at the top of the main plate. Due to the double symmetry of the system, only one half of Navier's distribution is modelled: in particular, $p = 0\ MPa$ on Kp 1, while $p = -\Delta\sigma_{nom}$ on Kp 2;
- Constraints: due to the antimetric loading, an antisymmetry BC is applied on Line 12, while in Line 10, as usual, a symmetry BC is imposed. Finally, a keypoint belonging to one of the two symmetry axes must be constrained along y-direction (u_y=0) in order to remove the system lability.

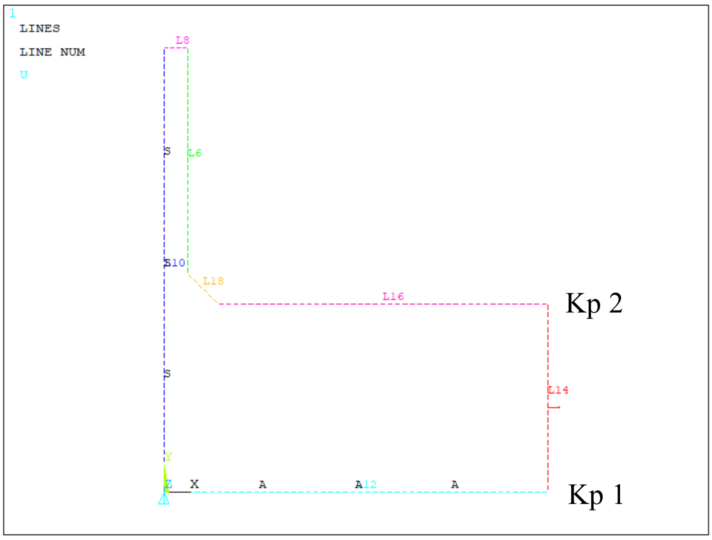

Figure 2.8: loads and constraints to Gurney #3 joint. The letter S refers to a Symmetry BC, the letter A to an Antisymmetry BC, while the red arrow refers to the linear pressure.

2.1.4 Gurney (1991), specimen #4

The fourth joint under investigation refers to a T-shape joint, first assessed by Gurney in 1991. Its dimensions are reported below:

2a [mm]	t [mm]	b [mm]
6	*6*	*6*

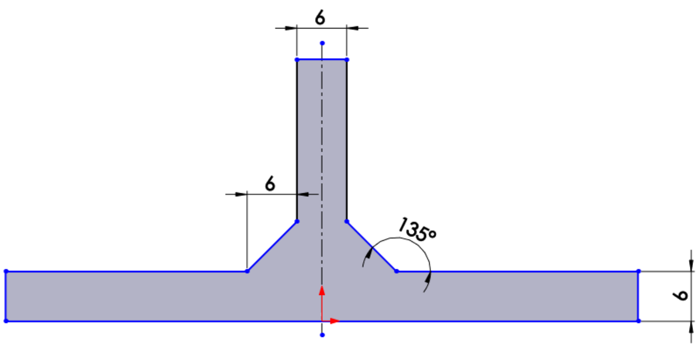

Figure 2. 9: Gurney #4, geometry. The quotes are expressed in [mm].

The experimental fatigue data are expressed in terms of nominal stress $\Delta\sigma_{nom}$:

R	$\Delta\sigma_{nom}$ [MPa]	N_f [cycles]
0	300	135 000
	260	237 000
	200	407 000
	190	573 000
	180	665 000
	160	1 525 000
	150	1 534 000
	140	2 601 000

Inside Ansys® environment, the modelling procedure is briefly described and shown in *Fig 2.10*:

- Symmetries: thanks to the symmetry of the T-shape joint, only ½ of the geometry is modelled, allowing to speed up the simulation timing process.
- Loading: Specimen #4 is bending loaded, and the load is applied on the main plate as a linear pressure. The bending solicitation brings to a Navier's linear stress distribution, therefore the nominal stress reported in the table above refers to the maximum stress reached at the top of the main plate. In order to model the stress distribution in a ½ joint, a linear pressure p is applied on Line 14. In particular, $p = \Delta\sigma_{nom}$ on Kp 1, while $p = -\Delta\sigma_{nom}$ on Kp 2.
- Constraints: a symmetry boundary condition is applied on Line 6. Moreover, a keypoint belonging to the vertical symmetry axis must be constrained along y-direction (u_y=0) in order to remove the system lability.

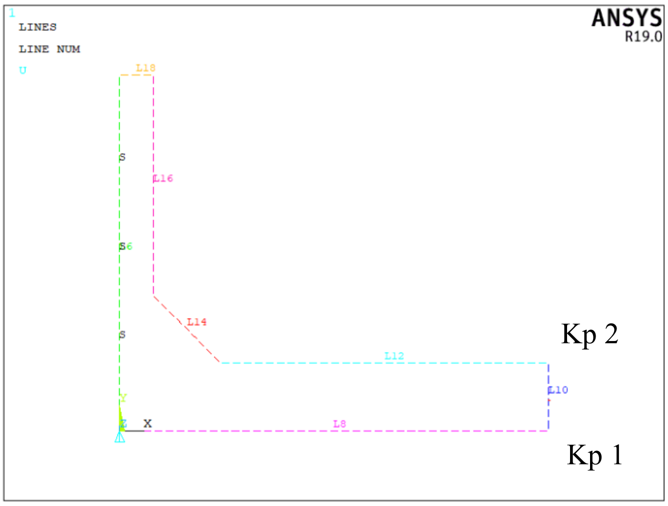

Figure 2. 10: loads and constraints to Gurney #4 joint. The letter S refers to a Symmetry BC, while the red arrow refers to the applied linear pressure.

2.2 Notch Stress Intensity Factor (NSIF) approach

According to the non-conventional linear elastic fracture mechanics extension to sharp V-notches, the V-notch region is characterised by a local non-linear stress concentration, caused by the structural geometry change and the weld profile itself; the intensity of the singular asymptotic stress field that follows is expressed by the notch stress intensity factors NSIFs under fracture modes I,II and III. From the knowledge of the NSIFs, it is possible to estimate the fatigue life of welded joints weakened by sharp V-notches.

From a preliminary analysis, the specimens are solicited under pure mode I: in fact, referring to William's eigenvalues graph in *Figure 1.11*, mode II is not singular ($\lambda_2 = 0$) for V-notch opening angles greater than 102.5°, in parallel with the fact that, due to the absence of out-of-plane shear stresses, mode III is also null.

In reference to *Figure 2.11*, the NSIF K_1 definition by Gross and Mendelson [13] is reported in equation (2.1):

$$K_1 \stackrel{\text{def}}{=} \sqrt{2\pi} \lim_{r \to 0} \left[\sigma_{\theta\theta_{r,\theta=0}} \cdot r^{1-\lambda_1} \right] \tag{2.1}$$

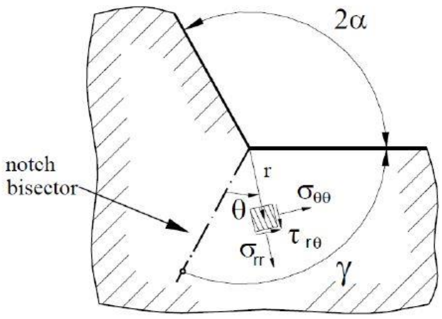

Figure 2. 11: local polar system of reference centred at the V-notch tip [15].

where:

- r is the radial distance from the V-notch tip;
- $\sigma_{\theta\theta_{r,\theta=0}}$ is the stress value for θ = 0° (i.e. along the V-notch bisector), r tending to 0 mm;
- λ_1 is the William's eigenvalue [16] and $1 - \lambda_1$ is the singularity grade of the local stress field, depending on the V-notch opening angle 2α.

Since for each dataset 2α = 135°, the corresponding eigenvalue λ_1 is equal to:

2α	**λ_1**
135°	*0.674*

2.2.1 NSIF K_1 analytical detection

Before proceeding, it is noted that the following work only refers to Maddox specimen #1; however, the procedure can be similarly extended to the other specimens.

In Ansys® APDL element library, Plane 182 element is chosen; the Key Option K1 is switched to *Simple Enhanced Strain*, while the Key Option K3 is set to *Plane Strain*.

Relying on formula (2.1), it is evident that a local stress distribution along the V-notch bisector is needed in order to obtain the NSIF K_1. Due to the non-linear stress increase at the V-notch area, the finite elements which has to "feel" the local stress must be very small (global size $\cong 10^{-5}$ mm). Thus, an appropriate mesh has to be laid on the model, paying close attention to the element size near the V-notch: in this regard, a smooth element transition towards the V-notch tip, without severe size jumps, is recommended.

To obtain an accurate mesh refinement, as well as a smooth transition, the following indications are considered:

1. Two circular areas, centred at the weld toe tip are created, with respective diameters $\Phi_1 = 0.0002\ mm$ and $\Phi_2 = 0.56\ mm$, as shown in *Figure 2.12*. The choice of the second diameter will be useful when dealing with the SED approach.

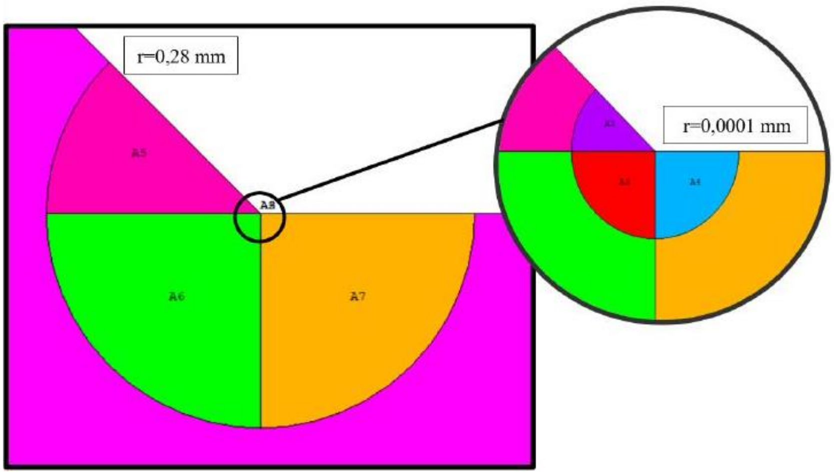

Figure 2. 12: two circular sectors centred at the weld toe tip.

2. Concerning the first circle meshing:
   a. The radial lines are divided in five parts, with a spacing ratio equal to 1;
   b. The 45° arc on the left is divided in four parts, with unitary spacing ratio;
   c. The 90° lower arcs are divided in 8 parts, with a spacing ratio equal to 1.
   d. A way to regularly guide the mesh consists in creating a concentration keypoint at the weld toe tip. The instructions in Ansys environment are shown below:

Meshing > SizeCNTRLS > ConcentratKPS > Create

Then, as options:

- *NPT*: the keypoint located at the tip is selected
- *DELR* = 0.00002
- *RRAT = 1.NTHET* = 4 (for 45° arc) or 8 (for 90° arc)

Finally, a free mesh algorithm is generated along the area under control.

3. Concerning the second circle meshing:
   a. The radial lines are divided in fifty parts, with a spacing ratio equal to 2000;
   b. The 45° arc on the left is divided in four parts, with unitary spacing ratio;
   c. The 90° lower arcs are divided in 8 parts, with a spacing ratio equal to 1;
   d. Finally, a mapped mesh is generated throughout the whole second circle.
4. For the remaining area, a free mesh algorithm is adopted, with global element size varying according to the welded joint into account.

At the end of this procedure, the mesh conformation should have an element length equal to 0.00005 mm at the weld toe, as displayed in *Figure 2.13*:

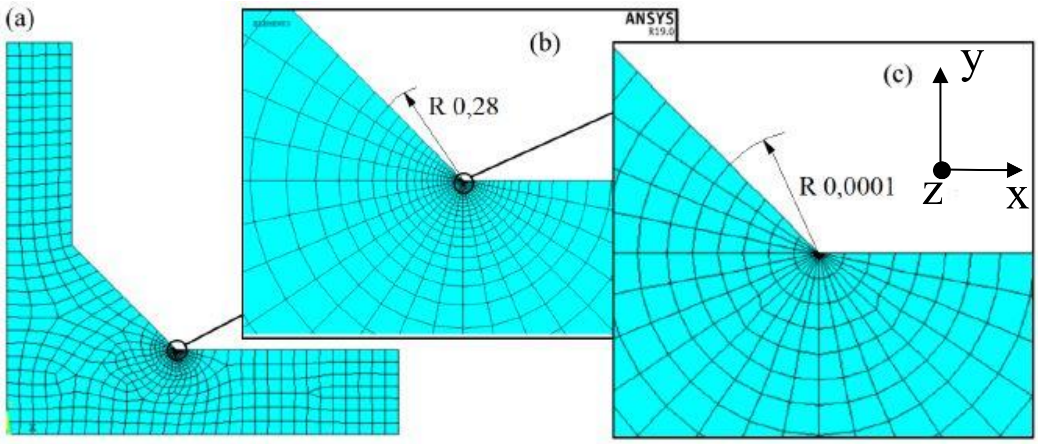

Figure 2. 13: mesh pattern for Maddox specimen #1. The gradually refined mesh reaches a size of 0.00005 mm at the V-notch tip. In black, the global coordinate system.

Once all the areas are meshed, the system can be solved:

Main Menu > Solution > Solve > Current LS

In order to plot the singular stress field along the V-notch bisector, a local X-Y-Z coordinate system, similar to the one illustrated in *Fig 2.11*, has to be defined with the following procedure:

1. The WorkPlane is displayed and offset to the keypoint at the weld toe:
   Utility Menu > Offset WorkPlane to > Keypoint
2. The WorkPlane is rotated by 112.5° clockwise about the out-of-plane global z-axis, according to the dispositions in *Figure 2.14*: the x-axis, being aligned with the V-notch bisector, replaces r in equation (2.1), while σ_{yy} replaces $\sigma_{\theta\theta_{r,\theta=0}}$.
   Utility Menu > Offset WP by Increments > Degrees

Figure 2. 14: work plane rotation by 112.5° clockwise about global z-axis.

3. The local coordinate system is now created in the WorkPlane origin:
   Utility Menu > Local Coordinate Systems > Create Local CS > At WP origin

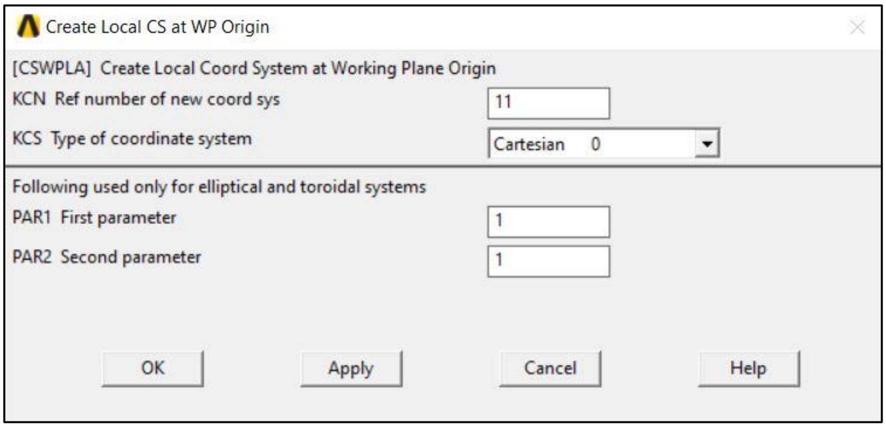

Figure 2. 15: Local Coordinate in the Work Plane origin. As KCN option, a number strictly higher than 10 must be chosen; thus, 11 is adopted.

4. The output results must be plotted in the new coordinate system. To do this:
   Main Menu > General Postproc > Options for Outp

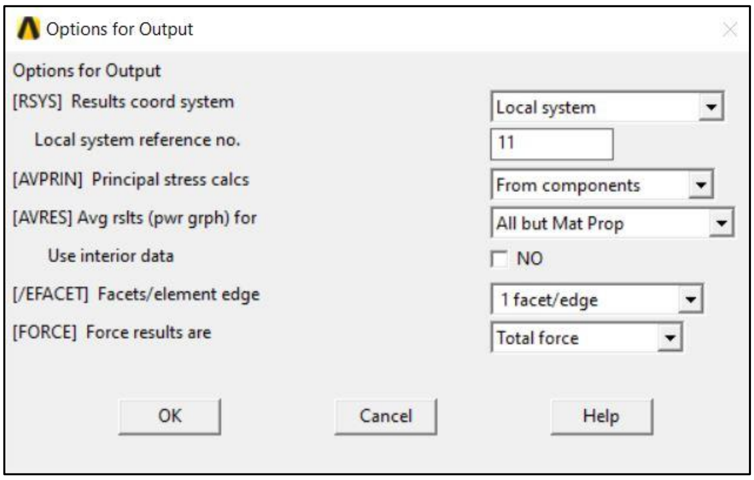

Figure 2. 16: Options for Output window.

5. The path is created by the selection of the nodes belonging to the V-notch bisector, as seen in *Figure 2.16*. The number of segment divisions (i.e. the spacing existing between two consecutive nodes) must be left to 1, in order to plot the nodal stress only:
   Main Menu > General Postproc > Path Operations > Define Path > By Nodes

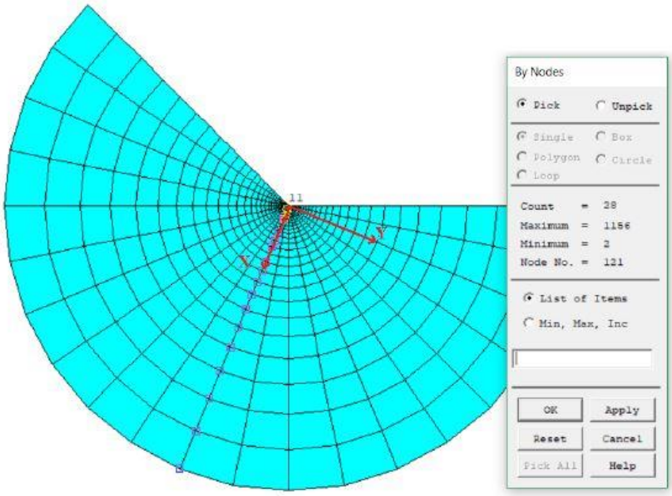

Figure 2. 16: nodes selection along the x-axis of the local system of reference, from x=0 to x=0.28 mm.

6. Both $\Delta\sigma_{yy}$ and x (respectively SY and S in Ansys®) are plotted along the local x-axis:
   Main Menu > General Postproc > Path Operations > Define Path > Map onto Path > S/SY

The found values are then exported in a double logarithmic $\Delta\sigma_{yy}$-x graph, displayed in *Figure 2.17*:

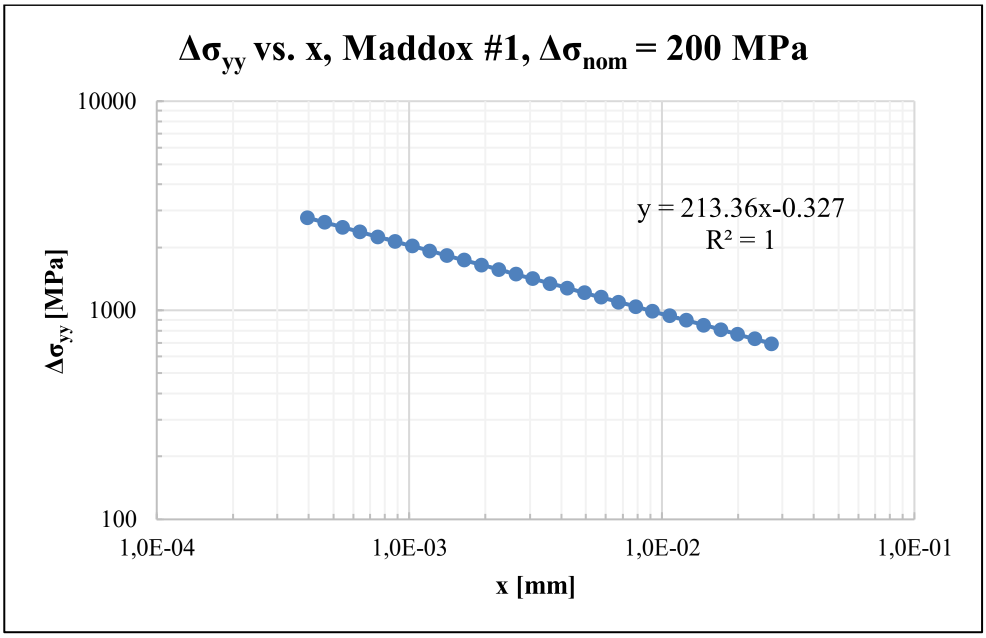

Figure 2. 17: singular stress field at weld toe, in case of 200 MPa nominal stress, Maddox #1. X is the distance from the weld toe tip along the local coordinate system.

For an external applied pressure $\Delta\sigma_{nom}$ = 200 MPa, the inverse slope of the asymptotic stress field k is equal to k=0.327, in good agreement with the theoretical k = 1-λ_1=0.326.

The K_1 is detected by averaging all the nodal K_1 values along the path. Relevant precautions concern the first K_1 nodal values, strongly depending on the mesh element size near the V-notch tip, which therefore must be excluded from the average; for the opposite reason, K_1 values too distant from the weld toe tip have to be excluded from the average. Hence, the K_1 average is performed in a range between $r = 3.95 \cdot 10^{-4}\ mm$ and $r = 2.73 \cdot 10^{-2}\ mm$, for a total of 28 nodal values. In each of these nodes, equation (2.1) is applied, to certify its constancy, graphically achieved in the K_1-x curve displayed in *Figure 2.18* for an external applied stress $\Delta\sigma_{nom}$ = 200 MPa:

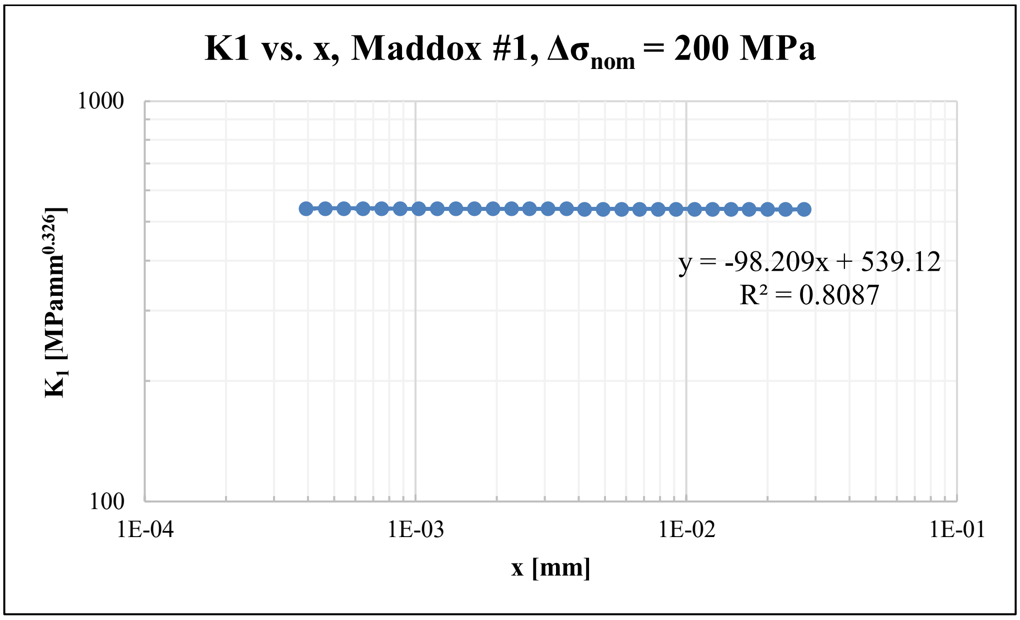

Figure 2. 18: K_1 constancy, in case of 200 MPa nominal stress, Maddox #1.

The analytical result of the NSIF K_1, given by (2.1), for an external applied nominal stress of 200 MPa, is equal to:

$$K_1 = 538.5\ MPamm^{0.326}$$

in good agreement with the line intercept, in *Figure 2.18*:

$$K_1 = 539.1\ MPamm^{0.326}$$

2.2.2 NSIF K_1 results

In linear elasticity hypothesis, the K_1 value resulting from different loading conditions can be found with expression (2.2):

$$K_{1,gen} = \frac{\Delta\sigma_{gen}}{\Delta\sigma_{ref}} \cdot K_{1,ref} \tag{2.2}$$

where:

- $K_{1,gen}$ is a generic K_1 that has to be detected;
- $\Delta\sigma_{gen}$ is the respective applied nominal stress;
- $K_{1,ref}$ is the reference NSIF already detected;
- $\Delta\sigma_{ref}$ is the reference nominal stress.

The re-elaborated results of each dataset are presented in terms of NSIF K_1.

#Specimen/load	$\Delta\sigma_{nom}$ [MPa]	K_1 [MPamm$^{0.326}$]	Nf [cycles]
Maddox #1 **Transverse NLC/axial**	200	538.5	192 000
	140	376.9	507 000
	100	269.2	2 937 000
	80	215.4	4 297 000
Gurney #2 **Transverse NLC/axial**	150	815.7	109 000
	120	652.5	224 000
	100	543.8	322 000
	65	353.5	1 153 000
	55	299.1	2 147 000
Gurney #3 **Transverse NLC/bending**	260	788.7	120 000
	220	667.4	200 000
	180	546.0	302 000
	140	424.7	744 000
	120	364.0	1 180 000
	110	333.7	2 158 000
Gurney #4 **T-joint/bending**	300	564.8	135 000
	260	489.5	237 000
	200	376.5	407 000
	190	357.7	573 000
	180	338.9	665 000
	160	301.2	1 525 000
	150	282.4	1 534 000
	140	263.6	2 601 000

Since the V-notch opening angle 2α=135° applies to each dataset, the corresponding grade of singularity of the stress field is the same; consequently, the comparison in terms of K_1 is allowed.

In *Figure 2.19*, the re-elaborated data are collected together in order to perform a statistical analysis; in agreement with the theory, the inverse slope is set to k=3.

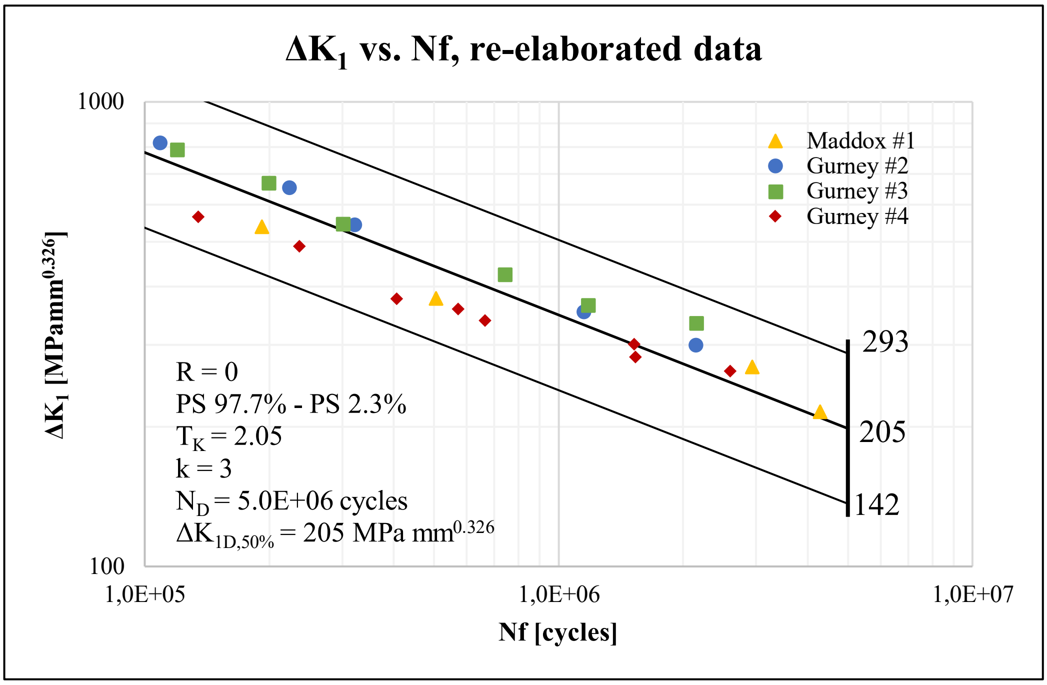

Figure 2. 19: fatigue strength in terms of NSIF K_1, re-elaborated data.

The experimental data are then entered inside the K_1 design curve proposed by Lazzarin and Tovo under prevailing mode I:

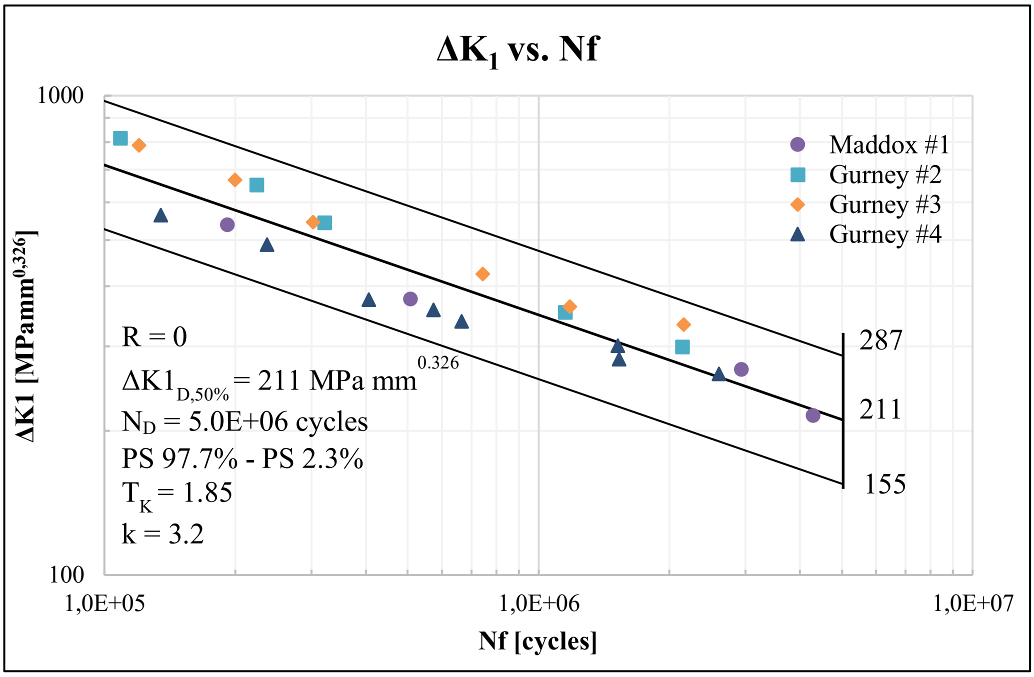

Figure 2. 20: data entry inside the K_1 design curve [5].

The following conclusions can be drawn:

1. The NSIFs approach has correctly foreseen the experimental crack initiation point at weld toe;
2. Since the totality of the experimental data fall above the PS 97.7% lines, the NSIF K_1 design curve has proven to be effective and conservative;
3. The theoretical scatter band amplitude T_K=1.85 is slightly lower than the re-elaborated T_K=2.05; this could be expected since in this work only 23 data have been employed.

2.3 Nominal stress approach

As Hobbacher affirms, the most common method for the fatigue assessment of welded joints is based on the nominal stress range, more particularly the maximum principal stress in the section where the crack is more likely to develop and propagate [1].

2.3.1 Nominal approach, results

The re-elaborated results of each dataset are presented in terms of maximum nominal stress calculated in the main plate of each joint category:

#Specimen/load	$\Delta\sigma_{nom}$ [MPa]	Nf [cycles]
Maddox #1 **Transverse NLC/axial**	200	192 000
	140	507 000
	100	2 937 000
	80	4 297 000
Gurney #2 **Transverse NLC/axial**	150	109 000
	120	224 000
	100	322 000
	65	1 153 000
	55	2 147 000
Gurney #3 **Transverse NLC/bending**	260	120 000
	220	200 000
	180	302 000
	140	744 000
	120	1 180 000
	110	2 158 000
Gurney #4 **T-joint/bending**	300	135 000
	260	237 000
	200	407 000
	190	573 000
	180	665 000
	160	1 525 000
	150	1 534 000
	140	2 601 000

In *Figure 2.21*, the re-elaborated data are collected together in order to perform a statistical analysis; in agreement with the theory, the inverse slope is set to k=3.

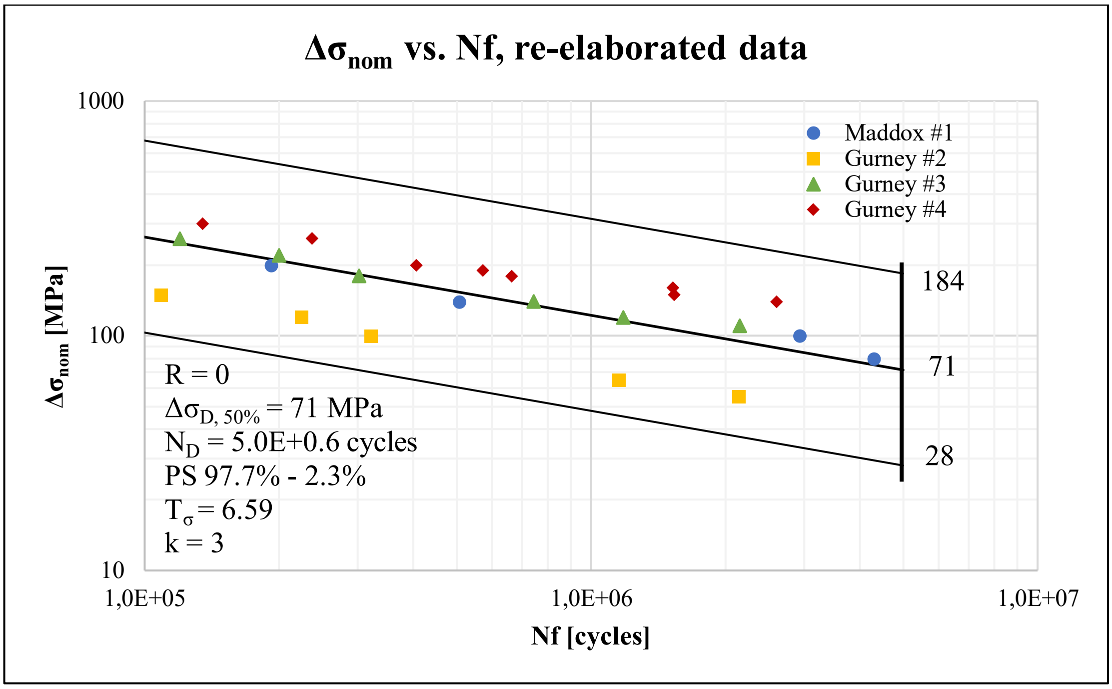

Figure 2. 21: fatigue strength in terms of nominal stress range, re-elaborated data.

Some observations can be drawn:

1. The scatter band amplitude $T_\sigma = 6.59$, is very large, due to the consistent data loss. This has to be expected since the fatigue strength of structural details is a local phenomenon which focuses on the crack development in the V-notch region;
2. In parallel with this, it can be demonstrated each singular dataset presents a slope k ranging between 2.9 and 3.73. Hence, this can contribute to the scatter band enlargement.

2.4 Strain Energy Density (SED) approach

As mentioned in Chapter 1, the SED approach, an energetic method introduced by Lazzarin and Zambardi in 2001 [6], deriving from Neuber's idea of the structural volume, ascribes as critical parameter for the fatigue strength of welded components the strain energy density (SED) value averaged over a circular sector of radius R_0 centred in the V-notch tip. R_0 is a material property, being equal to $R_0 = 0.28$ mm for steel structures and $R_0 = 0.12$ mm for aluminium alloys.

2.4.1 Modelling and meshing procedure

Before continuing, it is noted that the following instructions only refer to Maddox specimen #1; however, the procedure can be similarly extended to the other joints.

In Ansys® APDL element library, Plane 182 element is chosen; the Key Option K1 is switched to *Simple Enhanced Strain*, while the Key Option K3 is set to *Plane Strain*.

The first step consists in creating the circular sector of radius $R_0 = 0.28$ mm, centred in the V-notch tip, as illustrated in *Figure 2.23*:

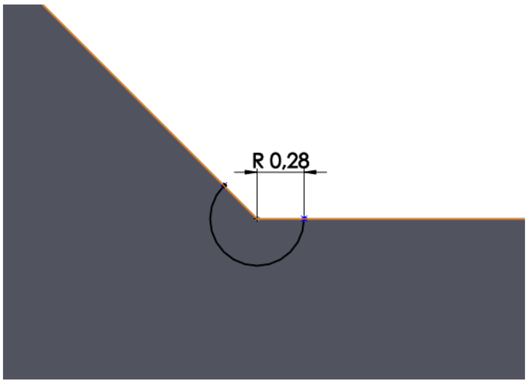

Figure 2. 23: modelling of the structural volume in Solidworks, Student Edition.

The meshing indications below are followed:

a) The element size of the lines of the structural volume is set to 0.06 mm:

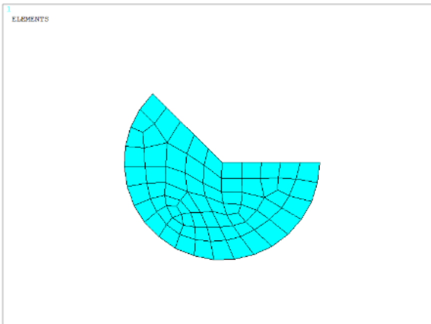

Figure 2. 24: element line size = 0.06 mm inside the circular sector, result.

b) The main plate and weld lines have a length of 0.05 mm, with a spacing ratio of 15, to guarantee a smooth element transition towards the circular sector. The resulting mesh conformation can be appreciated in *Figure 2.25*:

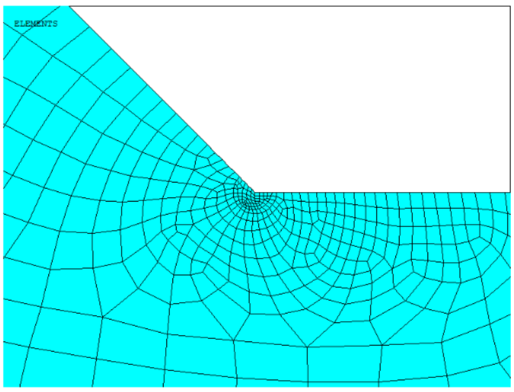

Figure 2. 25: smooth mesh transition towards the circular sector.

c) For the remaining area, a free mesh algorithm is adopted, with global element size proper to varying of the considered welded joint.

The system can now be solved:

Main Menu > Solution > Solve > Current LS

The averaged SED parameter is defined as the energy contained inside the structural volume. To obtain the average SED value, only the element belonging to the circular sector must be selected. In Ansys® APDL, the following commands have to be used:

Utility Menu > Select > Entities > Areas > From Full

Utility Menu > Select > Everything Below > Selected Areas

At this moment, a table containing both the energy (SENE) and volume (VOLU) of the selected elements has to be created:

Main Menu > General Postproc > Element Table

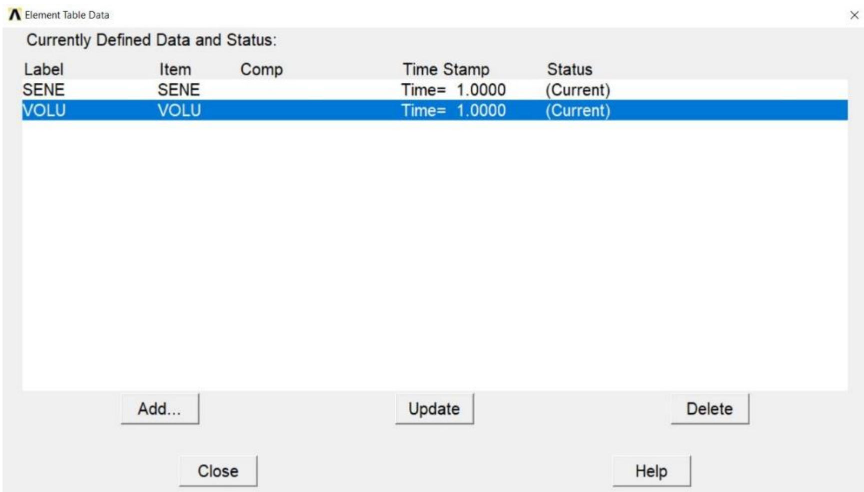

Figure 2. 36: element table in Ansys® APDL, where both SENE and VOLU are calculated.

Each single element SENE and VOLU values have now to be summed:

Main Menu > General Postproc > Element Table > Sum of Each Item

Finally, the SED value ($\Delta\overline{W}_{FEM}$ referring to FE software [33]) is calculated with equation (2.3) :

$$\overline{W}_{FEM} = \frac{\sum_{V(R_0)} W_{FEM,i}}{V(R_0)} = \frac{SENE}{VOLU} = \left[\frac{MJ}{m^3}\right] \tag{2.3}$$

For an external applied load equal to $\Delta\sigma_{nom}$ = 200 MPa, the resultant strain energy density is then equal to:

$$SENE = 5.72 \cdot 10^{-2}\, J$$

$$VOLU = 0.152844\, mm^3$$

$$SED = \frac{5.72 \cdot 10^{-2}}{0.152844} = 0.374\, \frac{MJ}{m^3}$$

If calculated with a FE software, the strain energy density does not necessarily require fine meshes [22]. To verify this, another simulation with different line size of the structural volume is performed:

a) The element size of the lines of the structural volume is set to 0.04 mm:

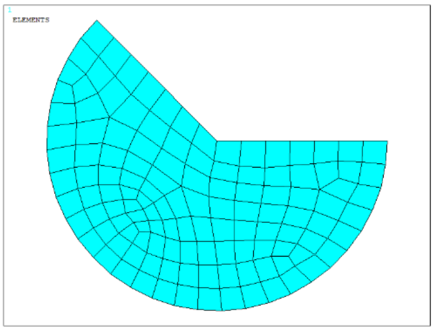

Figure 2. 27: average element size = 0.04 mm inside the circular sector.

b) The main plate and weld lines have a length of 0.04 mm, with a spacing ratio of 15, to guarantee a smooth element transition towards the circular sector;
c) For the remaining area, a free mesh algorithm is adopted, with global element size proper to varying of the considered welded joint.

For an external applied load equal to $\Delta\sigma_{nom}$ = 200 MPa, the resultant strain energy density calculated with (2.3) gives:

$$SENE = 5.70 \cdot 10^{-2}\, J$$

$$VOLU = 0.153434\, mm^3$$

$$SED = \frac{5.70 \cdot 10^{-2}}{0.153434} = 0.372\, \frac{MJ}{m^3}$$

which is in good agreement with the previous found value.

```
SUM ALL THE ACTIVE ENTRIES IN THE ELEMENT TABLE

TABLE LABEL     TOTAL
SENE        0.570268E-01
VOLU        0.153434
```

```
SUM ALL THE ACTIVE ENTRIES IN THE ELEMENT TABLE

TABLE LABEL     TOTAL
SENE        0.572008E-01
VOLU        0.152844
```

Figure 2. 28: SENE and VOLU values respectively for 0.006 mm and 0.004 mm meshes inside the circular sector.

2.4.2 SED, results

In linear elasticity hypothesis, the SED value resulting from different external loads can be found with equation (2.4):

$$SED_{gen} = \left(\frac{\Delta\sigma_{gen}}{\Delta\sigma_{ref}}\right)^2 \cdot SED_{ref} \tag{2.4}$$

where:

- SED_{gen} is a generic SED that has to be detected;
- $\Delta\sigma_{gen}$ is the nominal stress related to the generic SED;
- SED_{ref} is the reference strain energy density;
- $\Delta\sigma_{ref}$ is the reference nominal stress.

The experimental fatigue life results of each dataset are presented in terms of SED. It should be noted that since the unity of measurement is the same, i.e. energy, the method allows the comparison among fractures occurring at V-notch with different opening angles, for instance weld toes and roots.

#Specimen/load	$\Delta\sigma_{nom}$ [MPa]	SED [MJ/m^3]	Nf [cycles]
Maddox #1 **Transverse NLC/axial**	200	0.37	192 000
	140	0.18	507 000
	100	0.09	2 937 000
	80	0.06	4 297 000
Gurney #2 **Transverse NLC/axial**	150	0.86	109 000
	120	0.55	224 000
	100	0.38	322 000
	65	0.16	1 153 000
	55	0.11	2 147 000
Gurney #3 **Transverse NLC/bending**	260	0.80	120 000
	220	0.57	200 000
	180	0.38	302 000
	140	0.23	744 000
	120	0.17	1 180 000
	110	0.14	2 158 000
Gurney #4 **T-joint/bending**	300	0.41	135 000
	260	0.31	237 000
	200	0.18	407 000
	190	0.16	573 000
	180	0.15	665 000
	160	0.12	1 525 000
	150	0.10	1 534 000
	140	0.09	2 601 000

In *Figure 2.29*, the re-elaborated data are collected together in order to perform a statistical analysis; in agreement with the theory, the inverse slope is set to k=1.5.

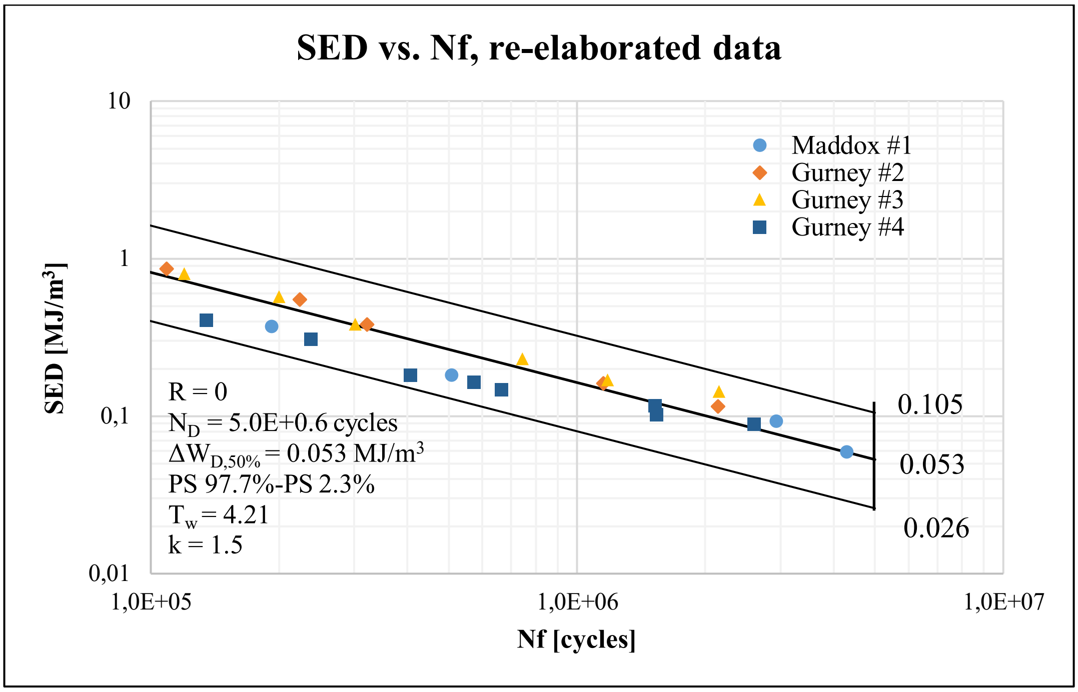

Figure 2. 29: fatigue strength in terms of SED, re-elaborated data.

The experimental data, are then entered inside the SED design curve proposed by Lazzarin and Zambardi:

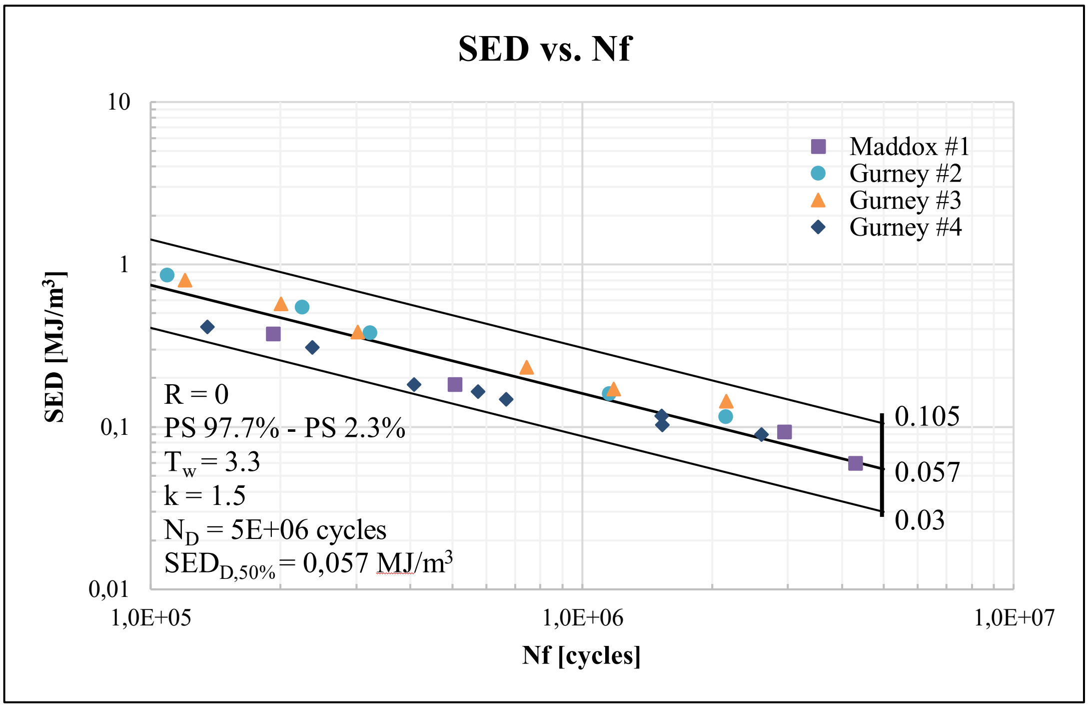

Figure 2. 30: data entry inside the SED design curve [6].

The following conclusions can be drawn:

1. The SED approach has correctly foreseen the experimental crack initiation point at weld toe;
2. Since the totality of the experimental data fall above the PS 97.7% lines, the SED design curve has proven to be effective and conservative;
3. The theoretical scatter band amplitude T_W=3.3 is lower than the re-elaborated T_W=4.45; this could be expected since in this work only 23 data have been employed against the 900 experimental data available to Lazzarin and Zambardi.

2.5 Peak Stress Method (PSM) approach

The analytical detection of notch stress intensity factors demonstrates a major drawback in engineering applications, due to the very refined (size = 10^{-5} mm) FE meshes demanded towards the V-notch tip [18], making both the modelling and simulation very onerous and time consuming.

The Peak Stress Method aims to overcome this problem by proposing a user-friendly FE method to rapidly obtain the NSIFs at singular sharp V-notches. Two PSM advantages are worth to be reminded:

- FE analyses require coarse meshes, with respect to the ones necessary for the analytical NSIFs calculation;
- Only the nodal stress at the V-notch tip is required to detect the NSIFs, instead of a number of *stress-distance* values.

Previously mentioned in Chapter 1, the estimated NSIFs under mode I,II and III are reported in equations (2.5)-(2.7):

$$K_1 \cong K^*_{FE} \cdot \sigma_{\theta\theta,\theta=0,peak} \cdot d^{1-\lambda_1} \tag{2.5}$$

$$K_2 \cong K^{**}_{FE} \cdot \tau_{r\theta,\theta=0,peak} \cdot d^{1-\lambda_2} \tag{2.6}$$

$$K_3 \cong K^{***}_{FE} \cdot \tau_{\theta z,\theta=0,peak} \cdot d^{1-\lambda_3} \tag{2.7}$$

where:

- K^*_{FE}, K^{**}_{FE}, K^{***}_{FE} are the PSM calibration constants related to mode I,II, III which depend on the element type, the element formulation, the adopted mesh pattern and the nodal stress evaluation procedure;

- $\sigma_{\theta\theta,\theta=0,peak}$, $\tau_{r\theta,\theta=0,peak}$, $\tau_{\theta z,\theta=0,peak}$ are the peak nodal stresses evaluated at the V-notch profile, with respect to a local coordinate system such as the one illustrated in *Figure 2.31*;

- d is the mesh global element size;

- λ_1, λ_2, λ_3 are William's eigenvalues [16], functions of the V-notch opening angle 2α.

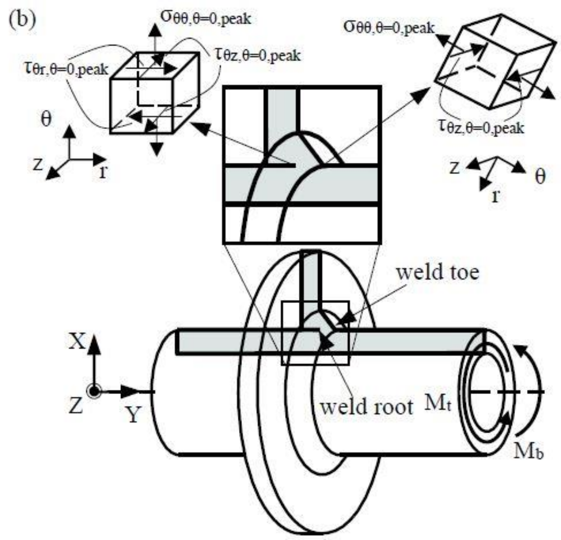

Figure 2. 31: definition of the nodal stresses at the V-notch [18].

The equivalent peak stress occurring in the singular tip is found with equation (2.8):

$$\sigma_{eq,peak} = \sqrt{f_{w1}^2 \cdot \sigma_{\theta,\theta=0,peak}^2 + f_{w2}^2 \cdot \tau_{r\theta,\theta=0,peak}^2 + f_{w3}^2 \cdot \tau_{\theta z,\theta=0,peak}^2} \tag{2.8}$$

where:

- $\sigma_{\theta\theta,\theta=0,peak}$, $\tau_{r\theta,\theta=0,peak}$, $\tau_{\theta z,\theta=0,peak}$ are the abovementioned nodal peak stresses;
- $f_{wi,i=1,2,3}$ are the peak stress corrective factors, assuming the expression (1.16):

$$f_{wi} = K_{FE}^{j} \cdot \sqrt{\frac{2e_i}{1-\nu^2}} \cdot \left(\frac{d}{R_0}\right)^{1-\lambda_i} \Bigg|_{\substack{i=1,2,3 \\ j=*,**,***}} \tag{2.9}$$

2.5.1 Modelling and meshing procedure

Before continuing, it is noted that the following instructions refer to Maddox specimen #1; however, the procedure can be similarly extended to the other specimens.

In Ansys® APDL element library, Plane 182 element is chosen; the Key Option K1 is switched to *Simple Enhanced Strain*, while the Key Option K3 is set to *Plane Strain*.

As previously affirmed, the weld toes are exclusively under mode I loading. Under mode I, the PSM requirements are listed in the table below:

		Mode I			
Element Type	**Mesh algorithm**	**$(a/d)_{min}$**	**2α**	**Mesh pattern 2α < 90°**	**Mesh pattern 2α > 90°**
Plane 182 *Kos: Simple Enhanced Strain + Plane Strain*	Free	3	0° < 2α < 135°	Four adjacent elements share the same node	Two adjacent elements share the same node

Under these restrictions, the mode I PSM calibration constant is equal to $K^*_{FE} = 1.38 \pm 3\%$.

The following PSM dispositions are thus adopted:

- Half joint main plate thickness a is equal to a = 13/2 = 6.5 mm;
- The mesh global element size is set to d = 1 mm;
- $\frac{a}{d} = \frac{6.5}{1} = 6.5 > 3$ the ratio is respected;
- The λ_1 and e_1 values associated to the weld toe (2α=135°) and required for f_{w1} detection are:

2α	λ_1	e_1
135°	*0.674*	*0.118*

Finally, the corrective stress factor calculated with equation (2.9) is f_{w1} = 1.064. The resulting mesh pattern can be appreciated in *Figure 2.32*:

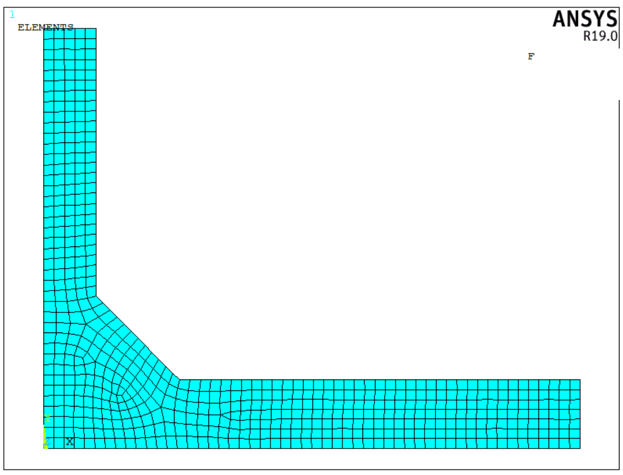

Figure 2. 32: mesh conformation required by PSM, d=1 mm.

After the geometry is loaded and constrained according to the indications in paragraph 2.1.1, the structure is then solved:

Main Menu > Solution > Solve > Current LS

The resulting first principal stress is plotted along the specimen:

Main Menu > General Postproc > Plot Results > Contour Plot > Nodal Solution > Stress

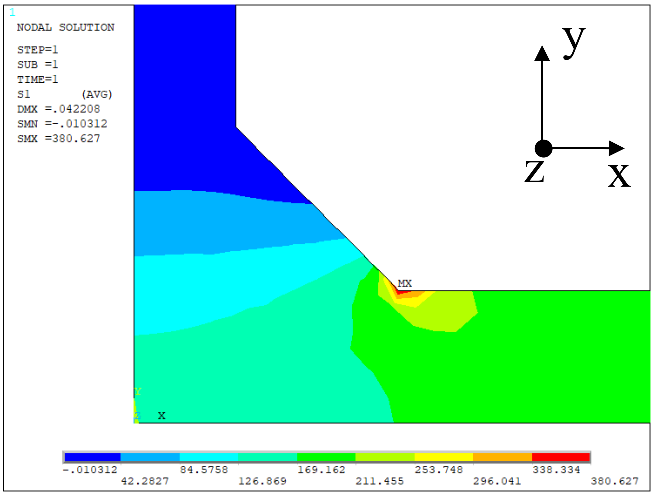

Figure 2. 33: plot of the first principal stress in Maddox #1, for an external applied nominal stress range of 200 MPa. In black, the global coordinate system.

In reference to *Figure 2.33*, the peak stress $\Delta\sigma_{\theta\theta,\theta=0,peak}$ has to be evaluated in the most solicited point of the structure, i.e. the weld toe tip. A rigorous procedure for the $\Delta\sigma_{\theta\theta,\theta=0,peak}$ detection should include the creation of a local coordinate system similar to the one adopted for the analytical K_1 detection. However, it can be demonstrated that, for 2D structures under pure mode I loading, the first principal stress $\Delta\sigma_{11}$ at the weld toe can be confused with the $\Delta\sigma_{yy}$ otherwise evaluated with the local coordinate system. To speed up the plotting procedure, the first principal stress is then used instead of $\Delta\sigma_{yy}$.

For an external applied pressure $\Delta\sigma_{nom}$=200 MPa, the maximum $\Delta\sigma_{11}$ located at the weld toe tip is equal to:

$$\Delta\sigma_{11} = \Delta\sigma_{\theta\theta,\theta=0,peak} = 380.6\ MPa$$

Once the peak stress is given, both K_1 and $\Delta\sigma_{eq,peak}$ can be respectively found with formulae (2.5) and (2.8):

$$\Delta K_1 \cong K_{FE}^{*} \cdot \Delta\sigma_{\theta\theta,\theta=0,peak} \cdot d^{1-\lambda_1} = 1.38 \cdot 380.63 \cdot 1^{1-0.674} = 525.5\ MPamm^{0.326}$$

$$\Delta\sigma_{eq,peak} = \Delta\sigma_{\theta\theta,\theta=0,peak} \cdot f_{w1} = 380.6 \cdot 1.064 = 407.3\ MPa$$

In linear elasticity hypothesis, $\Delta\sigma_{eq,peak}$ values for different external loading conditions can be found with expression (2.10):

$$\Delta\sigma_{eq,peak,gen} = \frac{\Delta\sigma_{gen}}{\Delta\sigma_{ref}} \cdot \Delta\sigma_{eq,peak,ref} \tag{2.10}$$

where:

- $\Delta\sigma_{eq,peak,gen}$ is a generic equivalent peak stress that has to be detected;
- $\Delta\sigma_{gen}$ is the nominal stress related to the generic equivalent peak stress;
- $\Delta\sigma_{eq,peak,ref}$ is the reference equivalent peak stress;
- $\Delta\sigma_{ref}$ is the reference nominal stress.

2.5.2 PSM, results

The experimental fatigue life results of each dataset are presented in terms of $\Delta\sigma_{eq,peak}$ as well as of K_1. Furthermore, the $\frac{a}{d}$ ratio adopted for each geometry is indicated. It should be noted that since the unity of measurement is the same, i.e. stress, the method allows the comparison among fractures occurring at V-notch with different opening angles, for instance weld toes and roots.

#Specimen/load/ratio	$\Delta\sigma_{nom}$ [MPa]	$\Delta\sigma_{eq,peak}$ [MPa]	K_1 [MPamm$^{0.326}$]	Nf [cycles]
Maddox #1 **Transverse NLC/axial** $\frac{a}{d} = 6.5$	200	407.3	528.3	192 000
	140	285.1	369.7	507 000
	100	203.6	264.1	2 937 000
	80	162.9	211.3	4 297 000
Gurney #2 **Transverse NLC/axial** $\frac{a}{d} = 50$	150	614.3	796.5	109 000
	120	491.4	637.2	224 000
	100	409.5	531.0	322 000
	65	266.2	345.2	1 153 000
	55	225.2	292.1	2 147 000
Gurney #3 **Transverse NLC/bending** $\frac{a}{d} = 50$	260	593.1	769.1	120 000
	220	501.9	650.8	200 000
	180	410.6	532.4	302 000
	140	319.4	414.1	744 000
	120	273.7	355.0	1 180 000
	110	250.9	325.4	2 158 000
Gurney #4 **T-joint/bending** $\frac{a}{d} = 3$	300	439.7	570.2	135 000
	260	381.1	494.2	237 000
	200	293.2	380.1	407 000
	190	278.5	361.1	573 000
	180	263.8	342.1	665 000
	160	234.5	304.1	1 525 000
	150	219.9	285.1	1 534 000
	140	205.2	266.1	2 601 000

In *Figure 2.34*, the re-elaborated data are collected together in order to perform a statistical analysis; in agreement with the theory, the inverse slope is set to k=3.

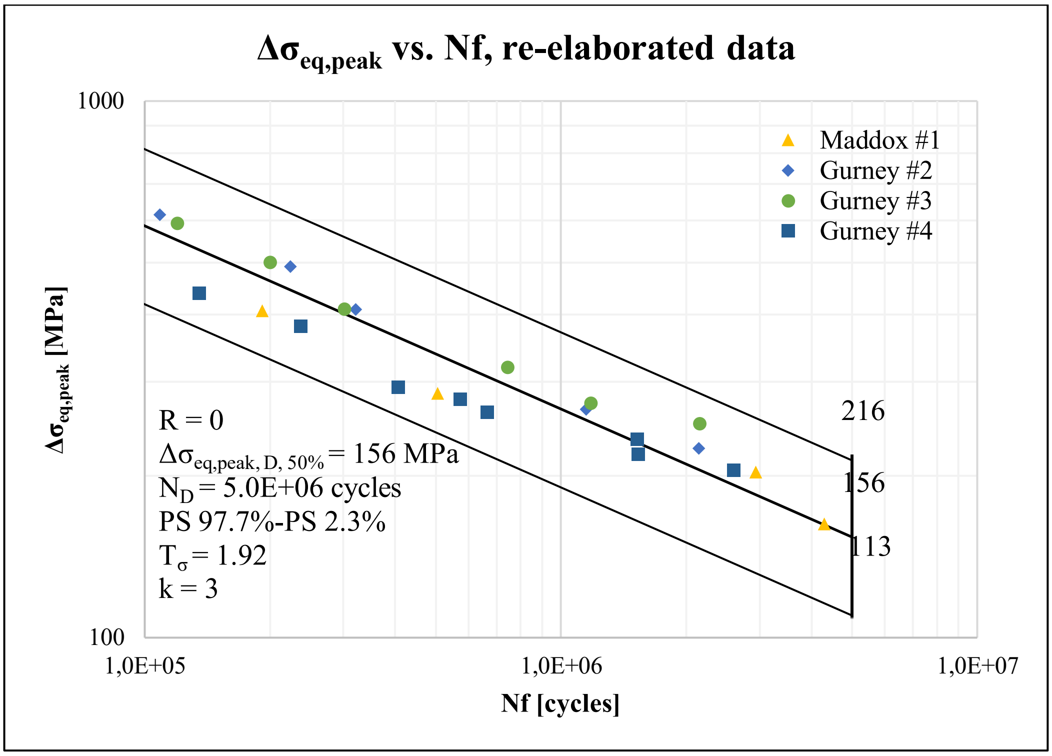

Figure 2. 34: fatigue strength in terms of $\Delta\sigma_{eq,peak}$, re-elaborated data.

The experimental data are then entered inside the $\Delta\sigma_{eq,peak}$ design curve proposed by Meneghetti and Lazzarin under prevailing mode I:

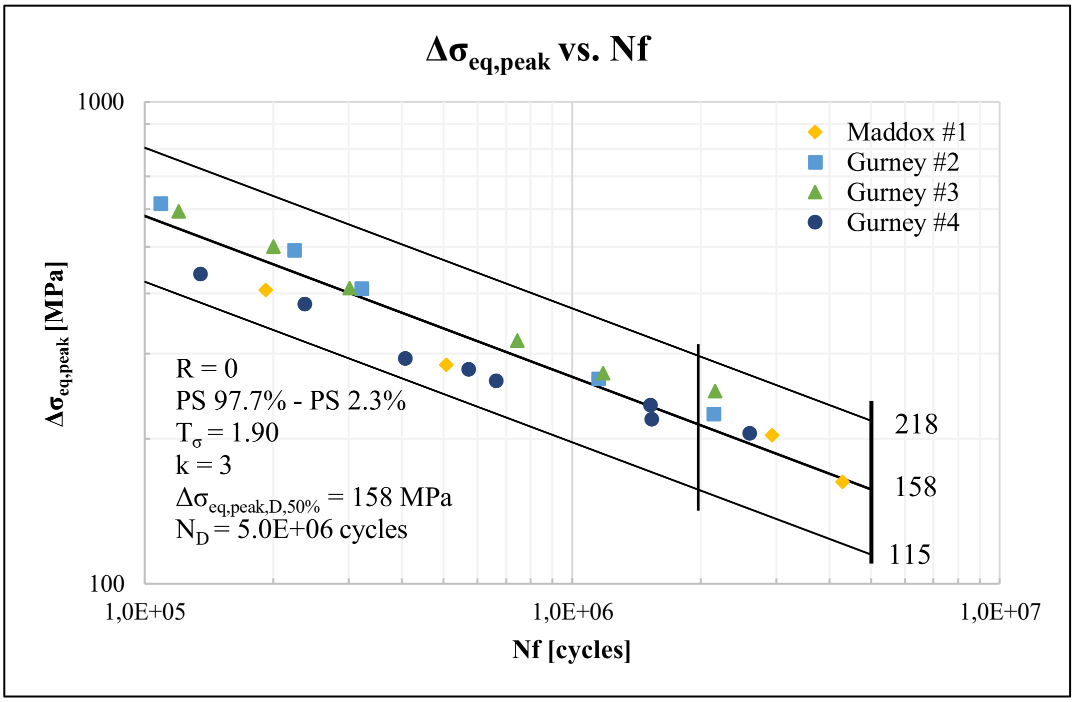

Figure 2. 35: data entry inside the PSM design curve [7].

The following conclusions can be drawn:

1. The PSM approach has correctly foreseen the experimental crack initiation point at weld toe;
2. Since the totality of the experimental data fall above the PS 97.7% line, the PSM design curve has proven to be effective and conservative;
3. The theoretical scatter band amplitude T_σ=1.90 is, engineering speaking, equal to the re-elaborated T_σ=1.92.

2.5.3 Analytical and PSM-esteemed K_1 comparison

One of the advantages of the PSM resides in the rapid estimation of the NSIFs. In this regard, a comparison between the PSM-esteemed and the analytical K_1 values is performed:

#Specimen/load	$K_{1,\,PSM}$ [MPamm$^{0.326}$]	$K_{1,\,analytical}$ [MPamm$^{0.326}$]	Rel error [%]
Maddox #1 **Transverse NLC/axial**	528.3	538.5	≅ 1.90%
	369.7	376.9	
	264.1	269.2	
	211.3	215.4	
Gurney #2 **Transverse NLC/axial**	796.5	815.7	≅ 2.36%
	637.2	652.5	
	531.0	543.8	
	345.2	353.5	
	292.1	299.1	
Gurney #3 **Transverse NLC/bending**	769.1	788.7	≅ 2.55%
	650.8	667.4	
	532.4	546.0	
	414.1	424.7	
	355.0	364.0	
	325.4	333.7	
Gurney #4 **T-joint/bending**	570.2	564.8	≅ 0.96%
	494.2	489.5	
	380.1	376.5	
	361.1	357.7	
	342.1	338.9	
	304.1	301.2	
	285.1	282.4	
	266.1	263.6	

In agreement with the theory, the totality of the relative errors falls below ±3%.

2.5.4 Convergence of $\Delta\sigma_{eq,peak}$ for various mesh sizes

Another advantage of the PSM is that, in respect of the $\frac{a}{d}$ ratio, convergence of $\Delta\sigma_{eq,peak}$ (and K_1) values with different mesh sizes can be achieved inside an $\pm 3\%$ error band. To assert this, a new assessment with a different $\frac{a}{d}$ ratio is performed for all the datasets, for a given external $\Delta\sigma_{nom}$.

#Specimen/load	$\Delta\sigma_{nom}$ [MPa]	$\Delta\sigma_{eq,peak,sim\#1}$ [MPa]	$\Delta\sigma_{eq,peak,sim\#2}$ [MPa]	Rel error [%]
Maddox #1 **Transverse NLC/axial**	200	407.3 $\left(\frac{a}{d}=6.5\right)$	413.2 $\left(\frac{a}{d}=3.25\right)$	≅ 1.41 %
Gurney #2 **Transverse NLC/axial**	150	614.3 $\left(\frac{a}{d}=50\right)$	624.7 $\left(\frac{a}{d}=5\right)$	≅ 1.70 %
Gurney #3 **Transverse NLC/bending**	260	593.1 $\left(\frac{a}{d}=50\right)$	596.7 $\left(\frac{a}{d}=17\right)$	≅ 0.61 %
Gurney #4 **T-joint/bending**	300	439.7 $\left(\frac{a}{d}=3\right)$	428.0 $\left(\frac{a}{d}=6\right)$	≅ 2.66 %

2.6 Square chord with circular brace joint (Gandhi)

The fifth investigated typology of welded joint in this Chapter is a tube-to-beam structure, tested by Gandhi in 1998 [32] under constant amplitude loading CAL. More precisely, the model consists in a circular hollow section tube (CHS) welded on top of a rectangular hollow section double cantilever beam (SHS).

Specific information on the component is reported below:

Weld condition	Fracture location	Load application
As-welded, non-load carrying, full penetration	*Weld toe, SHS and CHS sides, depending on the geometry*	*Axial, main plate, parent material*

The material properties are typical of structural steel:

Material model	Yield strength f_y	Young modulus	Poisson's ratio ν
API2H, linear elastic, isotropic	*355 MPa*	*206000 MPa*	*0.3*

In regard of the main geometrical quantities, *Figure 2.36* shows the most relevant information:

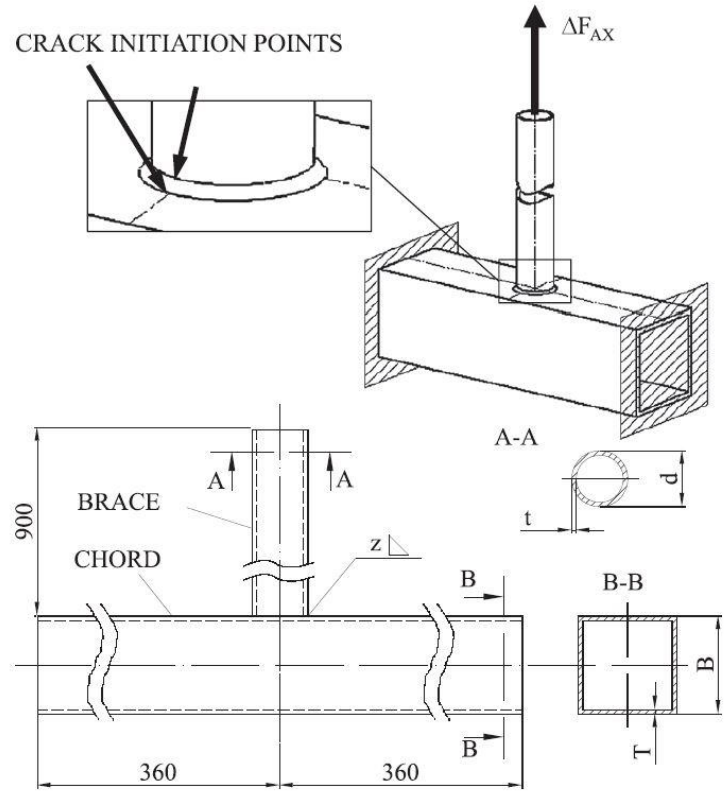

Figure 2. 36: Gandhi, geometry. The quotes are expressed in [mm] [32].

N°	*B* (mm)	*T* (mm)	*d* (mm)	*t* (mm)	*z* (mm)
1	200	10	51	6.3	6.3
2	200	10	82.5	6.3	6.3
3	200	10	159	6.3	6.3
4	200	10	76	4.5	4.5
5	200	10	82.5	8.8	8.8
6	300	12.5	127	8	8
7	200	6.3	88.9	4	4

Figure 2. 37: Gandhi, seven different geometries for the same specimen [32].

The weld profile parameters, related to geometry N° 1 in *Figure 2.37*, are described in the table below:

ρ weld toe tip [mm]	Weld leg [mm]	Weld flank angle	2α
≅ 0	*6.3*	*45°*	*SHS: 135°* *CHS: 135°*

The experimental data related to geometry N°1 is reported in terms of nominal stress $\Delta\sigma_{nom}$; two different fatigue lives N_f are defined:

R	**$\Delta\sigma_{nom}$ [MPa]**	**Nf [cycles]**
-0.36	*33.22*	*552 000 (complete fracture)* *350 000 (through-the-thickness crack)*

The FE model is created inside Ansys® CAD environment; the reference APDL commands are available in Appendix A.

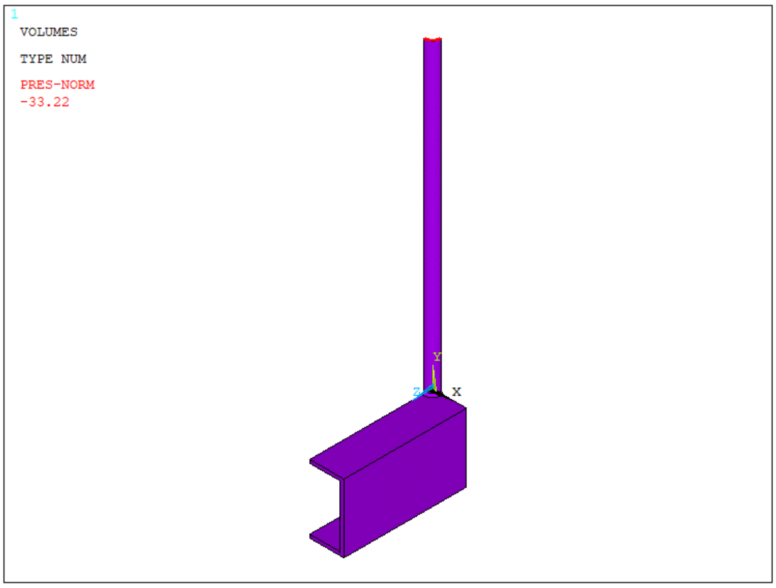

Figure 2. 38: Gandhi, geometry N°1, FE model.

Inside Ansys® environment, the modelling procedure is briefly described and shown in *Fig 2.38*:

- Symmetries: due to the double symmetry of the structure, only ¼ of the geometry is modelled, allowing to consistently speed up the computational process;
- Loading: the structure is axially loaded on the CHS top sectional area, and the load is applied as a red constant pressure equal to $p = -\Delta\sigma_{nom}$;
- Constraints: symmetry boundary conditions are applied along the light blue-highlighted areas; moreover, to represent the double cantilever SHS beam, all the displacements in the external C-shaped sectional area are constrained ($u_x = u_y = u_z = 0$).

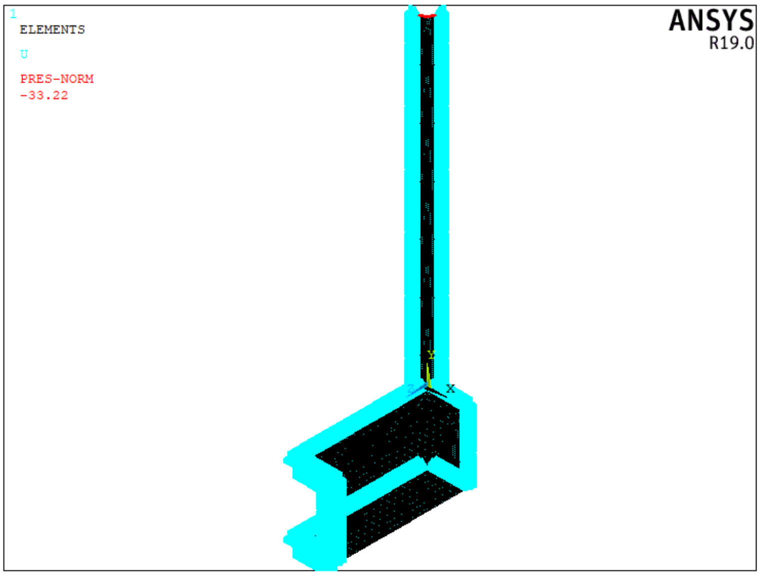

Figure 2. 40: Gandhi, geometry N°1, symmetry B.C on areas + constant pressure.

2.6.1 PSM, eight-node linear element (Brick 185)

The fatigue assessment is now performed in terms equivalent peak stress with the adoption of the Peak Stress Method for 3D structures, eight-node linear elements. As learned from Chapter 1, the submodelling technique is requested.

<u>Main model</u>

In Ansys® APDL element library, Tetra 187 element is chosen; the Key-option K1 left to *Pure displacement*, which means that the nodal forces are only dependent from the displacements.

The main model of the structure is illustrated in *Figure 3.4*. The cut boundary is determined with a stress convergence verification: three different meshes, with global element size respectively equal to 4, 5 and 8 mm, are laid on the main model.

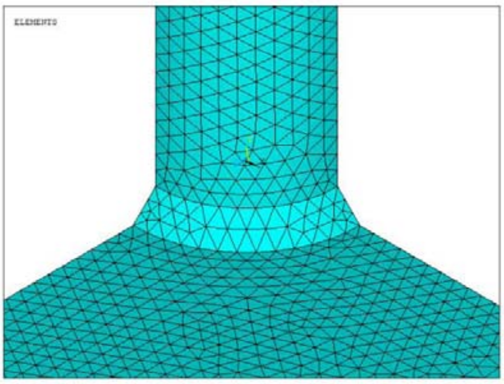

Figure 2.41: example of mesh with global element size 5 mm.

The first principal stress range $\Delta\sigma_{11}$ is then extracted along the z axis, starting from the weld toe tip, SHS side, as illustrated in *Figure 2.42*:

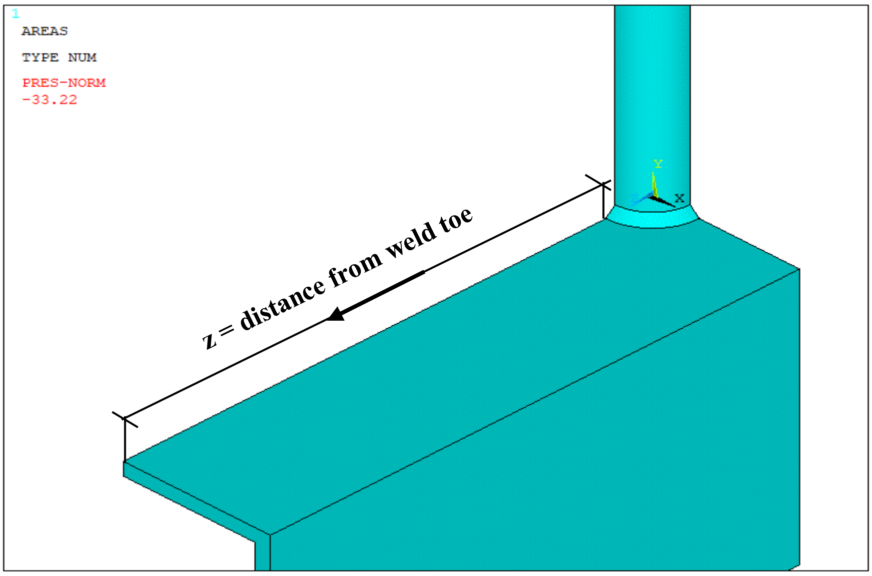

Figure 2. 42: path along which $\Delta\sigma_{11}$ is extracted.

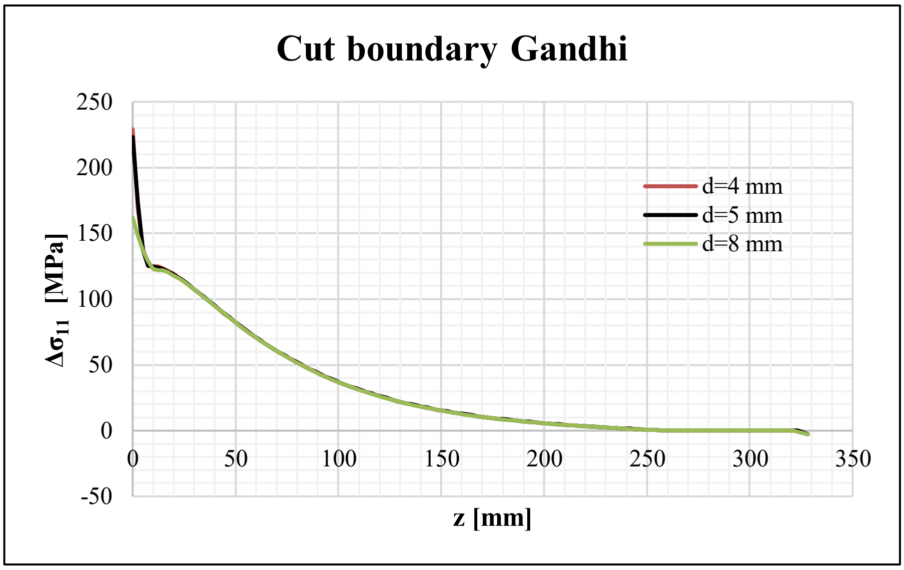

Figure 2. 43: convergence analysis for the cut boundary creation.

As it can be noticed in *Figure 2.43*, the local stresses cannot converge because the stress value is function of the element size. At x = 18.5 mm, compatibility between the results is clearly achieved, therefore the cut boundary is placed at that distance of 18.5 mm from the weld toe, SHS side.

<u>Submodel</u>

In Ansys® APDL element library, the adopted eight-node linear element is named Brick 185, with Key Option K1 switched to *Simple Enhanced Strain*.

When employing the submodelling technique, the submodel system of reference has to coincide with that of the main model, since the boundary conditions which are applied to the submodel are interpolated in the cut boundary coordinates with respect to the main model frame of reference.

From a preliminary analysis it can be inferred that mode I is prevailing at the weld toe, mode II is null since 2α > 102.5°, while mode III can be neglected; equation (2.5) is then employed.

Under mode I loading, the PSM Brick 185 requirements are listed below:

				Mode I	
Element Type	**Mesh algorithm**	**$(a/d)_{min}$**	**2α**	**Mesh pattern 2α < 90°**	**Mesh pattern 2α > 90°**
Brick 185 *KO: Simple Enhanced Strain*	Mapped	3	0° < 2α < 135°	Four adjacent elements share the same node	Two adjacent elements share the same node

Under these restrictions, the mode I PSM calibration constant is equal to $K_{FE}^{*} = 1.38 \pm 3\%$.

The following PSM dispositions are thus adopted:

- The SHS thickness a is equal to a = 10 mm;
- The mesh global element size is set to d = 1 mm;
- $\frac{a}{d} = \frac{10}{1} = 10 > 3$ the ratio is respected;
- The λ_1 and e_1 values associated to the weld toe, CHS and SHS sides (2α = 135°), required for the f_{w1} detection are:

2α	**λ_1**	**e_1**
135°	*0.674*	*0.118*

Finally, the corrective stress factor calculated with equation (2.9) is f_{w1} = 1.064.

One technique for the submodel creation consists in the revolution by 90° about the global y-axis, of the sectional area visible in *Figure 2.44*, on the right, which was pre-meshed before in respect of the PSM requirements. The number of extruded elements must be chosen so that to have cubic elements. To obtain a proper extrusion inside Ansys® APDL Preprocessor, the following commands are used:

Main Menu > Preprocessor > Modelling > Operate > Extrude > Elem Ext Opts

As Element type number, Brick 185 is selected; since the mesh size is d=1 mm, fifty element extrusion divisions bring to cubic elements. Finally, the area is extruded:

Main Menu > Preprocessor > Modelling > Operate > Extrude > Areas > About Axis

Once the volume is created, the mesh of the extruded area must be cleared, otherwise the constraints are going to be applied to nodes non-belonging to the FE model.

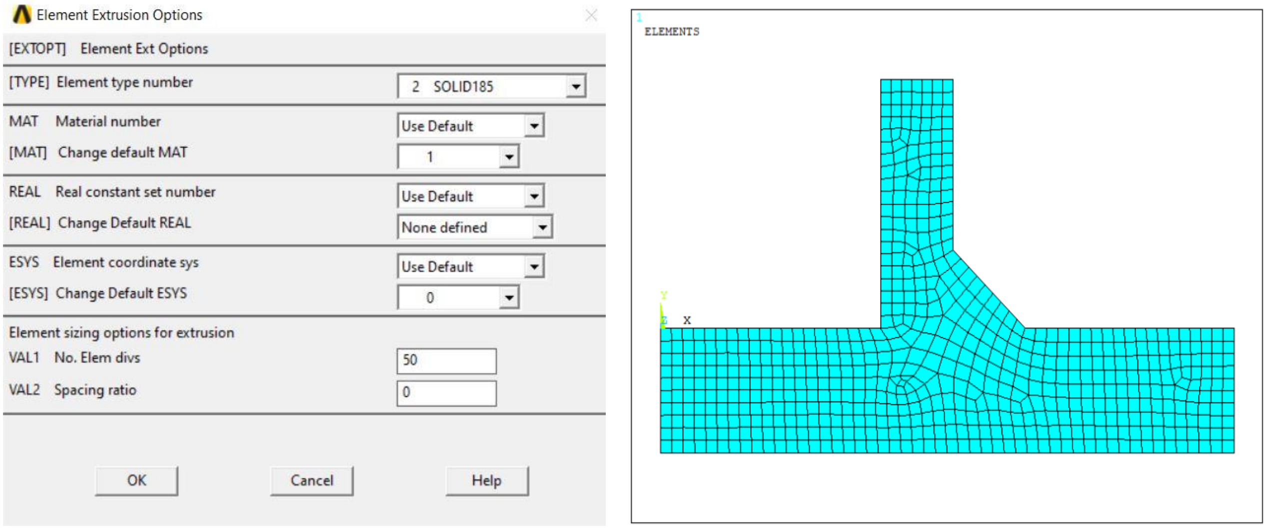

Figure 2. 44: on the left, the element extrusion options; on the right, the initial area which has to be extruded.

Concerning the constraints, symmetry boundary conditions are applied to the highlighted areas in *Figure 2.45* right side:

Main Menu > Loads > Define Loads > Apply >Displacements > Symmetry B.C on areas

Figure 2. 45: on the left, the selected areas for the cut boundary; on the right, selected areas for the symmetry boundary conditions.

To apply the nodal displacements to the cut boundary, represented by the highlighted areas in *Figure 2.45* left side, firstly the nodes attached to the cut boundary areas have to be selected:

Utility Menu > Select > Entities > Areas > From full

Utility Menu > Select > Entities > Nodes > Attached to > Areas, all

A file containing the nodal coordinates of the nodes belonging to the cut boundary has to be created:

Main Menu > Preprocessor > Modelling > Create > Nodes > Write Node File

When saving the file, the extension "file.node" is recommended.

The main model is then opened again and solved; the values of the displacements are interpolated in the cut boundary nodal coordinates, and the file is saved with the .cbdo extension, as seen in *Figure 2.46*:

Main Menu > General Postproc > Submodelling > Interpolate DOF

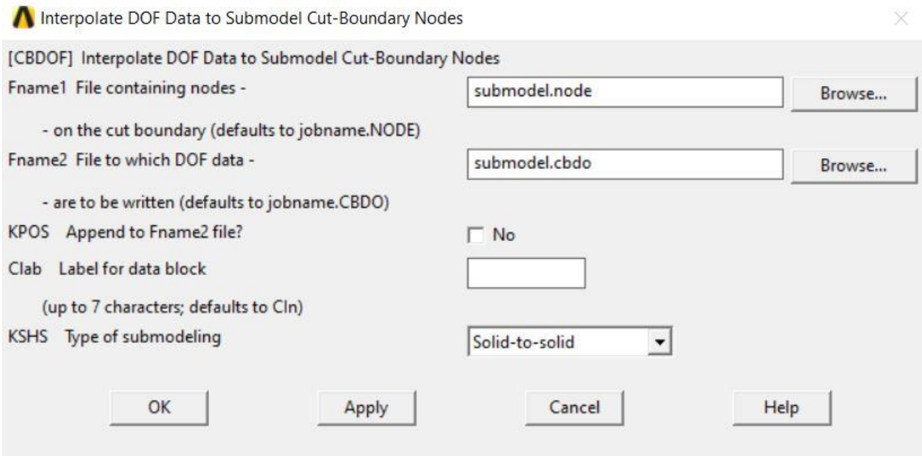

Figure 2. 46: interpolate DOF, window configuration.

Then, the submodel is opened again, and the nodal displacements are imposed on the cut boundary areas with the command:

Utility Menu > File > Read Input from > submodel.cbdo

Finally, the system can be solved:

Main Menu > Solution > Solve > Current LS

2.6.2 PSM Brick 185, analysis of results

Before proceeding, it is advised to immediately disable the POWERGRAPHICS option in Ansys® Toolbar, as seen in *Figure 2.47*, otherwise the output results are given by the average of only the superficial nodal stresses, without considering the inner ones.

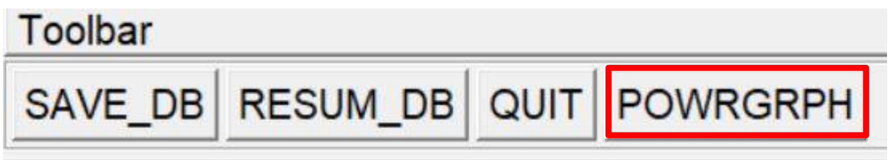

Figure 2. 47: POWERGRAPHICS disabled.

A rigorous procedure for the $\Delta\sigma_{\theta\theta,\theta=0,peak}$ detection should include the creation of a local coordinate system similar to the one adopted in paragraph 2.2.1 for the analytical K_1 detection, displayed in *Figure 2.31*. It can be demonstrated that under pure mode I loading, in case the stress flow is aligned with the external pressure direction, the first principal stress $\Delta\sigma_{11}$ at the weld toe can be confused with the local $\Delta\sigma_{yy}$ evaluated with a local coordinate system similar to that adopted in the PSM Tetra 187 analysis. Therefore, to speed up the simulation, the first principal stress replaces $\Delta\sigma_{yy}$, and it is displayed in *Figure 2.48*, for an external applied pressure of 33.22 MPa; the highest $\Delta\sigma_{11}$ is reached at the weld toe, SHS side:

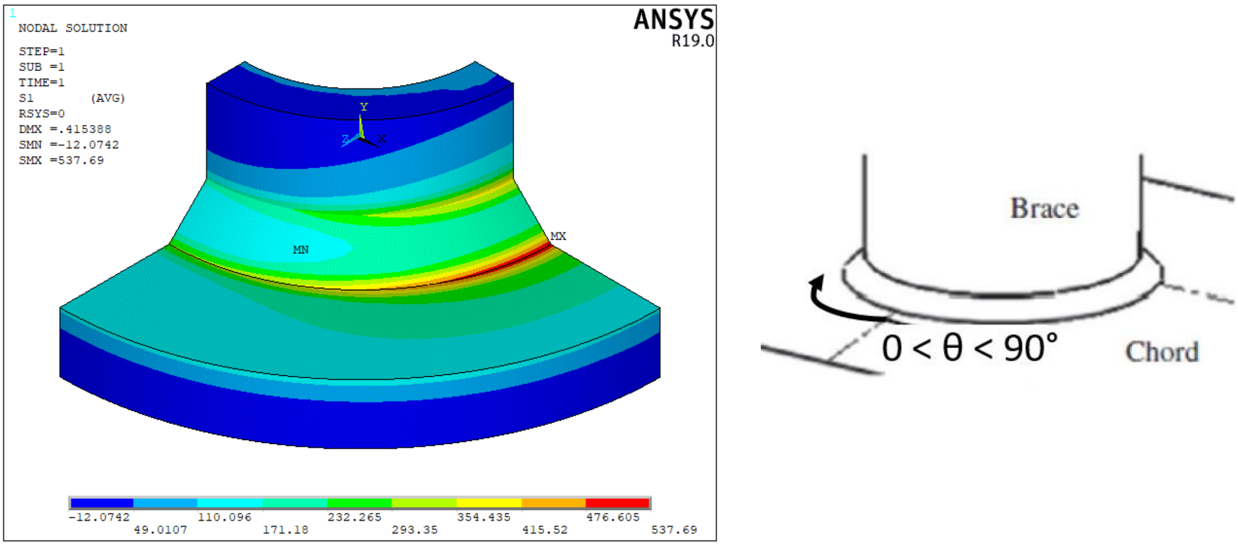

Figure 2. 48: one the left, first principal stress plot on the submodel; on the right, the angular coordinate θ used for the nodal stress extraction.

To obtain the nodal stress values at the V-notch profile, SHS and CHS sides, the nodes attached to the respective lines must be selected. The nodal selection has to be performed separately for each of the two profiles:

Utility Menu > Select > Entities > Lines > From full

Utility Menu > Select > Nodes > Attached to > Lines, all

The $\Delta\sigma_{11}$ nodal values are then plotted in an Excel graph with respect to the coordinate angular coordinate θ, ranging from 0° to 90°, illustrated in Figure 2.49*:*

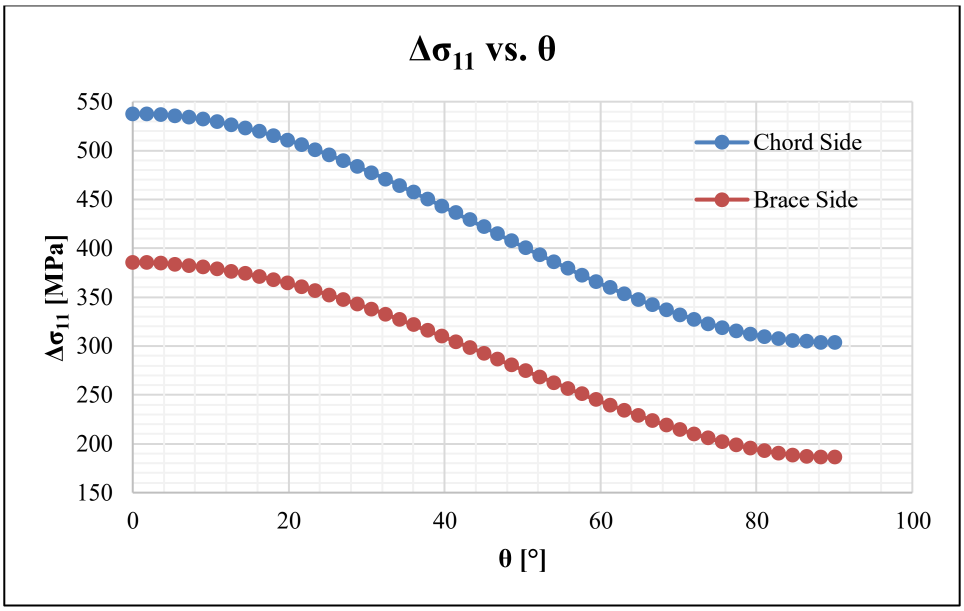

Figure 2. 49: first principal stress vs. θ, expressed in [°], CHS and SHS sides.

For an external applied pressure $\Delta\sigma_{nom}$=33.22 MPa, the maximum $\Delta\sigma_{11}$, located at θ=0 mm both at CHS and SHS sides, is respectively equal to:

$$\Delta\sigma_{11,chord\ side} = 537.7\ MPa$$

$$\Delta\sigma_{11,brace\ side} = 385.3\ MPa$$

Both the notch stress intensity factor ΔK_1 and the equivalent peak stress $\Delta\sigma_{eq,peak}$ are detected with formulae (2.5) and (2.8):

$$\Delta K_{1,chord\ side} \cong K_{FE}^{*} \cdot \Delta\sigma_{\theta\theta,\theta=0,peak} \cdot d^{1-\lambda_1} = 1.38 \cdot 537.7 \cdot 1^{1-0.674} = 742.0\ MPamm^{0.326}$$

$$\Delta\sigma_{eq,peak,chord\ side} = \Delta\sigma_{\theta\theta,\theta=0,peak} \cdot f_{w1} = 537.7 \cdot 1.064 = 572.2\ MPa$$

$$\Delta K_{1,brace\ side} \cong K_{FE}^{*} \cdot \Delta\sigma_{\theta\theta,\theta=0,peak} \cdot d^{1-\lambda_1} = 1.38 \cdot 385.3 \cdot 1^{1-0.674} = 531.7\ MPamm^{0.326}$$

$$\Delta\sigma_{eq,peak,brace\ side} = \Delta\sigma_{\theta\theta,\theta=0,peak} \cdot f_{w1} = 385.3 \cdot 1.064 = 410.1\ MPa$$

According to the PSM Brick 185 results, the chord side is more solicited than the brace side. The experimental fracture for Gandhi model N° 1 occurred at the weld toe, SHS side, hence the PSM foresees the crack initiation in the correct location.

It is now a matter of investigating whether the results differ in case the main model is composed of three volumes, one of them corresponding to the submodel, as shown in *Figure 2.50*. The volumes have to be glued, so that they can share the areas along their borders, congruent mesh. In Ansys® Mechanical APDL, the following commands can be used:

Main Menu > Preprocessor > Modelling > Operate > Booleans > Glue > Volumes

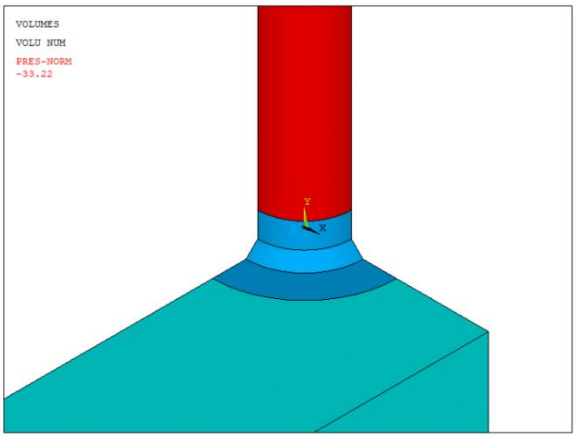

Figure 2. 50: Gandhi model N°1, three volumes. One coincides with the submodel volume.

Respectively, the maximum first principal stress $\Delta\sigma_{11}$ at chord and brace sides is now equal to:

$$\Delta\sigma_{11,chord\ side} = 538.6\ MPa$$

$$\Delta\sigma_{11,brace\ side} = 386.2\ MPa$$

in good agreement with the previous results. This last analysis confirms the non-necessity to account of the exact geometry of the submodel creation when employing the submodel technique.

2.6.3 PSM, ten-node quadratic element (Tetra 187)

The fatigue assessment is performed in terms of equivalent peak stress, with the adoption of the Peak Stress Method for 3D structures, ten-node quadratic elements.

From Ansys® APDL element library, Tetra 187 element is chosen; the Key Option K1 is left to *Pure displacement*, which means that the nodal forces are only dependent upon the displacements.

As it was previously stated, mode I is prevailing at the weld toe. Under mode I loading, the PSM Tetra 187 requirements are listed below:

		Mode I		
Element Type	**Mesh algorithm**	**$(a/d)_{min}$**	**2α**	**Mesh pattern**
Tetra 187 *KOs: Pure Displacement*	Free	1	135°	No particular indications

Under these restrictions, the mode I PSM calibration constant is equal to $K^*_{FE} = 1.21 \pm 10\%$.

The following dispositions are thus adopted:

- The SHS thickness a is equal to a = 10 mm;
- The mesh global element size is set to d = 5 mm;
- $\frac{a}{d} = \frac{10}{5} = 2 > 1$ the ratio is respected;
- The λ_1 and e_1 values associated to $2\alpha = 135°$ and required for f_{w1} detection are:

2α	**λ_1**	**e_1**
135°	*0.674*	*0.118*

Finally, the corrective stress factor calculated with equation (2.9) is equal to $f_{w1} = 1.58$.

2.6.4 Tetra 187, analysis of results

Before proceeding, the POWERGRAPHICS option in Ansys® Toolbar, as seen in *Figure 2.47*, is disabled.

With reference to the PSM Tetra 187 theory, two precautions are worth to be reported:

1. The resulting FE mesh is intrinsically irregular, the elements might have variable sizes and shapes even for a constant applied element size. Hence, the peak stress irregularly varies along the notch tip profile even in the case of a constant applied NSIF [18]. To overcome this issue, the outcoming peak stress values have to be averaged according to equation (2.10):

$$\bar{\sigma}_{ij,peak,n=k} = \left. \frac{\sigma_{ij,peak,n=k-1} + \sigma_{ij,peak,n=k} + \sigma_{ij,peak,n=k+1}}{3} \right|_{n=node} \tag{2.10}$$

2. Only peak stress values calculated at vertex nodes of the quadratic tetrahedral elements must be averaged;
3. Since affected by the nodal values in the adjacent areas, the V-notch profiles edge nodes must be excluded from the average.

The first principal stress $\Delta\sigma_{11}$ trend is plotted in *Figure 2.51*:

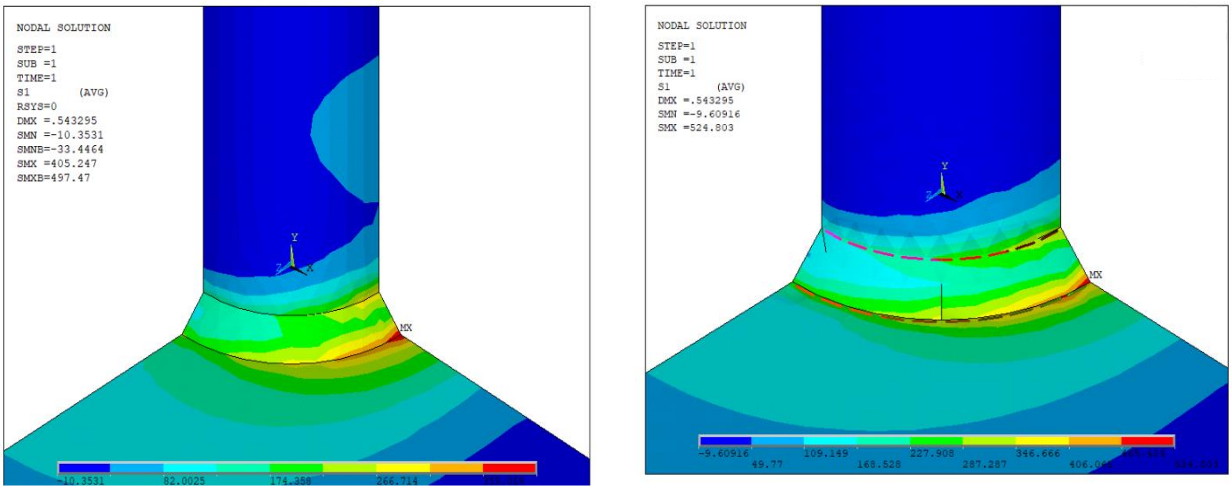

Figure 2. 51: on the left, the first principal stress plot with tetra elements. On the right, V-notch profiles selection at SHS and CHS sides.

The averaged as well as the non-averaged nodal $\Delta\sigma_{11}$ values are plotted in an Excel graph, in function of the angular coordinate θ:

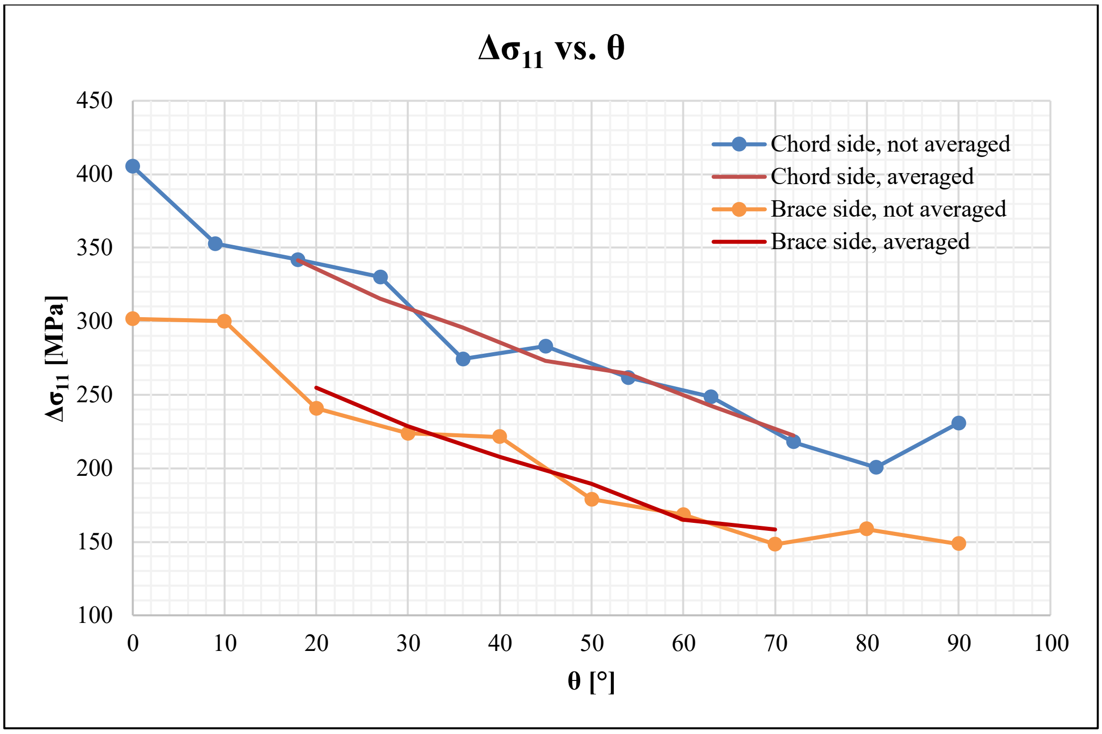

Figure 2. 52: first principal stress, averaged and non-averaged, vs. θ, chord and brace sides.

For an external applied pressure $\Delta\sigma_{nom}$=33.22 MPa, the maximum $\Delta\sigma_{11}$, located at θ=20° both at CHS and SHS sides, is respectively equal to:

$$\Delta\sigma_{11,chord\ side} = 341.5\ MPa$$

$$\Delta\sigma_{11,brace\ side} = 254.8\ MPa$$

Both the notch stress intensity factor ΔK_1 and the equivalent peak stress $\Delta\sigma_{eq,peak}$ are detected with formulae (2.5) and (2.8):

$$\Delta K_{1,chord\ side} \cong K_{FE}^{*} \cdot \Delta\sigma_{\theta\theta,\theta=0,peak} \cdot d^{1-\lambda_1} = 1.21 \cdot 341.5 \cdot 1^{1-0.674} = 698.3\ MPamm^{0.326}$$

$$\Delta\sigma_{eq,peak,chord\ side} = \Delta\sigma_{\theta\theta,\theta=0,peak} \cdot f_{w1} = 341.5 \cdot 1.58 = 538.5\ MPa$$

$$\Delta K_{1,brace\ side} \cong K_{FE}^{*} \cdot \Delta\sigma_{\theta\theta,\theta=0,peak} \cdot d^{1-\lambda_1} = 1.21 \cdot 254.8 \cdot 1^{1-0.674} = 521.1\ MPamm^{0.326}$$

$$\Delta\sigma_{eq,peak,brace\ side} = \Delta\sigma_{\theta\theta,\theta=0,peak} \cdot f_{w1} = 254.8 \cdot 1.58 = 401.8\ MPa$$

According to the PSM Tetra 187 results, the chord side is more solicited than the brace side, hence the PSM foresees the crack initiation in the correct location.

The relative errors between the $\Delta\sigma_{eq,peak}$ detected with PSM Brick 185 and PSM Tetra 187, SHS side, can be consulted in the table below:

	$\Delta\sigma_{eq,peak}$ [MPa]	ΔK_1 [MPamm$^{0.326}$]
Brick 185	572.2	742.0
Tetra 187	538.5	698.3
Relative error %	6.26 %	

2.6.5 Data entry in the PSM curve

The single available experimental data is entered inside the PSM design curve proposed by Meneghetti, Guzzella and Atzori (2014), under prevailing mode I. Nf=350 000 cycles (through-the-thickness crack) is taken as reference.

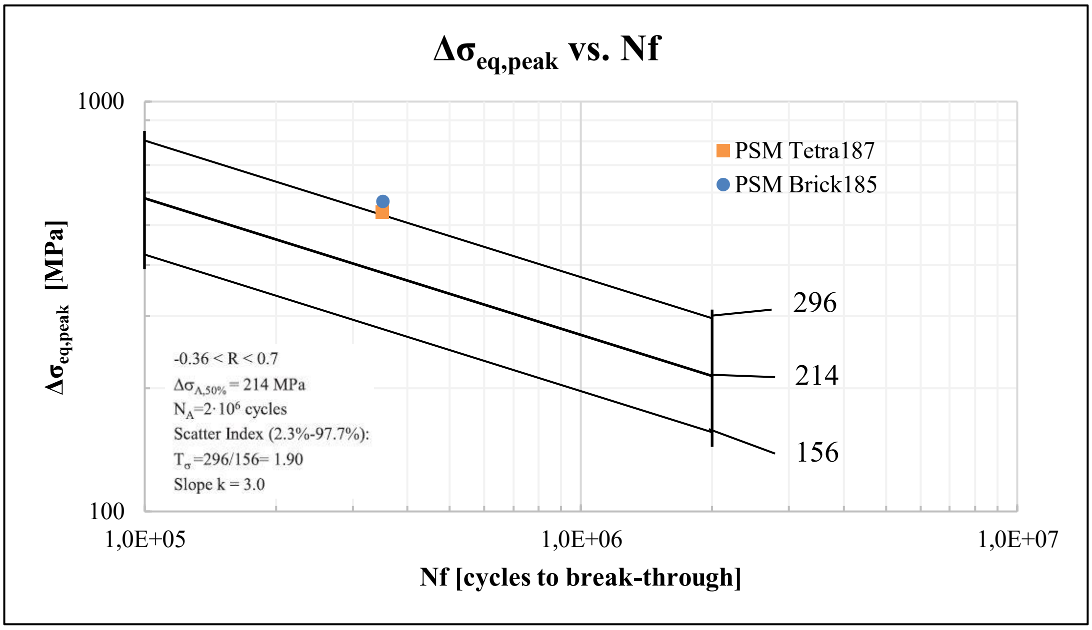

Figure 2. 53: data entry inside the PSM design curve [28].

The following conclusions can be drawn:

1. The PSM approach has correctly foreseen the experimental crack initiation point at weld toe;
2. Since the experimental data falls above the PS 2.3% line, the PSM design curve has proven to be very effective and conservative.

Conclusively, in *Figure 2.54*, the equivalent peak stress calculated at the weld toe, SHS side, both with tetrahedral and hexahedral elements is reported along with the respective error band provided by the literature ($\pm$10% for Tetra 187, and $\pm$3% for Brick 185):

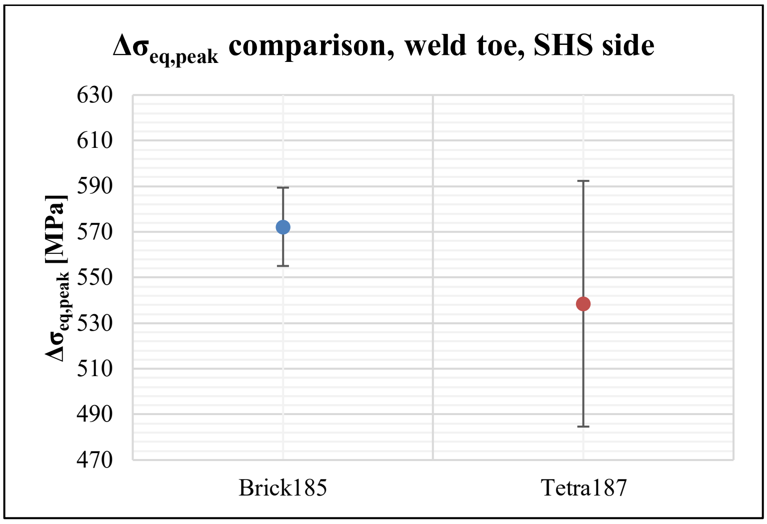

Figure 2.54: $\Delta\sigma_{eq,peak}$ detected with PSM Brick 185 and PSM Tetra 187 with the respective error band. The equivalent peak stress is between 555 MPa and 590 MPa.

Chapter 3: fatigue assessment of as-welded joints by local approaches

In this Chapter, the fatigue assessment on various welded joints is performed in terms of nominal stress, equivalent peak stress, strain energy density, structural hot-spot stress and 1-mm stress. The re-elaborated datasets are entered in their respective design curves, available in the literature; secondly, a fatigue life N_f comparison with respect to the experimental number of cycles allows to quantify the grade of conservativeness provided by each method.

The current work was performed at Aarhus University, under the guidance of the supervisor Associate Professor Halid Can Yildirim.

Re-elaborated datasets consist of three longitudinal stiffeners, one FAT 71 [34] and two FAT 63 class [35], as well as four FAT 80 transverse attachments (Yildirim et al, Okawa 2011 [36], Kuhlmann 2009 [37]).

The assessments are effectuated with the employment of the Finite Element FE software Ansys® Mechanical APDL 19.0, license from University of Padova; the simulations are achieved with the adoption of four-node linear element Plane182, *Simple Enhanced Strain* and *Plane strain* as Key Options K1 and K3, in case of 2D FE models; on the other hand, eight-node linear element Brick 185, *Simple Enhanced Strain* as Key Option K1, and ten-node quadratic element Tetra 187, *Pure Displacement* as Key Option K1, are chosen for the analysis of 3D structures. The elements are available in the Ansys® element library.

Exception made for longitudinal FAT 71 specimen, modelled inside Ansys® CAD environment, the rest of the components were designed inside SOLIDWORKS 2018 *Student Edition*, for then being imported in Ansys® APDL with the .IGS extension.

All the following joints are presented in as-welded condition. In compliance with the non-conventional LEFM extension to welded joints, the weld toe profile is assumed as a sharp V-notch, with tip radius equal to zero (the worst case), while the root is considered as a pre-crack in the structure.

3.1 Longitudinal attachment, FAT 71

The first welded joint to be assessed is a longitudinal stiffener, fatigue class FAT 71, tested by Yildirim in 2017 [34,38] under constant amplitude loading CAL.

Specific information on the component is reported below:

Weld condition	Fracture location	Load application	Main plate/gusset thickness
As-welded, non-load carrying, full penetration	*Weld toe*	*Axial, main plate, parent material*	*Main plate: 8 mm Gusset: 8 mm*

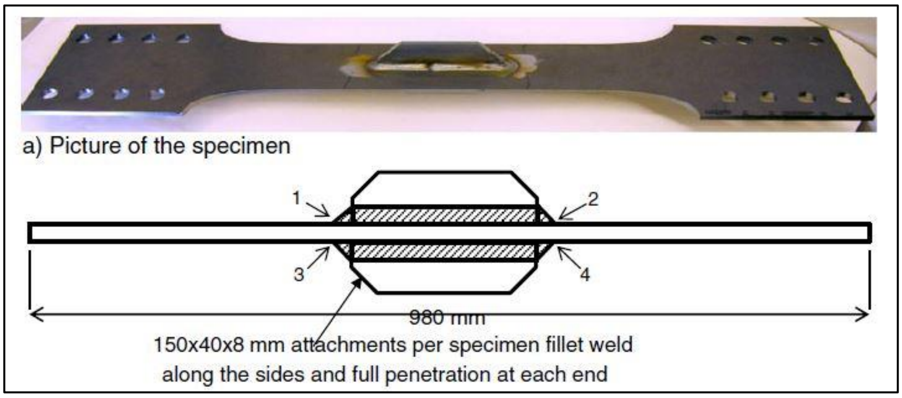

Figure 3. 1: longitudinal stiffener FAT 71, representation of the geometry [38].

The mechanical properties are described below:

Material	Yield strength f_y	Young modulus	Poisson's ratio ν
S700, HSS, linear elastic, isotropic	*700 MPa*	*206000 MPa*	*0.3*

In regard of the main geometrical quantities, *Figure 3.*1 and *Figure 3.2* show the most relevant information:

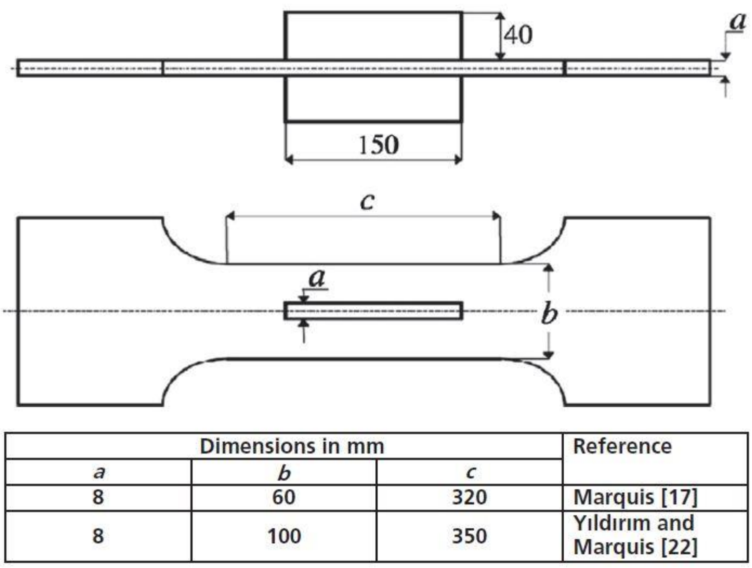

Figure 3. 2: geometrical parameters, expressed in [mm] [34].

Figure 3. 3: as-welded profile [39].

Even though the gusset, i.e. the attachment, is bevelled at its extremities, it is proved that it does not affect the fatigue resistance.

The weld profile parameters are described in the table below:

ρ weld toe tip [mm]	Weld throat [mm]	Weld flank angle	2α
0.4 – 1.32	*5.2*	*30°*	*Weld toe: 150°* *Gusset: 120°*

Since $\rho < 1.5$ mm, the assumption of a sharp V-notch ($\rho = 0$ mm) at the weld toe is coherent with the non-conventional LEFM extension to welded joints.

Referring to Hobbacher's recommendations [1], the influence of misalignments can be neglected in continuous welds longitudinally loaded. According to [38], angular distortions never exceeded 1°, therefore misalignments are neglected.

The experimental data are reported in terms of nominal stress $\Delta\sigma_{nom}$. In barred, the runouts.

R	**$\Delta\sigma_{nom}$ [MPa]**	**N_f [cycles]**
-1	159.7	229 600
	158.9	265 500
	158.5	679 800
	149.5	402 100
	136.7	2 808 000
	116.8	564 900
	104.5	844 100
	~~100.5~~	~~6 403 000~~

Due to the complex geometry of this type of joint, two different FE models are created, differing from each other for the shape of the weld junction: *Figure 3.4* shows on the left a simplified straight junction, while on the right a more realistic curve junction. The aim is to compare the outcoming results, so as to verify if a simplified model can be adopted instead of a more realistic one. Similar work was previously performed by Meneghetti, Guzzella and Atzori in 2014 [28].

As it was stated before, FAT 71 is modelled inside Ansys® CAD environment; the APDL commands are accessible in Appendix B.

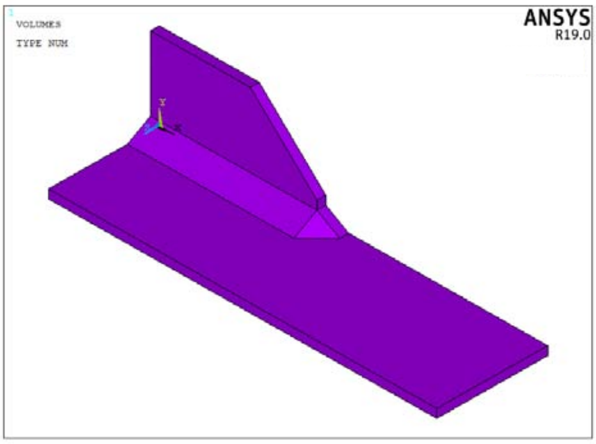

Figure 3. 4: representation of the straight weld junction.

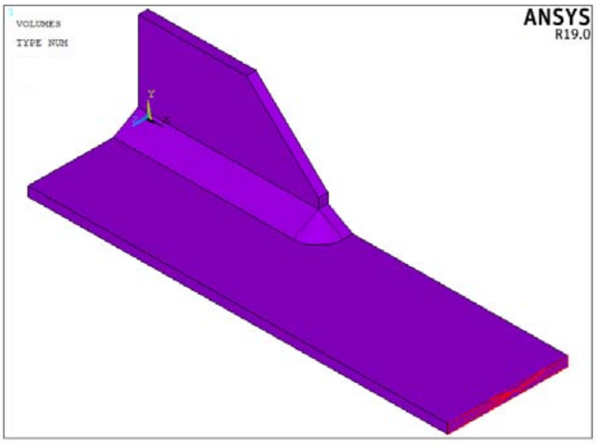

Figure 3. 5: representation of the curve weld junction.

In *Figure 3.6*, the modelling indications are described, which hold true for both the straight and the curve junction:

- Symmetries: due to the triple symmetry of the longitudinal stiffener, only 1/8 of the geometry is created, allowing to consistently speed up the computational time.
- Loading: the specimen is axially loaded, and the load is applied on the main plate as a constant pressure equal to $p = -\Delta\sigma_{nom}$, on Area 4.
- Constraints: symmetry boundary conditions are applied on Areas 6 (highlighted in the back), 9 and 15.

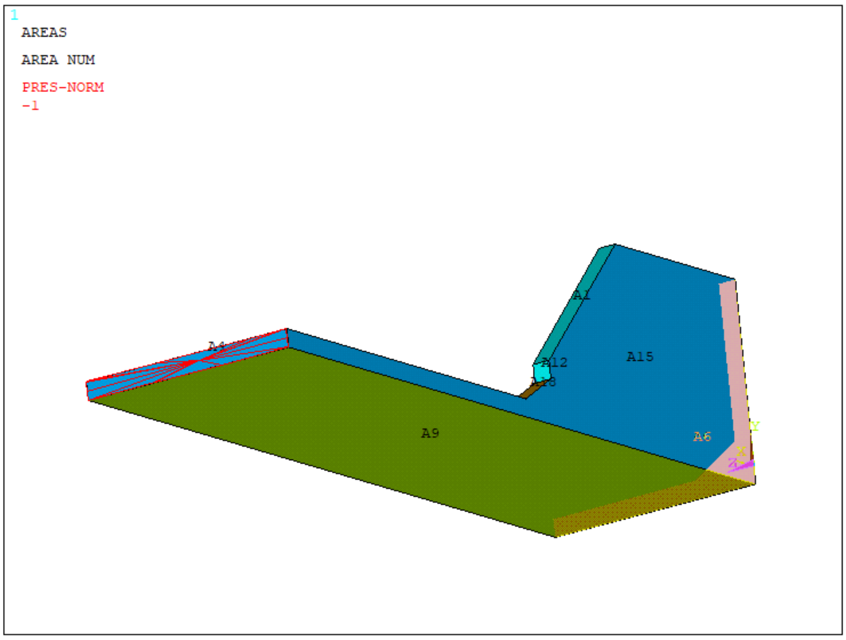

Figure 3. 6: red lines on area 4 indicate the applied pressure, while symmetry BC are applied on areas 9, 15 and 6 (highlighted in the back).

3.1.1 PSM Tetra 187

The fatigue assessment is performed in terms of equivalent peak stress, with the adoption of the Peak Stress Method for 3D structures, ten-node quadratic elements.

From Ansys® APDL element library, Tetra 187 element is chosen; the Key Option K1 is left to *Pure displacement*, which means that the nodal forces are only dependent upon the displacements.

From a preliminary analysis, it can be inferred that FAT 71 fillet weld is solicited under prevailing mode I at the attachment edge, while mode II is null since 2α > 102.5°; mode III is rigorously null in the attachment edge, while in the junction part it becomes singular.

An important observation refers to the V-notch opening angle 2α at weld toe, equal to 2α = 150°; in accordance with the literature, the PSM is not calibrated for V-notch opening angles higher than 135°. Therefore, in cases like this, it is common practise to extend the available calibration constants related to 2α=135°, even though the procedure is not rigorous. In support to this, the evidence in *Figure 1.21* that the PSM calibration constants tend to increase along with the V-notch opening angle.

Furthermore, another aspect concerns the parameters λ_3 and e_3, rigorously valid for axisymmetric structures, again extended for non-axial symmetric geometries like longitudinal stiffeners.

Under combined mode I and III loadings, the PSM Tetra 187 requirements at the weld toe and gusset are listed below:

Location: weld toe (2α=150°)		***Mode I***		
Element Type	**Mesh algorithm**	**$(a/d)_{min}$**	**2α**	**Mesh pattern**
Tetra 187 *KO: Pure Displacement*	Free	1	135° extended	No particular indications
		Mode III		
		$(a/d)_{min}$	**2α**	**Mesh pattern**
		3	135° extended	No particular indications

Location: gusset (2α=120°)		***Mode I***		
Element Type	**Mesh algorithm**	**$(a/d)_{min}$**	**2α**	**Mesh pattern**
Tetra 187 *KO: Pure Displacement*	Free	3	120°	No particular indications
		Mode III		
		$(a/d)_{min}$	**2α**	**Mesh pattern**
		3	120°	No particular indications

Hence, according to the table, a minimum ratio $\frac{a}{d} > 3$ must be respected.

Under these restrictions, at the weld toe (2α = 150°) the extended mode I calibration constant is equal to $K_{FE}^{*} = 1.21 \pm 10\%$, while the extended mode III constant is equal to $K_{FE}^{***} = 1.70 \pm 10\%$; at the gusset (2α = 120°) the mode I PSM calibration constant is equal to $K_{FE}^{*} = 1.05 \pm 15\%$, while the mode III constant is $K_{FE}^{***} = 1.70 \pm 10\%$.

The following PSM dispositions are thus adopted:

- Half the main plate thickness a is equal to a = 4 mm;
- The mesh global element size is set to d = 1 mm;
- $\frac{a}{d} = \frac{4}{1} = 4 > 3$ the ratio is respected;
- The λ_1, λ_3, e_1, e_3 values associated to the weld toe (2α = 150°) and gusset (2α = 120°) required for f_{w1} and f_{w3} detection respectively are:

2α	**λ_1**	**e_1**	**λ_3**	**e_3**
150° (weld toe)	*0.752*	*0.104*	*0.857*	*0.258*
120° (gusset)	*0.616*	*0.129*	*0.750*	*0.275*

Finally, the stress corrective factors under mode I and III at the weld toe calculated with equation (1.16) are $f_{w1} = 0.793$ and $f_{w3} = 1.536$, while at gusset they respectively are equal to $f_{w1} = 0.912$ and $f_{w3} = 1.817$.

3.1.2 PSM Tetra 187, analysis of results

Before proceeding, the POWERGRAPHICS option in Ansys® Toolbar is disabled, otherwise the results in output are given by the average of the superficial elements, with no consideration of the interior ones.

<u>Straight junction</u>

Once the geometry modelled in *Figure 3.4* is properly meshed, loaded and constrained, the system can be solved:

Main Menu > Solution > Solve > Current LS

The first principal stress $\Delta\sigma_{11}$ is plotted in *Figure 3.7*. As it can be seen, for an external pressure of 1 MPa, the maximum first principal stress is located at the weld toe and is equal to $\Delta\sigma_{11} = 2.28$ MPa.

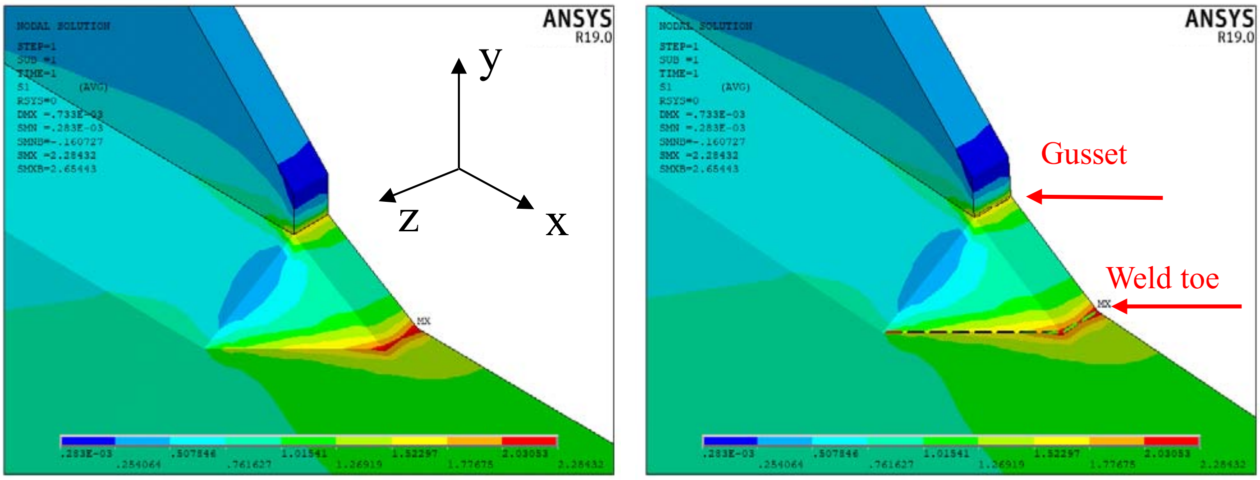

Figure 3. 7: on the left, the first principal stress trend. On the right, nodes attached to weld toe and gusset lines selection. In black, the global coordinate system.

In respect of the LEFM theory, the singular stress field along the V-notch profile has to be plotted in a local x-y-z coordinate system.

To create a local coordinate system in Ansys®, the procedure below can be followed:

2. The WorkPlane is displayed and offset to the keypoint attached to the weld toe, in the XY plane of symmetry:
   Utility Menu > Offset WorkPlane to > Keypoint
3. At weld toe, gusset edge, the WorkPlane is rotated by 105° anticlockwise about the out-of-plane z-axis (XY angle in Ansys®), while in weld junction it has to be pre-rotated by 45°

anticlockwise about the y-axis (ZX angle in Ansys®). At gusset, the WorkPlane is rotated by 150° anticlockwise about the z-axis;

Utility Menu > Offset WP by Increments > Degrees

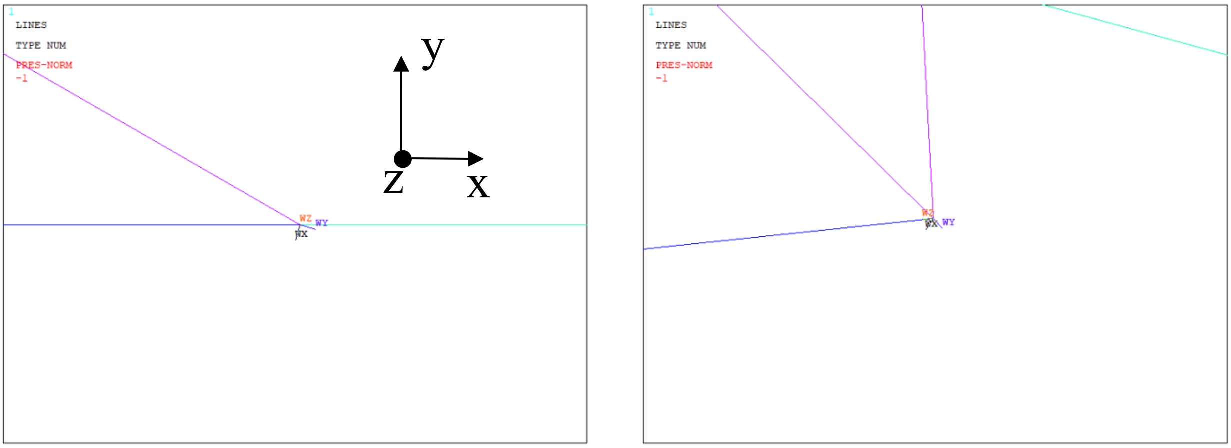

Figure 3. 8: on the left, WorkPlane placed at the weld toe, anterior part, side view. On the right, WorkPlane at the weld junction. The black SOR represents the global coordinate system.

4. The local coordinate system is now placed at the WorkPlane origin:
   Utility Menu > Local Coordinate Systems > Create Local CS > At WP origin

5. The output results must be plotted in the new coordinate system. To do this:
   Main Menu > General Postproc > Options for Outp > Local coordinate system

Finally, the peak stress along y-axis $\Delta\sigma_{yy,peak}$ calculated at the V-notch corresponds to the theoretical mode I $\Delta\sigma_{\theta\theta,\theta=0,peak}$ appearing in equation (1.15), while the mode III peak stress $\Delta\tau_{yz,peak}$ corresponds to $\tau_{\theta z,\theta=0,peak}$.

To have the local $\Delta\sigma_{yy,peak}$ values both at weld toe and gusset sides, the nodes attached to the respective lines have to be selected. The nodal selection has to be performed separately for each of the two profiles, as well as the creation of the local coordinate system:

Utility Menu > Select > Entities > Lines > From full

Utility Menu > Select > Nodes > Attached to > Lines, all

To plot and extrapolate the stress values along the selected nodes:

Main Menu > General Postproc > Path Operations > Define Path > By nodes

The results are then listed and plotted in an Excel graph. Once the procedure is achieved, the local coordinate system must be deleted and aligned back to the Global coordinate system. The following Ansys® commands can be used:

Utility Menu > WorkPlane > Local Coordinate System > Delete

Utility Menu > WorkPlane > Align WP with > Global Cartesian

In respect of the PSM Tetra 187 theory, the peak stress values have to be averaged with equation (1.17), with the exclusion of the edge nodes. Finally, the averaged nodal stress components related to mode I and III are combined inside equation (1.15) to obtain the equivalent peak stress along the V-notch profiles of the weld toe and the gusset.

$$\Delta\sigma_{eq,peak,avg} = \sqrt{f_{w1}^2 \cdot \sigma_{\theta,\theta=0,peak,avg}^2 + f_{w3}^2 \cdot \tau_{\theta z,\theta=0,peak,avg}^2} \tag{3.1}$$

Both at weld toe, gusset edge, and gusset, mode III influence associated to the stress component $\Delta\tau_{yz,peak,avg}$ is practically null, and therefore neglectable, while in the junction part it becomes singular. However, the increase of $\tau_{yz,\theta=0,peak,avg}$ is accompanied by a greater decrease of $\sigma_{\theta\theta,\theta=0,peak,avg}$, therefore the overall $\Delta\sigma_{eq,peak,avg}$ tends to decrease.

The averaged nodal $\Delta\sigma_{eq,peak,avg}$ values are plotted in an Excel graph with respect to the coordinate z, defined as the nodal distance from the XY plane of symmetry:

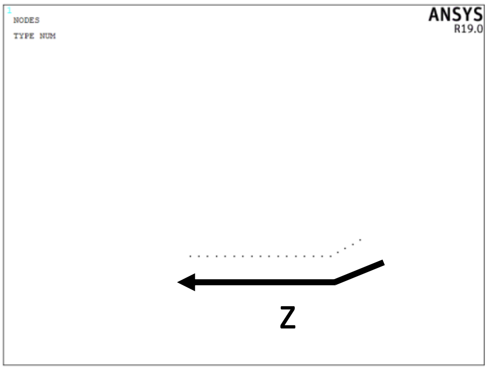

Figure 3. 9: nodes attached to the weld toe, gusset edge and junction, plus the direction of selection z.

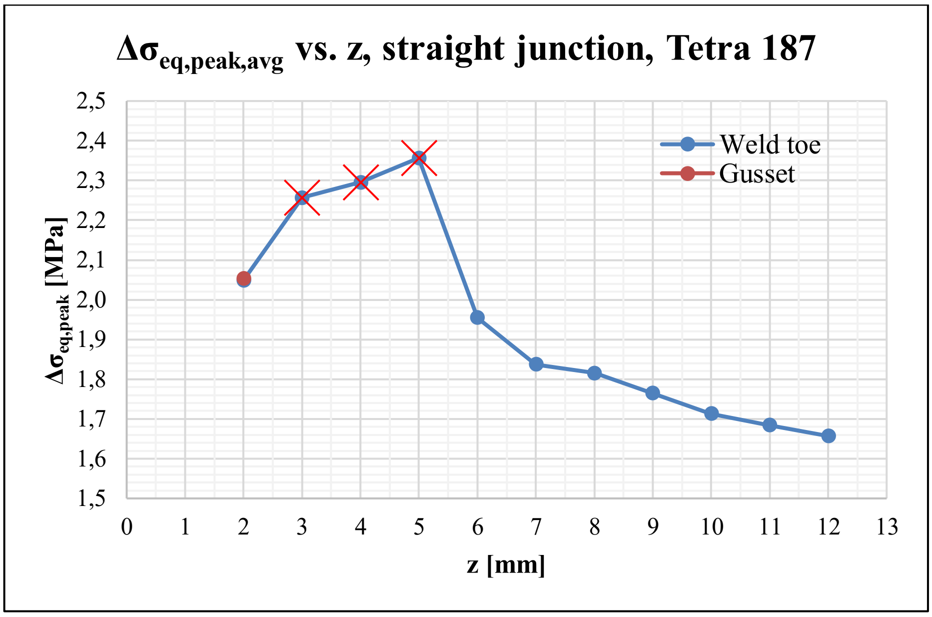

Figure 3. 10: averaged equivalent peak stress vs. z, straight junction, Tetra 187.

Some relevant observations must be drawn:

1. Due to the intrinsically irregular mesh, the peak stress irregularly varies along the notch tip profile even in the case of a constant applied NSIF;
2. The edge nodes (at z = 0, 4 mm) are not selected; for this reason, nodes at z = 1, 3, 5 mm cannot be averaged. As evidence of the edge nodes influence, an equivalent peak stress raise can be observed between z = 3 and 5 mm, it is to say when the straight junction begins. However, those nodal values must not be considered;
3. Since $\Delta\sigma_{eq,peak}$ in the weld junction is decreasing after 6 mm, the plotting can be interrupted;

For an external applied pressure $\Delta\sigma_{nom}$ = 1 MPa, the maximum $\Delta\sigma_{eq,peak,avg}$, located at z = 2 mm both at weld toe and gusset, is respectively equal to:

$$\Delta\sigma_{eq,peak,weld\ toe} = 2.05\ MPa$$

$$\Delta\sigma_{eq,peak,gusset} = 2.05\ MPa$$

According to the PSM Tetra 187 results, both weld toe and gusset seem equally solicited. Hence, since the experimental results show fractures occurring at the weld toe, $\Delta\sigma_{eq,peak,weld\ toe}$ is chosen for the fatigue assessment. It is noted that K^{*}_{FE} and K^{***}_{FE} are not calibrated at the weld toe, where 2α = 150°, and consequently the result at weld toe could not be reliable.

Curve junction

Once the geometry modelled in *Figure 3.5* is properly meshed, loaded and constrained, the system can be solved:

Main Menu > Solution > Solve > Current LS

The first principal stress $\Delta\sigma_{11}$ is plotted in *Figure 3.11*. As it can be seen, for an external pressure of 1 MPa, the maximum first principal stress is located at the weld toe and is equal to $\Delta\sigma_{11}$ = 2.21 MPa.

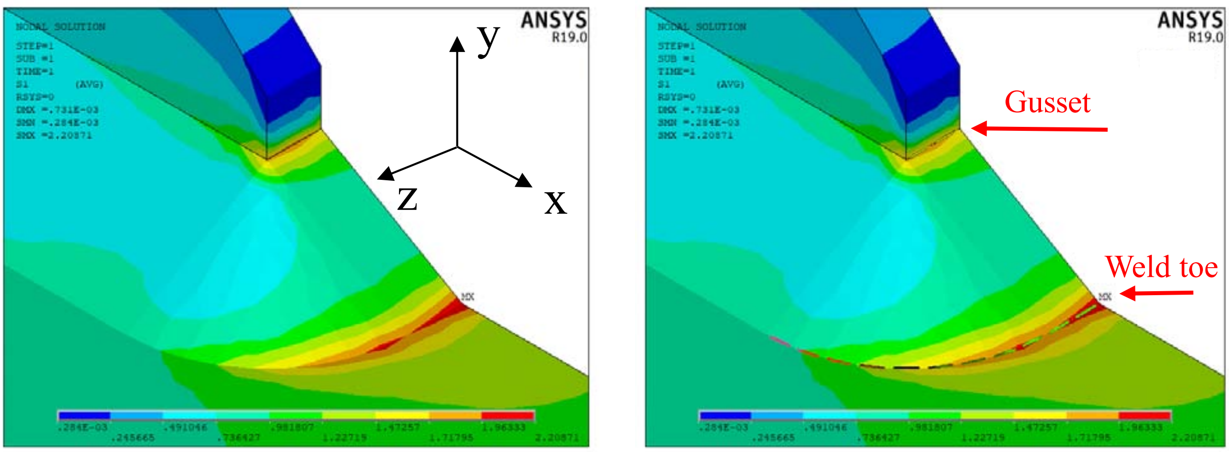

Figure 3. 11: on the left, the first principal stress trend. On the right, nodes attached to weld toe and gusset lines selection. In black, the global coordinate system.

The previous instructions can be followed for the detection of the equivalent peak stress along the weld toe and the gusset profiles. For an external applied pressure $\Delta\sigma_{nom}$=1 MPa, $\Delta\sigma_{eq,peak}$ is plotted along the weld toe and the gusset profiles:

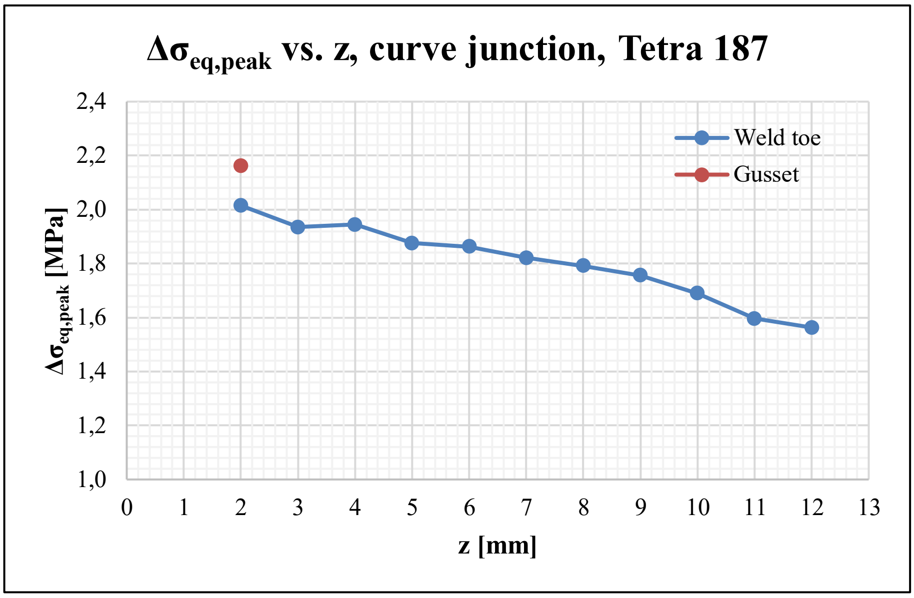

Figure 3. 12: averaged equivalent peak stress vs. z, curve junction, Tetra 187.

Some relevant observations must be drawn:

1. Due to the intrinsically irregular mesh, the peak stress irregularly varies along the notch tip profile even in the case of a constant applied NSIF;
2. The edge node at z=0 mm is not selected; for this reason, the node at z=1 mm, cannot be averaged. This time, the equivalent peak stress raise is not happening because the free edge at z=4 mm is replaced by the curve junction;
3. Since $\Delta\sigma_{eq,peak}$ in the weld junction is decreasing after 5 mm, the plotting can be interrupted;

For an external applied pressure $\Delta\sigma_{nom}$=1 MPa, the maximum $\Delta\sigma_{eq,peak,avg}$, located at z=2 mm both at weld toe and gusset, is respectively equal to:

$$\Delta\sigma_{eq,peak,weld\ toe} = 2.01\ MPa$$

$$\Delta\sigma_{eq,peak,gusset} = 2.16\ MPa$$

According to the PSM Tetra 187 results, the gusset is 7.5% more solicited than the weld toe. Hence, the PSM foresees a crack initiation in the wrong location. However, since the experimental results show fractures occurring at the weld toe, $\Delta\sigma_{\mathrm{eq,peak,weld\ toe}}$ is chosen for the fatigue assessment. One of the reasons could lie in the fact that $\mathrm{K}^*_{\mathrm{FE}}$ and $\mathrm{K}^{***}_{\mathrm{FE}}$ are not calibrated at the weld toe, where 2α = 150°, and consequently the results could appear lower than they actually are.

3.1.3 PSM Brick 185

The fatigue assessment is now performed in terms equivalent peak stress with the adoption of the Peak Stress Method for 3D structures, eight-node linear elements.

Even in this case, since the PSM calibration constants are not available at the weld toe, where the V-notch opening angle 2α equal to 150°, it is common practise to extend the available calibration constants related to $2\alpha = 135°$, even though the procedure is not rigorous. Under the same aspect, the parameters λ_3 and e_3, valid for axisymmetric structures, are non-rigorously extended. First the main model, then the submodel creation is described.

<u>Main model</u>

From Ansys® APDL element library, Tetra 187 element is chosen; the Key Option K1 is left to *Pure displacement*, which means that the nodal forces are only dependent from the displacements.

The main model of the structure is illustrated in *Figure 3.4*. The cut boundary is determined with a stress convergence verification: three different meshes, with global element size respectively equal to 2, 4 and 5 mm, are laid on the main model.

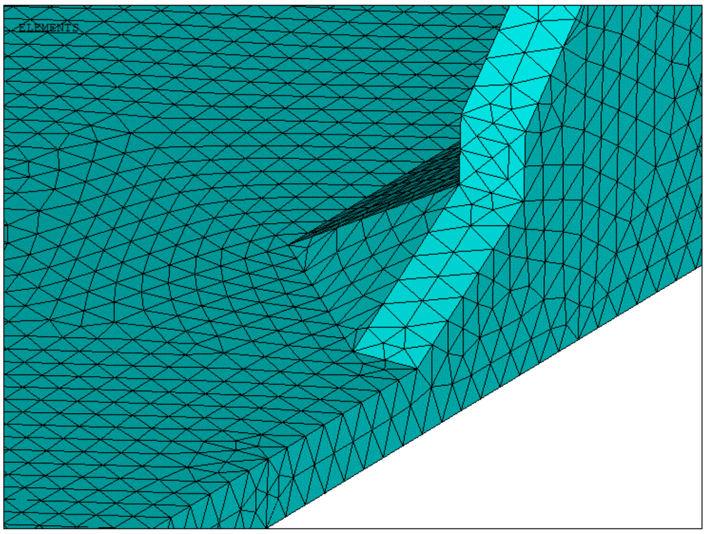

Figure 3. 13: mesh example with global element size 2 mm.

The first principal stress range $\Delta\sigma_{11}$ is then extracted along the longitudinal direction, starting from the weld toe tip, as illustrated in *Figure 3.14*:

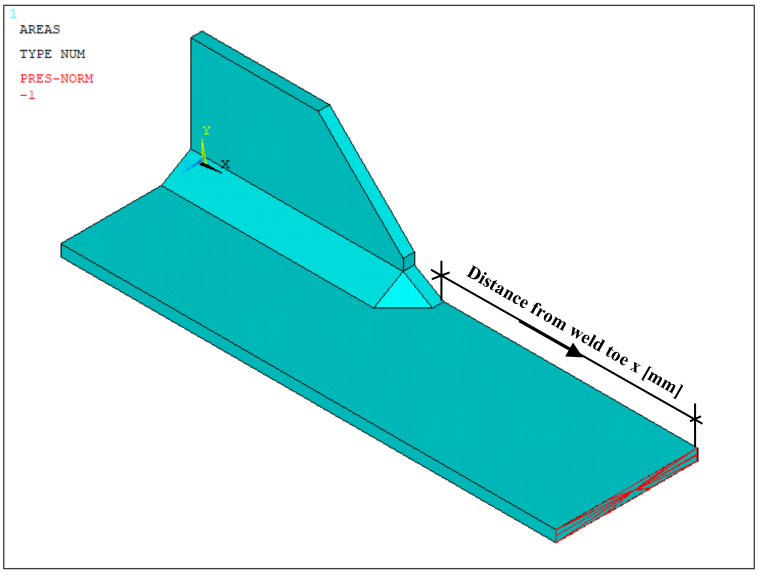

Figure 3. 14: path along which $\Delta\sigma_{11}$ is extracted.

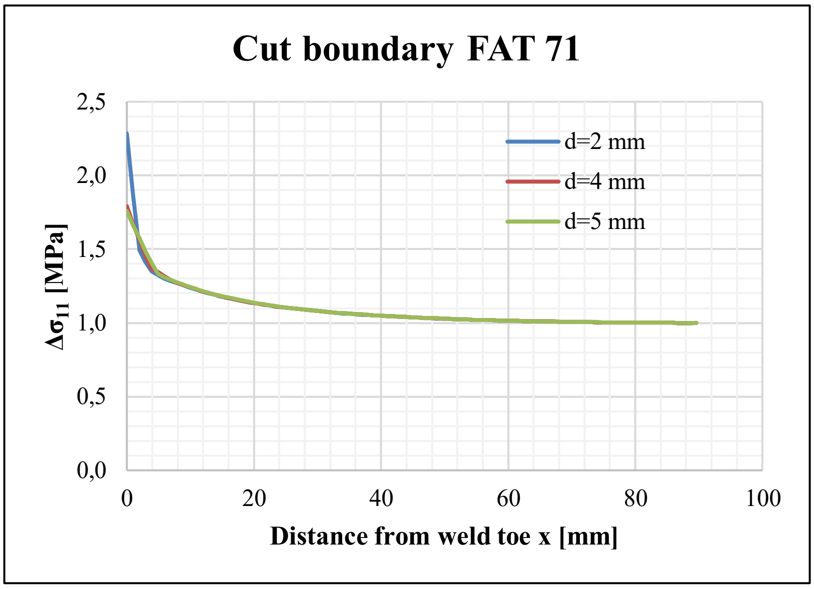

Figure 3. 15: convergence check for the cut boundary creation.

As it can be noticed in *Figure 3.15*, the local stresses cannot converge because the stress value is function of the element size. At x = 15 mm, compatibility between the results is clearly achieved, therefore the cut boundary is placed at that distance of 15 mm from the weld toe.

Submodel

In Ansys® APDL element library, Brick 185 element is chosen; the Key Option K1 is switched to *Simple Enhanced Strain*.

As it was shown in Chapter 2, the submodel system of reference has to coincide with that of the main model, since the boundary conditions which are applied to the submodel are interpolated in the cut boundary coordinates with respect to the main model frame of reference.

From the previous considerations, mode I is prevailing at the V-notch profiles, while mode II is null since 2α > 102.5° and mode III, although singular in the weld toe junction, can be neglected at the weld toe, attachment edge. Therefore, only the weld toe, gusset edge, under mode I is considered in this analysis. Similar considerations were previously stated by Meneghetti, Guzzella and Atzori [28] in 2014.

Under mode I loading, the PSM Brick 185 requirements at the weld toe and gusset are listed below:

Location: weld toe (2α=150°) ***Mode I***

Element Type	Mesh algorithm	$(a/d)_{min}$	2α	Mesh pattern 2α < 90°	Mesh pattern 2α > 90°
Brick 185 *KOs: Simple Enhanced Strain*	Mapped	3	135° extended to 150°	Four adjacent elements share the same node	Two adjacent elements share the same node

Location: gusset (2α=120°) ***Mode I***

Element Type	Mesh algorithm	$(a/d)_{min}$	2α	Mesh pattern 2α < 90°	Mesh pattern 2α > 90°
Brick 185 *KO: Simple Enhanced Strain*	Mapped	3	0° < 2α < 135°	Four adjacent elements share the same node	Two adjacent elements share the same node

Hence, according to the table, a minimum ratio $\frac{a}{d} > 3$ must be respected.

Under these restrictions, at the weld toe (2α = 150°) the extended mode I calibration constant is equal to $K_{FE}^{*} = 1.38 \pm 3\%$; at the gusset (2α = 120°) the mode I PSM calibration constant is again equal to $K_{FE}^{*} = 1.38 \pm 3\%$.

The following PSM dispositions are thus adopted:

- Half the main plate thickness a is equal to a = 4 mm;
- The mesh global element size is set to d = 0.5 mm;
- $\frac{a}{d} = \frac{4}{0.5} = 8 > 3$ the ratio is respected;
- The λ_1 and e_1 values associated to the weld toe (2α = 150°) and gusset (2α = 120°) required for f_{w1} detection respectively are:

2α	λ_1	e_1
150° (weld toe)	*0.752*	*0.104*
120° (gusset)	*0.616*	*0.129*

Finally, the corrective stress factors under mode I and III at the weld toe with equation (1.16) are f_{w1}=0.762 while at gusset side they respectively are equal to f_{w1}=0.918.

The submodel is created with the extrusion by 4 mm (half the gusset thickness) along the global z-axis of the sectional area, visible in *Figure 3.16* on the right, which was pre-meshed in respect of the PSM requirements. The number of extruded elements must be chosen so that to have cubic elements. To obtain a proper extrusion inside Ansys® APDL Preprocessor, the following commands are used:

Main Menu > Preprocessor > Modelling > Operate > Extrude > Elem Ext Opts

As Element type number, Brick 185 is selected; since the mesh size is d=0.5 mm, eight element extrusion divisions bring to cubic elements. Finally, the area is extruded:

Main Menu > Preprocessor > Modelling > Operate > Extrude > Areas > By XYZ Offset > z=4 mm

Once the volume is created, the mesh of the extruded area must be cleared, otherwise the constraints are going to be applied to nodes non-belonging to the FE model.

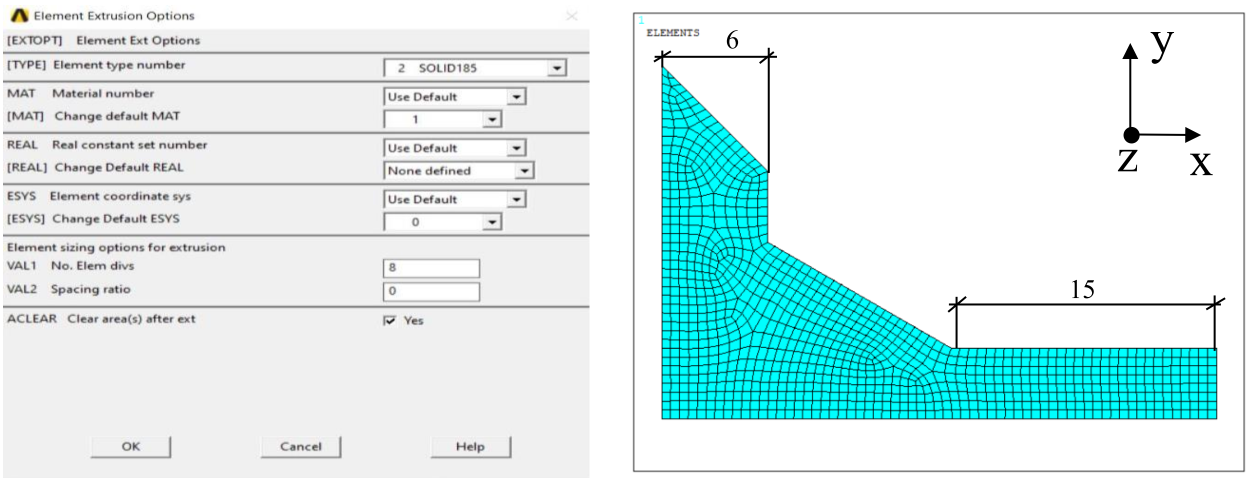

Figure 3. 16: on the left, the element extrusion options; on the right, the initial area which has to be extruded. The mesh pattern requested by the PSM is respected.

Concerning the constraints, symmetry BC are applied to the highlighted areas in *Figure 3.17*, right side:

Main Menu > Loads > Define Loads > Apply >Displacements > Symmetry B.C on areas

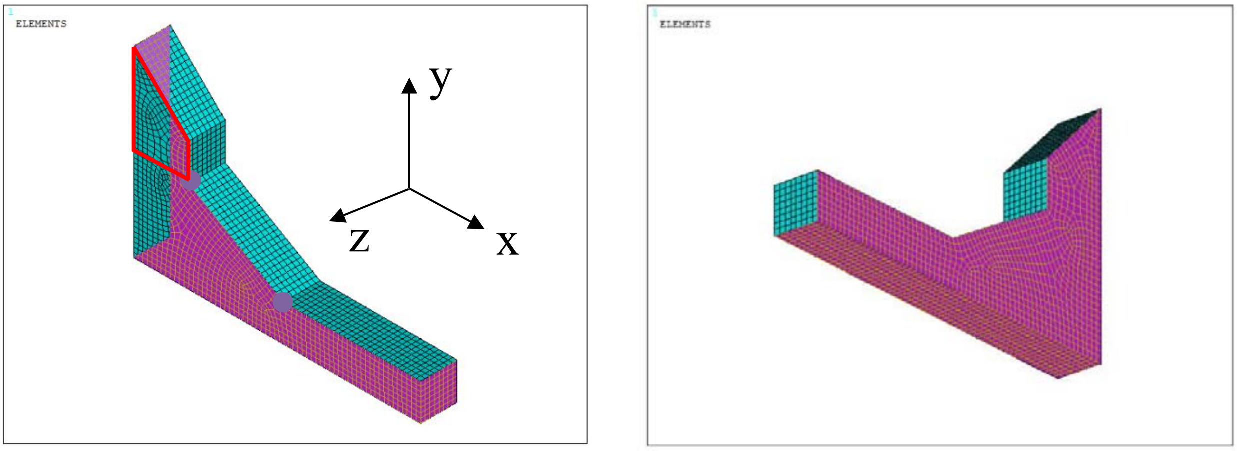

Figure 3. 17: on the left, the selected areas for the cut boundary; on the right, selected areas for the symmetry boundary conditions. In black, the global coordinate system.

To apply the nodal displacements to the cut boundary, represented by the highlighted areas in *Figure 3.17* left side, firstly the nodes attached to the cut boundary areas have to be selected:

Utility Menu > Select > Entities > Areas > From full

Utility Menu > Select > Entities > Nodes > Attached to > Areas, all

A file containing the nodal coordinates of the nodes belonging to the cut boundary has to be created:

Main Menu > Preprocessor > Modelling > Create > Nodes > Write Node File

When saving the file, the extension "file.node" is recommended.

However, the designed submodel in *Figure 3.17* presents two issues of paramount importance:

1. The yellow dots point out the location in which non-converging displacements, also called singular displacements, will be applied. These displacements come from the free edge displacements;

2. The red lines circumscribe an area in which wrong displacements are still added.

The main model is then opened again and solved; the values of the displacements are interpolated in the cut boundary nodal coordinates, and the file is saved with the .cbdo extension, as seen in *Figure 3.18*:

Main Menu > General Postproc > Submodelling > Interpolate DOF

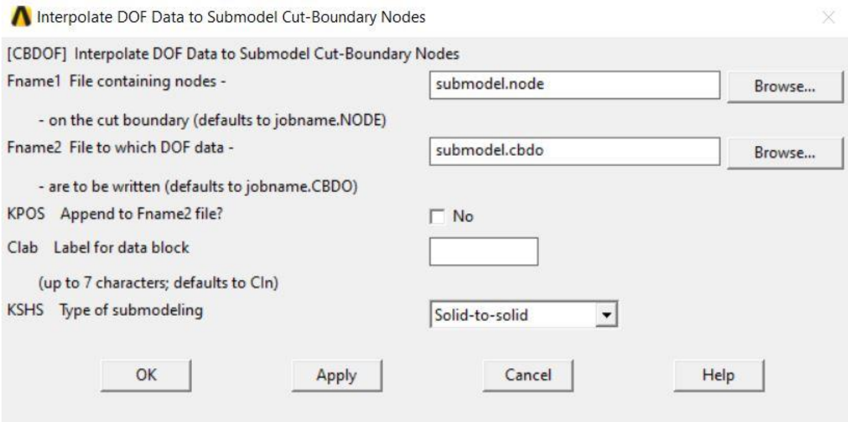

Figure 3. 18: interpolate DOF, window configuration.

Then, the submodel is opened again, and the nodal displacements are input on the cut boundary areas with the command:

Utility Menu > File > Read Input from > submodel.cbdo

Finally, the system can be solved:

Main Menu > Solution > Solve > Current LS

3.1.4 PSM Brick 185, analysis of results

As done before, POWERGRAPHICS option in Ansys® Toolbar is disabled.

It can be demonstrated that under pure mode I loading, in case the stress flow is aligned with the external pressure direction, the first principal stress $\Delta\sigma_{11}$ at the weld toe can be confused with the local $\Delta\sigma_{yy}$ evaluated with a local coordinate system similar to that adopted in the PSM Tetra 187 analysis. Therefore, to speed up the simulation, the first principal stress is replaced to $\Delta\sigma_{yy}$, and it is displayed in *Figure 3.19*, for an external applied pressure of 1 MPa.

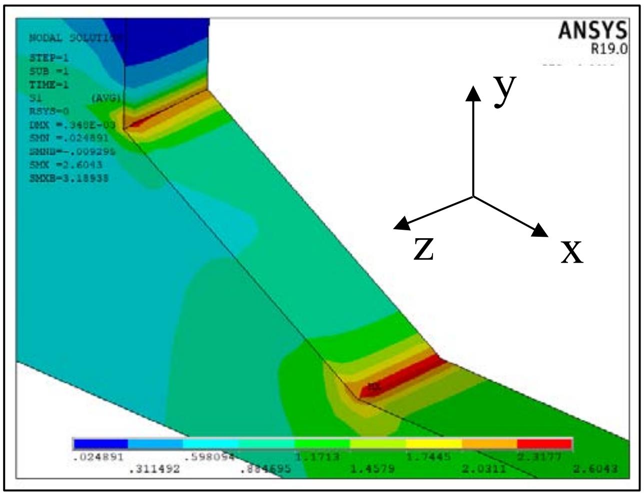

Figure 3. 19: first principal stress plot on the submodel along z.

To obtain the nodal stress values at weld toe, as well as the gusset, the nodes attached to the respective lines must be selected. The nodal selection has to be performed separately for each of the two profiles.

Utility Menu > Select > Entities > Lines > From full

Utility Menu > Select > Nodes > Attached to > Lines, all

The $\Delta\sigma_{eq,peak}$ nodal values are calculated with equation (1.15), for then being plotted in an Excel graph with respect to the coordinate z, i.e. the distance from the XY plane of symmetry. For an external applied pressure $\Delta\sigma_{nom}$ = 1 MPa, $\Delta\sigma_{eq,peak}$ is plotted along the weld toe and the gusset profiles:

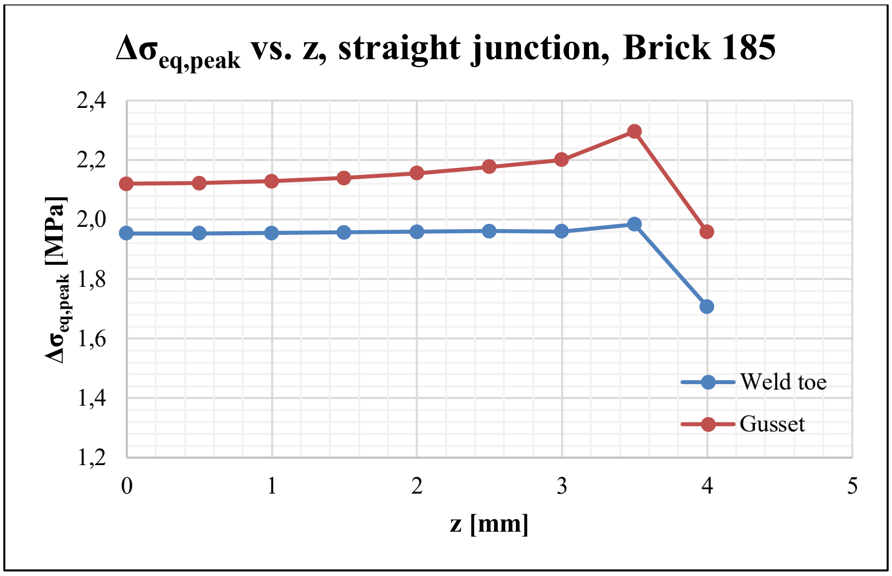

Figure 3. 20: equivalent peak stress vs. z, straight junction, Brick 185.

Some relevant observations must be drawn:

1. Despite the small thickness of the longitudinal attachment, with the Brick element adoption all the nodes belonging to the V-notch profiles can be selected;
2. As expected, due to the singular displacements, $\Delta\sigma_{eq,peak}$ tends to increase along with z: the maximum equivalent peak stress is located at z = 3.5 mm;
3. Since the stress raise is due to numerical integration issues, it is decided to rely on the values at z = 0 mm, confirmed by the fact that the experimental data show fractures occurring at the centre of the stiffener edge.

For an external applied pressure $\Delta\sigma_{nom}$ = 1 MPa, the maximum $\Delta\sigma_{eq,peak}$, located at z = 0 mm both at weld toe and gusset, is respectively equal to:

$$\Delta\sigma_{eq,peak,weld\ toe} = 1.95\ MPa$$

$$\Delta\sigma_{eq,peak,gusset} = 2.12\ MPa$$

According to the PSM Brick 185 results, the gusset side is 8.7% more solicited than the weld toe. Hence, the PSM foresees a crack initiation in the wrong location. However, since the experimental results show fractures occurring at the weld toe, $\Delta\sigma_{eq,peak,weld\ toe}$ is chosen for the fatigue assessment. One of the reasons could lie in the fact that K^*_{FE} is not calibrated at the weld toe, where $2\alpha = 150°$, and consequently the results could appear lower than they actually are.

Curve junction

The same previous dispositions can be followed for the detection of the equivalent peak stress in the curve junction model. For an external applied pressure $\Delta\sigma_{nom}$=1 MPa, $\Delta\sigma_{eq,peak}$ is plotted along the weld toe and the gusset profiles:

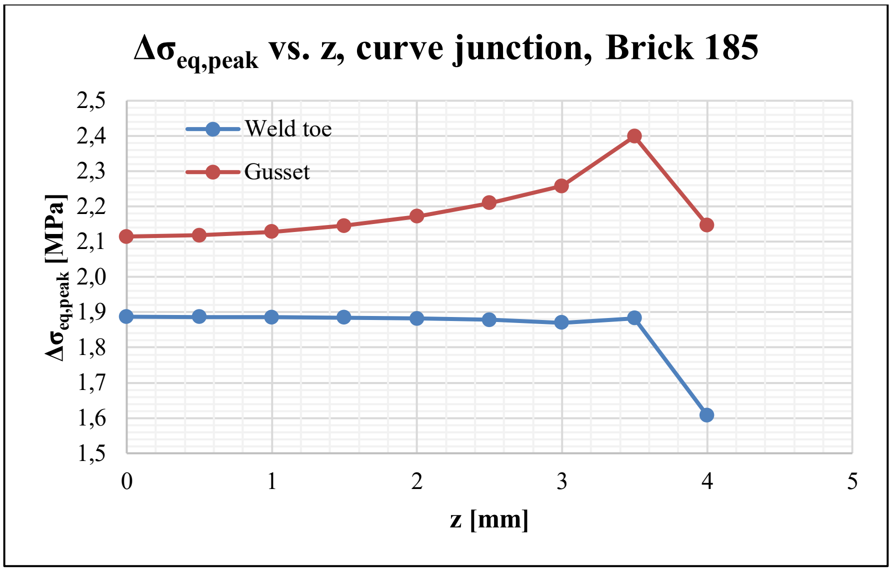

Figure 3. 21: equivalent peak stress with respect to the coordinate z, curve junction, Brick 185.

Some relevant observations must be drawn:

1. Despite the small thickness of the longitudinal attachment, with the Brick element adoption all the nodes belonging to the V-notch profiles can be selected;
2. As expected, due to the singular displacements, $\Delta\sigma_{eq,peak}$ at gusset side tends to increase along with z: the maximum equivalent peak stress is located at z = 3.5 mm; on the other hand, the presence of a curve junction eliminates the problem at the weld toe, where the stress raise is not evident;
3. Since the stress raise is due to numerical integration issues, it is decided to rely on the values at z = 0 mm, confirmed by the fact that the experimental data show fractures occurring in the centre of the stiffener edge.

For an external applied pressure $\Delta\sigma_{nom}$=1 MPa, the maximum $\Delta\sigma_{eq,peak}$, located at z=0 mm both at weld toe and gusset, is respectively equal to:

$$\Delta\sigma_{eq,peak,weld\ toe} = 1.89\ MPa$$

$$\Delta\sigma_{eq,peak,gusset} = 2.11\ MPa$$

According to the PSM Brick 185 results, the gusset side is 11.6% more solicited than the weld toe. Hence, the PSM foresees a crack initiation in the wrong location. However, since the experimental results show fractures occurring at the weld toe, $\Delta\sigma_{eq,peak,weld\ toe}$ is chosen for the fatigue assessment. Again, one of the reasons could lie in the fact that K^*_{FE} is not calibrated at the weld toe, where $2\alpha = 150°$, and consequently the results could appear lower than they actually are.

In the table below, all the $\Delta\sigma_{eq,peak}$, detected with the adoption of a straight and a curve junction, are reported along with the relative errors: all the errors fall below the engineering ±5%. Conclusively, it is proved that, in compliance with the right measures to be taken, the modelling of the two geometries seems to bring to the same results:

WELD TOE (K_{FE} not calibrated)	**Straight junction**	**Curve junction**	**Error straight/curve**
Tetra 187	*2.05*	*2.02*	*1.99%*
Brick 185	*1.95*	*1.89*	*3.17%*

GUSSET (K_{FE} calibrated)	**Straight junction**	**Curve junction**	**Error straight/curve**
Tetra 187	*2.05*	*2.16*	*5.4%*
Brick 185	*2.12*	*2.11*	*0.5%*

Finally, the equivalent peak stresses calculated at the weld toe with the two approaches are reported in the graphs below along with their respective error band provided by the literature (±15% for Tetra 187, and ±3% for Brick 185):

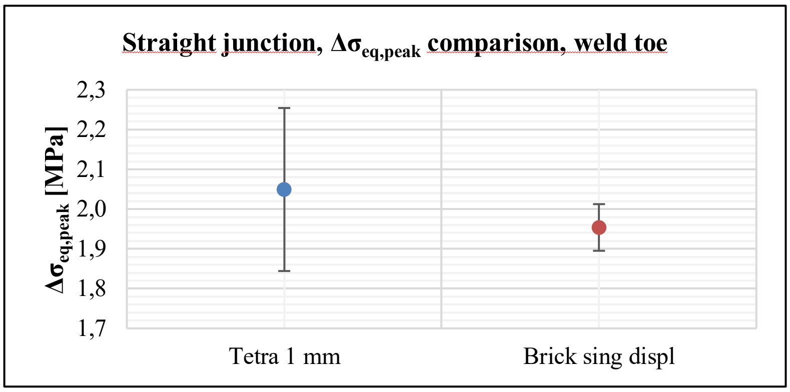

Figure 3. 22: with the modelling of a straight junction, $\Delta\sigma_{eq,peak}$ is between 1.90 MPa and 2.02 MPa.

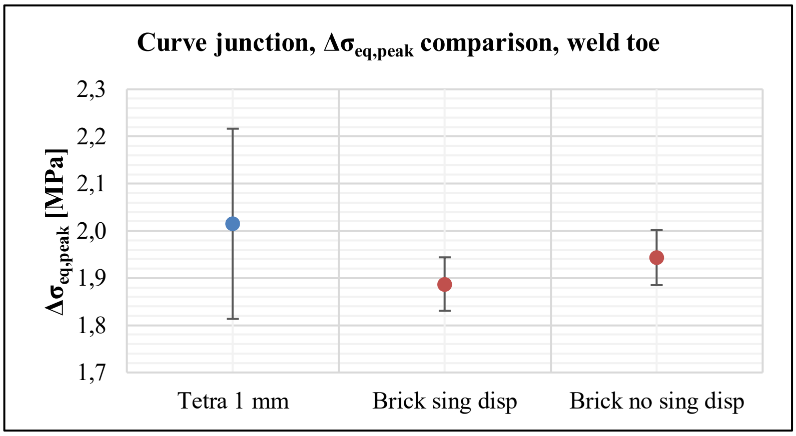

Figure 3. 23: with the modelling of a straight junction, $\Delta\sigma_{eq,peak}$ is between 1.83 MPa and 1.94 MPa. Please do not consider the "Brick no sing disp" value.

3.1.5 Data entry in the PSM curve

In the previous analyses, 1 MPa was applied to the main plate of the specimen; under linear elasticity hypotheses, the effective equivalent peak stress related to a specific $\Delta\sigma_{nom}$ can be detected with (3.2):

$$\Delta\sigma_{eq,peak} = \Delta\sigma_{eq,peak,1\ MPa} \cdot \Delta\sigma_{nom} \tag{3.2}$$

where:

- $\Delta\sigma_{eq,peak}$ is the effective equivalent peak stress for a specific external load;
- $\Delta\sigma_{nom}$ is the nominal applied stress;
- $\Delta\sigma_{eq,peak,1\ MPa}$ is the equivalent peak stress for a nominal stress equal to 1 MPa.

The results in terms of equivalent peak stress, calculated both with the PSM Tetra 187 and Brick 185, can be consulted in the Appendix C.

The experimental data are then entered inside the PSM design curve proposed by Meneghetti, Guzzella and Atzori under prevailing mode I:

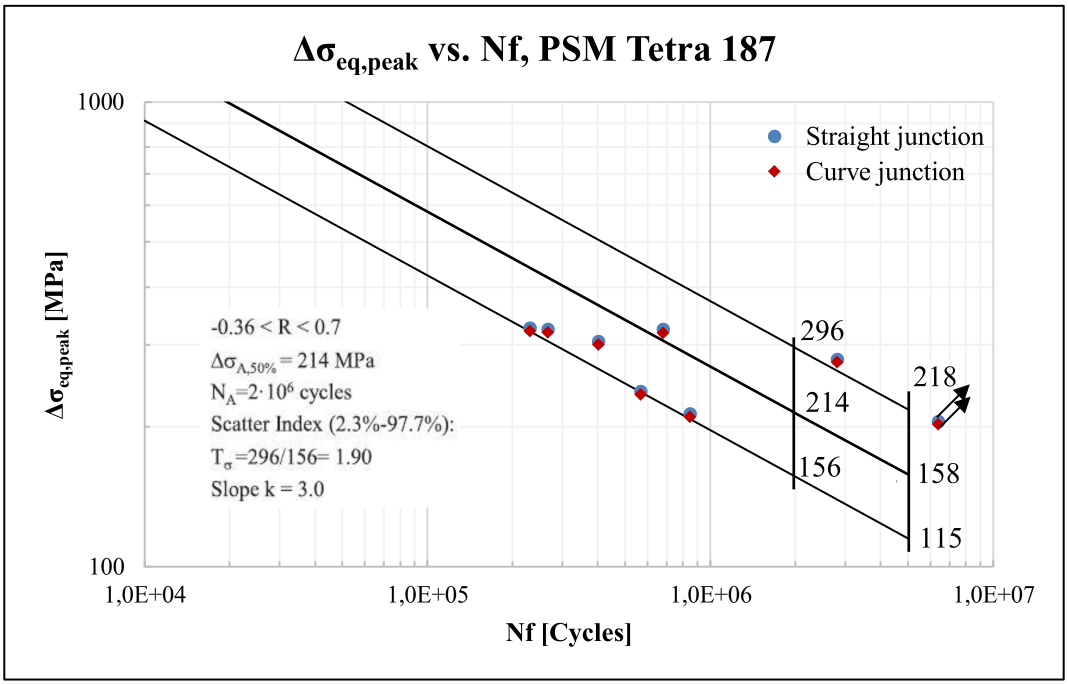

Figure 3. 24: data entry inside the PSM design curve, Tetra 187, straight and curve junction [28].

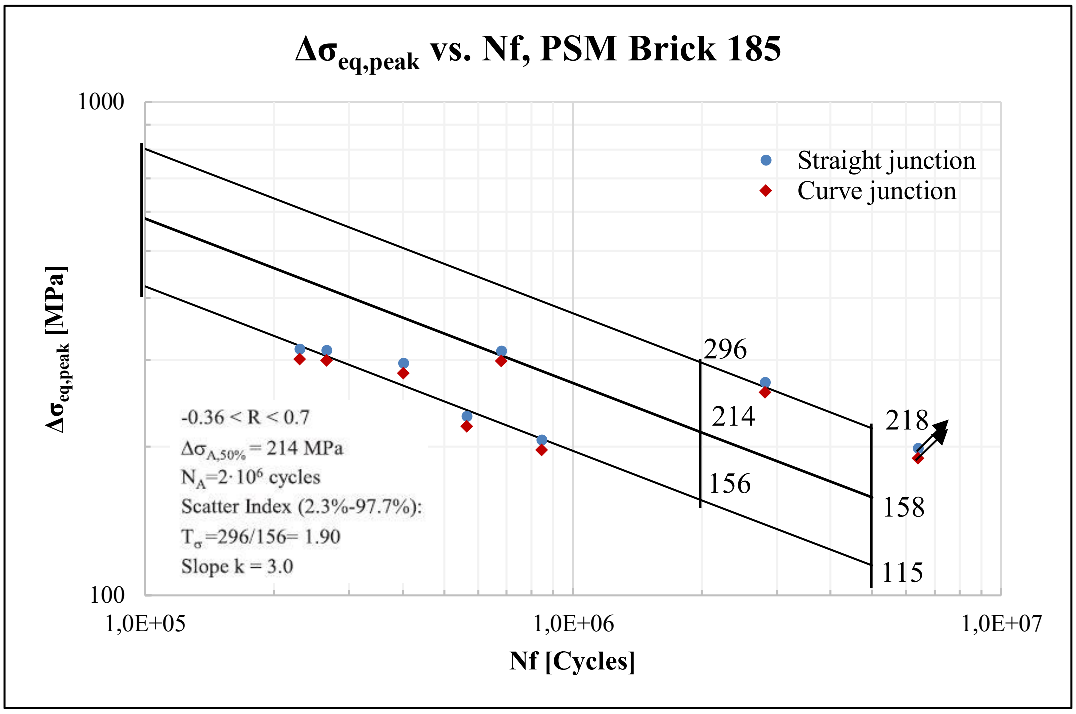

Figure 3. 25: data entry inside the PSM design curve, Brick 185, straight and curve junction [28].

The following conclusions can be drawn:

1. Either modelling with a straight or a curve weld junction, compatibility of results is achieved. Therefore, from now on, only FE models with curve junctions are going to be modelled;
2. Both the PSM Tetra 187 and Brick 185 approaches have erroneously foreseen the experimental crack initiation point at gusset side. However, since the experimental reality shows fractures occurring at the weld toe, those $\Delta\sigma_{eq,peak}$ values have been taken into account;
3. Most of the experimental data fall below the PS 50% curve, and, in case of Brick 185 elements, under the PS 97.7% curve: the PSM seems to lack of conservativeness. Several reasons could compete to this: first, the PSM underestimates the effects of non-uniform high residual stresses superimposed to external loads, as well as the real weld geometry; second, the PSM constants K_{FE} are not calibrated at the weld toe profile, where the V-notch opening angles is equal to 2α=150°.

3.1.6 SED for data validation

To check if the PSM low data are mostly due to the second problem, the SED method, valid for opening angles ranging between $0 < 2\alpha < 150°$, is employed.

In Ansys® APDL element library, Tetra 187 element is chosen; the Key-option K1 left to Pure displacement, which means that the nodal forces are only dependent from the displacements.

The SED method for 3D as-welded structures is based on the creation of a cylindrical sector of radius R0 = 0.28 mm, centred at the V-notch tip, extruded of 0.14 mm, (i.e. R0/2 due to the XY plane symmetry). The resulting volume is displayed in *Figure 3.26*:

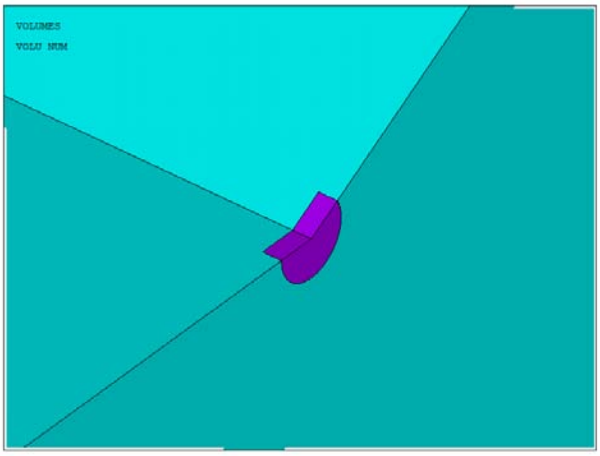

Figure 3. 26: structural volume for the average SED detection.

Concerning the meshing procedure, the structural volume lines are meshed with an element size equal to 0.04 mm, while the external lines are meshed in order to have smooth transition towards the cylindrical sector. Finally, a global element size of 1 mm is laid on the remaining volume. The output is illustrated in *Figure 3.27*:

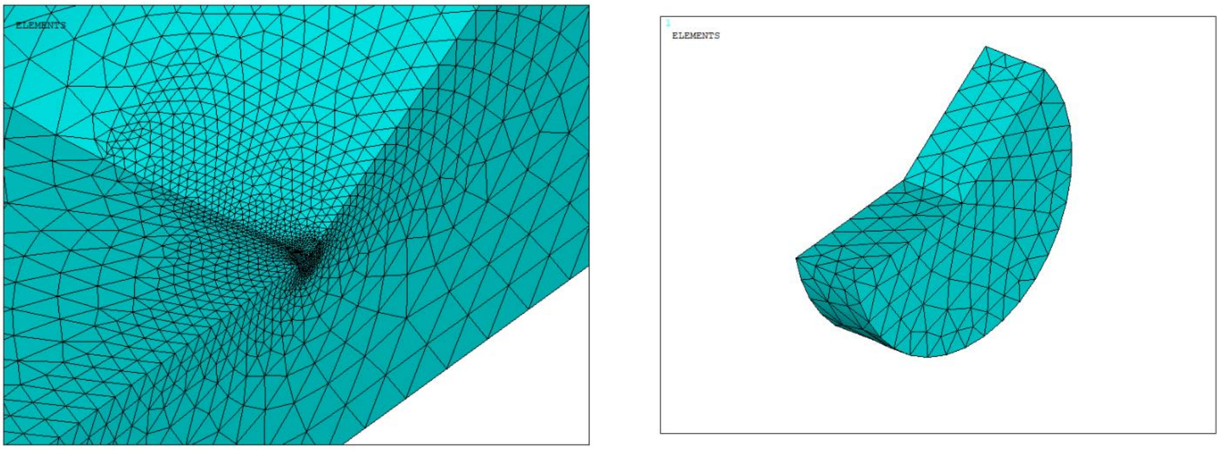

Figure 3. 27: on the left, the resulting mesh; on the right, representation of the structural volume, mesh size 0.04 mm.

The system can now be solved:

Main Menu > Solution > Solve > Current LS

3.1.7 SED, analysis of results

The averaged SED parameter is defined as the energy contained inside the structural volume. To obtain the average SED value, only the elements belonging to the cylindrical sector must be selected. In Ansys® APDL, the following commands have to be used:

Utility Menu > Select > Entities > Volumes > From Full

Utility Menu > Select > Everything Below > Selected Volumes

At this moment, a table containing both the energy (SENE) and volume (VOLU) of the selected elements has to be created:

Main Menu > General Postproc > Element Table

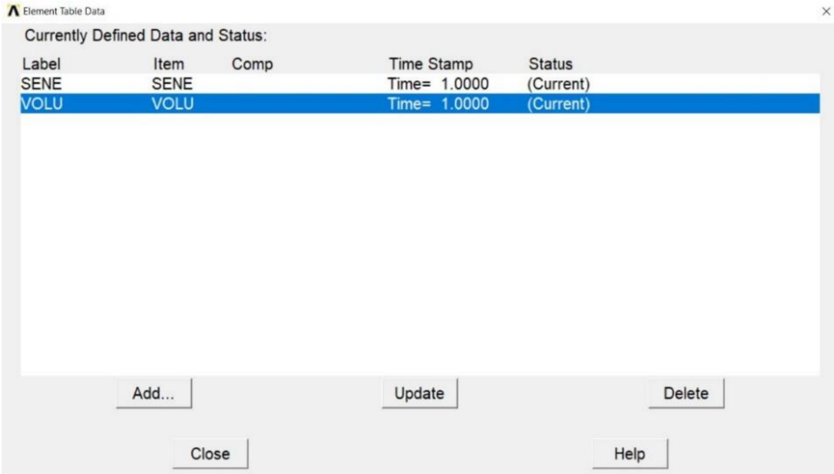

Figure 3. 28: element table in Ansys® APDL, where both SENE and VOLU are calculated.

Each single element SENE and VOLU values have now to be summed:

Main Menu > General Postproc > Element Table > Sum of Each Item

Finally, the SED value ($\Delta\overline{W}_{FEM}$ referring to FE software) is calculated as [33]:

$$\Delta\overline{W}_{FEM} = \frac{\sum_{V(R_0)} W_{FEM,i}}{V(R_0)} = \frac{SENE}{VOLU} = \left[\frac{MJ}{m^3}\right] \tag{3.3}$$

For an external applied pressure equal to $\Delta\sigma_{nom}$ = 159.72 MPa (i.e. the first experimental data), the resultant strain energy density detected with (3.3) is equal to:

$$SENE = 6.03 \cdot 10^{-3}\, J$$

$$VOLU = 0.0201126\, mm^3$$

$$SED = \frac{6.03 \cdot 10^{-3}}{0.0201126} = 0.300\ \frac{MJ}{m^3}$$

3.1.8 Data entry in the SED curve

In linear elasticity hypothesis, the SED value resulting from different external loads can be found with equation (3.4):

$$SED_{gen} = \left(\frac{\Delta\sigma_{gen}}{\Delta\sigma_{ref}}\right)^2 \cdot SED_{ref} \tag{3.4}$$

where:

- SED_{gen} is a generic SED that has to be detected;
- $\Delta\sigma_{gen}$ is the nominal stress related to the generic SED;
- SED_{ref} is the reference strain energy density;
- $\Delta\sigma_{ref}$ is the reference nominal stress.

The experimental data, consultable in Appendix C, are then entered inside the PSM design curve proposed by Lazzarin and Zambardi:

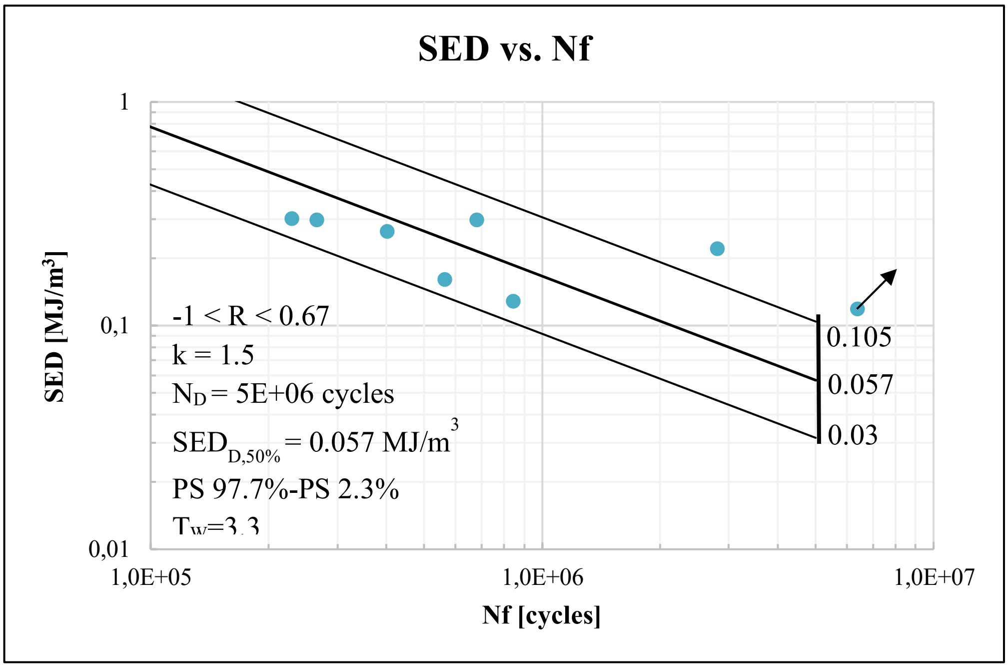

Figure 3. 29: data entry inside the SED design curve, Tetra 187, curve junction [6].

The following conclusions can be drawn:

1. The SED approach has correctly foreseen the experimental crack initiation point at weld toe;
2. Since the experimental data falls above the PS 97.7% line, the SED design curve has proven to be effective and conservative. Therefore, it is advised to validate a new PSM calibration constant for V-notch opening angles $2\alpha > 135°$.

3.1.9 Structural Hot-Spot Stress

In this paragraph, the fatigue assessment of the longitudinal stiffener FAT 71 is performed following the IIW recommendations [1] for the hot-spot stress extrapolation. In reference to the guideline, type "a" hot-spot is detected with the employment of fine mesh, as shown in *Figure 1.6*.

Proper mesh indications, concerning the stress extrapolation region, are given in the table below:

Element Type	Mesh algorithm	Main plate thickness t	Max element size	Adopted el. size
Brick 185 *KO: Simple Enhanced Strain*	Mapped	8 mm (4 mm modelled)	0.4*(t/2) = 1.6 mm	0.4 mm

According to [1], the structural hot-spot stress is extrapolated at two reference points located at 0.4t and 1.0t distance from the weld toe tip, it is to say 3.2 mm and 8 mm. In regard of the type of extrapolated stress, the graph below in *Figure 3.30* shows that, for an external pressure $\Delta\sigma_{nom}$=1 MPa applied on the parent material, after 1.2 mm σ_{11} and σ_{xx} are perfectly coincident, therefore the choice is indifferent.

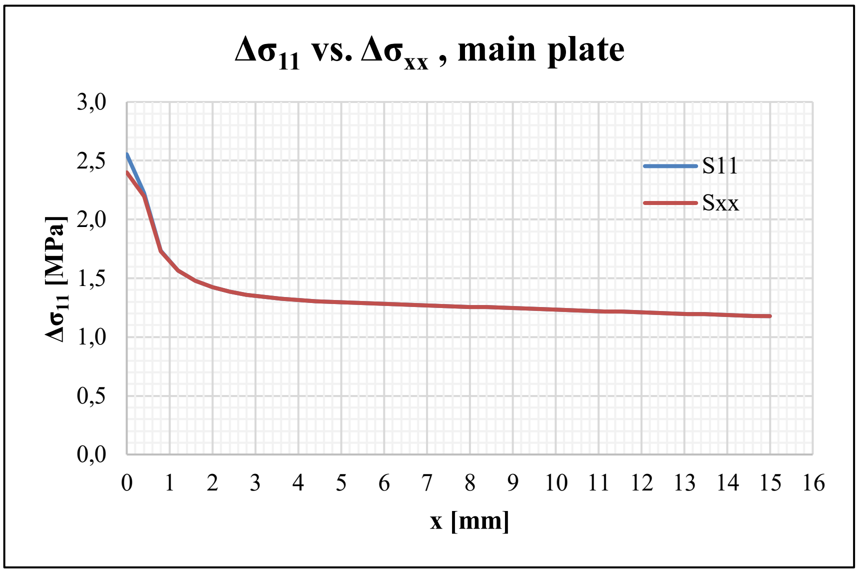

Figure 3. 30: $\Delta\sigma_{11}$ and $\Delta\sigma_{xx}$ plot starting from the weld toe tip.

The mesh pattern can be seen in *Figure 3.31*:

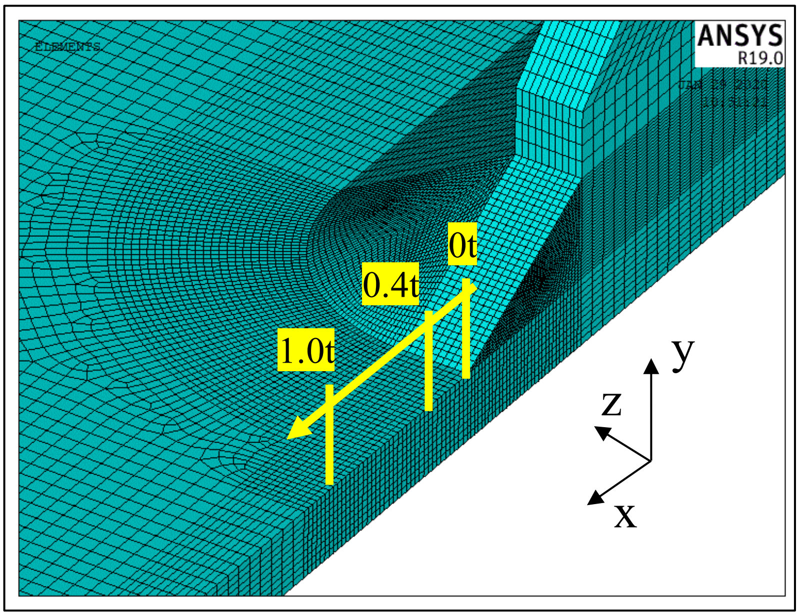

Figure 3. 31: mapped mesh pattern and extrapolation points indication.

For an external applied pressure equal to $\Delta\sigma_{nom}$=1 MPa, the resultant extrapolated stresses at the reference points are:

$$\Delta\sigma_{0.4t} = 1.34\ MPa$$

$$\Delta\sigma_{1.0t} = 1.26\ MPa$$

The structural hot-spot stress SHSS is finally detected with equation (1.2):

$$\Delta\sigma_{hs} = 1.67 \cdot \Delta\sigma_{0.4t} - 0.67 \cdot \Delta\sigma_{1.0t} = 1.39\ MPa \tag{3.5}$$

3.1.10 1-mm Stress

The fatigue assessment of the longitudinal stiffener FAT 71 is then performed with the employment of the 1-mm stress [3] method, proposing a stress extrapolation 1-mm below the weld toe tip, along the y direction in *Figure 3.32*.

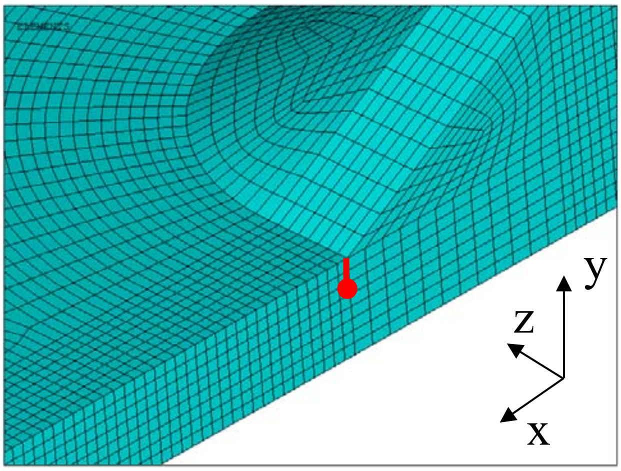

Figure 3. 32: mapped mesh conformation, d=0.5 mm, and indication of the node at 1-mm distance from the weld toe tip.

From a practical point of view, three main issues have to be discussed:

1. With respect to the SHSS approach, at 1-mm distance from the weld toe a 3% difference between σ_{11} and σ_{xx}, evidenced in *Figure 3.33,* is present:

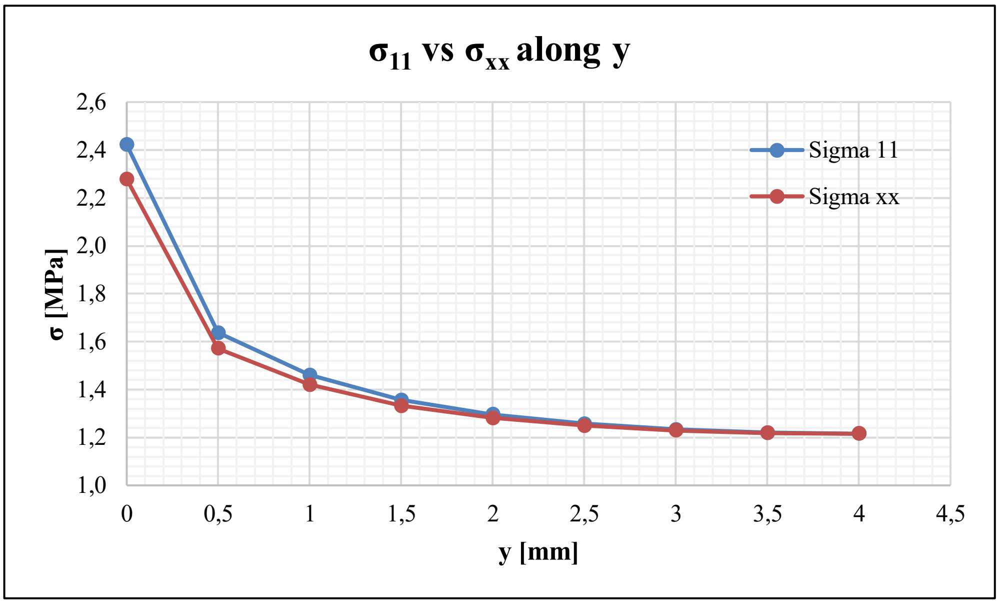

Figure 3. 33: differences between σ_{11} and σ_{xx} normal to the weld toe, element size 0.5 mm, 1 MPa applied stress.

   In his paper, as displayed in *Figure 1.8*, Xiao depicts σ_{xx}; on the other hand, Nussbaumer [40] in his round robin study on local approaches suggests the adoption of σ_{11}. However, it is clear that the stress difference is lower than the engineering $\pm5\%$;
2. Concerning the element choice, Nussbaumer [40] underlines that, even though bringing to the same result, quadratic elements usually need finer meshes than linear ones;

3. With regard to the element size, Xiao and Yamada [3] employ linear square 0.05 x 0.05 mm elements for 2D models and linear cubic 1x1x1 mm elements for 3D models.

Regardless of the choices, convergence analyses are recommended: as illustrated in *Figure 3.34*, the convergence is achieved for an element size of d = 0.5 mm, which is smaller than the one adopted by the authors.

Conclusively, the adopted measures for this simulation are shown in the table below:

Element	Mesh algorithm	Element size	Extrapolated Stress
Brick 185 *KOs: Simple Enhanced Strain*	Mapped	0.5 mm	$\Delta\sigma_{xx}$

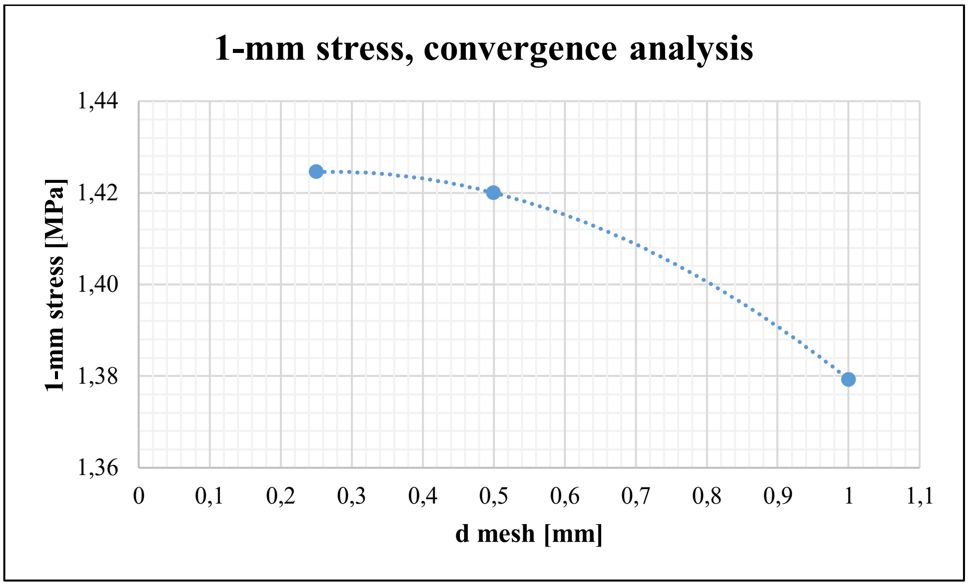

Figure 3. 34: convergence of 1-mm stress to varying of the element size.

For an external applied pressure equal to $\Delta\sigma_{nom}$=1 MPa, the resultant 1-mm stress $\Delta\sigma_{1\text{-mm}}$ is equal to:

$$\Delta\sigma_{1-mm} = 1.42\ MPa$$

3.1.11 Data entry in the IIW curves

Nominal approach

The experimental data in terms of nominal stress, reported at the beginning of paragraph 3.1, are entered inside the FAT 71 design curve proposed by the IIW guideline:

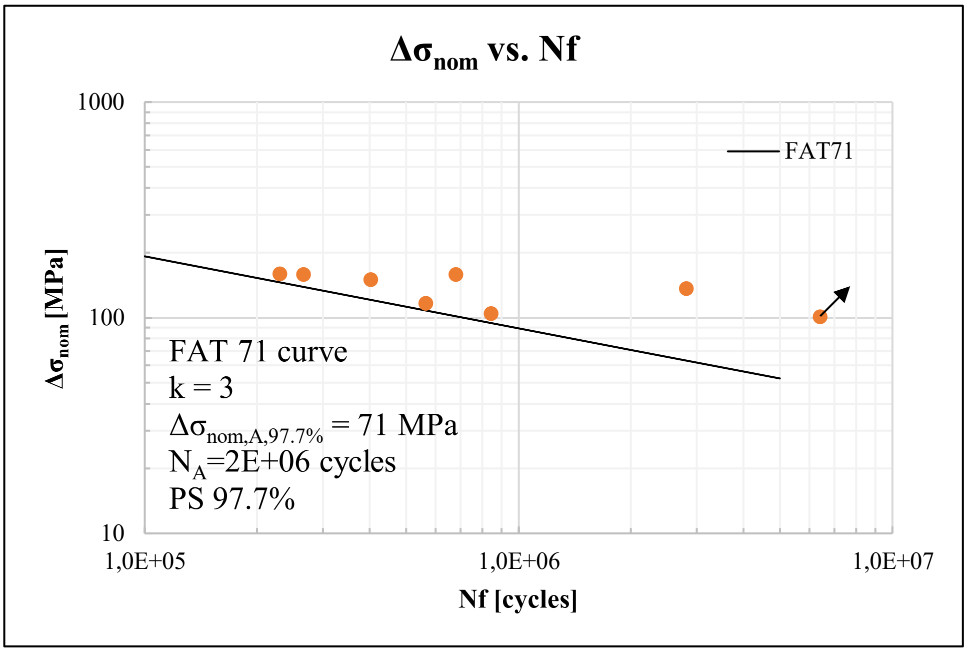

Figure 3. 35: data entry inside the FAT 71 design curve, global approach [1].

SHSS approach

In the previous analyses, 1 MPa was applied to the main plate of the specimen; under linear elasticity hypotheses, the effective SHSS related to a specific $\Delta\sigma_{nom}$ can be detected with (3.6)

$$\Delta\sigma_{hs} = \Delta\sigma_{hs,1\,MPa} \cdot \Delta\sigma_{nom} \tag{3.6}$$

where:

- $\Delta\sigma_{hs}$ is the effective hot-spot stress for a specified external load;
- $\Delta\sigma_{nom}$ is the nominal applied stress;
- $\Delta\sigma_{hs,1\,MPa}$ is the hot-spot stress for a nominal stress equal to 1 MPa.

The experimental data in terms of hot-spot stress, reported in Appendix C, are entered inside the FAT 100 design curve, for non-load carrying specimens, proposed by the IIW guideline:

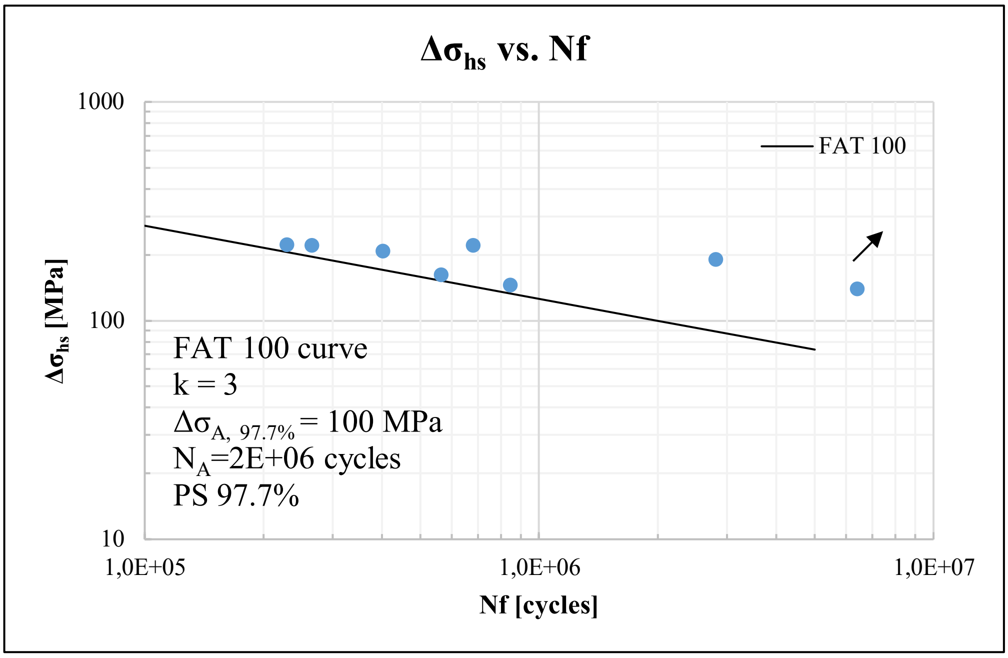

Figure 3. 36: data entry inside the hot-spot FAT 100 design curve [1].

<u>1-mm stress approach</u>

In the previous analyses, 1 MPa was applied to the main plate of the specimen; under linear elasticity hypotheses, the effective 1-mm stress related to a specific $\Delta\sigma_{nom}$ can be detected with (3.7)

$$\Delta\sigma_{1-mm} = \Delta\sigma_{1-mm,1\,MPa} \cdot \Delta\sigma_{nom} \tag{3.7}$$

where:

- $\Delta\sigma_{1-mm}$ is the effective 1-mm stress for a specified external load;
- $\Delta\sigma_{nom}$ is the nominal applied stress;
- $\Delta\sigma_{1-mm,1\,MPa}$ is the hot-spot stress for a nominal stress equal to 1 MPa.

The experimental data in terms of 1-mm stress, reported in Appendix C, are entered inside the reference detail design curve, proposed by Xiao and Yamada:

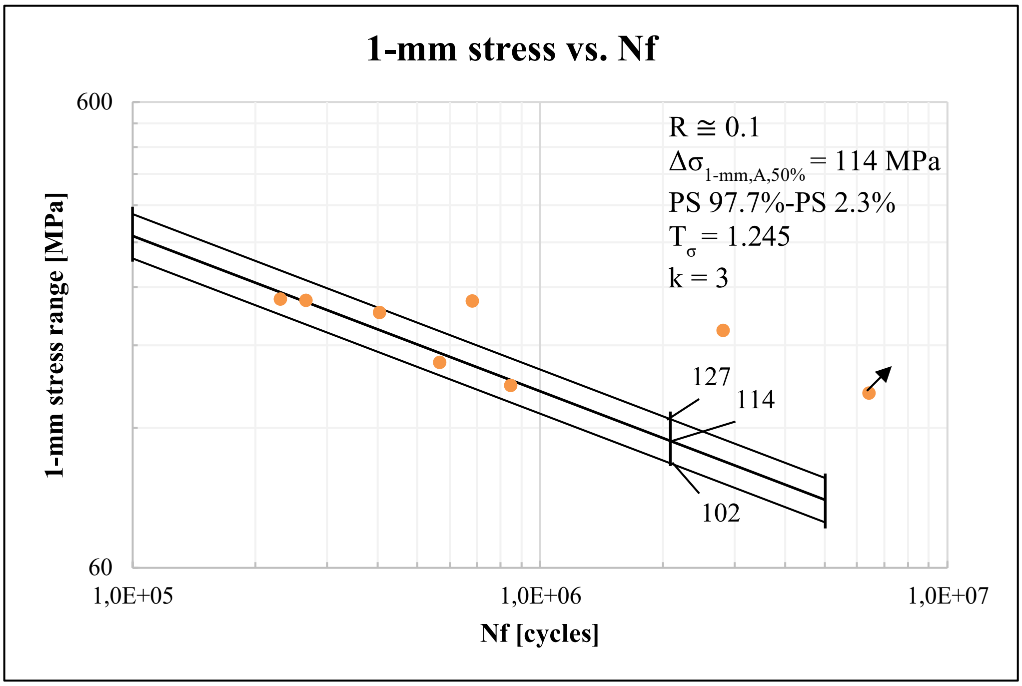

Figure 3. 37: data entry inside 1-mm design curve [3].

The following conclusions can be drawn:

1. These methods have correctly been applied to the FAT 71 welded joint, for weld toe fractures;
2. Since the experimental data falls above the PS 97.7% line, both the design curves have proven to be effective and conservative.

3.1.12 Fatigue life comparison

The fatigue life comparison is performed in terms of equivalent nominal stress. For a PS 97.7%, at 2 million cycles, the corresponding equivalent stress is found with formula (3.8):

$$\sigma_{nom,2\cdot10^6} = \frac{\sigma_{ref,2\cdot10^6}}{\sigma_{ref,1\ MPa}} \tag{3.8}$$

where:

- $\sigma_{nom,2\cdot10^6}$ is the equivalent nominal fatigue class that has to be detected;
- $\sigma_{ref,2\cdot10^6}$ is the real stress $(\sigma_{eq,peak}, \sigma_{hs}, \sigma_{1-mm})$ at two million cycles;
- $\sigma_{ref,1\ MPa}$ is the reference stress for a nominal stress of 1 MPa.

Starting from the $\sigma_{nom,2\cdot10^6}$, the equivalent nominal fatigue class is then created, knowing that the imposed inverse slope is equal to k=3. Finally, the experimental data are inserted in the graph in *Figure 3.38*:

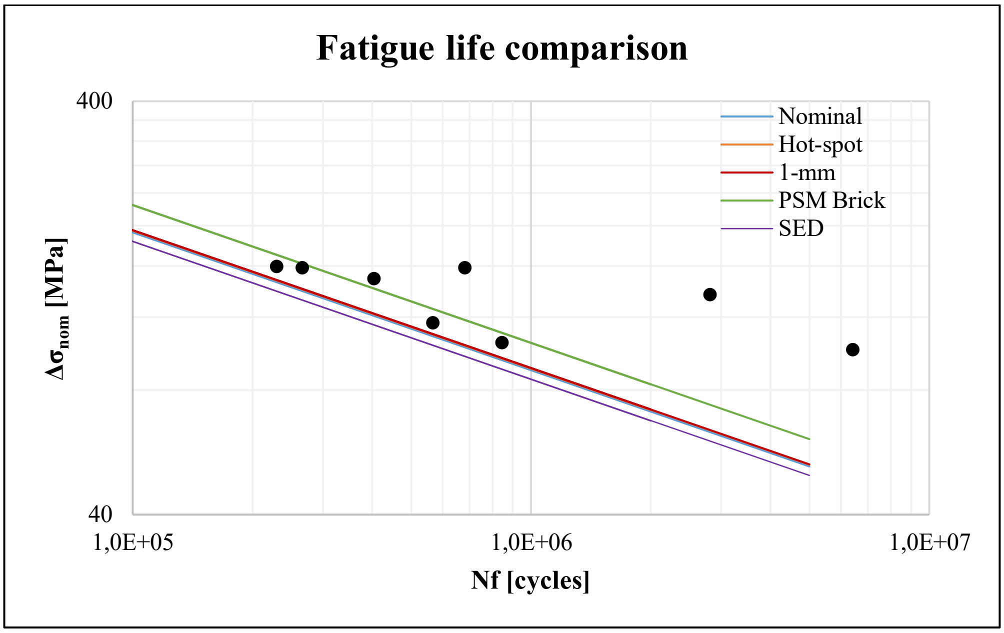

Figure 3. 38: fatigue life in terms of "equivalent" nominal stress.

Some relevant conclusions can be drawn:

- PSM is the least conservative method, because it is not calibrated for this specimen;
- SED method, since calibrated, is the most conservative one. With respect to the PSM, it foresees nearly 100 000 fatigue cycles less;
- IIW global and local approaches give similar results in terms of fatigue life.

3.2 Longitudinal attachment, FAT 63

The second welded joint category to be assessed is a longitudinal stiffener, fatigue class FAT 63, tested by Yildirim et al. in 2013 [35] under constant amplitude loading CAL.

Specific information on the components is reported below:

Weld condition	**Fracture location**	**Load application**	**Main plate/gusset thickness**
As-welded, non-load carrying, full penetration	*Weld toe*	*Axial, main plate, parent material*	*Main plate:5-20 mm* *Gusset: 5-20 mm*

The mechanical properties are described below:

Materials	**Yield strength f_y**	**Young modulus**	**Poisson's ratio ν**
S700MC, HSS, linear elastic, isotropic	*700 MPa*	*206000 MPa*	*0.3*
S690QL, HSS, linear elastic, isotropic	*690 MPa*		

In regard of the main geometrical quantities, *Figure 3.39* shows the most relevant information. Only the three specimens highlighted in *Figure 3.40* are assessed:

- S700MC, main plate and gusset thickness = 10 mm;
- S690QL, main plate and gusset thickness = 10 mm;
- S690QL, main plate and gusset thickness = 20 mm.

Since both the geometry and material steel grade f_y are common, the first two models are together analysed as a single 10-mm specimen, while the third one is assessed separately as a 20-mm specimen.

As affirmed by Hobbacher in his IIW guideline [1], the influence of misalignments can be neglected in continuous welds longitudinally loaded.

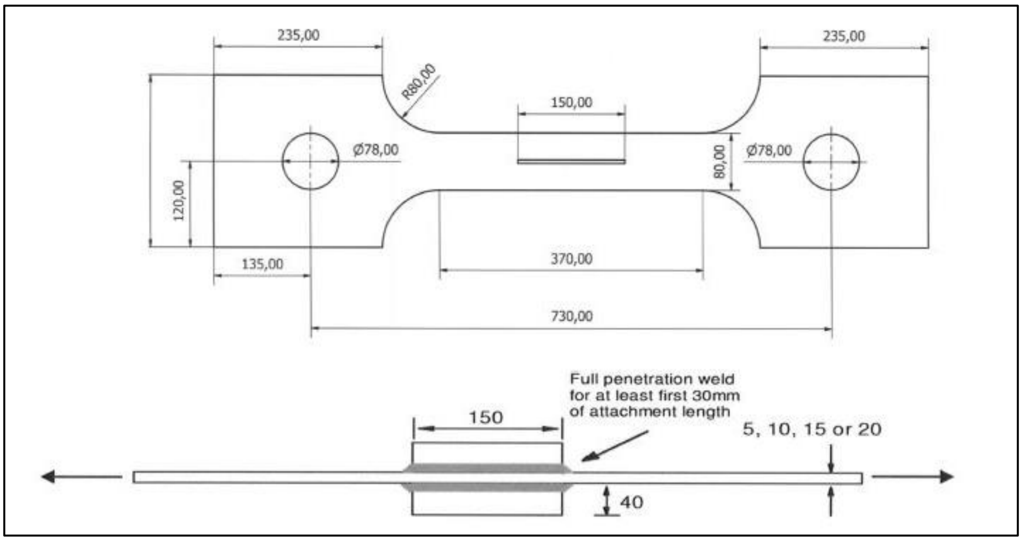

Figure 3. 39 geometrical parameters, expressed in [mm] [35].

Material grade	Thickness	supplier / brand name
S700 MC	5 mm	AM S700 MC
S700 MC	10 mm	AM S700 MC
S690 QL	10 mm	SSAB Weldox 700
S690 QL	20 mm	AM Supralsim 690
S960 MC	5 mm	SSAB Domex 960
S960 QL	10 mm	AM SuperElso 960
S960 QL	15 mm	SSAB Weldox 960

Figure 3. 40: list of the several main plate and gusset thicknesses and material steel grade [35].

Since no information is available, assumptions on the weld profile parameters have to be made:

1. The radius of the weld toe tip ρ is set to 0, to obtain a V-notch (worst case);

2. Concerning the weld throat and flank angle, reference is made to *Figure 3.41*, which displays the shape of the weld preparation for each longitudinal attachment.

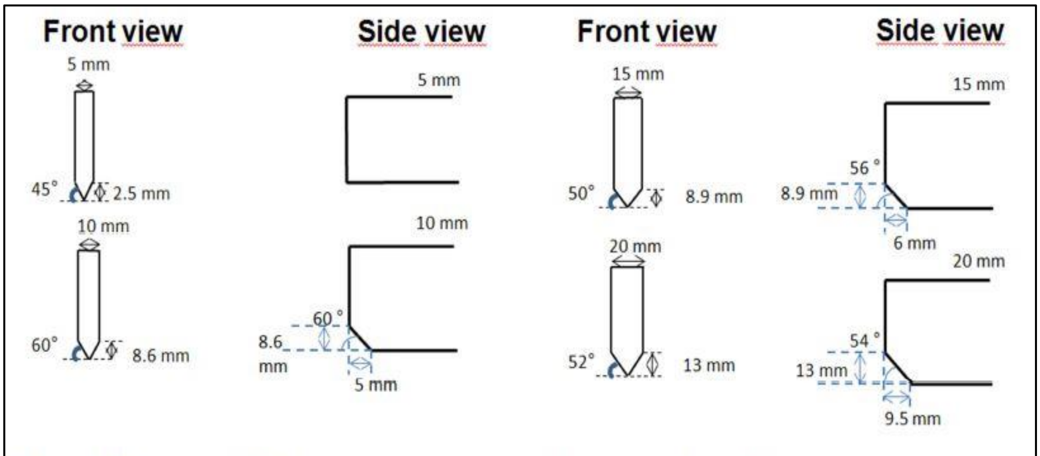

Figure 4: *Overview of the different welding preparations depending on the thickness*

Figure 3. 41: Overview of the different welding preparations depending on the thickness [35].

Focusing on the front and side views of the 10-mm and 20-mm gussets, the weld profile is supposed to be obtained by the mirroring the bevel. To justify this choice, *Figure 3.42*, taken from the FATWELDHSS report [35], represents the shape of the 10-mm specimen weld toe after laser re-melting treatment. As it can be noticed, before the operation the weld flank has an angle of nearly 60°.

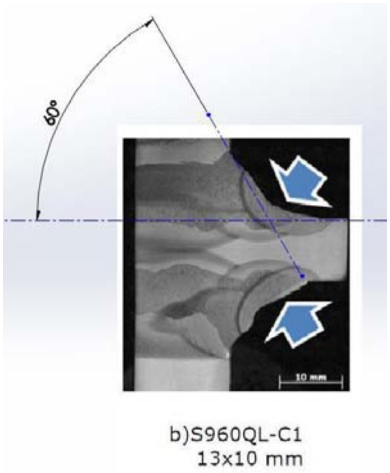

Figure 3. 42: Macro-sections of laser re-melted welded fatigue samples S960QL. The image is only taken to validate the assumption. No analyses were performed with this kind of treatment [35].

Concerning the 20-mm specimen, the 54° angle is brought to 60°, keeping the weld leg equal to 13 mm, so that the PSM can be properly applied, besides increasing the singularity at the V-notch, in safety advantage.

As a result of these assumptions, the weld profile parameters are described in the table below:

t [mm]	ρ weld toe tip [mm]	Weld throat [mm]	Weld flank angle
10	*0*	*4.3*	*60°*
20	*0*	*6.5*	*60°*

The experimental data are reported in terms of nominal stress $\Delta\sigma_{nom}$. In barred, the runouts.

t = 10 mm

Steel Grade	**R**	**$\Delta\sigma_{nom}$ [MPa]**	**N_f [cycles]**
S690QL	0.1	~~50~~	~~10 000 000~~
		~~70~~	~~10 000 000~~
		90	3 466 968
		200	204 202
		250	112 546
		350	47 716
S700MC	0.5	~~50~~	~~10 000 000~~
		70	2 333 651
		90	893 070
		200	88 800
		250	49 800
		300	33 700

t = 20 mm

Steel Grade	**R**	**$\Delta\sigma_{nom}$ [MPa]**	**N_f [cycles]**
S690QL	0.1	70	3 600 954
		90	1 513 276
		200	125 887
		250	113 433
		350	41 521
S690QL	0.5	~~70~~	~~10 000 000~~
		90	1 612 500
		125	828 000
		200	136 936
		250	85 459
		300	49 546

Among the conclusions of the previous fatigue assessment on longitudinal attachment FAT 71, either modelling with a straight or a curve junction compatibility of results is achieved; as a consequence, the FE models are designed only with a curve weld junction: *Figure 3.43* and *Figure 3.44* respectively display the 10-mm and 20-mm specimens. The modelling, constraints and loading procedures follow the same dispositions adopted for the preceding longitudinal FAT 71.

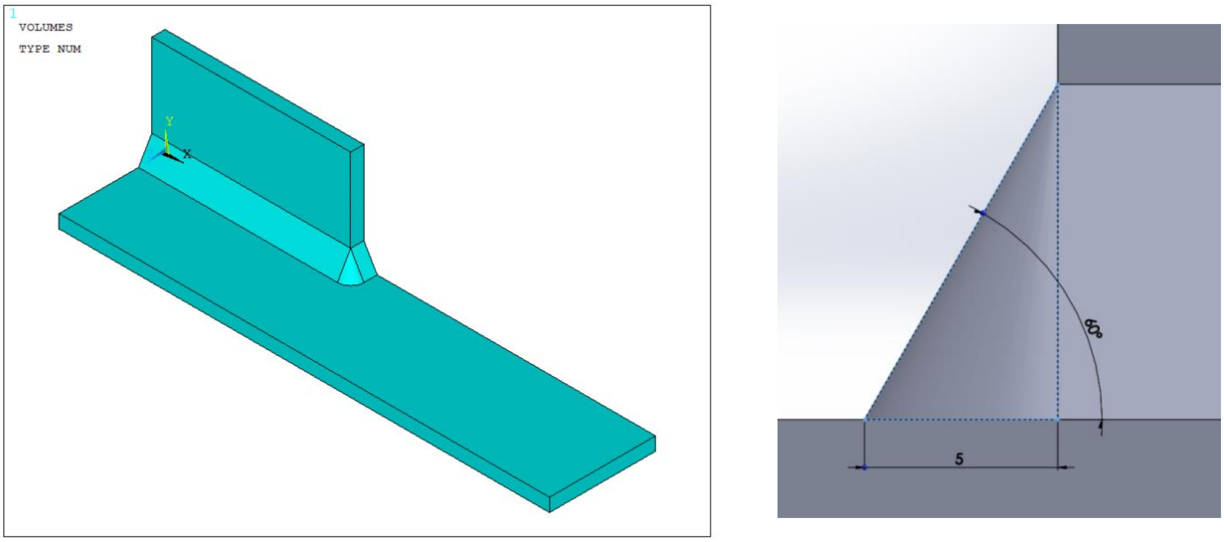

Figure 3. 43: FAT 63 10-mm model, with an enlargement on the weld profile.

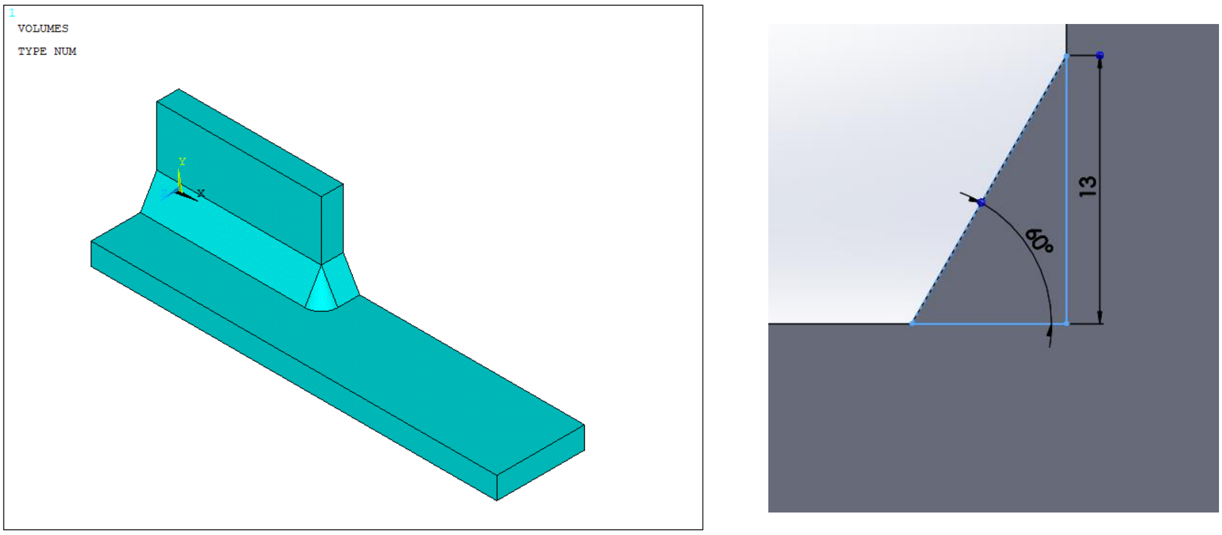

Figure 3. 44: FAT 63 20-mm model, with an enlargement on the weld profile.

3.2.1 PSM Tetra 187

The fatigue assessment is performed in terms of equivalent peak stress, with the adoption of the Peak Stress Method for 3D structures, ten-node quadratic elements.

From Ansys® APDL element library, Tetra 187 element is chosen; the Key Option K1 is left to *Pure displacement*, which means that the nodal forces are only dependent upon the displacements.

From a preliminary analysis, it can be inferred that FAT 63 fillet weld is solicited under prevailing mode I at the attachment edge, while mode II is null since $2\alpha > 102.5°$; mode III is rigorously null in the attachment edge, while in the junction part it becomes singular.

The weld toe V-notch opening angle is equal to $2\alpha = 120°$, therefore the PSM calibration constants are valid; vice versa, the gusset now has an opening angle equal to $2\alpha = 150°$, therefore the available

K_{FE} related to 2α = 135° are extended to 2α = 150°, even though the procedure is not rigorous. Regarding the parameters λ_3 and e_3, valid for axisymmetric structures, the invalid extension to non-axisymmetric geometries is applied too.

Under combined mode I and III loadings, the PSM Tetra 187 requirements at the weld toe and gusset, which hold true for both 10-mm and 20-mm specimens, are listed below:

Location: weld toe (2α=120°)

Element Type	Mesh algorithm	***Mode I***		
		$(a/d)_{min}$	**2α**	**Mesh pattern**
Tetra 187 *KO: Pure Displacement*	Free	1	120°	No particular indications
		Mode III		
		$(a/d)_{min}$	**2α**	**Mesh pattern**
		3	120°	No particular indications

Location: gusset (2α=150°)

Element Type	Mesh algorithm	***Mode I***		
		$(a/d)_{min}$	**2α**	**Mesh pattern**
Tetra 187 *KO: Pure Displacement*	Free	1	135° extended	No particular indications
		Mode III		
		$(a/d)_{min}$	**2α**	**Mesh pattern**
		3	135° extended	No particular indications

Hence, according to the table, a minimum ratio $\frac{a}{d} > 3$ must be respected.

Under these restrictions, at the weld toe (2α = 120°) the mode I calibration constant is equal to $K^{*}_{FE} = 1.05 \pm 15\%$, while the mode III constant is equal to $K^{***}_{FE} = 1.70 \pm 10\%$; at the gusset (2α = 150°) the extended mode I PSM calibration constant is equal to $K^{*}_{FE} = 1.21 \pm 10\%$, while the extended mode III constant is $K^{***}_{FE} = 1.70 \pm 10\%$.

For the 10-mm specimen, the following PSM dispositions are thus adopted:

- Half the main plate thickness a is equal to a = 5 mm;
- The mesh global element size is set to d = 1 mm;
- $\frac{a}{d} = \frac{5}{1} = 5 > 3$ the ratio is respected;
- The λ_1, λ_3, e_1, e_3 values associated to the weld toe (2α = 120°) and gusset (2α = 150°) required for f_{w1} and f_{w3} detection respectively are:

2α	λ_1	e_1	λ_3	e_3
120° (weld toe)	*0.616*	*0.129*	*0.750*	*0.275*
150° (gusset)	*0.752*	*0.104*	*0.857*	*0.258*

Finally, the corrective stress factors under mode I and III at the weld toe calculated with equation (1.16) are $f_{w1} = 0.912$ and $f_{w3} = 1.820$ while at gusset they respectively are equal to $f_{w1} = 0.876$ and $f_{w3} = 1.654$.

For the 20-mm specimen, the following PSM dispositions are thus adopted:

- Half the main plate thickness a is equal to a = 10 mm;
- The mesh global element size is set to d = 1 mm;
- $\frac{a}{d} = \frac{10}{1} = 10 > 3$ the ratio is respected;
- The λ_1, λ_3, e_1, e_3 values associated to the weld toe main plate side ($2\alpha = 120°$) and at gusset ($2\alpha = 150°$) required for f_{w1} and f_{w3} detection are the same as the 10-mm specimen.

3.2.2 PSM Tetra 187, analysis of results

For the equivalent peak stress detection, the same procedures and dispositions of the previous FAT 71 analysis, consultable in paragraph 3.1, are followed.

<u>10-mm specimen</u>

The averaged nodal $\Delta\sigma_{eq,peak,avg}$ values are plotted in an Excel graph with respect to the coordinate z, defined as the nodal distance from the XY plane of symmetry:

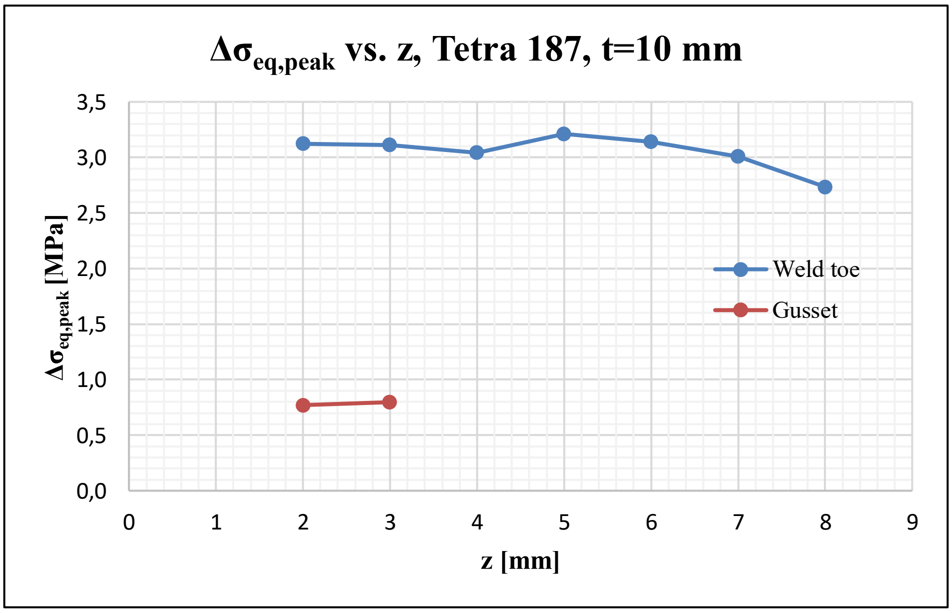

Figure 3. 45: averaged equivalent peak stress vs. z, t=10 mm.

Some relevant observations must be drawn:

1. Due to the intrinsically irregular mesh, the peak stress irregularly varies along the notch tip profile even in the case of a constant applied NSIF;
2. The edge node at z=0 mm is not selected; for this reason, the node at z=1 mm, cannot be averaged. The equivalent peak stress raise is not happening because the free edge at z=5 mm is replaced by the curve junction;
3. Since $\Delta\sigma_{eq,peak}$ in the weld junction is decreasing after 5 mm, the plotting can be interrupted;

For an external applied pressure $\Delta\sigma_{nom}$=1 MPa, the maximum $\Delta\sigma_{eq,peak,avg}$, located at z=2 mm both at weld toe and gusset, is respectively equal to:

$$\Delta\sigma_{eq,peak,avg,weld\ toe} = 3.13\ MPa$$

$$\Delta\sigma_{eq,peak,avg,gusset} = 0.80\ MPa$$

According to the PSM Tetra 187 results, the gusset is much less solicited than the weld toe. Hence, the PSM foresees a crack initiation in the exact location; one of the reasons lies in the fact that K^{*}_{FE} and K^{***}_{FE} are now calibrated at the weld toe, where $2\alpha = 120°$.

<u>20-mm specimen</u>

The averaged nodal $\Delta\sigma_{eq,peak,avg}$ values are plotted in an Excel graph with respect to the coordinate z, defined as the nodal distance from the XY plane of symmetry:

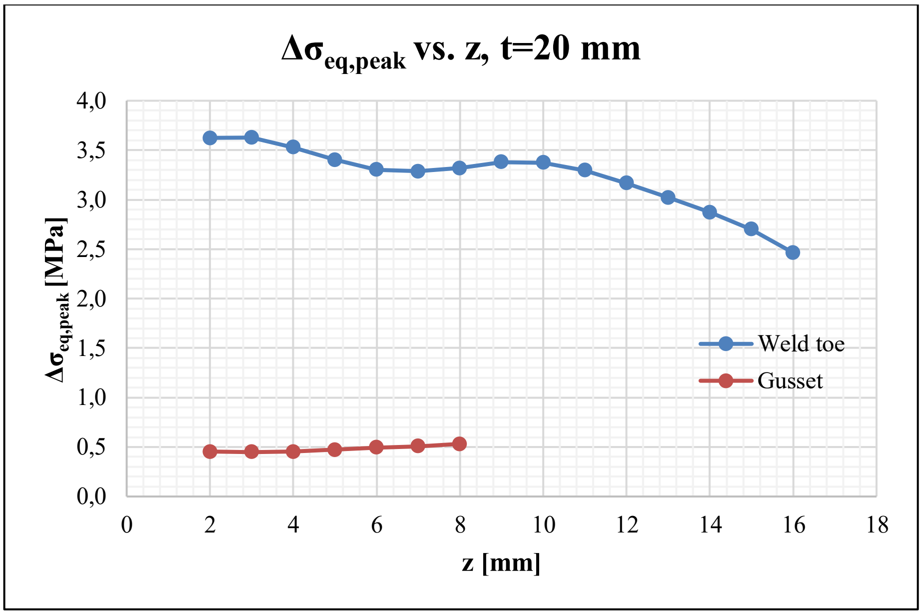

Figure 3. 46: averaged equivalent peak stress vs. z, t=20 mm.

Respectively, the maximum average equivalent peak stress $\Delta\sigma_{eq,peak,avg}$ at weld toe and gusset side, for z = 2 mm for an external applied pressure $\Delta\sigma_{nom}$ = 1 MPa, is equal to:

$$\Delta\sigma_{eq,peak,avg,weld\ toe} = 3.63\ MPa$$

$$\Delta\sigma_{eq,peak,avg,gusset} = 0.53\ MPa$$

Even this time, the gusset is much less solicited than the weld toe, and the PSM correctly foresees the crack development point at the weld toe.

3.2.3 PSM Brick 185

The fatigue assessment is now performed in terms equivalent peak stress with the adoption of the Peak Stress Method for 3D structures, eight-node linear elements.

The weld toe V-notch opening angle is equal to 2α=120°, therefore the PSM calibration constants are valid; vice versa, the gusset has now an opening angle equal to 2α=150°, therefore the available PSM calibration constants related to 2α=135° are extended to 2α=150°, even though the procedure is not rigorous. Regarding the parameters λ_3 and e_3, valid for axisymmetric structures, the invalid extension to non-axisymmetric geometries is applied too.

<u>Main model</u>

From Ansys® APDL element library, Tetra 187 element is chosen; the Key Option K1 is left to *Pure displacement*, which means that the nodal forces are only dependent from the displacements.

The 10-mm and 20-mm main models are respectively illustrated in *Figure 3.43* and *3.44*. The appropriate location of the cut boundary is determined with a convergence analysis.

- For the 10-mm specimen, three different meshes, with global element size respectively equal to 0.8, 1 and 2 mm, are laid on the main model;
- For the 20-mm specimen, three different meshes with global element size respectively equal to 1.5, 2 and 3 mm are laid.

The first principal stress range $\Delta\sigma_{11}$ is then extracted along the longitudinal direction, starting from the weld toe tip, as illustrated in *Figure 3.47*:

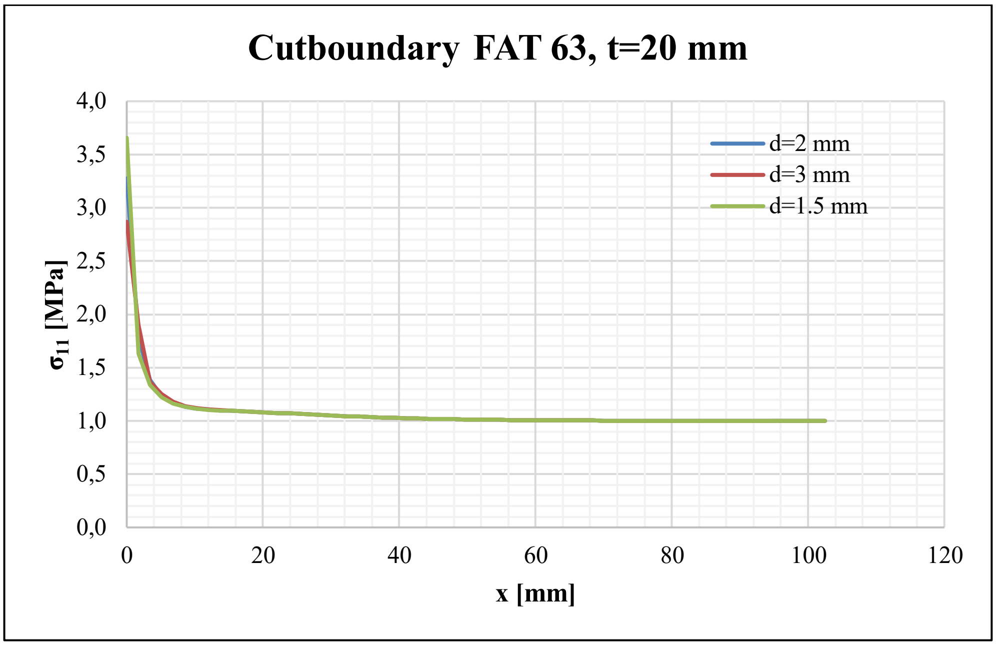

Figure 3. 47: convergence analysis for the cut boundary creation, example of t=20 mm.

As it can be noticed in *Figure 3.47*, the local stresses cannot converge because the stress value is function of the element size. At x = 15 mm, compatibility between the results is clearly achieved, therefore the cut boundary is placed at that distance of 15 mm from the weld toe.

Submodel

In Ansys® APDL element library, Brick 185 element is chosen; the Key Option K1 is switched to *Simple Enhanced Strain*.

Since mode III loading has a neglectable influence on the overall results in terms of $\Delta\sigma_{eq,peak}$, only mode I is considered in this analysis. The submodel creation follows the same dispositions previously adopted for the FAT 71 specimen.

Under mode I loading, the PSM Brick 185 requirements at the weld toe and gusset, which hold true for both 10-mm and 20-mm specimens, are listed below:

Location: weld toe (2α=120°) ***Mode I***

Element Type	Mesh algorithm	$(a/d)_{min}$	2α	Mesh pattern $2\alpha < 90°$	Mesh pattern $2\alpha > 90°$
Brick 185 *KOs: Simple Enhanced Strain*	Mapped	3	$0° < 2\alpha < 135°$	Four adjacent elements share the same node	Two adjacent elements share the same node

Location: gusset (2α=150°) **Mode I**

Element Type	**Mesh algorithm**	**$(a/d)_{min}$**	**2α**	**Mesh pattern 2α < 90°**	**Mesh pattern 2α > 90°**
Brick 185 *KOs: Simple Enhanced Strain*	Mapped	3	135° extended	Four adjacent elements share the same node	Two adjacent elements share the same node

Hence, according to the table, a minimum ratio $\frac{a}{d} > 3$ must be respected.

Under these restrictions, the mode I PSM calibration constant is equal to $K^*_{FE} = 1.38 \pm 3\%$.

For the t = 10 mm, the following PSM dispositions are thus adopted:

- Half the main plate thickness a is equal to a = 5 mm;
- The mesh global element size is set to d = 0.5 mm;
- $\frac{a}{d} = \frac{5}{0.5} = 10 > 3$ the ratio is respected;
- The λ_1 and e_1 values associated to the weld toe (2α = 120°) and gusset (2α = 150°) required for f_{w1} detection respectively are:

2α	**λ_1**	**e_1**
120° (weld toe)	*0.616*	*0.129*
150° (gusset)	*0.674*	*0.104*

Finally, the corrective stress factors under mode I at the weld toe calculated with equation (1.16) is $f_{w1} = 0.918$, while at the gusset $f_{w1} = 0.797$.

For the t = 20 mm, the following PSM dispositions are instead adopted:

- Half the main plate thickness a is equal to a=10 mm;
- The mesh global element size is set to d=1 mm;
- $\frac{a}{d} = \frac{10}{1} = 10 > 3$ the ratio is respected;
- The λ_1 and e_1 values associated to the weld toe main plate side (2α=120°) required for f_{w1} detection are the same as the previous ones.

Finally, the corrective stress factors under mode I at the weld toe with equation (1.16) is $f_{w1}=1.198$, while at the gusset $f_{w1}=0.999$.

The submodels are created with the extrusion of the sectional areas by 5 mm and 10 mm (half the two gusset thicknesses) along the global Z-axis, which are pre-meshed in respect of the PSM requirements. The resulting meshes are visible in *Figure 3.48* and *Figure 3.49*, on the right. The number of extruded elements must be chosen so that to have cubic elements.

- For the t=10 mm, ten element extrusion divisions may lead to cubic elements:

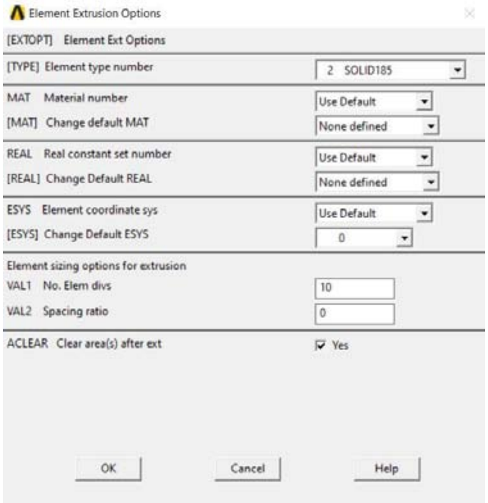

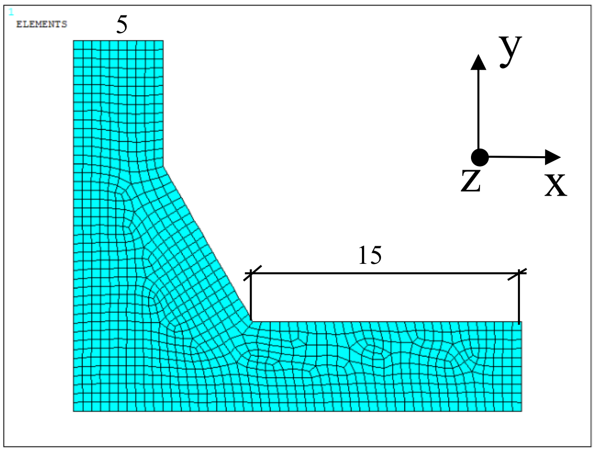

Figure 3. 48: on the left, the element extrusion options; on the right, the initial area which has to be extruded, t = 10 mm. The mesh pattern requested by the PSM is respected. In black, the global coordinate system.

- For the t=20 mm, ten element extrusion divisions may lead to cubic elements:

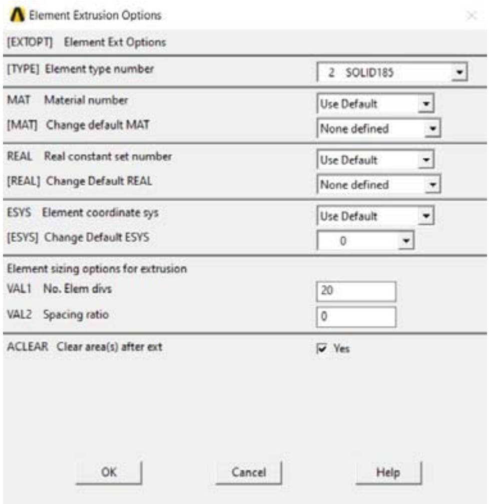

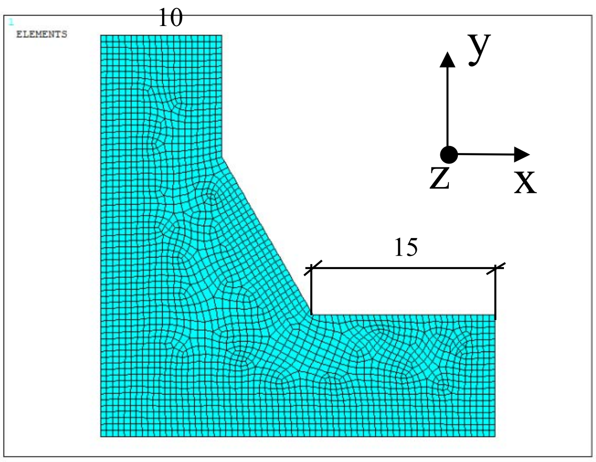

Figure 3. 49: on the left, the element extrusion options; on the right, the initial area which has to be extruded, t = 20 mm. The mesh pattern requested by the PSM is respected. In black, the global coordinate system.

Once the volume is created, the mesh of the extruded area must be cleared, otherwise the constraints are going to be applied to nodes non-belonging to the FE model.

The modelling, constraints and loading procedures can be consulted in the previous FAT 71 analysis, paragraph 3.1.

3.2.4 PSM Brick 185, analysis of results

Before proceeding, the POWERGRAPHICS option in Ansys® Toolbar is disabled.

As said before, $\Delta\sigma_{11}$ can be adopted instead of the local $\Delta\sigma_{yy}$. The $\Delta\sigma_{eq,peak}$ nodal values are calculated with equation (1.15), for then being plotted in an Excel graph with respect to the coordinate z, i.e. the distance from the XY plane of symmetry, illustrated in *Figure 3.50*.

<u>10-mm specimen</u>

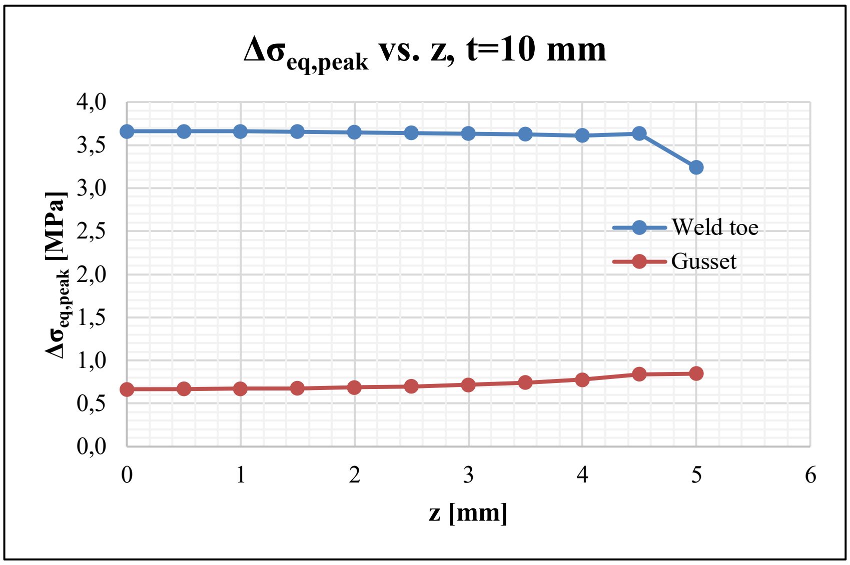

Figure 3. 50: equivalent peak stress vs. z, Brick 185, t=10 mm.

Some relevant observations must be drawn:

1. Despite the small thickness of the longitudinal attachment, with the Brick element adoption all the nodes belonging to the V-notch profiles can be selected;
2. As expected, due to the singular displacements, $\Delta\sigma_{eq,peak}$ at gusset side tends to increase along with z: the maximum equivalent peak stress is located at z=5 mm; on the other hand, the presence of a curve junction eliminates the problem at the weld toe, where the stress raise is not evident;
3. Since the stress raise is due to numerical integration issues, it is decided to rely on the values at z=0 mm, confirmed by the fact that the experimental data show fractures occurring in the centre of the attachment edge.

For an external applied pressure $\Delta\sigma_{nom}$=1 MPa, the maximum $\Delta\sigma_{eq,peak}$, located at z=0 mm both at weld toe and gusset, is respectively equal to:

$$\Delta\sigma_{eq,peak,weld\ toe} = 3.66\ MPa$$

$$\Delta\sigma_{eq,peak,gusset} = 0.67\ MPa$$

According to the PSM Brick 185 results, the gusset is much less solicited than the weld toe. Hence, the PSM foresees a crack initiation in the exact location; one of the reasons lies in the fact that K^*_{FE} is now calibrated at the weld toe, where $2\alpha = 120°$.

20-mm specimen

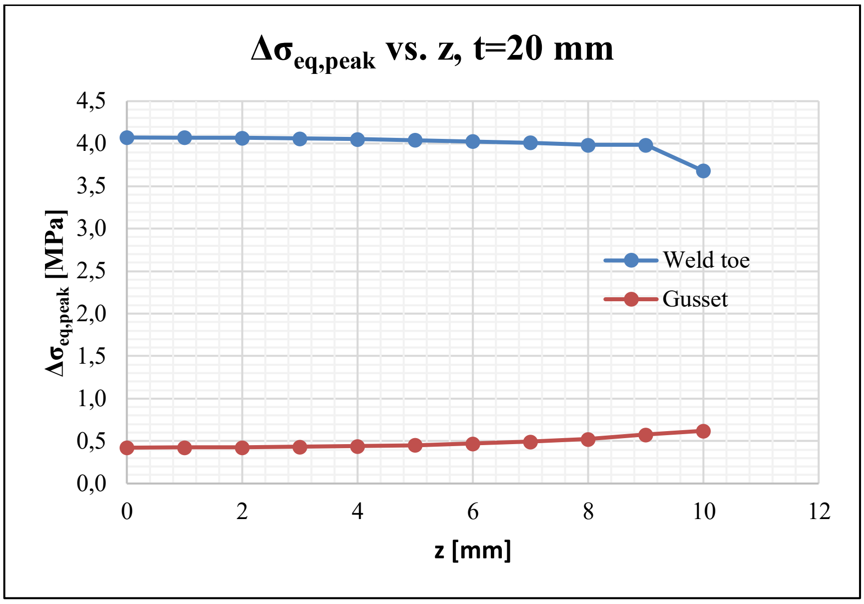

Figure 3. 51: equivalent peak stress vs. z, Brick 185, t=20 mm.

For an external applied pressure $\Delta\sigma_{nom}$=1 MPa, the maximum $\Delta\sigma_{eq,peak}$, located at z=0 mm both at weld toe and gusset, is respectively equal to:

$$\Delta\sigma_{eq,peak,weld\ toe} = 4.07\ MPa$$

$$\Delta\sigma_{eq,peak,gusset} = 0.42\ MPa$$

Same overall conclusions can be made for the 20-mm specimen.

The equivalent peak stress calculated at the weld toe both with tetrahedral and hexahedral elements is reported in the graphs below along with the respective error band provided by the literature ($\pm$15% for Tetra 187, and $\pm$3% for Brick 185):

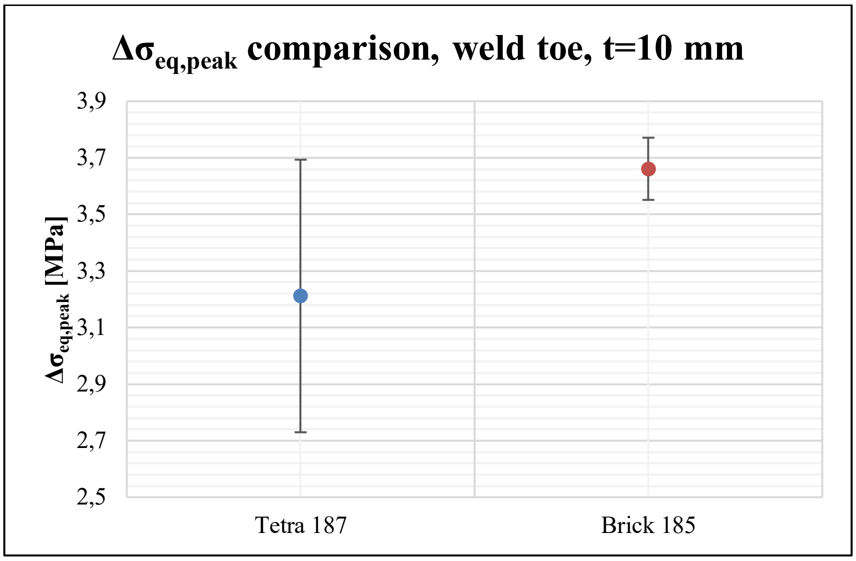

Figure 3. 52: for the 10-mm specimen, $\Delta\sigma_{eq,peak}$ is between 3.55 MPa and 3.7 MPa.

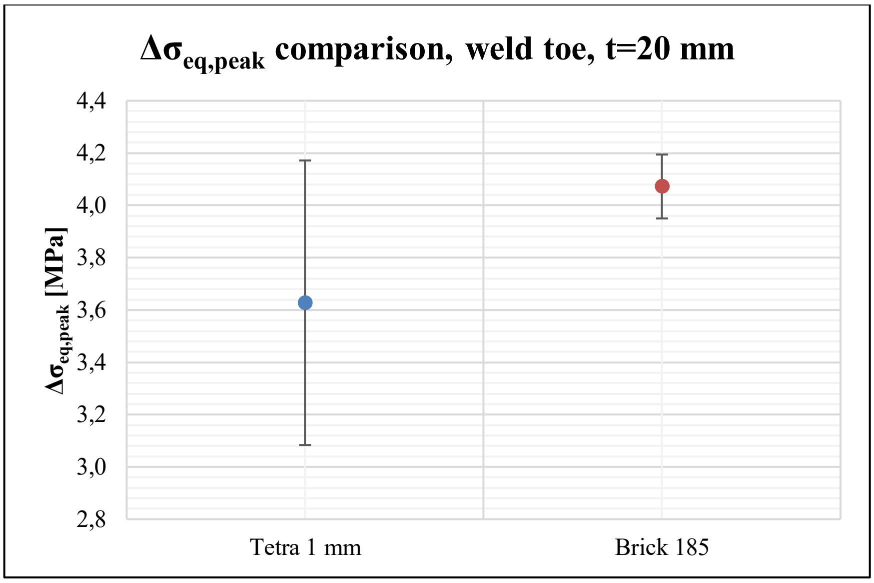

Figure 3. 53: for the 20-mm specimen, $\Delta\sigma_{eq,peak}$ is between 3.96 MPa and 4.2 MPa.

3.2.5 Data entry in the PSM curve

In the preliminary analysis, 1 MPa was applied to the main plate of the specimen; to obtain the effective equivalent peak stress related to the applied nominal stress, the equation (3.2) can be adopted.

The experimental data, available in Appendix D, are then entered inside the PSM design curve proposed by Meneghetti, Guzzella and Atzori under prevailing mode I:

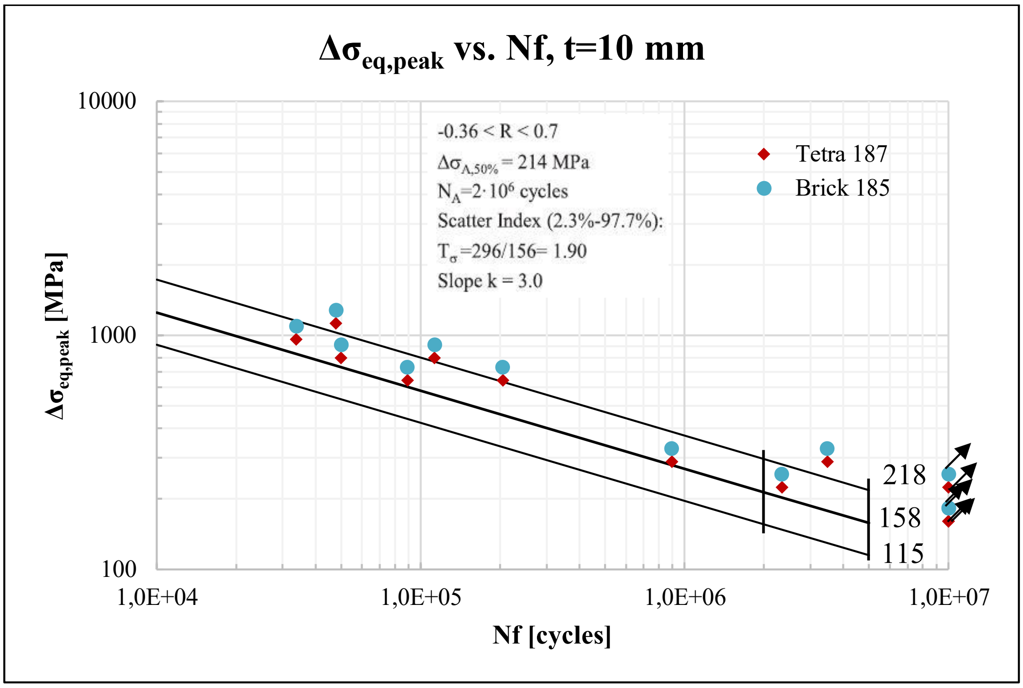

Figure 3. 54: data entry inside the PSM design curve, t=10 mm [28].

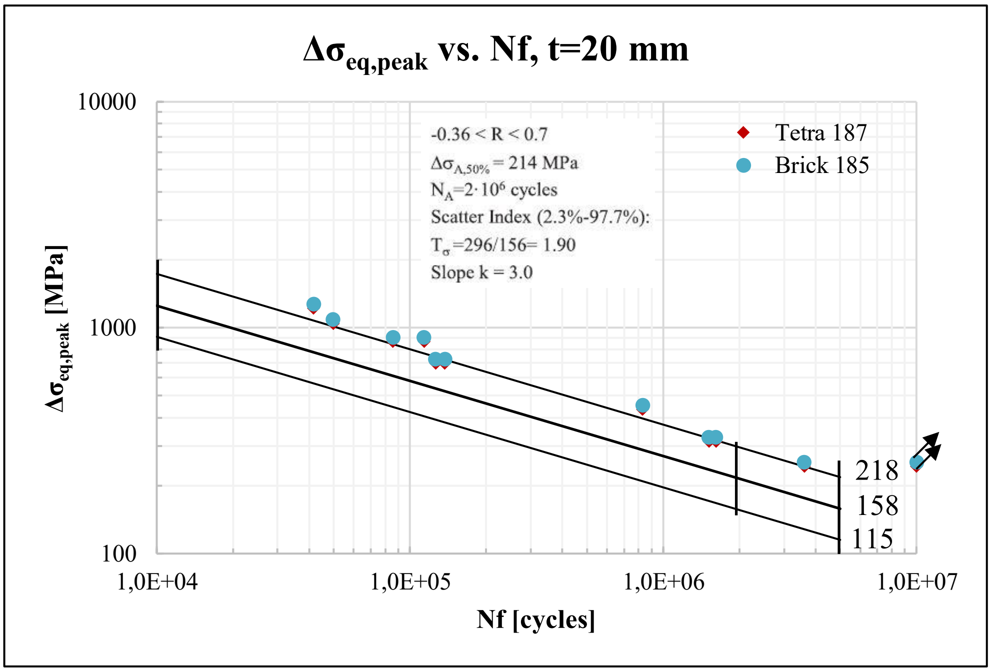

Figure 3. 55: data entry inside the PSM design curve, t=20 mm [28].

The following conclusions can be drawn:

1. Both the PSM Tetra 187 and Brick 185 approaches have correctly foreseen the experimental crack initiation point at weld toe;
2. Since the experimental data falls above the PS 50% line, the PSM design curve has proven to be effective and conservative.

3.2.6 Structural Hot-Spot Stress

The fatigue assessment of the longitudinal stiffener FAT 63 is performed following the IIW recommendations [1] for the hot-spot stress extrapolation. In reference to the guideline, type "a" hot-spot is detected with the employment of fine mesh, as shown in *Figure 1.6*.

Proper mesh indications, concerning the stress extrapolation region, are given in the table below:

<u>10-mm specimen</u>

Element Type	**Mesh algorithm**	**Main plate thickness t**	**Max element size**	**Adopted el. size**
Brick 185 *KO: Simple Enhanced Strain*	Mapped	10 mm (5 mm modelled)	0.4*(t/2) = 2 mm	1 mm

According to [1], the structural hot-spot stress has to be extrapolated at two reference points located at 0.4t and 1.0t distance from the weld toe tip, it is to say 4 mm and 10 mm. As for the previous FAT 71 simulation, both σ_{11} and σ_{xx} can be independently chosen.

The mesh pattern is similar to the one represented in *Figure 3.31*.

For an external applied pressure equal to $\Delta\sigma_{nom}$=1 MPa, the resultant extrapolated stresses at the reference points are:

$$\Delta\sigma_{0.4t} = 1.29\ MPa$$

$$\Delta\sigma_{1.0t} = 1.21\ MPa$$

The SHSS can be finally detected with expression (3.5):

$$\Delta\sigma_{hs} = 1.67 \cdot \Delta\sigma_{0.4t} - 0.67 \cdot \Delta\sigma_{1.0t} = 1.35\ MPa$$

<u>20-mm specimen</u>

Element Type	**Mesh algorithm**	**Main plate thickness t**	**Max element size**	**Adopted el. size**
Brick 185 *KOs: Simple Enhanced Strain*	Mapped	20 mm (10 mm modelled)	0.4*(t/2) = 4 mm	1 mm

The structural hot-spot stress is extrapolated at two reference points located at 0.4t and 1.0t distance from the weld toe tip, it is to say 8 mm and 20 mm.

For an external applied pressure equal to $\Delta\sigma_{nom}$=1 MPa, the resultant extrapolated stresses at the reference points are:

$$\Delta\sigma_{0.4t} = 1.14\, MPa$$

$$\Delta\sigma_{1.0t} = 1.08\, MPa$$

The SHSS can be finally detected with expression (3.5):

$$\Delta\sigma_{hs} = 1.67 \cdot \Delta\sigma_{0.4t} - 0.67 \cdot \Delta\sigma_{1.0t} = 1.18\, MPa$$

As it can be noticed, the 20-mm specimen SHSS is lower than the 10-mm one. This goes against the size effect theory, by which the thicker the main plate (and the attachment), the more the stress concentration at the weld and consequently the lower the fatigue life of the joint. This issue happens because, according to this method, the extrapolation points depend on the main plate thickness t: thicker plates would result in extrapolation points more distant from the weld toe tip, which then would cause a less steep linearized stress curve slope. This, as also Xiao and Yamada [3] affirm in their paper, is due to the fact that the hot-spot stress extrapolation cannot account for the size and thickness effect.

3.2.7 1-mm Stress

The fatigue assessment of the longitudinal stiffener FAT 63 is now performed with the employment of the 1-mm stress [3], proposing a stress extrapolation 1-mm below the weld toe tip, along the y direction referring to *Figure 3.32*.

In respect of the previous precautions emerged during the FAT 71 analysis, the adopted measures for this simulation are shown in the table below:

<u>10-mm specimen</u>

Element	Mesh algorithm	Element size	Extrapolated Stress
Brick 185 *KO: Simple Enhanced Strain*	Mapped	0.5 mm	$\Delta\sigma_{xx}$

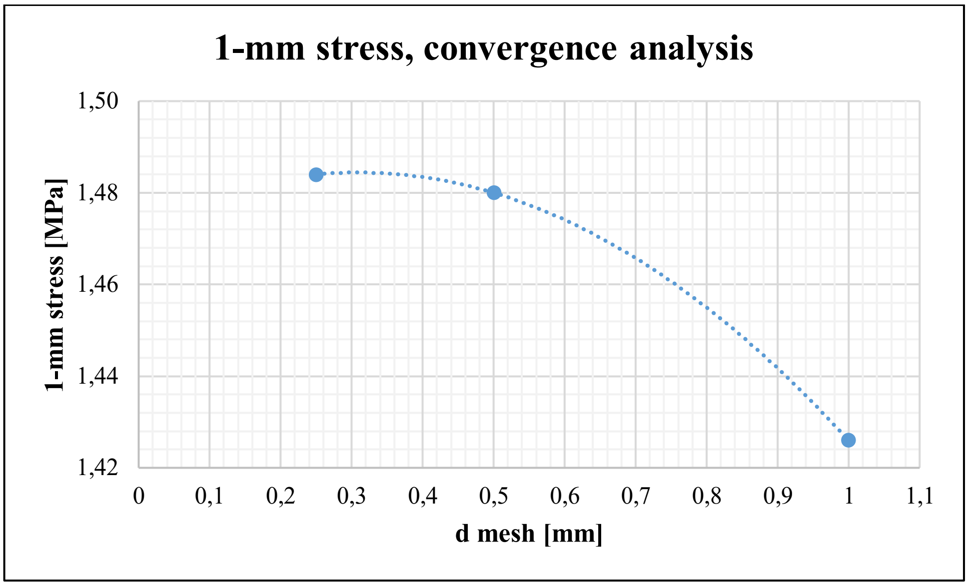

Figure 3. 56: convergence of 1-mm stress to varying of the element size, t=10 mm.

With these dispositions, the resulting $\Delta\sigma_{1\text{-mm}}$ is equal to:

$$\Delta\sigma_{1-mm} = 1.48\ MPa$$

<u>20-mm specimen</u>

Element	Mesh algorithm	Element size	Extrapolated Stress
Brick 185 KOs: Simple Enhanced Strain	Mapped	0.5 mm	$\Delta\sigma_{xx}$

With these dispositions, the resulting $\Delta\sigma_{1\text{-mm}}$ is equal to:

$$\Delta\sigma_{1-mm} = 1.65\ MPa$$

As it is noted, since the 1-mm method is able to account for the thickness effect, the stress value at 1-mm distance from the weld toe tip is higher for the 20-mm specimen.

3.2.8 Data entry in the IIW curves

<u>Nominal approach</u>

The experimental data in terms of nominal stress, reported at the beginning of paragraph 3.2, are entered inside the FAT 63 design curve proposed by the IIW guideline:

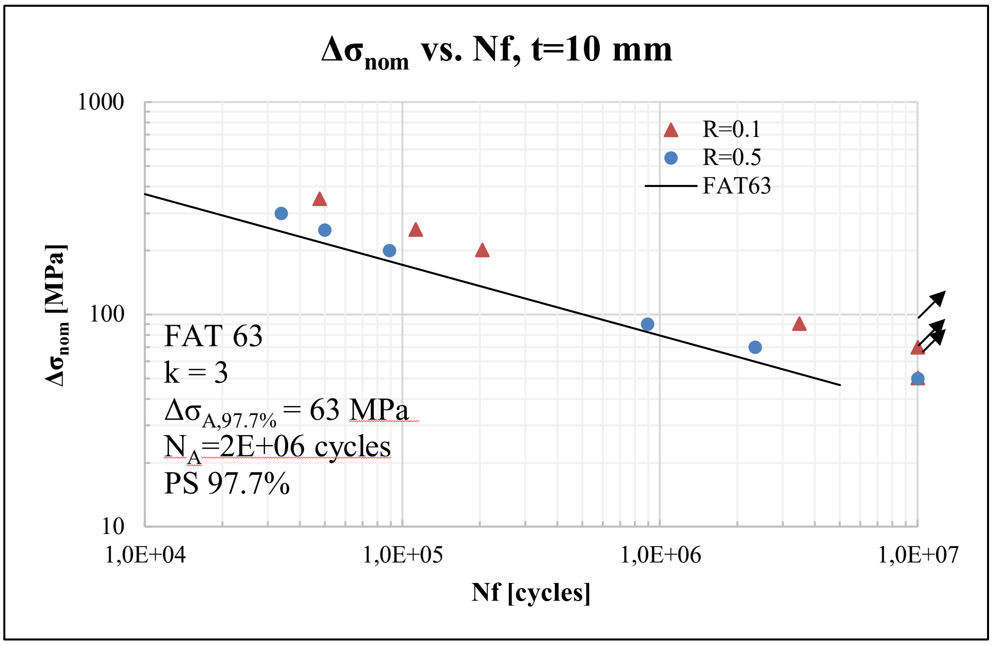

Figure 3. 57: data entry inside the FAT 63 design curve, global approach, t=10 mm [1].

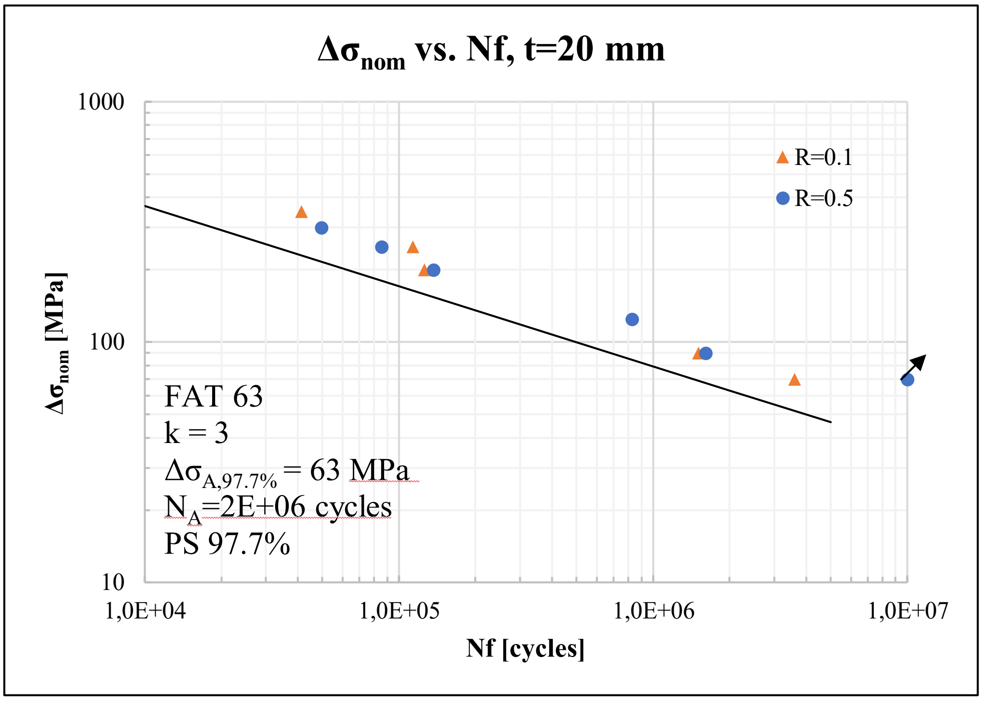

Figure 3. 58: data entry inside the FAT 63 design curve, global approach, t=20 mm. [1].

SHSS approach

In the previous analyses, 1 MPa was applied to the main plate of the specimen; under linear elasticity hypotheses, the effective SHSS related to a specific $\Delta\sigma_{nom}$ can be detected with (3.6).

The experimental data in terms of hot-spot stress, reported in Appendix D, are entered inside the FAT 100 design curve, for non-load carrying specimens, proposed by the IIW guideline:

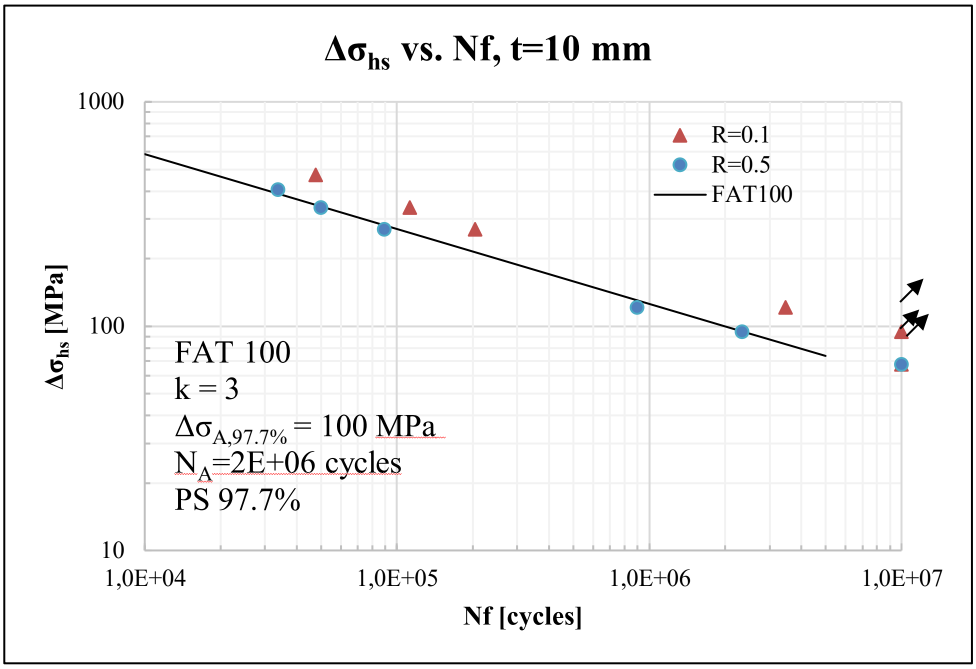

Figure 3. 59: data entry inside the FAT 100 design curve, hot-spot approach, t=10 mm [1].

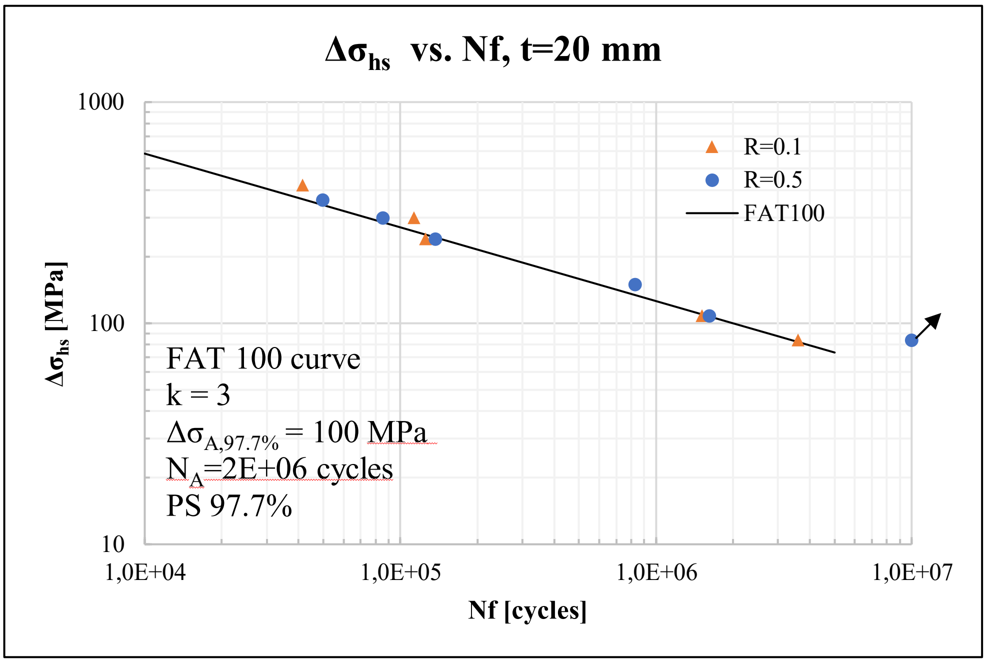

Figure 3. 60: data entry inside the FAT 100 design curve, hot-spot approach, t=20 mm [1].

<u>1-mm stress approach</u>

In the previous analyses, 1 MPa was applied to the main plate of the specimen; under linear elasticity hypotheses, the effective 1-mm stress related to a specific $\Delta\sigma_{nom}$ can be detected with (3.7).

The experimental data in terms of 1-mm stress, reported in Appendix D, are entered inside the reference detail design curve, proposed by Xiao and Yamada:

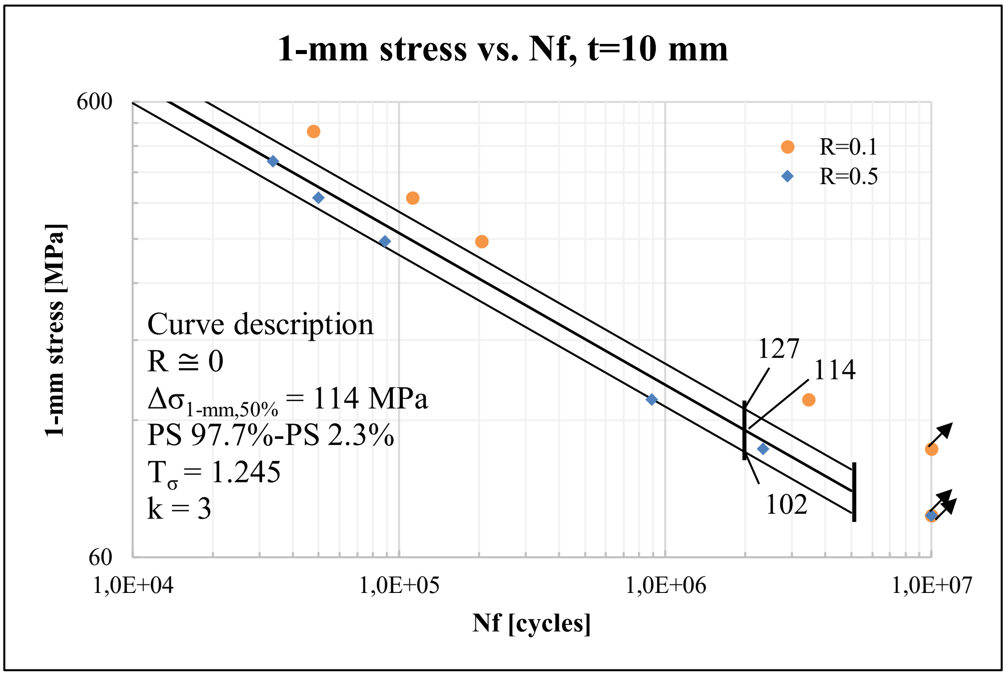

Figure 3. 61: data entry inside Xiao design curve, 1-mm stress approach, t=10 mm [3].

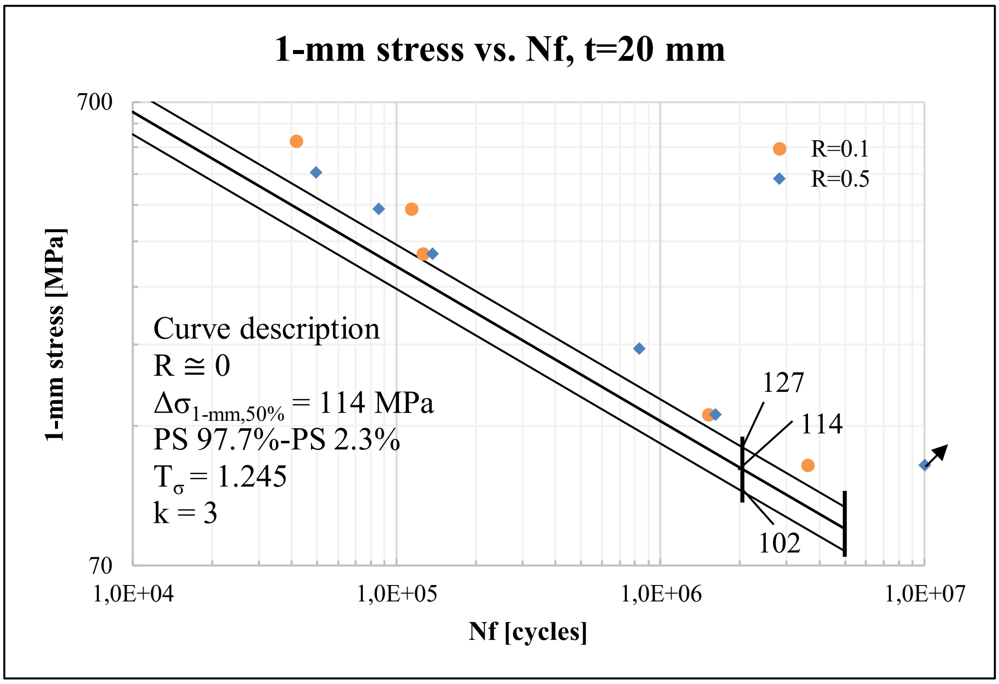

Figure 3. 62: data entry inside Xiao design curve, 1-mm stress approach, t=20 mm [3].

The following conclusions can be drawn:

1. These methods have correctly been applied to the FAT 63 welded joint, for weld toe fractures;
2. Concerning the nominal and the 1-mm stress approaches, since the experimental data fall above the PS 97.7% line, their respective design curves have proven to be effective and conservative;
3. Regarding the hot-spot stress approach, along with the fact that the extrapolation points are dependent on the main plate thickness, some data fall slightly below the PS 97.7% curve, therefore the method has not proven to be as conservative as the others.

3.2.9 Fatigue life comparison

The fatigue life comparison is performed in terms of equivalent nominal stress. For a PS 97.7%, at 2 million cycles, the corresponding equivalent stress is found with formula (3.8):

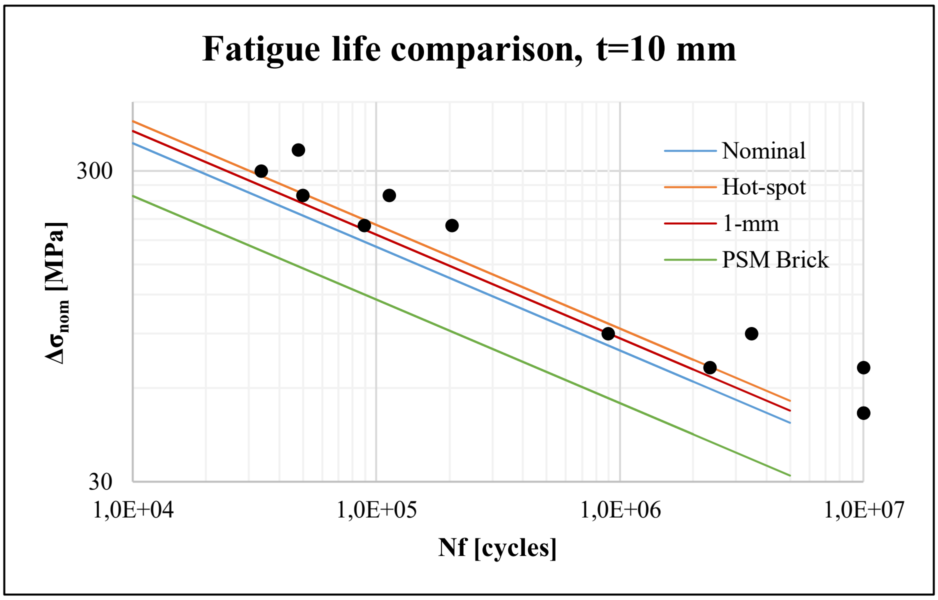

Figure 3. 63: fatigue life comparison, t=10 mm.

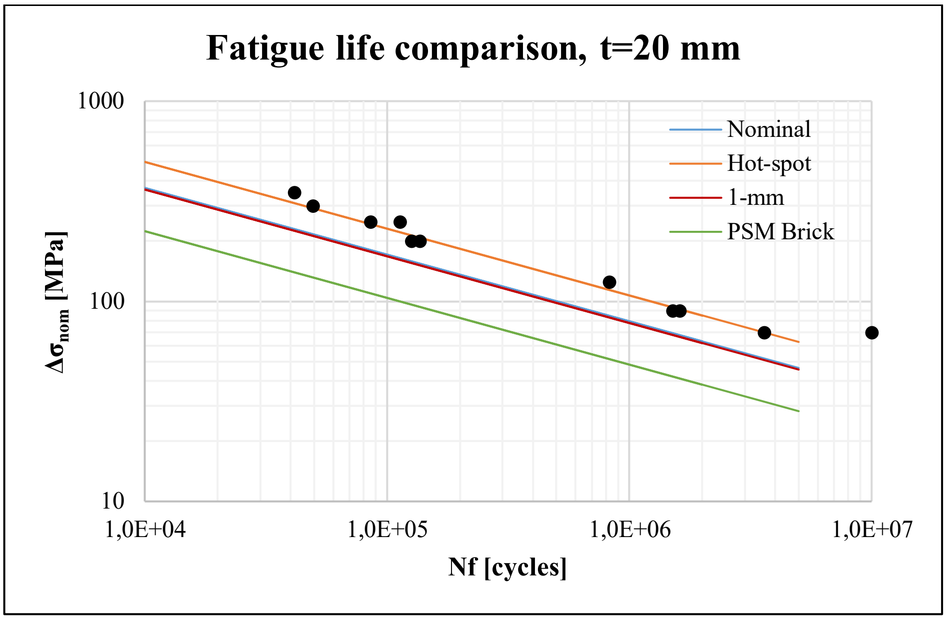

Figure 3. 64: fatigue life comparison, t=20 mm.

Some relevant conclusions can be drawn for these specimens:

- Now that K_{FE} are calibrated at the weld toe ($2\alpha = 120°$), the PSM is appears to be the most conservative method for the fatigue assessment;
- The nominal and 1-mm stress methods give similar results in terms of fatigue life;
- The hot-spot stress reveals to be the least conservative method.

3.3 Transverse attachment, FAT 80 (Yildirim et al.)

Two non-load carrying FAT 80 transverse NLC joints, recently analysed by Yildirim et al., have also been assessed in terms of nominal stress, hot-spot stress, 1-mm stress, equivalent peak stress and strain energy density. At the moment, the experimental data are classified, therefore no additional information on the material, the geometries, the experimental data and the re-elaborated results can be given. However, some general conclusions are worth to be reported:

1. Important assumptions were made with regard to the weld profile geometry;
2. The influence of misalignment in the as-welded condition was consistent and therefore had to be considered in the analyses;
3. By modelling the transverse attachment in two or three dimensions, the results are generally coincident;
4. For V-notch opening angles higher than 135°, the PSM still remains less conservative (K_{FE} are not calibrated), while the SED approach, valid for $0 < 2\alpha < 150°$, proves to be conservative. This confirms the fact that K_{FE}, under modes I, II and III, for $2\alpha > 135°$ should be validated;
5. Generally, all the local and nominal approaches have proven to be well conservative, exception made for the hot-spot approach, presenting some issues which are also going to be discussed in the next paragraph.

3.4 Transverse attachment, FAT 80 (Okawa)

The fourth typology of welded joint to be investigated is a transverse NLC joint, fatigue class FAT 80, tested by Okawa in 2011 [36] under constant amplitude loading CAL.

Specific information on the component is reported below:

Weld condition	Fracture location	Load application	Main plate/gusset thickness
As-welded, non-load carrying, full penetration	*Weld toe*	*Axial, main plate, parent material*	*Main plate: 20 mm* *Gusset: 10 mm*

The mechanical properties are described below:

Material	Yield strength f_y	Young modulus	Poisson's ratio ν
AH36, HSS, linear elastic, isotropic	*392 MPa*	*206000 MPa*	*0.3*

In regard of the main geometrical quantities, *Figure 3.65* shows the most relevant information:

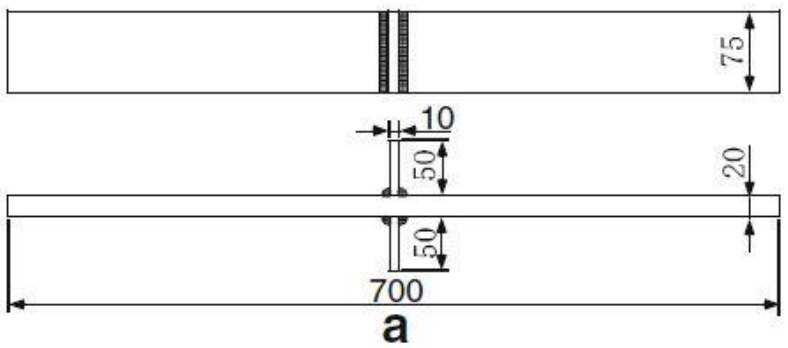

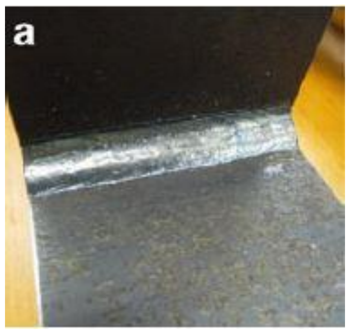

Figure 3. 65: on the left, schematic representation of the AW geometry; on the right, an enlargement of the weld [36].

The weld profile parameters are described in the table below:

ρ weld toe tip [mm]	Weld leg [mm]	Weld flank angle	2α
≅ 0	*8*	*45°*	*Main plate: 135°* *Gusset: 135°*

Since ρ < 1.5 mm, the assumption of a sharp V-notch (ρ = 0 mm) at the weld toe is coherent with the non-conventional LEFM extension to welded joints.

In case of transverse attachments, the influence of the misalignment cannot be neglected. However, since no information is available, they are neglected, knowing that this choice can consistently alter the final results.

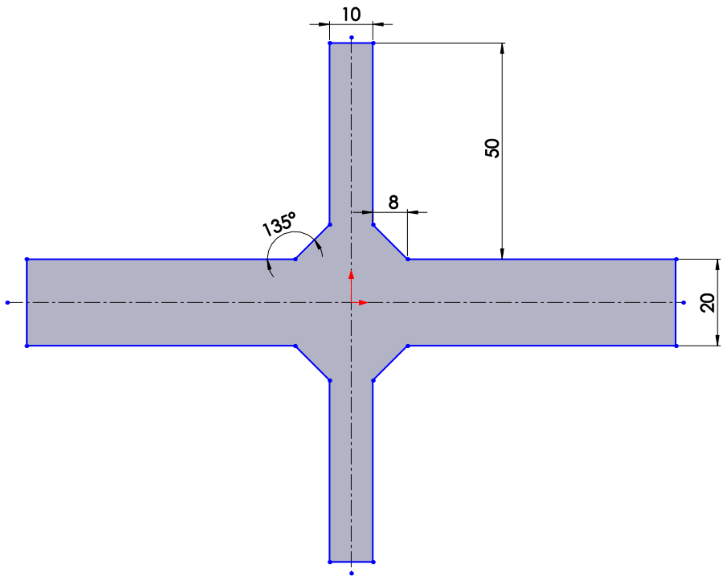

Figure 3. 66: Okawa, geometry. The quotes are expressed in [mm].

The experimental data are reported in terms of nominal stress $\Delta\sigma_{nom}$. In barred, the runouts.

R	**$\Delta\sigma_{nom}$ [MPa]**	**N_f [cycles]**
0.1	200	164 000
	150	354 000
	100	1 320 000
	~~80~~	~~5 000 000~~

Since the simulations on FAT 80 (Yildirim et al.) showed compatibility between 2D and 3D models for transverse attachments, the next fatigue assessment are performed with the adoption of 2D FE models, allowing to consistently speed up the computational times.

Inside Ansys® APDL environment, the modelling procedure is briefly described and shown in *Figure 3.67*.

- <u>Symmetries</u>: due to the double symmetry of the transverse NLC joint, only ¼ of the geometry is created, allowing to consistently speed up the computational time;
- <u>Loading</u>: the specimen is axially loaded, and the load is applied on the main plate as a constant pressure equal to $p = -\Delta\sigma_{nom}$, on Line 16;
- <u>Constraints</u>: symmetry BC are applied on Lines 6 and 18.

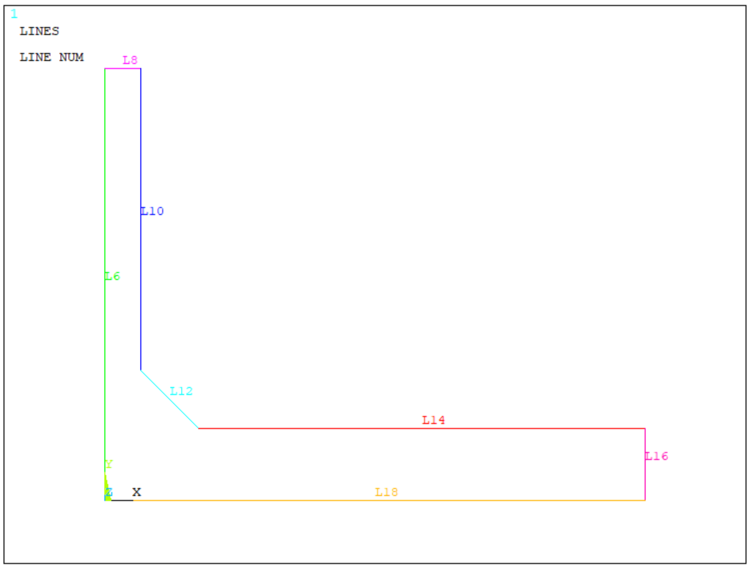

Figure 3. 67: reference lines for loads and constraints application to Okawa joint.

Modelling the total main plate length of the welded joint is not necessary: in fact, the latter shall be sufficient to represent the stress flowing from the "infinite".

3.4.1 PSM Plane 182

The fatigue assessment is performed in terms of equivalent peak stress, with the adoption of the Peak Stress Method for 2D structures, four-node linear elements.

From Ansys® APDL element library, Plane 182 element is chosen; the Key Option K1 is switched to *Simple Enhanced Strain*, while K3 is changed to *Plane Strain*.

From a preliminary analysis, it can be inferred that Okawa FAT 80 fillet weld is solicited under prevailing mode I at the attachment edge, while mode II is null since 2α > 102.5°; mode III is influence can be neglected.

Since the V-notch opening angle 2α is equal to 135°, the PSM calibration constants are valid both at gusset and weld toe.

Under mode I loading, the PSM Plane 182 requirements are listed below:

Location: weld toe, gusset **_Mode I_**

Element Type	**Mesh algorithm**	**$(a/d)_{min}$**	**2α**	**Mesh pattern 2α < 90°**	**Mesh pattern 2α > 90°**
Plane 182 *KOs: Simple Enhanced Strain + Plane Strain*	Free	3	0 < 2α < 135°	Four adjacent elements share the same node	Two adjacent elements share the same node

Under these restrictions, the mode I PSM calibration constant is equal to $K_{FE}^{*} = 1.38 \pm 3\%$, at both gusset and weld toe locations.

The following PSM dispositions are thus adopted:

- Half the main plate thickness a is equal to a = 10 mm;
- The mesh global element size is set to d = 2 mm;
- $\frac{a}{d} = \frac{10}{2} = 5 > 3$ the ratio is respected;
- The λ_1 and e_1 values associated to the weld toe and gusset ($2\alpha = 135°$) required for f_{w1} detection respectively are:

2α	**λ_1**	**e_1**
135°	*0.674*	*0.118*

Finally, the stress corrective factors under mode I calculated with equation (1.16) is $f_{w1} = 1.334$. The resulting mesh pattern can be appreciated in *Figure 3.68*:

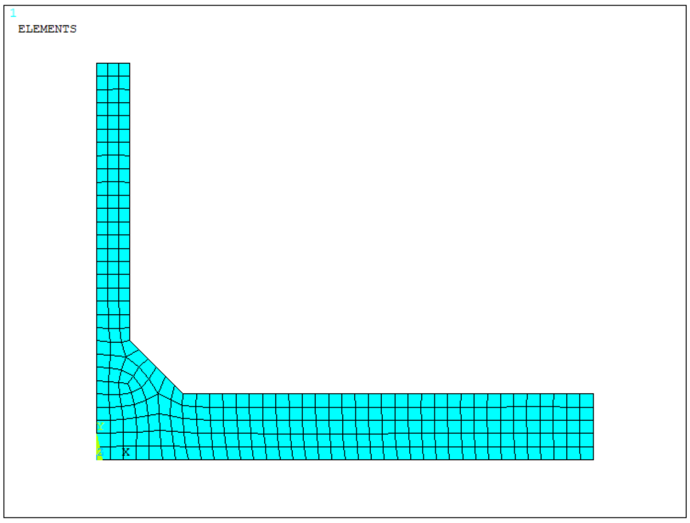

Figure 3. 68: mesh conformation required by PSM, d=2 mm.

3.4.2 PSM Plane 182, analysis of results

After the geometry is loaded and constrained according to the previous indications, the structure is solved:

Main Menu > Solution > Solve > Current LS

For an external applied pressure $\Delta\sigma_{nom}$=1 MPa, the first principal stress is plotted:

Main Menu > General Postproc > Plot Results > Contour Plot > Nodal Solution > 1st pr. stress

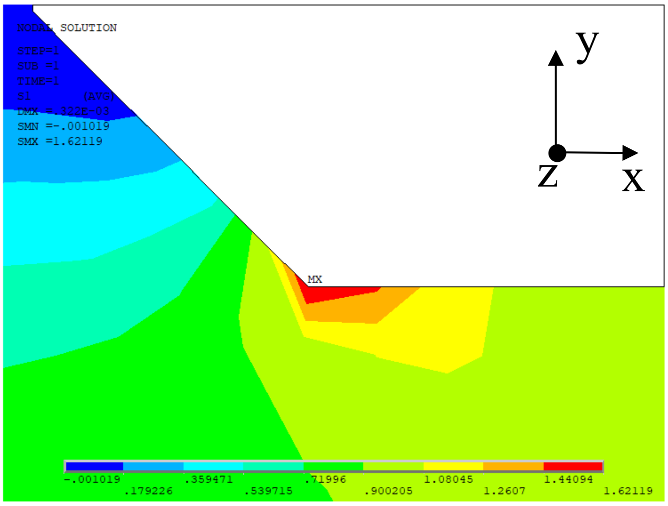

Figure 3. 69: plot of the first principal stress in Okawa, for an external applied stress of 1 MPa. In black, the global coordinate system.

The peak stress $\Delta\sigma_{\theta\theta,\theta=0,peak}$ (i.e. the $\Delta\sigma_{yy}$ of the Ansys® local coordinate system) has to be evaluated at the most solicited point of the structure. As it was declared in Chapter 2, under mode I loading $\Delta\sigma_{yy}$ can be confused with $\Delta\sigma_{11}$ both at weld toe and gusset.

For an external applied pressure $\Delta\sigma_{nom}$=1 MPa, the maximum $\Delta\sigma_{11}$ located at the weld toe tip is equal to:

$$\Delta\sigma_{11} = \Delta\sigma_{\theta\theta,\theta=0,peak} = 1.62\ MPa$$

Once the peak stress is given, both K_1 and $\Delta\sigma_{eq,peak}$ can be respectively found with formulae (2.5) and (2.8):

$$\Delta K_1 \cong K_{FE}^{*} \cdot \Delta\sigma_{\theta\theta,\theta=0,peak} \cdot d^{1-\lambda_1} = 1.38 \cdot 1.62 \cdot 2^{1-0.674} = 2.80\ MPamm^{0.326}$$

$$\Delta\sigma_{eq,peak} = \Delta\sigma_{\theta\theta,\theta=0,peak} \cdot f_{w1} = 1.62 \cdot 1.334 = 2.16\ MPa$$

If the global element size is set to d=1 mm, the respective stress corrective factor becomes f_{w1}=1.064 and the results are the same as before:

$$\Delta\sigma_{11} = \Delta\sigma_{\theta\theta,\theta=0,peak} = 2.03\ MPa$$

$$\Delta K_1 \cong K_{FE}^{*} \cdot \Delta\sigma_{\theta\theta,\theta=0,peak} \cdot d^{1-\lambda_1} = 1.38 \cdot 2.03 \cdot 1^{1-0.674} = 2.80\ MPamm^{0.326}$$

$$\Delta\sigma_{eq,peak} = \Delta\sigma_{\theta\theta,\theta=0,peak} \cdot f_{w1} = 2.03 \cdot 1.064 = 2.16\ MPa$$

In agreement with the experimental reality, the PSM correctly foresees the weld toe as the most solicited part of the joint.

3.4.3 Data entry in the PSM curve

In the preliminary analysis, 1 MPa was applied to the main plate of the specimen; to obtain the effective equivalent peak stress related to the applied nominal stress, the equation (3.2) can be adopted. The results can be consulted in Appendix E.

The experimental data are then entered inside the PSM design curve proposed by Meneghetti and Lazzarin under prevailing mode I:

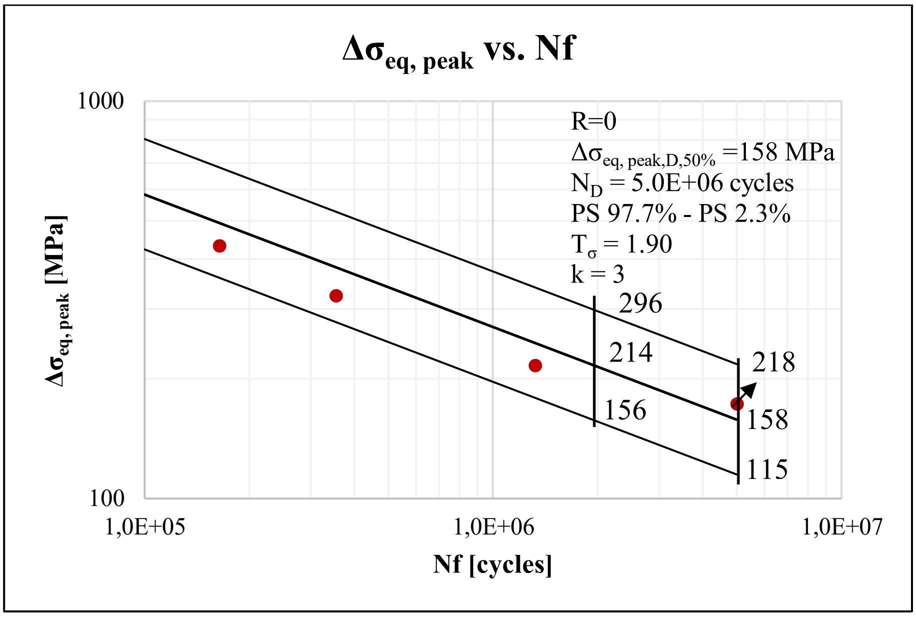

Figure 3. 70: data entry inside the PSM design curve [7]

The following conclusions can be drawn:

1. The PSM has correctly foreseen the experimental crack initiation point at weld toe;
2. Even without considering the effect of misalignments, since the experimental data fall above the PS 97.7% line, the PSM design curve has proven to be effective and conservative.

3.4.4 Structural Hot-Spot Stress

In this paragraph, the fatigue assessment of the Okawa FAT 80 welded joint is performed following the IIW recommendations [1] for the hot-spot stress extrapolation. In reference to the guideline, type "a" hot-spot is detected with the employment of fine mesh, as shown in *Figure 1.6*.

Proper mesh indications, concerning the stress extrapolation region, are given in the table below.

Element Type	Mesh algorithm	Main plate thickness t	Max element size	Adopted el. size
Plane 182 *KOs: Simple Enhanced Strain + Plane Strain*	Mapped	20 mm (10 mm modelled)	0.4*(t/2) = 4 mm	1 mm

The mesh pattern can be seen in *Figure 3.71*:

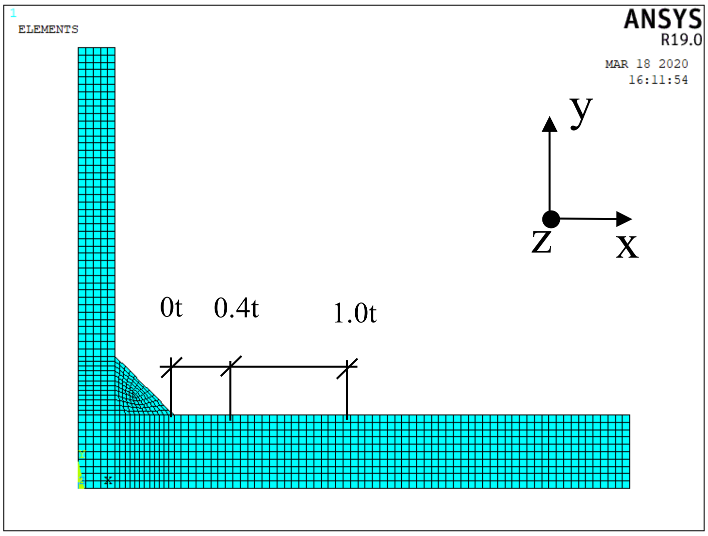

Figure 3. 71: mapped mesh for the hot-spot stress detection. In black, the global coordinate system.

According to [1], the structural hot-spot stress has to be extrapolated at two reference points located at 0.4t and 1.0t distance from the weld toe tip, it is to say 8 mm and 20 mm. In regard of the type of extrapolated stress, the graph below in *Figure 3.72* shows that, for an external pressure $\Delta\sigma_{nom}$=1 MPa applied on the parent material, after 3 mm σ_{11} and σ_{xx} are perfectly coincident, therefore the choice is indifferent.

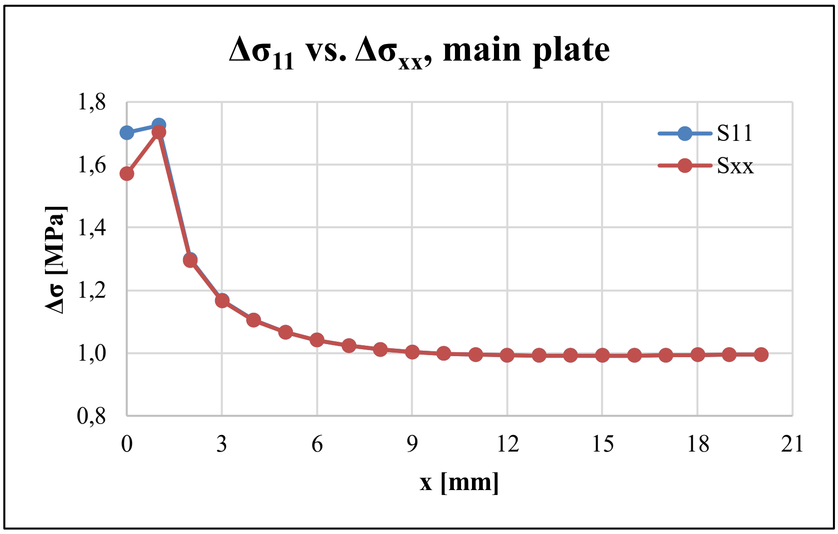

Figure 3. 72: $\Delta\sigma_{11}$ and $\Delta\sigma_{xx}$ plot starting from the weld toe tip.

For an external applied pressure equal to $\Delta\sigma_{nom}$=1 MPa, the resultant extrapolated stresses at the reference points are:

$$\Delta\sigma_{0.4t} = 1.01\ MPa$$

$$\Delta\sigma_{1.0t} = 1.00\ MPa$$

The structural hot-spot stress SHSS is finally detected with equation (3.5):

$$\Delta\sigma_{hs} = 1.67 \cdot \Delta\sigma_{0.4t} - 0.67 \cdot \Delta\sigma_{1.0t} = 1.02\ MPa$$

Therefore, the analysis shows that the SHSS tends to be equal to the nominal stress. To check whether the result is converging, a further simulation is run, with element size 0.1 mm, but the result was the same. Even Xiao and Yamada [3] in their research pointed out that on transverse NLC joints the calculated SHSS were found to be very close to nominal stresses, confirming the fact that SHSS cannot predict the thickness effect.

3.4.5 1-mm Stress

The fatigue assessment of the Okawa specimen is now performed with the employment of Xiao and Yamada [3] method, proposing a stress extrapolation 1-mm below the weld toe tip, along the y direction referring to *Figure 3.73*.

In respect of the previous precautions emerged during the FAT 71 analysis, the adopted measures for this simulation are shown in the table below:

Element	**Mesh algorithm**	**Element size**	**Extrapolated Stress**
Plane 182 *KOs: Simple Enhanced Strain + Pure Displacement*	Mapped	0.05 mm	$\Delta\sigma_{xx}$

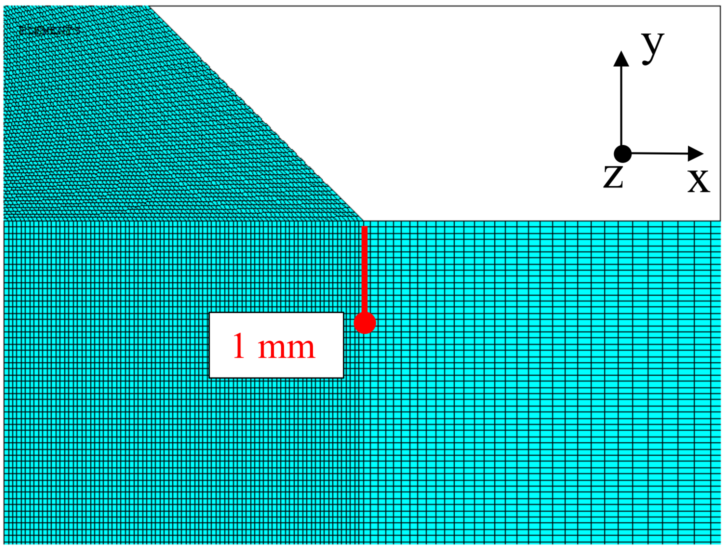

Figure 3. 73: very fine mesh (d=0.05 mm) near the weld toe, according to Xiao's article. In black, the global coordinate system.

For an external applied load $\Delta\sigma_{nom}$=1 MPa , the resulting extrapolated $\Delta\sigma_{1\text{-}mm}$ is equal to:

$$\Delta\sigma_{1-mm} = 1.18\ MPa$$

3.4.6 Data entry in the IIW curves

Nominal approach

The experimental data in terms of nominal stress, reported at the beginning of paragraph 3.4, are entered inside the FAT 80 design curve proposed by the IIW guideline:

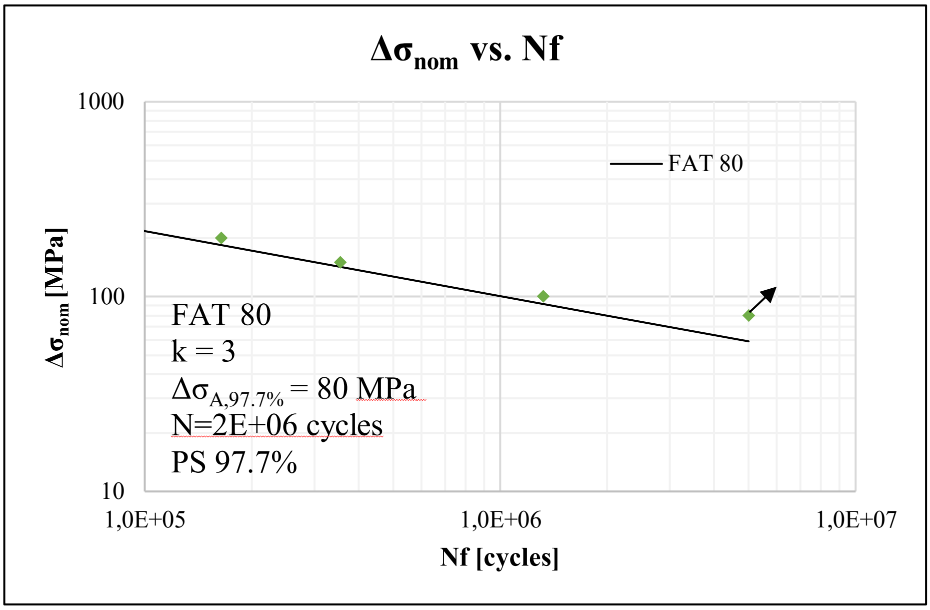

Figure 3. 74: data entry inside the FAT 80 design curve, global approach [1].

SHSS approach

In the preliminary analysis, 1 MPa was applied to the main plate of the specimen; under linear elasticity hypotheses, the effective SHSS related to a specific $\Delta\sigma_{nom}$ can be detected with (3.6). The results can be consulted in Appendix E.

The experimental data in terms of hot-spot stress are entered inside the FAT 100 design curve, for non-load carrying specimens, proposed by the IIW guideline:

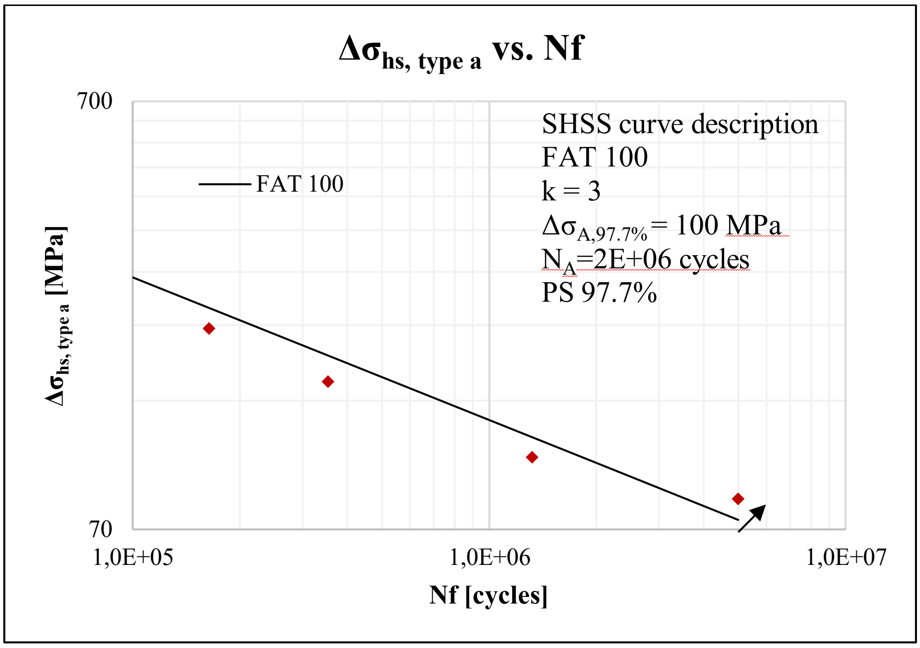

Figure 3. 75: data entry inside the FAT 100 design curve, hot-spot approach [1].

<u>1-mm stress approach</u>

In the previous analyses, 1 MPa was applied to the main plate of the specimen; under linear elasticity hypotheses, the effective 1-mm stress related to a specific $\Delta\sigma_{nom}$ can be detected with (3.7).

The experimental data in terms of 1-mm stress, reported in Appendix E, are entered inside the reference detail design curve, proposed by Xiao and Yamada:

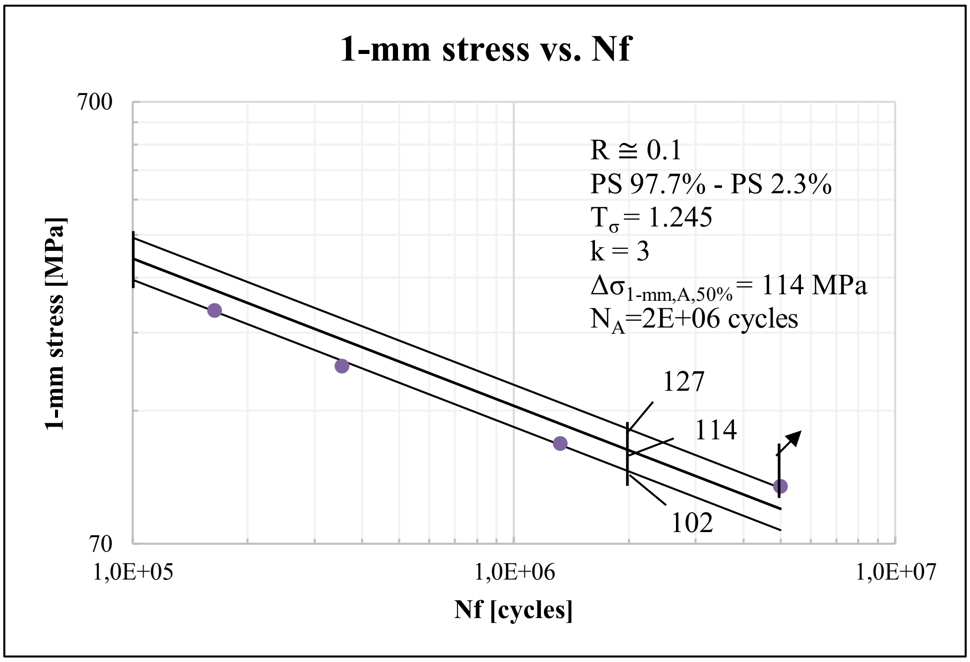

Figure 3. 76: data entry inside the 1-mm design curve [3].

The following conclusions can be drawn:

1. These methods have correctly been applied to the welded joint, for weld toe fractures;
2. Concerning the nominal approach, since the experimental data fall above the PS 97.7% line, the design curve has proven to be effective and conservative;
3. Concerning the hot-spot approach, since the misalignments have been neglected and the found SHSS has a value very close to the nominal one, the experimental data fall below the PS 97.7% line. Consequently, the method has not proven to be effective and conservative;
4. Regarding the 1-mm stress approach, almost the totality of the data fall above the PS 97.7% line, exception made for one point slightly below it, meaning that bending stresses actually are consistent.

3.4.7 Fatigue life comparison

The fatigue life comparison is performed in terms of equivalent nominal stress. For a PS 97.7%, at 2 million cycles, the corresponding equivalent stress is found with formula (3.8):

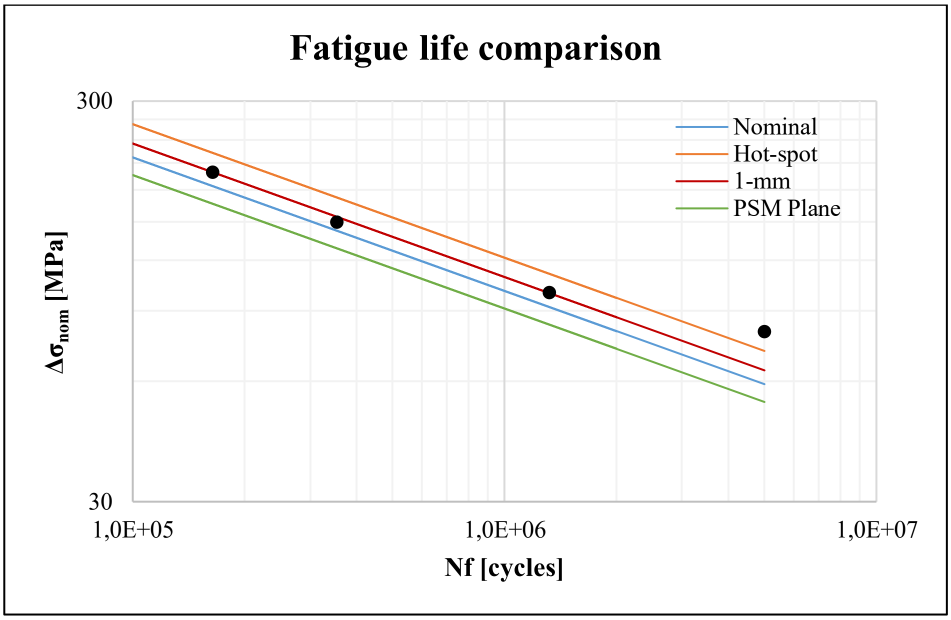

Figure 3. 77: fatigue life comparison.

Several conclusions can be drawn:

- PSM is again the most conservative method;
- Nominal approach, already covering a misalignment stress magnification factor equal to k_m=1.2 [1] for transverse NLC joints, results to be conservative too;
- Due to the small k_m=1.05 covered by the hot-spot FAT curves, and the hot-spot values similar to the nominal stress, the SHSS approach lacks conservativeness: as it is noted in *Figure 3.77*, the esteemed fatigue life greatly exceeds the experimental number of cycles;
- Concerning the 1-mm curve, if the outlier data is taken, such as in this case, the predicted fatigue life slightly overcomes the experimental one by 30 000 cycles.

3.5 Transverse attachment, FAT 80 (Kuhlmann 2009)

The fifth and last welded joint to be investigated is a transverse stiffener, fatigue class FAT 80, tested by Kuhlmann in 2009 [37] under constant amplitude loading CAL.

Specific information on the component is reported below:

Weld condition	Fracture location	Load application	Main plate/gusset thickness
As-welded, non-load carrying, full penetration	*Weld toe*	*Axial, main plate, parent material*	*Main plate: 12 mm* *Gusset: 12 mm*

The mechanical properties of the specimens are described below. In brackets, the measured f_y.

Materials	Yield strength f_y	Young modulus	Poisson's ratio ν
S355J2, linear elastic, isotropic *S690QL, linear elastic, isotropic*	*355 (422) MPa* *690 (781) MPa*	*206000 MPa*	*0.3*

In regard of the main geometrical quantities, *Figure 3.78* shows the most relevant information:

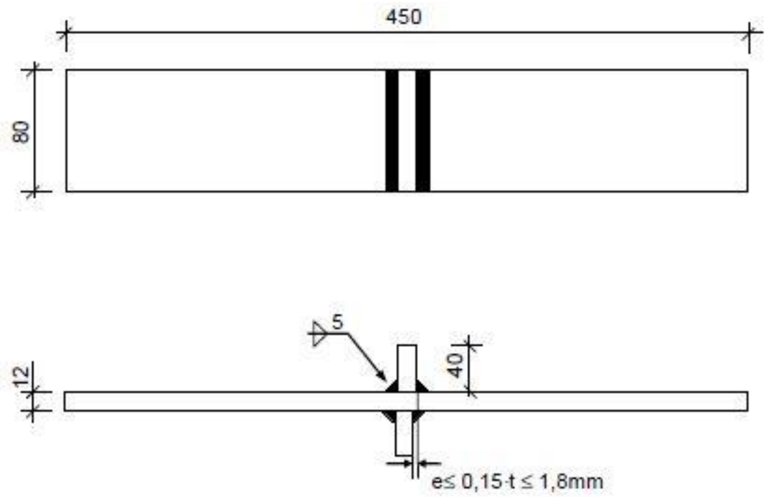

Figure 3. 78: on the left, schematic representation of the as-welded geometry; on the right, a picture of the resulting weld [37].

The weld profile parameters are described in the table below:

ρ weld toe tip [mm]	Weld leg [mm]	Weld flank angle	2α
≅ 0	*7*	*45°*	*Main plate: 135°* *Gusset: 135°*

Since ρ < 1.5 mm, the assumption of a sharp V-notch (ρ=0 mm) at the weld toe is coherent with the non-conventional LEFM extension to welded joints.

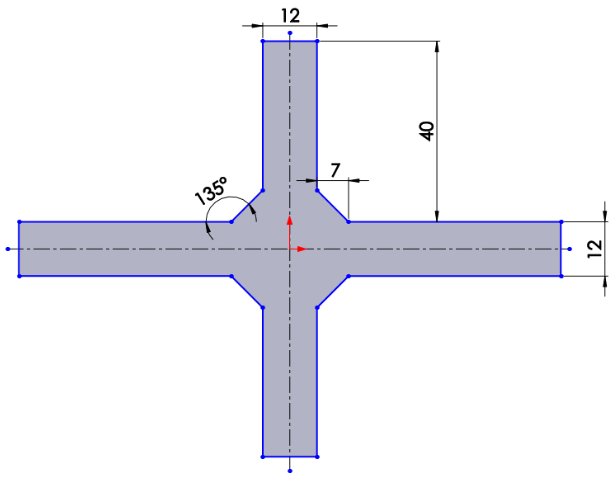

Figure 3. 79: Kuhlmann (2009), geometry. The quotes are expressed in [mm].

Modelling the total main plate length of the welded joint is not necessary: in fact, the latter shall be sufficient to represent the stress flowing from the "infinite".

In Kuhlmann's paper, no information on misalignments, as well as superimposed bending loads, can be found. With all chances, specific piece of information might be found in the article Appendix [37]. However, misalignments are in first place neglected.

The experimental data are reported in terms of nominal stress $\Delta\sigma_{nom}$.

R	**f_y [MPa]**	**$\Delta\sigma_{nom}$ [MPa]**	**N_f [cycles]**
0.1	441	300	67 921
		300	64 159
		170	574 631
		170	456 289
		125	1 400 261
		125	3 712 215
		225	185 219
		225	168 630
		125	1 933 751
0.1	781	300	106 797
		300	123 652
		225	537 534
		225	415 846
		190	1 028 720
		190	575 000
		190	1 034 355
		150	3 517 443
		150	1 833 757

Since the simulations on FAT 80 (Yildirim et al.) showed compatibility between 2D and 3D models for transverse attachments, the next fatigue assessment are performed with the adoption of 2D FE models, allowing to consistently speed up the computational times.

Inside Ansys® APDL environment, the modelling procedure is briefly described and shown in *Figure 3.80*.

- <u>Symmetries</u>: due to the double symmetry of the transverse NLC joint, only ¼ of the geometry is created, allowing to consistently speed up the computational time;
- <u>Loading</u>: the specimen is axially loaded, and the load is applied on the main plate as a constant pressure equal to $p = -\Delta\sigma_{nom}$, on Line 16;
- <u>Constraints</u>: symmetry boundary conditions are applied on Lines 6 and 18.

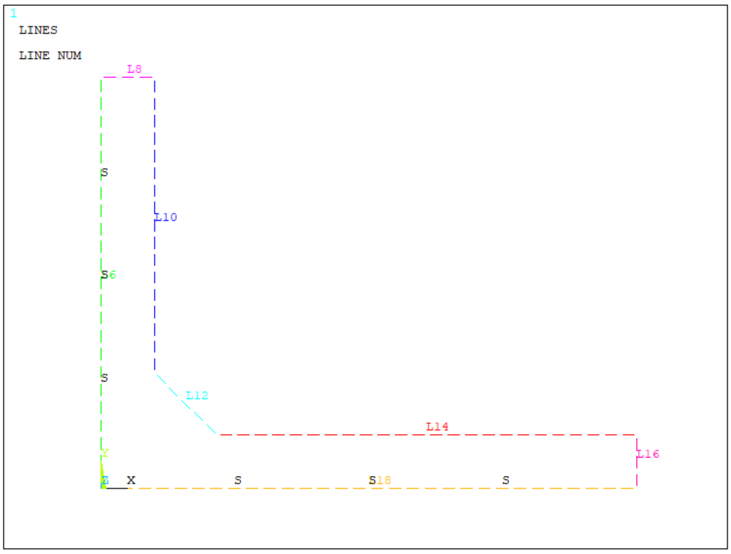

Figure 3. 80: loads and constraints application to Kuhlmann (2009). The letter S refers to a Symmetry BC.

3.5.1 PSM Plane 182

The fatigue assessment is performed in terms of equivalent peak stress, with the adoption of the Peak Stress Method for 2D structures, four-node linear elements.

From Ansys® APDL element library, Plane 182 element is chosen; the Key Option K1 is switched to *Simple Enhanced Strain*, while K3 is changed to *Plane Strain*.

Under mode I loading, the PSM Plane 182 requirements are listed below:

Location: weld toe, gusset **Mode I**

Element Type	**Mesh algorithm**	**$(a/d)_{min}$**	**2α**	**Mesh pattern 2α < 90°**	**Mesh pattern 2α > 90°**
Plane 182 *KOs: Simple Enhanced Strain + Plane Strain*	Free	3	0 < 2α < 135°	Four adjacent elements share the same node	Two adjacent elements share the same node

Under these restrictions, the mode I PSM calibration constant is equal to $K_{FE}^{*} = 1.38 \pm 3\%$, at both gusset and weld toe locations.

The following PSM dispositions are thus adopted:

- Half the main plate thickness a is equal to a = 6 mm;
- The mesh global element size is set to d = 2 mm;
- $\frac{a}{d} = \frac{6}{2} = 3 \geq 3$ the ratio is respected;
- The λ_1 and e_1 values associated to $2\alpha = 135°$ required for f_{w1} detection respectively are:

2α	**λ_1**	**e_1**
135°	*0.674*	*0.118*

Finally, the stress corrective factors under mode I calculated with equation (1.16) is $f_{w1} = 1.334$.

3.5.2 PSM Plane 182, analysis of results

For an external applied pressure $\Delta\sigma_{nom}$=1 MPa, the first principal stress is plotted:

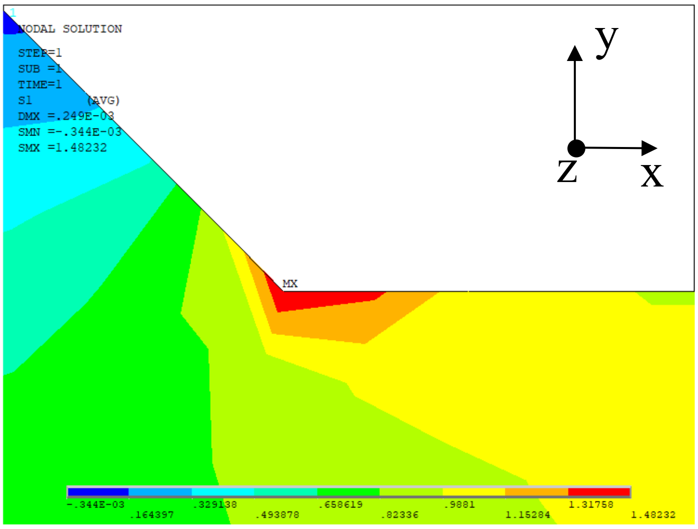

Figure 3. 81: plot of the first principal stress in Kuhlmann, for an external applied stress equal to 1 MPa. In black, the global coordinate system.

With reference to Chapter 2, the peak stress $\sigma_{\theta\theta,\theta=0,peak}$ (i.e. the $\Delta\sigma_{yy}$ of the Ansys® local coordinate system) has to be evaluated at the most solicited point of the structure. As it was previously demonstrated, under mode I loading $\Delta\sigma_{yy}$ can be confused with $\Delta\sigma_{11}$ both at weld toe and gusset.

For an external applied pressure $\Delta\sigma_{nom}$=1 MPa, the maximum $\Delta\sigma_{11}$ located at the weld toe tip is equal to:

$$\Delta\sigma_{11} = \Delta\sigma_{\theta\theta,\theta=0,peak} = 1.48\ MPa$$

Once the peak stress is given, both K_1 and $\Delta\sigma_{eq,peak}$ can be respectively found with formulae (2.5) and (2.8):

$$\Delta K_1 \cong K_{FE}^* \cdot \Delta\sigma_{\theta\theta,\theta=0,peak} \cdot d^{1-\lambda_1} = 1.38 \cdot 1.48 \cdot 2^{1-0.674} = 2.56\ MPamm^{0.326}$$

$$\Delta\sigma_{eq,peak} = \Delta\sigma_{\theta\theta,\theta=0,peak} \cdot f_{w1} = 1.48 \cdot 1.334 = 1.97\ MPa$$

If the global element size is set to d=1 mm, the respective stress corrective factor becomes f_{w1}=1.064 and the results are the same as before:

$$\Delta\sigma_{11} = \Delta\sigma_{\theta\theta,\theta=0,peak} = 1.85\ MPa$$

$$\Delta K_1 \cong K_{FE}^* \cdot \Delta\sigma_{\theta\theta,\theta=0,peak} \cdot d^{1-\lambda_1} = 1.38 \cdot 1.85 \cdot 1^{1-0.674} = 2.55\ MPamm^{0.326}$$

$$\Delta\sigma_{eq,peak} = \Delta\sigma_{\theta\theta,\theta=0,peak} \cdot f_{w1} = 1.85 \cdot 1.064 = 1.97\ MPa$$

In agreement with the experimental reality, the PSM correctly foresees the weld toe as the most solicited part of the joint.

3.5.3 Data entry in the PSM curve

In the preliminary analysis, 1 MPa was applied to the main plate of the specimen; to obtain the effective equivalent peak stress related to the applied nominal stress, the equation (3.2) can be adopted. The results can be consulted in Appendix F.

The experimental data are then entered inside the PSM design curve proposed by Meneghetti and Lazzarin under prevailing mode I:

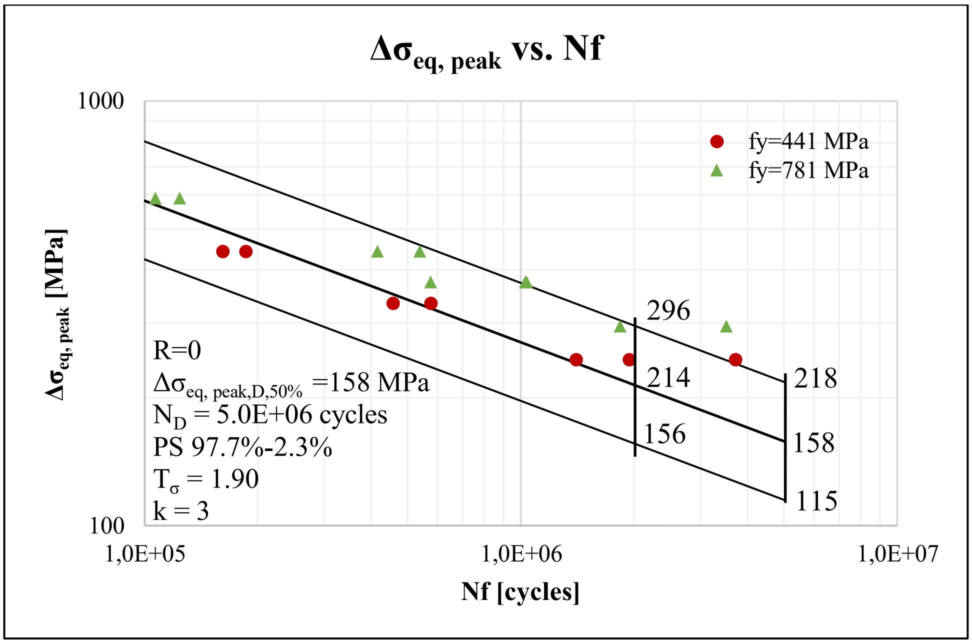

Figure 3. 82: data entry inside the PSM design curve [7].

The following conclusions can be drawn:

1. The totality of the data, re-elaborated in terms of the Peak Stress Method Plane 182, fall inside the PSM curve, confirming its effectiveness;
2. Since the collected experimental data refer to R=0.1, all the PSM data were correctly inserted in the literature scatter band;
3. Even though misalignments are not considered, all the experimental data fall inside the curve.

3.5.4 Structural Hot-Spot Stress

The fatigue assessment of the Kuhlmann FAT 80 welded joint is performed following the IIW recommendations [1] for the hot-spot stress extrapolation. In reference to the guideline, type "a" hot-spot is detected with the employment of fine mesh, as shown in *Figure 1.6*.

Proper mesh indications, concerning the stress extrapolation region, are given in the table below:

Element Type	Mesh algorithm	Main plate thickness t	Max element size	Adopted el. size
Plane 182 *KOs: Simple Enhanced Strain + Plane Strain*	Mapped	12 mm (6 mm modelled)	0.4*(t/2) = 2.4 mm	0.6 mm

A pressure equal to $\Delta\sigma_{nom}$ = 1 MPa is applied on the parent material, as a preliminary analysis, and the solution is launched.

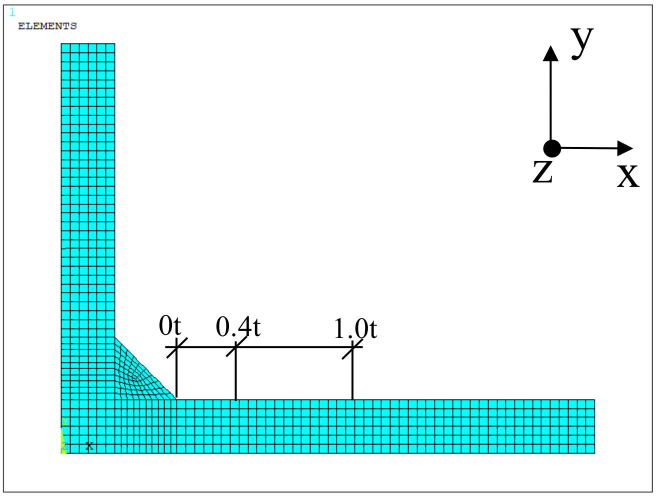

Figure 3. 83: mapped mesh for the hot-spot stress detection. In black, the global coordinate system.

According to [1], the structural hot-spot stress has to be extrapolated at two reference points located at 0.4t and 1.0t distance from the weld toe tip, it is to say 4.8 mm and 12 mm. In regard of the type of extrapolated stress, previously it was demonstrated that both σ_{11} and σ_{xx} can be independently chosen. The mesh pattern can be seen in *Figure 3.83*.

For an external applied pressure equal to $\Delta\sigma_{nom}$=1 MPa, the resultant extrapolated stresses at the reference points are

$$\Delta\sigma_{0.4t} = 1.00\ MPa$$

$$\Delta\sigma_{1.0t} = 0.99\ MPa$$

The structural hot-spot stress SHSS is finally detected with equation (3.5):

$$\sigma_{hs} = 1.67 \cdot \Delta\sigma_{0.4t} - 0.67 \cdot \Delta\sigma_{1.0t} = 1.01\ MPa$$

Therefore, the analysis shows that the SHSS tends to be very close to the nominal stress. As Xiao and Yamada [3] point out in their research, this result is another confirmation of the fact that SHSS cannot predict the thickness effect.

3.5.5 1-mm Stress

The fatigue assessment of the Kuhlmann FAT 80 specimen is now performed with the employment of Xiao and Yamada [3] method, proposing a stress extrapolation 1-mm below the weld toe tip, along the y direction referring to *Figure 3.84*.

In respect of the previous precautions emerged during the FAT 71 analysis, the adopted measures for this simulation are shown in the table below:

Element	Mesh algorithm	Element size	Extrapolated Stress
Plane 182 *KOs: Simple Enhanced Strain + Pure Displacement*	Mapped	0.05 mm	$\Delta\sigma_{xx}$

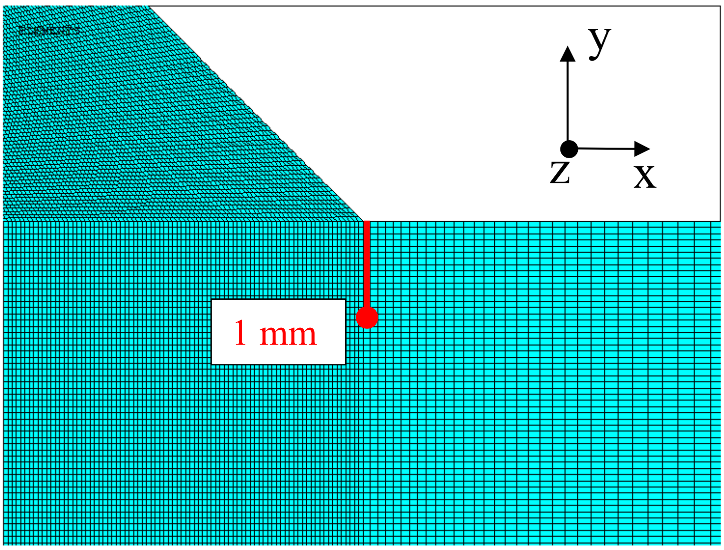

Figure 3. 84: very fine mesh (size = 0.05 mm) near the weld toe, according to Xiao's article, and indication of the reference node at 1-mm distance. In black, the global coordinate system.

For an external applied load $\Delta\sigma_{nom}$=1 MPa , the resulting extrapolated $\Delta\sigma_{1\text{-}mm}$ is equal to:

$$\Delta\sigma_{1-mm} = 1.08\ MPa$$

3.5.6 Data entry in the IIW curves

<u>Nominal approach</u>

The experimental data in terms of nominal stress, reported at the beginning of paragraph 3.5, are entered inside the FAT 80 design curve proposed by the IIW guideline.

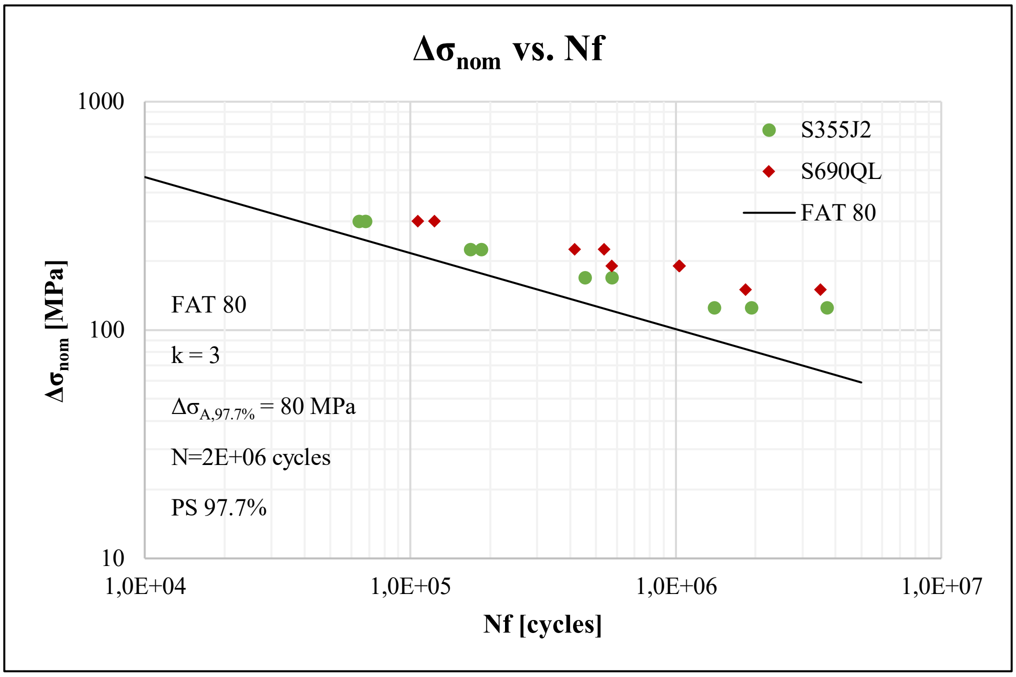

Figure 3. 85: data entry inside the FAT 80 design curve, global approach [1].

<u>SHSS approach</u>

In the preliminary analysis, 1 MPa was applied to the main plate of the specimen; under linear elasticity hypotheses, the effective SHSS related to a specific $\Delta\sigma_{nom}$ can be detected with (3.6).

The results can be consulted in Appendix F. The experimental data in terms of hot-spot stress are entered inside the FAT 100 design curve, for non-load carrying specimens, proposed by the IIW guideline:

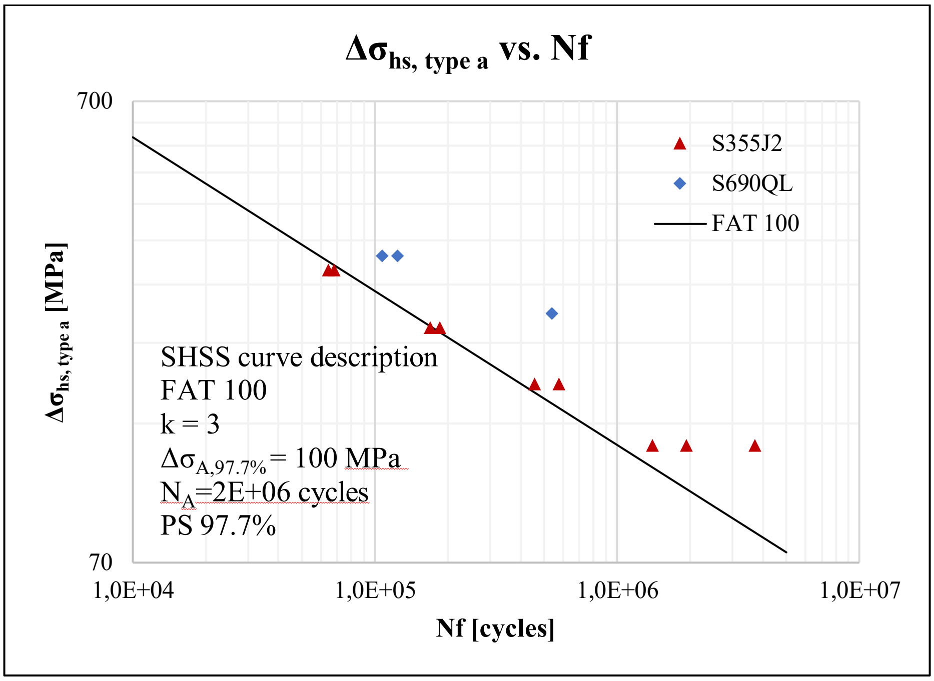

Figure 3. 86: data entry inside the FAT 100 design curve, hot-spot approach [1].

<u>1-mm stress approach</u>

In the previous analyses, 1 MPa was applied to the main plate of the specimen; under linear elasticity hypotheses, the effective 1-mm stress related to a specific $\Delta\sigma_{nom}$ can be detected with (3.7).

The experimental data in terms of 1-mm stress, reported in Appendix F, are entered inside the reference detail design curve, proposed by Xiao and Yamada:

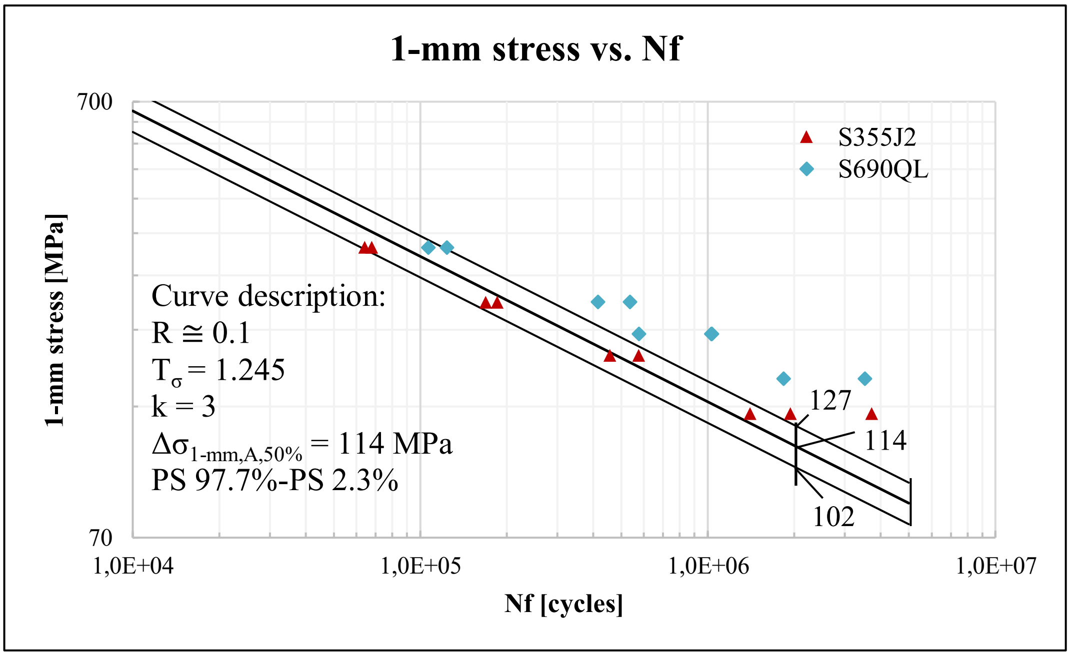

Figure 3. 87: data entry inside the 1-mm design curve [3].

The following conclusions can be drawn:

1. These methods have correctly been applied to the welded joint, for weld toe fractures;
2. Even though misalignments have not been considered, not all the hot-spot experimental data fall above the PS 97.7% line. However, the influence of misalignment seems to be not to important in this case;
3. Concerning the 1-mm and the nominal stress, the design curves have proven to be effective and conservative, confirming the fact that bending stresses could be neglected in this case.

3.5.7 Fatigue life comparison

The fatigue life comparison is performed in terms of equivalent nominal stress. For a PS 97.7%, at 2 million cycles, the corresponding equivalent stress is found with formula (3.8):

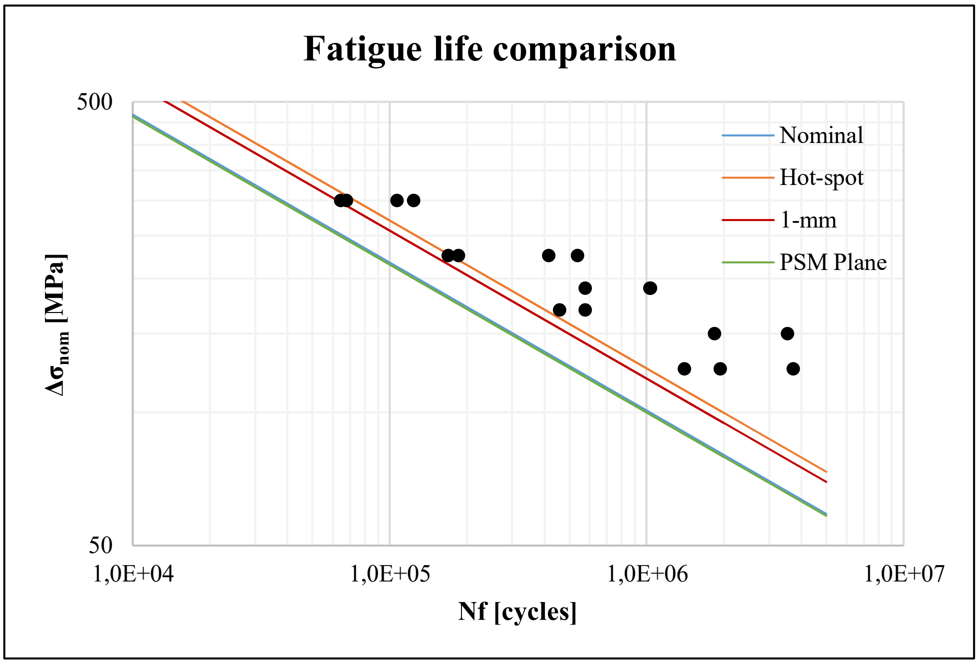

Figure 3. 88: fatigue life comparison.

Some relevant conclusions can be drawn:

- PSM is the most conservative method, along with the nominal approach;
- IIW local approaches give similar results in terms of fatigue life;
- Hot-spot stress method again demonstrates to be the least conservative because for several data the experimental fatigue life is higher than the foreseen one.

Chapter 4: principles of post-weld treatments on welded joints for the weld toe improvement

Nowadays, various post-weld techniques are employed to enhance the fatigue resistance of the welded structures, improving both the weld profile and the residual stress conditions located in the weld toe region. Various methods for the weld toe improvement have been furthering over the years: in 2007, Haagensen and Maddox [41] approved the best practice recommendations concerning four common weld toe post-weld treatment techniques for steel and aluminium structures: burr-grinding, TIG re-melting (i.e. TIG dressing), hammer peening and needle peening. In principle, both hammer and needle peening induce a plastic deformation at the weld toe, while TIG dressing and grinding remove the embedded defects in the proximity of weld toe, allowing besides a smooth transition between the main plate and the weld toe. Classic post-weld improvement techniques differ from each other according to the way they are implemented and the results they give: while TIG dressing and grinding have the advantage of reducing the local stress concentrations at the weld toe with surface quality refinements, on the other hand hammer and needle peening have the extra capacity of introducing beneficial compressive residual stresses in the weld toe region. Each technique could be contemporarily applied to the weld profile, which would result in a greater fatigue life enhancement for the component.

As affirmed by Hobbacher, the grade of improvement each technique bestows depends on the applied load, the material, the structural detail, the stress ratio R and the global dimension of the welded joint. The benefit factors upgrade the as-welded FAT classes [1].

As the name suggests, weld toe improvements are suitable only in weld toe crack propagation cases, which examples are illustrated in *Figure 4.1*. Other examples, where the improvement may not be effective, are instead shown in *Figure 4.2*:

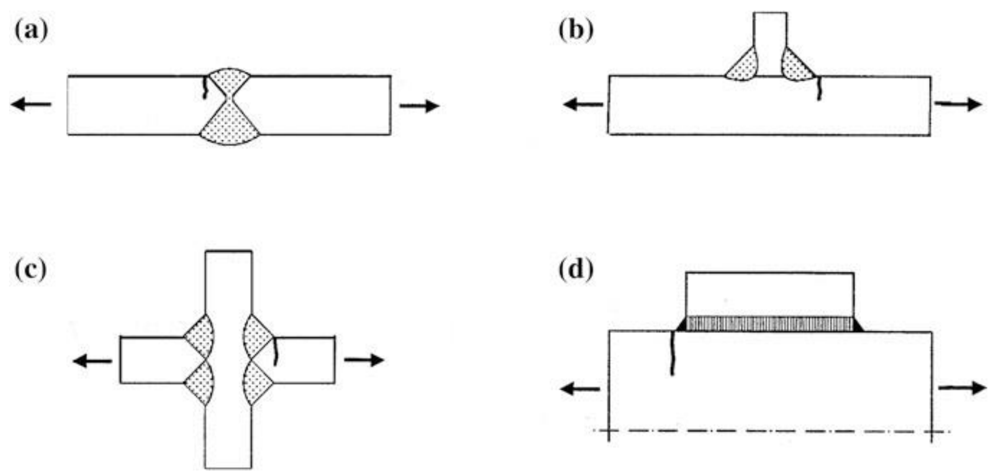

Figure 4. 1: some examples of joints that can be improved [1].

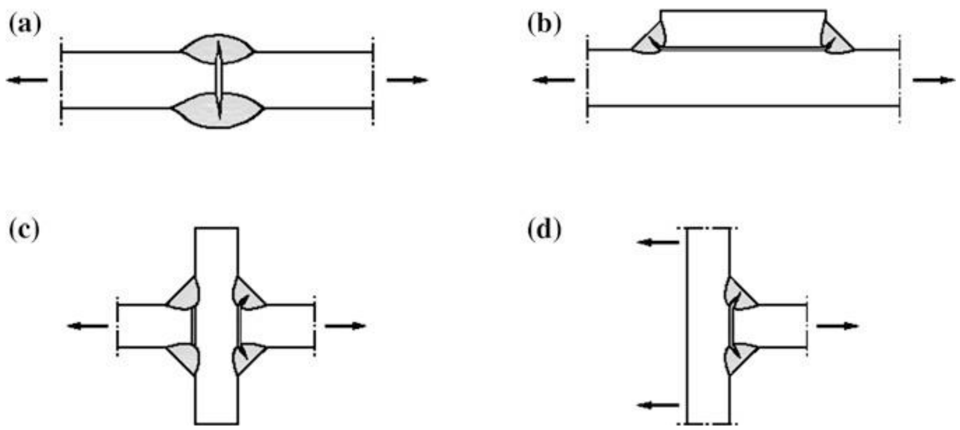

Figure 4. 2: some examples of joints which improvement could not effective [1].

4.1 The High Frequency Mechanical Impact treatment

In the past decades, the High Frequency Mechanical Impact (HFMI) has revealed itself as a trustworthy, user-friendly and efficient technique for post-weld fatigue life improvement of welded joints. Alongside the aforementioned TIG dressing, grinding, hammer and needle peening, the HFMI is denoted as a fatigue strength increase technology dedicated both to new structures as well as maintenance operations on already existing mechanical components.

The reference guideline, "IIW recommendations for the HFMI treatment" from Marquis and Barsoum [9], can be consulted in the Bibliography section.

4.1.1 Backgrounds of the HFMI treatment

In a HFMI treatment, the impacted material is highly plastically deformed causing changes in the material microstructure and the local geometry as well as the residual stress state in the region of impact.

The original technology for high frequency mechanical impact was developed in 2002 at the Northern Scientific and Technological Foundation in Russia in association with Paton Welding Institute in the Ukraine [42]. Between 2002 and 2012, several scientific papers regarding HFMI technologies proved the benefits of this peculiar weld toe post-weld treatment in terms of fatigue strength increment and weld toe surface quality refinement. Over the past decade, numerous HFMI peening equipment manufacturers have been emerging along with the proposal of customized indenters of different steel grade and pin tip radius. The peening devices have alternate power sources, among which ultrasonic impact treatment (UIT), ultrasonic peening (UP), ultrasonic peening treatment (UPT), high frequency impact treatment (HiFiT), pneumatic impact treatment (PIT) and ultrasonic needle peening (UNP) are cited in [43]. The common mechanism behind consists in accelerating high strength steel cylindrical indenters against the weld toe, with frequencies about 90 Hz, so that the impacted material endures a local plastic deformation. The material microstructure modifies, as well as the local weld toe local geometry. As main emerging outcome, the tensile residual stresses localised in the weld toe region, which are typically found in as-welded conditions, are efficiently brought into highly compressive.

In *Figure 4.3*, some examples of HFMI treatments from different companies are displayed.

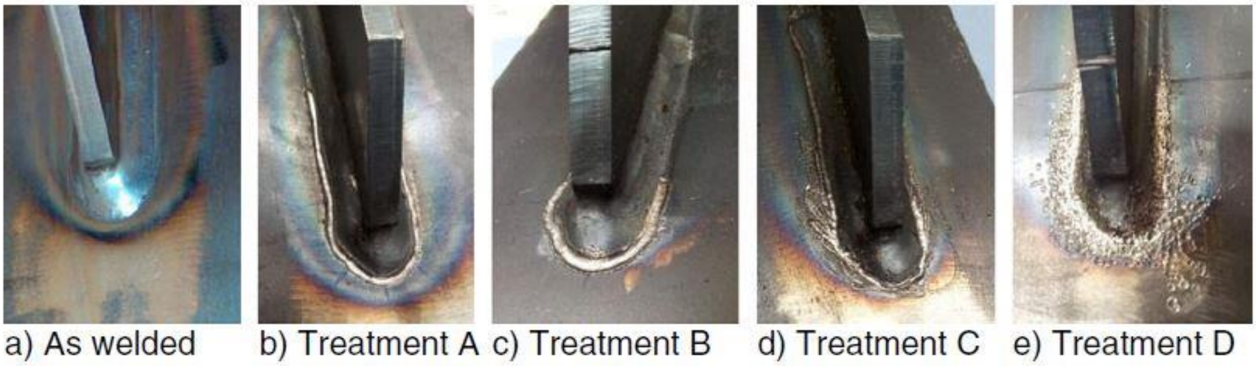

Figure 4. 3: different HFMI grooves, outcome of four different companies [38].

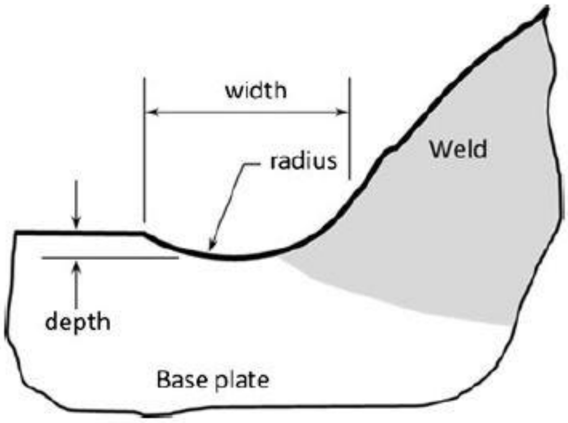

Figure 4. 4: sketch of HFMI region [9].

In 2016, Gary B. Marquis and Zuheir Barsoum published the IIW Recommendations for HFMI treatment for improving the fatigue strength of welded joints [9]. The guideline proves to be applicable to joints made of structural steel, main plate ranging from 5 to 50 mm and steel grade f_y varying from 235 MPa to 960 MPa. However, it is noted that nowadays parallel research is currently being conducted also on aluminium and stainless-steel structures.

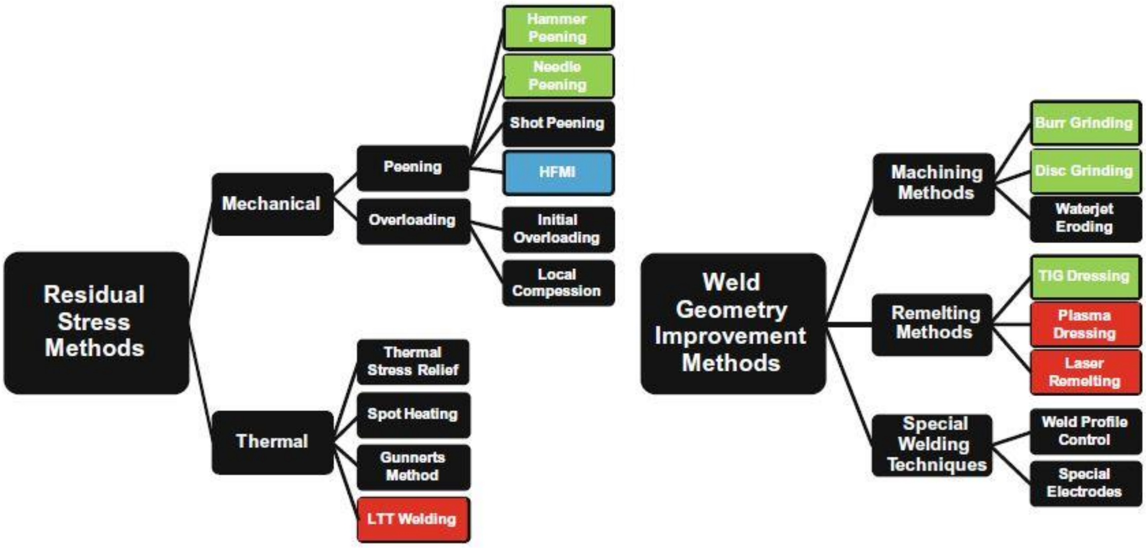

Figure 4. 5: overview of the various weld improvement techniques. Green is covered by IIW recommendations, red is planned/in progress, and the blue refers to HFMI [9].

The table below, taken from the IIW guideline [9], shows the benefits guaranteed by the main post-weld improvement operations:

Method	**Weld geometry improvement**		**Mechanical effects**
	Smoothing transition	*Eliminate defects*	*Induce compressive residual stresses*
Grinding	x	x	-
TIG dressing	x	x	-
Hammer/needle peening	x	x	x
HFMI	x	x	x

As it is noted, both hammer peening and HFMI treatment have the advantage to simultaneously refine the local weld geometry and its surface quality, and to induce compressive residual stresses at the weld toe. However, as Marquis and Barsoum assert, HFMI operations are esteemed more user-friendly and the spacing between alternate impacts on the work piece is very small resulting in a finer surface finish [9].

As for the other operations, the HFMI treatment solely applies to weld toe, since due to technical issues the operation cannot be performed in other singularities such as weld roots. As a consequence, in case of potential fractures occurring at the root, an eventual HFMI treatment at the weld toe might not be effective.

Figure 4.6 displays examples of improper impacts between the indenter and the weld toe, which could result in a facilitated potential crack initiation.

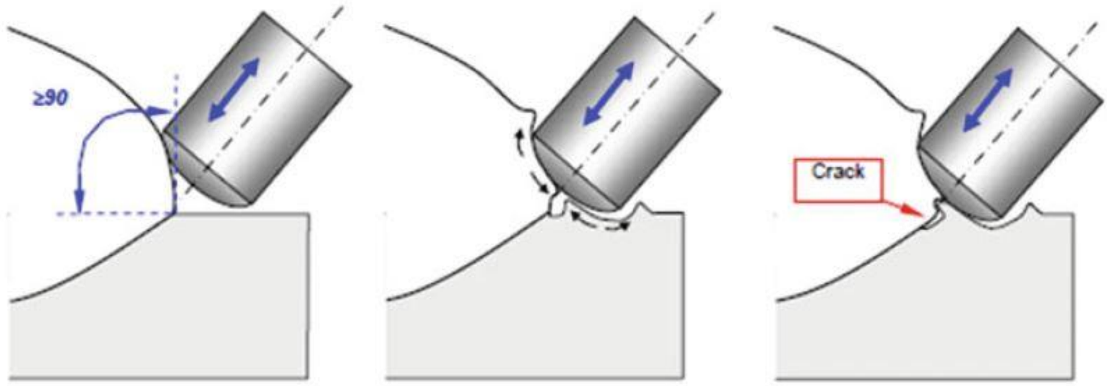

Figure 4. 6: initiation of a crack-like defect due to an inappropriately treated weld toe presenting a steep angle, or due to a too large-sized indenter [9].

Generally, the weld toe improvement operations consistently vary according to the employed tool. The table below, taken from Marquis and Barsoum guideline [9], illustrates some procedure parameters for two HFMI tools with alternate power sources and indenter configurations.

Parameter	**HFMI tool**	
	HiFIT	**UIT**
Power source	*Pneumatic*	*Ultrasonic magneto strictive*
Number of indenters	*1*	*1 - 4*
Angle of the axis of the indenter w.r.t the plate surface Φ	*60° - 80°*	*30° - 60°* *40° - 80°*
Angle of the axis of the indenter w.r.t the direction of travel ψ	*70° - 90°*	*90°*
Working speed	*3 - 5 mm/s*	*5 - 10 mm/s* *5 - 25 mm/s*
Other		*The self-weight of the tool is sufficient. Minimum 5 passes.*

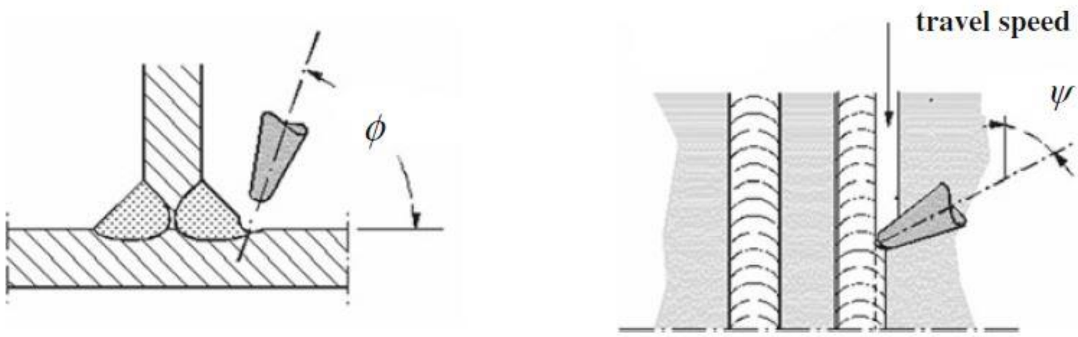

Figure 4. 7: on the left, inclinations of the indenter with respect to the plate surface; on the right, with the respect to the direction of travel [9].

Concerning the inclination angle of the indenter with respect to the plate surface Φ, it is common practise to match Φ and the V-notch bisector.

The guideline also gives advices on visual inspections for the qualitative and quantitative measurement of the weld toe groove. Concerning qualitative aspects, a well-treated weld toe should appear smooth, shiny, continuous, with no breaks or visible lines as well as undercuts or porosities. A significant example is represented in *Figure 4.8*:

Figure 4. 8: a shiny and defect free HFMI groove [9].

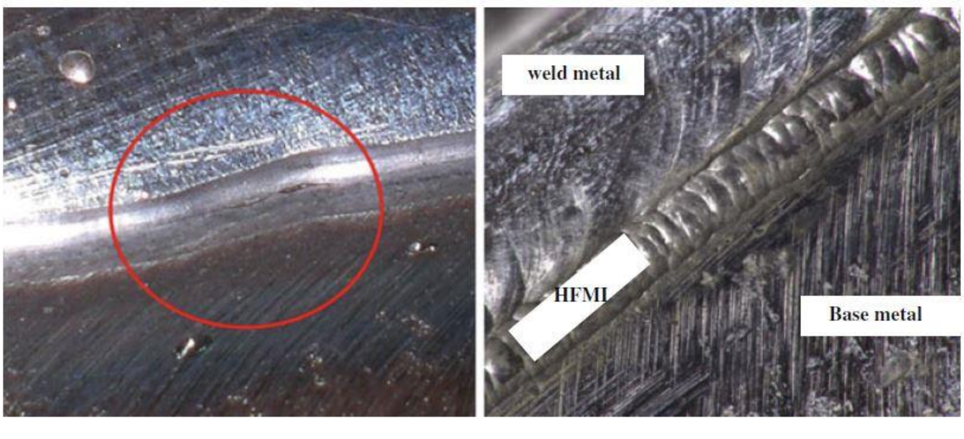

Figure 4. 9: on the left, HFMI groove presenting an imperfection; on the right, a non-smooth HFMI groove which needs further peening [9].

HFMI operations often bring to consistent local cold forming of the material near the weld fusion line. In case the pin tips are exceedingly impacted in one single location at the weld toe, the arising plastic deformation might form imperfections in the groove edge, as illustrated in *Figure 4.10*. The resulting crack-like defect must be eliminated by light grinding, along with a further weld toe treatment [9].

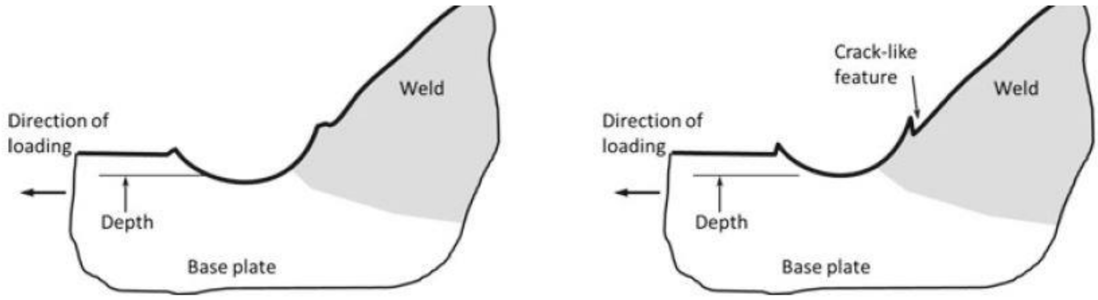

Figure 4. 10:on the left, normal on the right, the creation of a crack-like feature at the side of the HFMI groove [9].

Focusing on quantitative measurements, the guideline [9] cites some typical post-weld treatment geometrical quantities:

- Groove depth = 0.1 – 0.6 mm;
- Groove width = 3 – 6 mm;
- The radius depends on the employed pin tip diameters, as well as the number of passes.

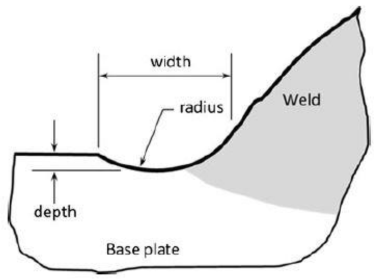

Marquis and Barsoum bestow two observations: first, it is noted that a unique optimal HFMI groove dimension does not exist, since each configuration depends on both the steel yield strength and the diameter of the indenter. Second, it is advisable to have a minimum groove depth of at least 0.1 – 0.2 mm to ensure an efficient quality treatment.

4.2 Fatigue assessment of HFMI-treated welded joints (IIW recommendations)

According to the IIW guideline on HFMI-treated joints [9], the fatigue assessment of HFMI specimens is currently available in terms of global approach (nominal stress), as well as local approaches (structural hot-spot stress, effective notch stress). In the next paragraph, the theory behind the first two approaches is explained.

4.2.1 Global approach (nominal stress)

The beneficial effects of the HFMI treatment are available only for welded joints having FAT classes between FAT 50 and FAT 90; upper classes refer to complex structural geometries or non-welded details mainly governed by root failures, while lower classes have not been investigated yet.

Many factors, such as main plate thickness and size, steel grade f_y, overloads, stress ratio and variable amplitude loading VAL, may involve the reduction, as well as the modification, of the reference nominal FAT classes for the HFMI-treated joints. In the following pages, a description of their effects and characteristics is made.

Thickness and size effect

As for the as-welded specimens, HFMI-treated joints are affected by the thickness and size effect. In fact, the larger the main plate (and the stiffener) thickness is, the higher the local stress concentration at the weld toe and, consequently, the lower the fatigue strength. The reduction factor for plate thicknesses greater than 25 mm, taken from the IIW guideline [1], shown in equation (4.1), holds true even for HFMI-treated joints:

$$f(t) = \left(\frac{25}{t_{eff}}\right)^{0.2} \tag{4.1}$$

where:

- $t_{eff} = \frac{L}{2}$ if $\frac{L}{t} < 2$
- $t_{eff} = t$ if $\frac{L}{t} \geq 2$

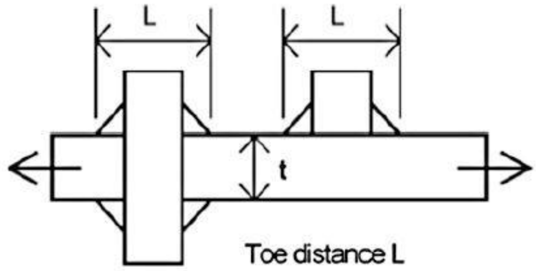

Figure 4. 11: description of L and t [9].

Steel grade

The influence of the material steel strength on the grade of improvement in the joint is displayed in *Figure 4.12*:

- If $f_y < 355$ MPa, four FAT classes increment in strength, starting from the reference nominal FAT class in as-welded condition, is recommended;
- If $f_y > 355$ MPa, one FAT classes increment in strength (about 12.5%) for every 200 MPa increment in yield resistance f_y is recommended.

These solutions have proved to be conservative for all the collected data.

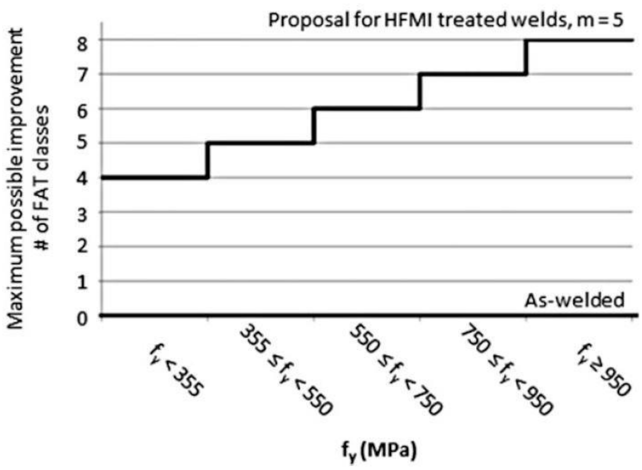

Figure 4. 12: numbers of FAT class increment to varying of f_y [9].

The turning up observation refers to the fact that HFMI operations have the tendency to increase their beneficial effect along with the material steel grade f_y.

Stress ratio

In as-welded joints, the presence of high tensile residual stresses in the crack region modifies the local stress cycle with respect of the applied external one. As a consequence, it is proved that the stress ratio R does not affect the fatigue endurance of as-welded joints, since its dependence is mostly due to the residual stress entity. On the contrary, in case of HFMI-treated joints, in which the local residual stresses are compressive, the influence of R on the fatigue strength is explained as a penalty factor which can strongly alter the service life of the component.

As it can be seen in *Figure 4.13*, the general trend assumes that the higher the stress ratio is, the lower the fatigue endurance, expressed in terms of maximum applicable $\Delta\sigma_{nom}$, becomes. This hold even truer for higher material steel grades f_y.

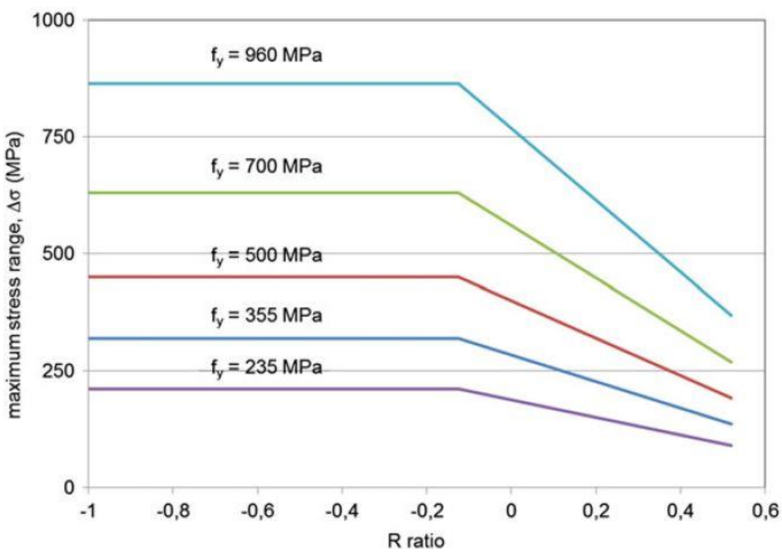

Figure 4. 13: $\Delta\sigma_{nom,\,max}$ vs. R, CAL condition [9].

The table below, taken from Marquis and Barsoum's guideline, quantifies the number of FAT classes reduction to varying of R.

Stress Ratio R	**Minimum FAT classes reduction**
$R \leq 0.15$	*No reduction*
$0.15 < R \leq 0.28$	*One FAT class*
$0.28 < R \leq 0.4$	*Two FAT classes*
$0.4 < R \leq 0.52$	*Three FAT classes*
$0.52 < R$	*No data available*

Loading effects

Eventual overloads on the structures might lead to a plastic redistribution of the material in the weld toe region, resulting in the beneficial compressive residual stress decrement, thus compromising the efficacy of the HFMI treatment [44].

The table below, consultable in the IIW guideline for HFMI-treated joints [9], summarizes the limitations on the maximum applied stress, which holds true for both as-welded and improved joints:

Type of load	**AW**	**HFMI + hammer/needle peening**
$\boldsymbol{\Delta\sigma_{nom,max}}$ **[MPa]**	$1.5\ f_y$	$0.8\ f_y$ *due to overloads* **R < 0.5*
$\boldsymbol{\Delta\tau_{nom,max}}$ **[MPa]**	$1.5\ \frac{f_y}{\sqrt{3}}$	
$\boldsymbol{\Delta\sigma_{hs,max}}$ **[MPa]**	$2\ f_y$	

Variable amplitude loading

Given a variable amplitude loading history, the latter can be expressed in terms of an equivalent constant amplitude loading history with the adoption of formula (4.2), based on Miner's damage sum hypothesis:

$$\Delta\sigma_{eq} = \left(\frac{1}{D} \cdot \frac{\sum \Delta\sigma_i^m N_i + \Delta\sigma_k^{(m-m')} + \sum \Delta\sigma_j^{m'} N_j}{\sum N_i + \sum N_j}\right)^{\frac{1}{m}} \tag{4.2}$$

where:

- $\Delta\sigma_{eq}$ is the equivalent applied stress in terms of CAL;
- $N_{i,j}$ are the number of cycles spent at their respective stress range $\Delta\sigma_{i,j}$;
- $\Delta\sigma_k$ is the stress range related to the knee point at $N = 1 \cdot 10^7$ cycles;

- D is the damage sum, ranging from 0 to 1;
- m is the inverse slope above the knee point;
- m' is the inverse slope below the knee point.

Nominal FAT classes for HFMI-treated joints

The assumed inverse slope of the nominal FAT classes for HFMI joints is equal to $m = 5$. As for the as-welded state, FAT classes are defined at $N_A = 2 \cdot 10^6$ cycles. The knee point is defined at $N_D = 1 \cdot 10^7$ cycles, where the slope changes to $m' = 22$ in case of CAL, while $m' = (2m - 1)$ in case of VAL.

Between *Figure 4.14* and *Figure 4.18*, the nominal S-N curves for HFMI-treated joints, under constant amplitude loading CAL, are illustrated to varying of the steel grade f_y and for a stress ratio R < 0.15:

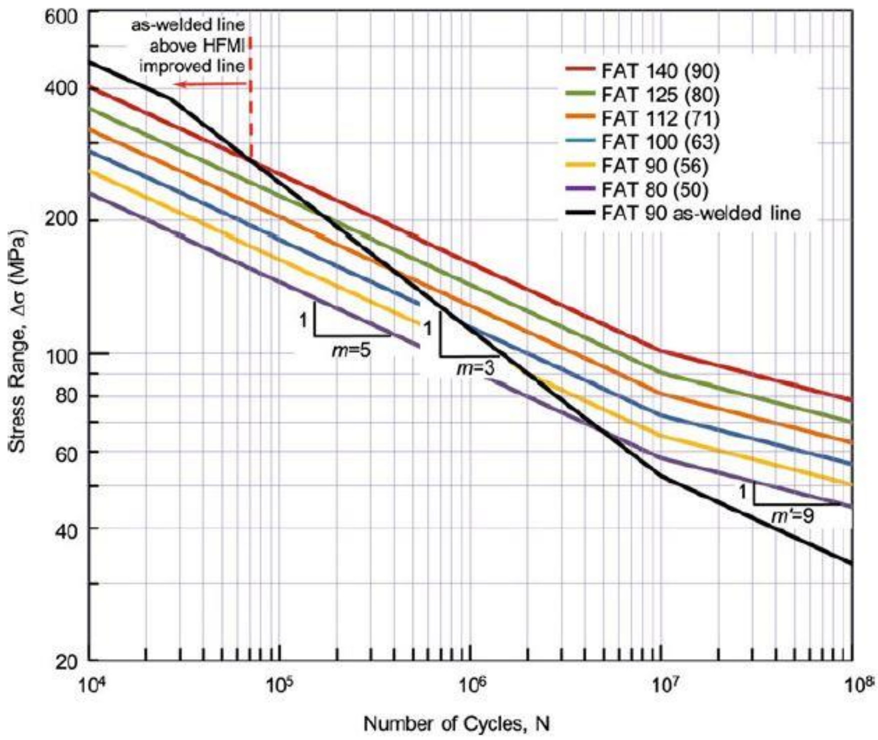

Figure 4. 14: nominal S-N curves for HFMI-treated welded joints, f_y < 355 MPa, R < 0.15. The terms in brackets refer to the reference FAT class in AW condition. In black, the FAT 90 as-welded line [9].

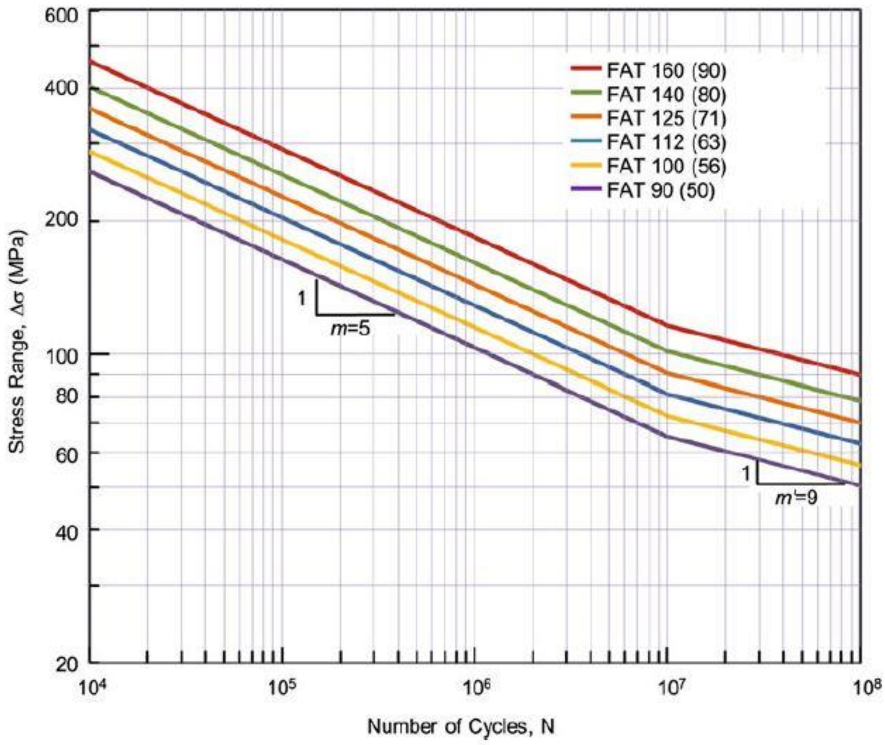

Figure 4. 15: nominal S-N curves for HFMI-treated welded joints, 355 MPa < f_y < 550 MPa, R < 0.15. The terms in brackets refer to the reference FAT class in AW condition [9].

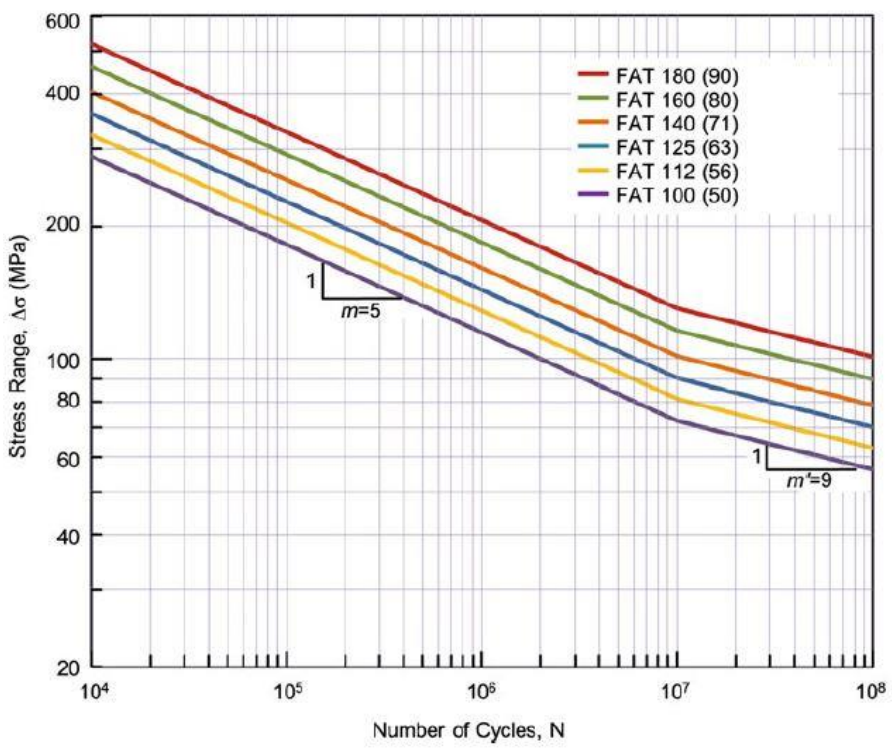

Figure 4. 16: nominal S-N curves for HFMI-treated welded joints, 550 MPa < f_y < 750 MPa, R < 0.15. The terms in brackets refer to the reference FAT class in AW condition [9].

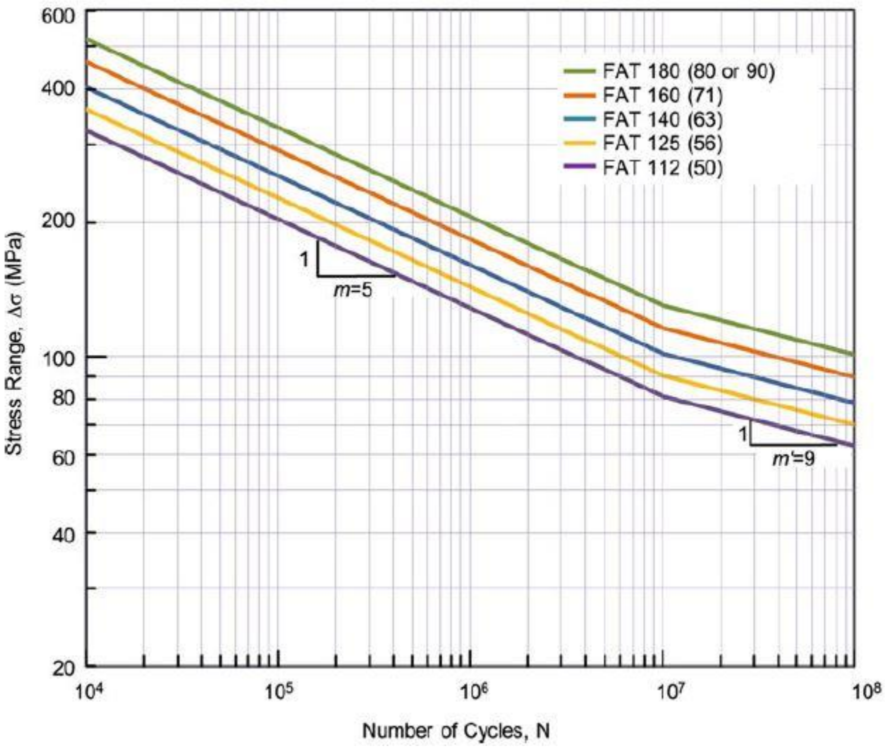

Figure 4. 17: nominal S-N curves for HFMI-treated welded joints, 750 MPa < f_y <950 MPa, R < 0.15. The terms in brackets refer to the reference FAT class in AW condition [9].

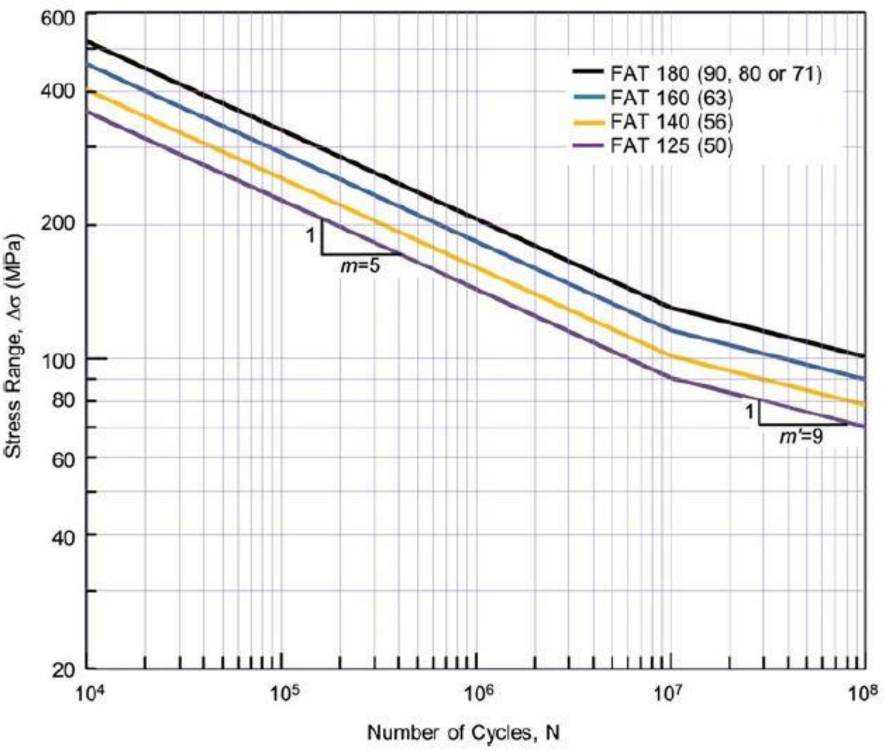

Figure 4. 18: nominal S-N curves for HFMI-treated welded joints, 950 MPa < f_y , R < 0.15. The terms in brackets refer to the reference FAT class in AW condition [9].

In *Figure 4.14*, both the as-welded FAT 90 and its respective HFMI FAT 140 curves are represented; due to their different slopes, there is an intersection point, named N_{int} in this thesis. Therefore, for a given number of cycles $N < N_{int}$ the AW line predicts a higher number of cycles to failure with respect to the HFMI prevision. Conclusively, the benefits of the post-weld improvement techniques are effective only from N_{int} onwards. The specific N_{int} to varying of the f_y range are illustrated below:

f_y [MPa]	N_{int} [cycles]
$f_y < 355$	*72 000*
$355 < f_y < 550$	*30 000*
$550 < f_y < 750$	*12 500*
$f_y > 750$	*< 10 000*

As it can be noted, N_{int} diminishes as f_y increases. This trend highlights the fact that HFMI treatments proves to be more beneficial for higher strength steels.

4.2.2 Local approaches (hot-spot stress)

As far as the structural hot-spot stress for HFMI-treated joints is concerned, the numerical extrapolation with the employment of FE software follows the same recommendations given by Hobbacher in his IIW guideline [1], which can be consulted in Chapter 1.

In AW conditions, two hot-spot stress design curves are proposed for structural steels: FAT 90 and FAT 100. In case of HFMI improved joints, Marquis and Barsoum [9] highlight the fact that the respective FAT classes are function of the steel grade range, as it can be seen in the following table:

	LC fillet welds		NLC fillet welds	
f_y [MPa]	FAT	$k_{S,min}$	FAT	$k_{S,min}$
	As-welded, m = 3			
All f_y	*90*	-	*100*	-
	Improved by HFMI, m = 5			
$f_y < 355$	*140*	-	*160*	-
$355 < f_y < 550$	*160*	-	*180*	-
$550 < f_y < 750$	*180*	-	*200*	*1.15*
$750 < f_y < 950$	*200*	*1.15*	*225*	*1.25*
$f_y > 950$	*225*	*1.25*	*250*	*1.40*

When extrapolating the SHSS, the verification of the equation (4.3), dealing with structural hot-spot stress concentration k_S, is recommended:

$$k_s = \frac{\sigma_{hs}}{\sigma_{nom}} > k_{s,min} \tag{4.3}$$

In case of relatively small structural hot-spot stress concentrations, computational issues might arise. In cases like this, Marquis and Barsoum assert that the hot-spot stress system must be limited so as not to result in a S-N curve greater that FAT 180 in the nominal stress system [9].

4.3 Fatigue assessment of HFMI-treated welded joints (University of Padova)

According to the current state of the art, both the Peak Stress Method and the Strain Energy Density have been employed for the fatigue assessment of welded joints in as-welded and stress-relieved conditions. Investigations in cases of local beneficial compressive residual stresses, such as for HFMI-treated joints, have never been conducted.

Referring to the literature [38], the HFMI groove radius at the weld toe typically ranges between 1.5 mm and 4.5 mm: the possibility of assuming the weld toe radius equal to zero, as it was done in case of as-welded specimens, is too restrictive. Consequently, the welds of HFMI-treated joints are then assumed as blunt V-notches, so that the PSM can be employed in combination with the SED method for blunt notches.

4.3.1 Principles of SED for blunt notches

In 2005, the SED method, initially proposed in 2001 by Lazzarin and Zambardi [6] for sharp V-notches, was secondly extended to blunt notches on PMMA specimens [10]. The theory behind follows the same principles previously expressed in 2001 for sharp notches in steel and aluminium alloys structures. A sketch of a blunt notch along with its polar system of reference is displayed in *Figure 4.19*:

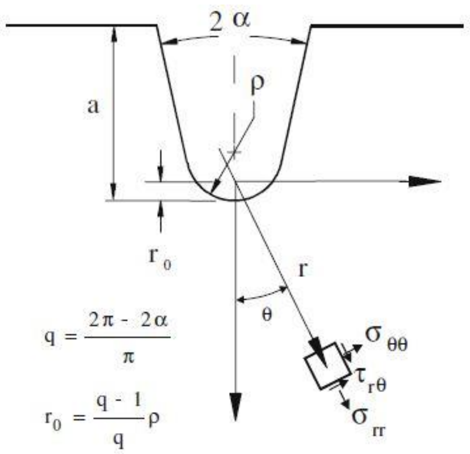

Figure 4. 19: polar coordinate system and stress components of a blunt V-notch [45].

Two parameters are fundamental for the proper modelling of the rounded circular sector. Their respective expression, found by Neuber in 1958 [45], is reported in equations (4.4) and (4.5):

$$q = \frac{2\pi - 2\alpha}{\pi} \tag{4.4}$$

$$r_0 = \frac{q-1}{1} \cdot \rho \tag{4.5}$$

where:

- 2α is the notch opening angle;
- ρ is the notch radius;
- r_0 is the distance from the origin of the analytical frame and the notch tip.

In *Figure 4.20 (c)* a schematic representation of the resulting volume can be appreciated:

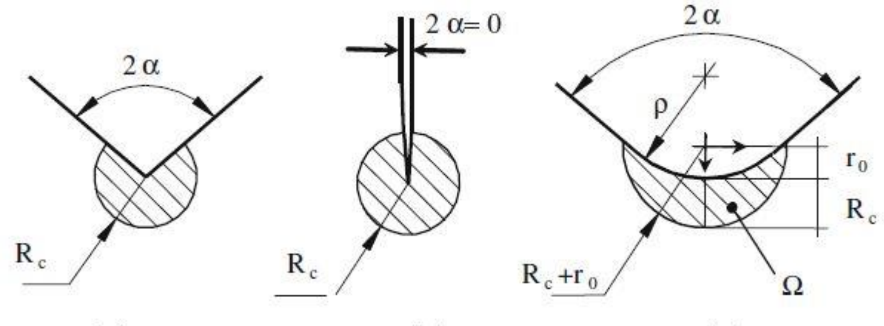

Figure 4. 20: from left to right, schematic representations of a sharp V-notch, a crack and a blunt notch. Ω refers to the area enclosed by the structural volume [10].

As highlighted by Lazzarin in 2005 [10], when mixed modes are effective at the notch the maximum first principal stress, clearly linked to the highest strain energy deformation, appears not to be aligned with the blunt notch bisector. In such cases, the structural volume has to be rigidly rotated by an angle φ about the centre of the blunt notch, so as the maximum principal stress is entirely included in the volume. According to *Figure 4.21*, the circular sector has its centre translated to point O':

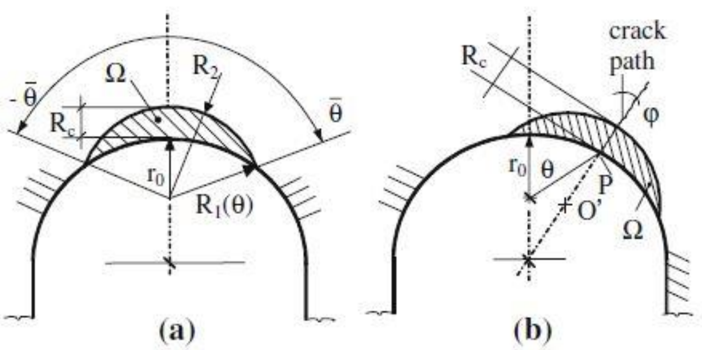

Figure 4. 21: on the left, example of circular sector under mode I; on the right, under combined modes [10].

In the particular event of a radiused weld toe, like the case of a post-weld HFMI treatment, the averaged strain energy density $\Delta\overline{W}$ inside this crescent-shape structural volume could be analytically calculated making use of equation (1.9). In a FE environment, the average SED ($\Delta\overline{W}_{FEM}$) might be instead detected with the employment of the so-called "direct approach", with formula (1.10) [33]:

$$\Delta\overline{W}_{FEM} = \frac{\sum_{V(R_0)} W_{FEM,i}}{V(R_0)} \tag{4.6}$$

4.3.2 PSM in combination with SED for blunt notches

Under linear elastic hypothesis, the equivalent peak stress is detected with (4.7) [33]:

$$c_w \cdot \Delta\overline{W}_{FEM} = \frac{1-\nu^2}{2E} \cdot \Delta\sigma_{eq,peak}^2 \rightarrow \Delta\sigma_{eq,peak} = \sqrt{c_w \cdot \frac{2E \cdot \Delta\overline{W}_{FEM}}{1-\nu^2}} \tag{4.7}$$

where:

- $\Delta\sigma_{eq,peak}$ is the equivalent peak stress;
- $\Delta\overline{W}_{FEM}$ is the average strain energy density inside the crescent-shape circular sector;
- c_w is the parameter accounting of the stress ratio R;
- E is the Young modulus;
- ν is the Poisson's ratio.

Chapter 5: fatigue assessment of HFMI-treated joints by local approaches

In this Chapter, the fatigue assessment on various HFMI-treated welded joints is performed in terms of structural hot-spot stress and equivalent peak stress. The aim is to investigate the effectiveness of the PSM in combination with the SED approach for blunt notches, currently valid for as-welded and stress-relieved welded joints, for the fatigue assessment of HFMI-treated joints. Along with it, the assessment in terms of the structural hot-spot stress refers to the dispositions available in the IIW guideline [9]. The re-elaborated datasets are entered in their respective design curves in order to quantify the grade of effectiveness and conservativeness provided by each method.

The current work was performed at Aarhus University, under the guidance of the supervisor Associate Professor Halid Can Yildirim.

Re-elaborated datasets consist of the same as-welded geometries previously analysed in Chapter 3: three longitudinal stiffeners, one FAT 71 [34, 38] and two FAT 63 class [35], as well as five FAT 80 transverse attachments (Yildirim et al., Okawa 2011 [36], Kuhlmann 2009 [37], 2006 [46]).

The assessments are effectuated with the employment of the Finite Element FE software Ansys® Mechanical APDL 19.0, license from University of Padova; the simulations are achieved with the adoption of four-node linear element Plane182, *Simple Enhanced Strain* and *Plane strain* as Key Options K1 and K3, in case of 2D FE models; on the other hand, ten-node quadratic element Tetra187, *Pure Displacement* as Key Option K1, are chosen for the analysis of 3D structures. The elements are available in the Ansys® element library.

Due to the complex geometry of the HFMI groove in the weld toe location, all the specimens were modelled inside SOLIDWORKS 2018 *Student Edition*, for then being imported in Ansys® APDL with the .IGS extension.

According to the literature [38], the HFMI groove radius typically ranges between 1.5 mm and 4.5 mm; thus, in order to correctly apply the PSM in combination with the SED method, the assumption of blunt V-notches has to be made. As far as the c_w factor is concerned, since it is valid for only as-welded and stress-relieved welded joints, c_w is non-rigorously left to 1. On the other hand, the SHSS approach for HFMI-treated joints follows the same procedures previously discussed for the hot-spot detection for as-welded joints.

The influence of misalignments on HFMI-treated joints is not considered critical. Along with the fact that no information quantifying the k_m was inferred from the specimens in Chapter 3, misalignments are again neglected in the following analyses.

5.1 Longitudinal attachment, FAT 71

The first welded joint to be assessed is the longitudinal stiffener, fatigue class FAT 71, tested by Yildirim in 2017 [34] under constant amplitude loading CAL.

Specific information on the component is reported below:

Weld condition	Fracture location	Load application	Main plate/gusset thickness
HFMI, non-load carrying, full penetration	*Weld toe*	*Axial, main plate, parent material*	*Main plate: 8 mm* *Gusset: 8 mm*

The mechanical properties are described below:

Material	Yield strength f_y	Young modulus	Poisson's ratio ν
S700, HSS, linear elastic, isotropic	*700 MPa*	*206000 MPa*	*0.3*

The geometry of the specimen can be referred to *Figure 3.1* and *Figure 3.2*, Chapter 3, along with the weld profile parameters.

In regard of the HFMI groove geometry, the article states that the longitudinal stiffener is taken from [38], in which *Figure 5.1* lists the HFMI groove radii, denominated ρ_{HFMI} in this elaborate, resulting from different post-weld operations. Overall, it is seen that 1.8 mm < ρ_{HFMI} < 4.55 mm.

Manufacturer	Radius (mm)	SD	Width (mm)	SD	Depth (mm)	SD
A	1.80	0.20	2.39	0.32	0.16	0.05
B	3.81	0.46	4.10	0.37	0.22	0.11
C	3.03	0.60	3.11	0.43	0.17	0.03
D	4.55	1.11	5.45	1.05	0.29	0.08
Average	3.30	0.59	3.76	0.54	0.21	0.07

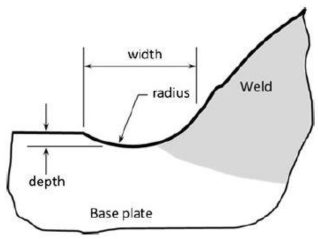

Figure 5. 1: values of HFMI-improved weld measurements, and respective standard deviations SD [38].

From this table, referring to manufacturer A, the groove radius is assumed ρ_{HFMI}=1.8 mm (worst case), the depth is taken 0.16 mm, the width is 2.39 mm. Concerning the indenter inclination angle, in agreement with the recommendations, the operation is assumed to be performed along the V-notch bisector, i.e. 75° in this case.

Henceforth, the HFMI region is summed up in the table below, and displayed in *Figure 5.2*:

ρ_{HFMI} [mm]	Depth [mm]	Width [mm]
≅ 1.80	*0.16*	*2.39*

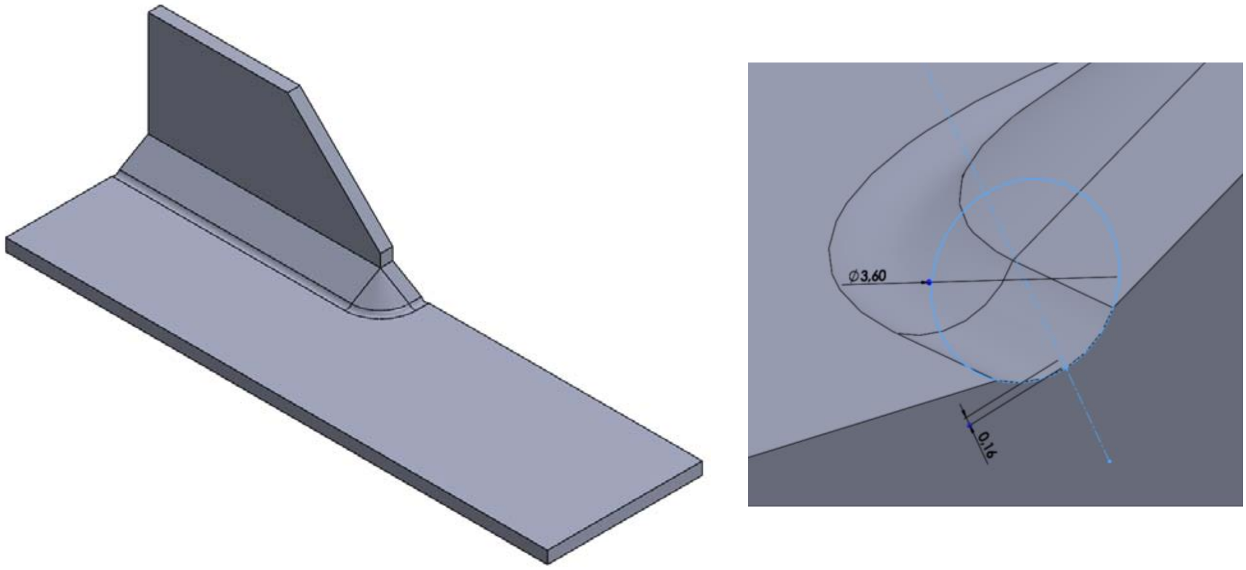

Figure 5. 2: representation of the HFMI treatment along the weld toe profile, with geometrical references.

The experimental data are reported in terms of nominal stress $\Delta\sigma_{nom}$:

R	**$\Delta\sigma_{nom}$ [MPa]**	**N_f [cycles]**
-1	464	499 700
	450	552 400
	446	208 600
	410	1 949 000
	337	964 800
	337	858 400
	317	447 500
	305	469 700
	257	2 907 000
	255	1 980 000

Since the compressive residual stresses at the weld toe are thought to be one of the main reasons for the improvement of fatigue endurance, their values, measured with X-ray diffraction in the longitudinal direction perpendicular to the weld toe, are reported in *Figure 5.3*.

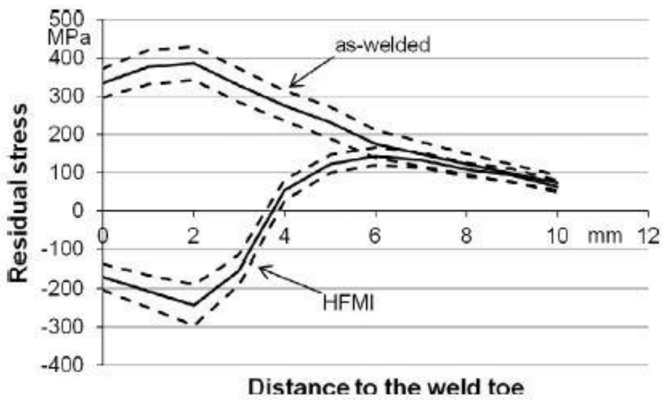

Figure 5. 3: residual stress distributions along the surface in both as-welded and HFMI conditions [34].

5.1.1 SED and PSM for blunt notches

Before proceeding, the POWERGRAPHICS option in Ansys® Toolbar is disabled, otherwise the results in output are given by the average of the superficial elements, with no consideration of the interior ones.

In Ansys® APDL element library, Tetra 187 element is chosen; the Key Option K1 is left to *Pure Displacement*.

As shown in *Figure 5.4*, the SED method for blunt notches is based on the creation of a rounded cylindrical sector, i.e. the structural volume, at the radiused weld toe, which can be rigidly rotated so as to capture the whole maximum principal stress (thus related to the highest strain energy density).

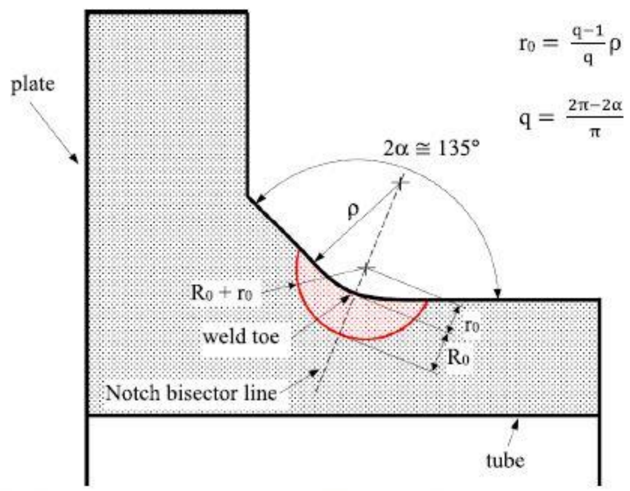

Figure 5. 4: example of the structural volume creation at a radiused weld toe for the SED detection [33].

The first step consists in detecting the inclination with respect to the blunt notch bisector of the most stressed area (highlighted in red in Ansys®): after meshing the structure with an arbitrary global element size, an external nominal stress $\Delta\sigma_{nom}$=1 MPa is applied on the main plate, the system is solved, and the first principal stress $\Delta\sigma_{11}$ is plotted:

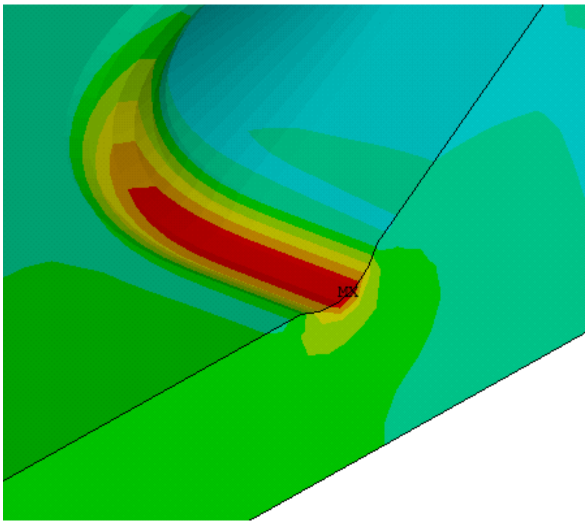

Figure 5. 5: plot of the first principal stress near the weld toe region.

As it is noted, the highest stress is located exactly around the blunt notch bisector, thus the structural volume can be designed along it. The circular sector is created according to equations (4.4) and (4.5), also reported in *Figure 5.4*:

$$q = \frac{2\pi - 2\alpha}{\pi} = 2 - \frac{150}{180} = 1.17$$

$$r_0 = \frac{q-1}{1} \cdot \rho_{HFMI} = \frac{0.17}{1.17} \cdot 1.8 = 0.26\ mm$$

$$R_0 + r_0 = 0.28 + 0.26 = 0.54\ mm$$

Following the modelling dispositions of *Figure 5.4*, first the rounded circular sector is designed as shown in *Figure 5.6:*

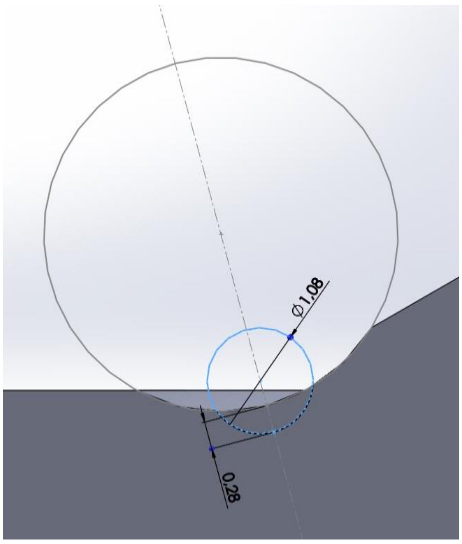

Figure 5. 6: structural volume, inclination and geometrical quantities.

For 3D specimens, due to the symmetries, the area has to be extruded by 0.14 mm (i.e. $R_0/2$):

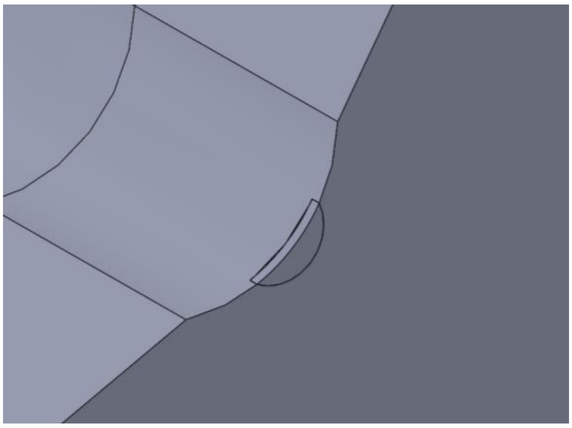

Figure 5. 7: illustration of half of the outcome rounded cylindrical sector.

Inside Ansys® APDL environment, the following meshing procedures are employed:

a) The circular sector lines size is set to 0.06 mm:

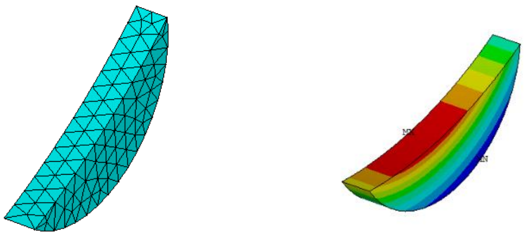

Figure 5. 8: on the left, meshed structural volume. On the right, the proof that the highest stress is contained inside it.

b) The edge HFMI groove lines size is set to 0.1 mm;
c) The edge weld lines size is set to 0.1 mm, with a spacing ratio of 10, to guarantee a smooth element transition towards the groove. The resulting mesh conformation can be appreciated in *Figure 5.9*.

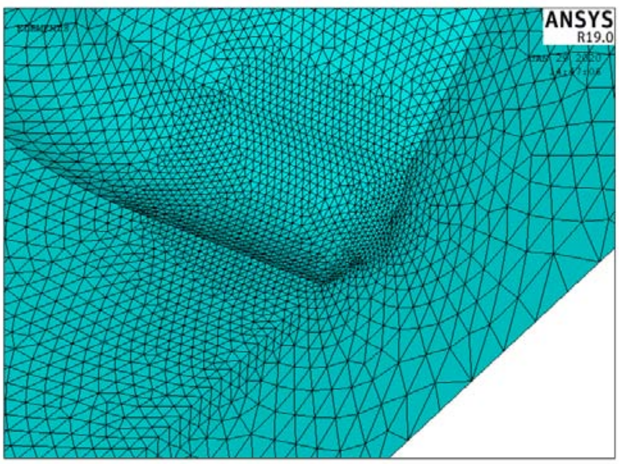

Figure 5. 9: resulting mesh conformation.

d) The remaining geometry is free meshed, with a global element size equal to 1 mm.
The system can now be solved:

Main Menu > Solution > Solve > Current LS

The averaged SED parameter is defined as the energy contained inside the rounded structural volume. To obtain the average SED value, only the elements belonging to the cylindrical sector must be selected. In Ansys® APDL, the following commands have to be used:

Utility Menu > Select > Entities > Volumes > From Full

Utility Menu > Select > Everything Below > Selected Volumes

At this moment, a table containing both the energy (SENE) and volume (VOLU) of the selected elements has to be created:

Main Menu > General Postproc > Element Table

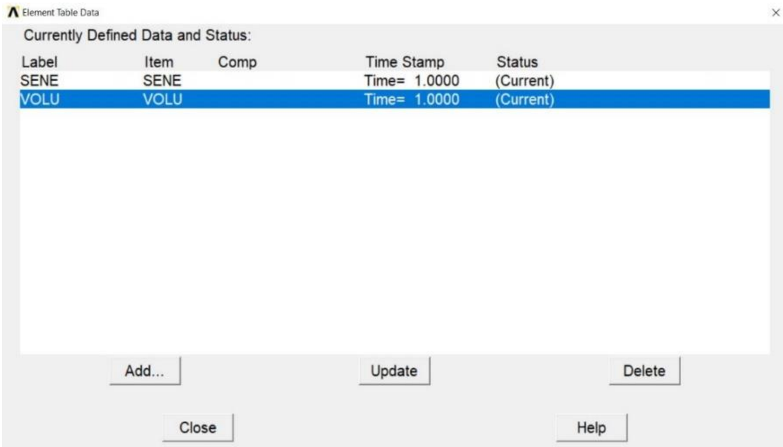

Figure 5. 10: element table in Ansys® APDL, where both SENE and VOLU are calculated.

Each single element SENE and VOLU values now have to be summed:

Main Menu > General Postproc > Element Table > Sum of Each Item

Finally, the SED value ($\Delta\overline{W}_{FEM}$ referring to FE software) is calculated with equation (2.3):

$$\overline{W}_{FEM} = \frac{\sum_{V(R_0)} W_{FEM,i}}{V(R_0)} = \frac{SENE}{VOLU} = \left[\frac{MJ}{m^3}\right] \tag{5.1}$$

For an external applied load equal to $\Delta\sigma_{nom}$ = 464 MPa, the resultant strain energy density is then equal to:

$$SENE = 8.54 \cdot 10^{-2}\, J$$

$$VOLU = 0.0294846\, mm^3$$

$$SED = \frac{8.54 \cdot 10^{-2}}{0.0294846} = 2.9\ \frac{MJ}{m^3}$$

Finally, the equivalent peak stress is calculated with equation (4.7):

$$\Delta\sigma_{eq,peak} = \sqrt{c_w \cdot \frac{2E \cdot \Delta\bar{W}_{FEM}}{1-\nu^2}} = 1145\ MPa$$

5.1.2 Data entry in the PSM curve

In linear elasticity hypothesis, the $\Delta\sigma_{eq,peak}$ values resulting from different external loads can be found with equation (2.4). The results can be consulted in Appendix C.

The experimental data, following the work made in Meneghetti, Campagnolo, Babini [33], are then entered inside the PSM design curve proposed by Meneghetti Guzzella and Atzori:

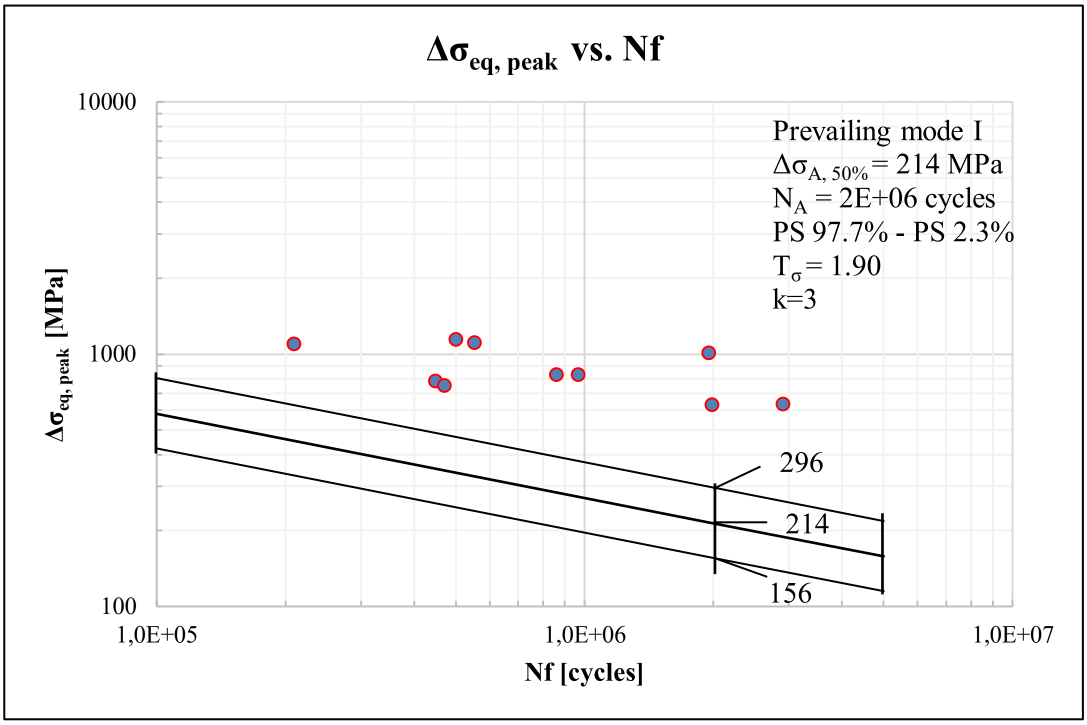

Figure 5. 11: data entry inside the PSM design curve [28].

The following conclusions can be drawn:

1. The PSM in combination with the SED approach for blunt notches has correctly foreseen the experimental crack initiation point at weld toe;
2. Since the experimental data falls above the PS 2.3% line, the PSM design curve has proven to be effective and very conservative. However, this result is expected since the two methods have only been calibrated for as-welded and stress-relieved welded joints, in which the beneficial effects of compressive residual stresses are not present.

5.1.3 Data entry in the IIW curve

With reference to Chapter 3, paragraph 3.1.9, for an external applied load $\Delta\sigma_{nom}$=1 MPa, the related SHSS was $\Delta\sigma_{hs}$=1.39 MPa. In linear elasticity hypotheses, the effective SHSS related to a specific $\Delta\sigma_{nom}$ can be detected with (3.6). The experimental results can be consulted in Appendix C.

In agreement with the IIW recommendations on HFMI-treated welded joints [9], the hot-spot FAT class for 550 < f_y < 750, non-load carrying fillet welds, minimum $k_{S,min}$=1.15, corresponds to FAT 200:

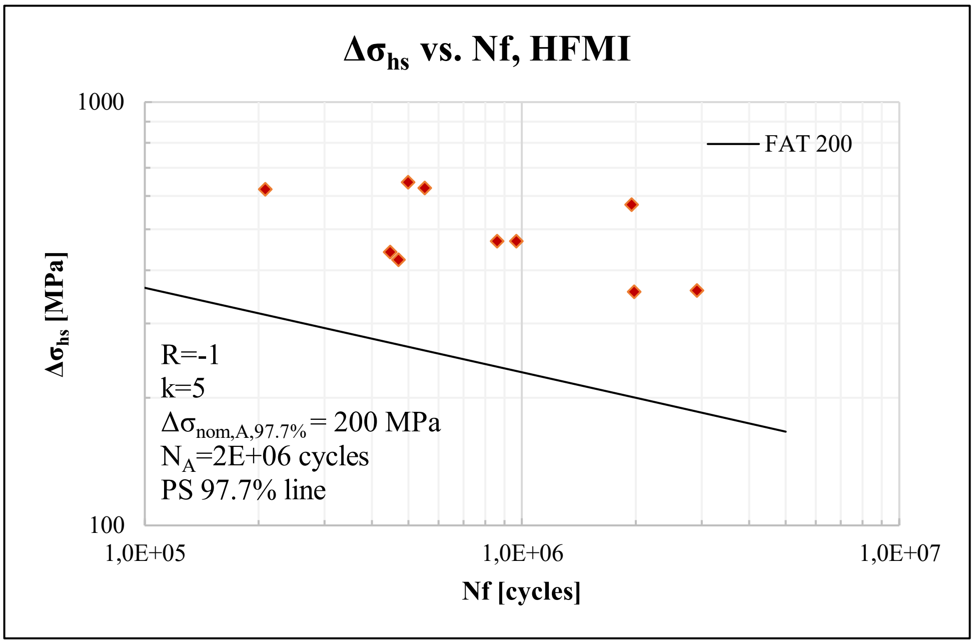

Figure 5. 12: data entry inside the FAT 200 and FAT 140 design curves, hot-spot approach [9].

The following conclusions can be drawn:

1. These methods have correctly been applied to weld toe fractures;
2. Even though misalignments have not been considered, since the experimental data fall above the PS 97.7% line, the hot-spot design curve has proven to be effective and very conservative.

5.2 Longitudinal attachment, FAT 63

The second welded joint category to be assessed is a longitudinal stiffener, fatigue class FAT 63, tested by Yildirim et al. Marquis in 2013 [35] under constant amplitude loading CAL.

Only the three specimens highlighted in *Figure 3.40* are analysed:

- S700MC, main plate and gusset thickness = 10 mm;
- S690QL, main plate and gusset thickness = 10 mm;
- S690QL, main plate and gusset thickness = 20 mm.

Since both the geometry and material steel grade f_y are common, the first two models are together analysed as a single 10-mm specimen, while the third one is assessed separately as a 20-mm specimen.

Specific information on the components is reported below:

Weld condition	Fracture location	Load application	Main plate/gusset thickness
HFMI, non-load carrying, full penetration	*Weld toe + parent material*	*Axial, main plate, parent material*	*Main plate:5-20 mm* *Gusset: 5-20 mm*

The mechanical properties are described below:

Materials	Yield strength f_y	Young modulus	Poisson's ratio ν
S700MC, HSS, linear elastic, isotropic	*700 MPa*	*206000 MPa*	*0.3*
S690QL, HSS, linear elastic, isotropic	*690 MPa*		

The geometry of the two analysed specimens (10-mm and 20-mm thickness) can be referred to *Figure 3.39*, Chapter 3, along with the weld profile.

In regard of the HFMI groove geometry, since no information can be inferred relevant assumptions must be made: according to the report [35], the radius of the pin of the indenter ranges between 3 mm and 8 mm. Then, as first try, ρ_{HFMI} could be made to correspond to the smaller pin radius, i.e. ρ_{HFMI}=3 mm. However, evidence proves that often ρ_{HFMI} is smaller than the pin tip radius. Therefore, concerning the 10-mm specimen, for which ρ_{HFMI}=3 mm would be exaggerated, the weld toe groove diameter is assumed ρ_{HFMI}=1.8 mm, with reference to the article [38]; for the 20-mm specimen, on the author of the report Professor Yildirim's advice, again ρ_{HFMI}=1.8 mm. Always referring to [38] and *Figure 5.1*, a value of 0.16 mm is chosen as penetration depth. In regard of the indenter inclination angle, the report states that the range of oscillation angle during treatment relative to the initial position of 45° is between 35° and 55°. Thus, the latter is assumed along the V-notch bisector, i.e. 60° in this case.

Hence, the HFMI region is summed up in the table below, and displayed in *Figure 5.13*:

t [mm]	ρ_{HFMI} [mm]	Depth [mm]
10	*≅ 1.8*	*0.16*
20	*≅ 1.8*	*0.17*

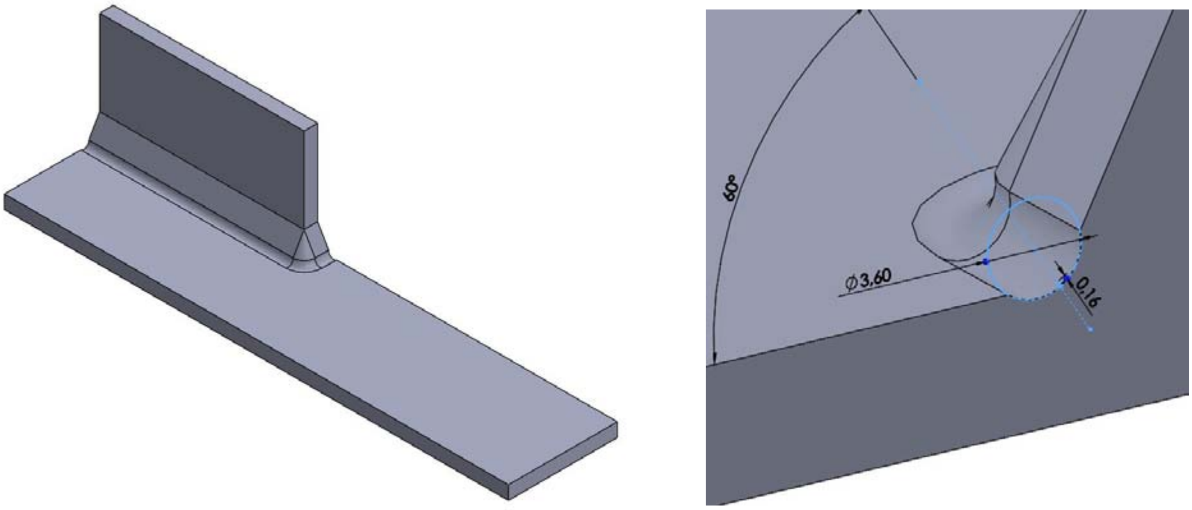

Figure 5. 13: representation of the HFMI treatment along the weld toe profile, with geometrical references, 10-mm specimen.

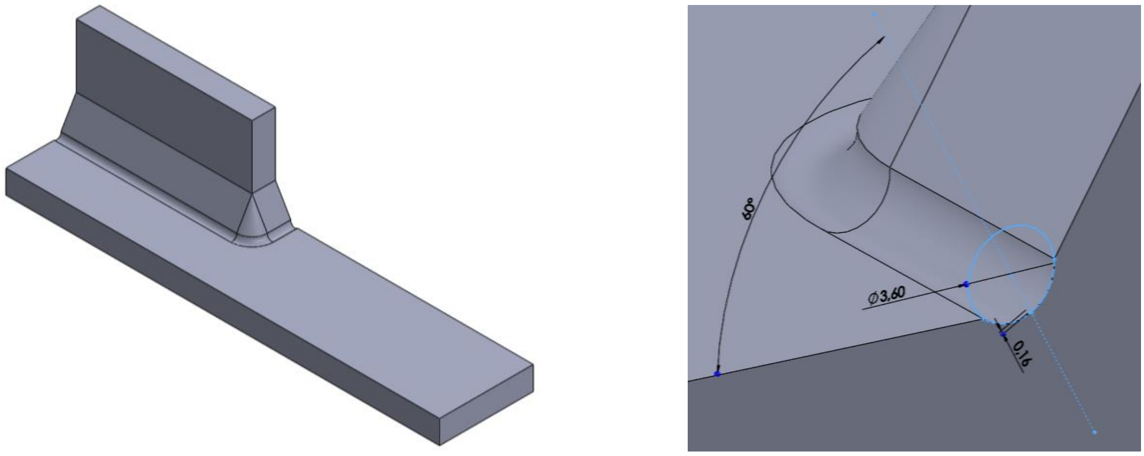

Figure 5. 14: representation of the HFMI treatment along the weld toe profile, with geometrical references, 20-mm specimen.

The experimental data are reported in terms of nominal stress $\Delta\sigma_{nom}$. In barred, the runouts.

t=10 mm

Steel grade	**R**	**$\Delta\sigma_{nom}$ [MPa]**	**N_f [cycles]**	**Failure**
S690QL S700MC	0.1	300	158 200	Weld toe
		150	2 031 700	Weld toe
		~~90~~	~~10 000 000~~	Runout
		200	2 235 000	PM
		250	3 547 800	Weld toe
		350	101 200	Weld toe
		~~175~~	~~10 000 000~~	Runout
		150	532 122	Weld toe
		~~90~~	~~6 000 000~~	Runout
		200	350 000	PM
		350	187 828	Weld toe
		250	855 162	Weld toe
		~~150~~	~~6 000 000~~	Runout
		~~90~~	~~2 000 000~~	Runout
		~~200~~	~~6 000 000~~	Runout
		350	82 506	Weld toe
		400	98 500	Weld toe
		~~225~~	~~10 000 000~~	Runout
		~~90~~	~~10 000 000~~	Runout
		~~200~~	~~10 000 000~~	Runout
		250	317 200	Weld toe
		350	223 200	Weld toe
		225	18 010	Weld toe
		~~70~~	~~2 000 000~~	Runout
		~~90~~	~~2 000 000~~	Runout
		200	299 234	PM
		250	179 511	PM
		350	134 300	Weld toe
S700MC	0.5	250	33 391	Weld toe
		200	84 895	Weld toe

t=20 mm

Steel grade	R	$\Delta\sigma_{nom}$ [MPa]	N_f [cycles]	Failure
S690QL	0.1	275	141 700	Weld toe
		~~150~~	~~10 000 000~~	Runout
		225	2 411 800	PM
		250	4 267 720	PM
		350	480 227	PM
		200	480 200	Weld toe
		200	2 241 008	PM
		250	231 323	Weld toe
		350	80 830	Weld toe
		400	184 642	Weld toe
		275	5 068 136	PM
		300	470 640	Weld toe
		~~250~~	~~10 000 000~~	Runout
		350	123 655	Weld toe
S690QL	0.5	200	343 210	Weld toe
		125	1 019 256	Weld toe
		150	644 530	Weld toe
		275	56 926	Weld toe

Since the compressive residual stresses at the weld toe are thought to be one of the main reasons for the improvement of fatigue endurance, their values, measured with X-ray diffraction, are reported in *Figure 5.15*.

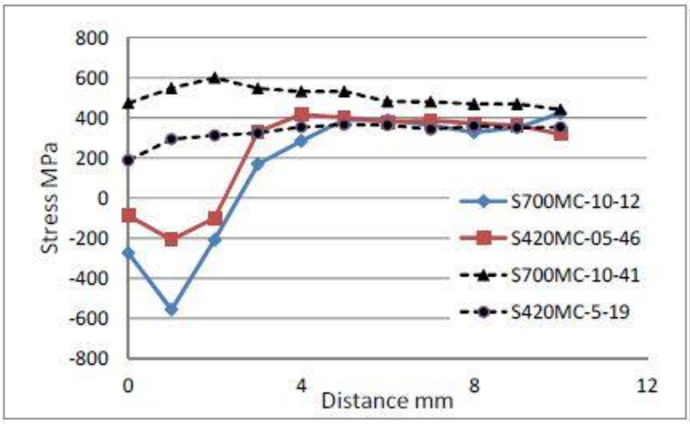

Figure 5. 15: residual stress distributions along the surface in both as-welded (black) and HFMI conditions [35].

5.2.1 SED and PSM for blunt notches

Before proceeding, the POWERGRAPHICS option is disabled in Ansys® Toolbar. Furthermore, since the HFMI groove geometry is the same, the following dispositions apply to both specimens.

In Ansys® APDL element library, Tetra 187 element is chosen; the Key Option K1 is left to *Pure Displacement*.

The first step consists in detecting the inclination with respect to the blunt notch bisector of the most stressed area (highlighted in red in Ansys®): after meshing the structure with an arbitrary global element size, an external nominal stress $\Delta\sigma_{nom}$=1 MPa is applied on the main plate, the system is solved, and the first principal stress $\Delta\sigma_{11}$ is plotted. This time, the highest stress is not located exactly around the blunt notch bisector, thus it is a matter of quantifying the grades of rotation.

The circular sector is created according to equations (4.4) and (4.5):

$$q = \frac{2\pi - 2\alpha}{\pi} = 2 - \frac{120}{180} = 1.33$$

$$r_0 = \frac{q-1}{1} \cdot \rho_{HFMI} = \frac{0.33}{1.33} \cdot 1.8 = 0.45\, mm$$

$$R_0 + r_0 = 0.28 + 0.45 = 0.73\, mm$$

As seen is *Figure 5.*16, the rounded circular sector has to be rigidly rotated by 11° anticlockwise about the global z-axis in order to capture the highest stress:

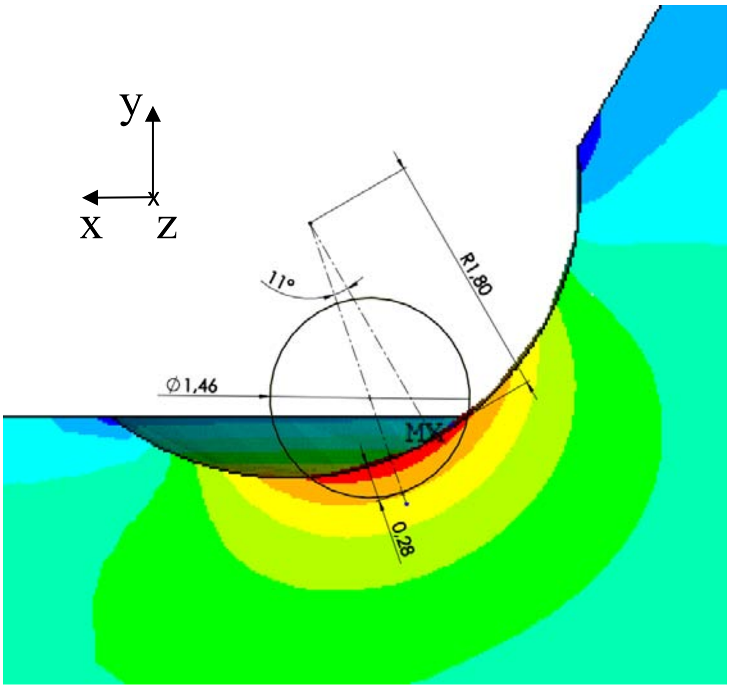

Figure 5. 16: structural volume, inclination and geometrical quantities. In black, the global coordinate system.

The meshing procedure follows the same dispositions previously mentioned for the FAT 71 longitudinal stiffener.

10-mm specimen

For an external applied load equal to $\Delta\sigma_{nom}$=300 MPa, the resultant strain energy density is then equal to:

$$SENE = 6.70 \cdot 10^{-2}\,J$$

$$VOLU = 0.0375393 mm^3$$

$$SED = \frac{6.70 \cdot 10^{-2}}{0.0375393} = 1.78\,\frac{MJ}{m^3}$$

Finally, the equivalent peak stress is calculated with equation (4.7):

$$\Delta\sigma_{eq,peak} = \sqrt{c_w \cdot \frac{2E \cdot \Delta\overline{W}_{FEM}}{1-\nu^2}} = 898\,MPa$$

20-mm specimen

For an external applied load equal to $\Delta\sigma_{nom}$=275 MPa, the resultant strain energy density is then equal to:

$$SENE = 6.57 \cdot 10^{-2}\,J$$

$$VOLU = 0.0375393\,mm^3$$

$$SED = \frac{6.57 \cdot 10^{-2}}{0.0375393} = 1.75\,\frac{MJ}{m^3}$$

Finally, the equivalent peak stress is calculated with equation (4.7):

$$\Delta\sigma_{eq,peak} = \sqrt{c_w \cdot \frac{2E \cdot \Delta\overline{W}_{FEM}}{1-\nu^2}} = 890\,MPa$$

5.2.2 Data entry in the PSM curve

In linear elasticity hypothesis, the $\Delta\sigma_{eq,peak}$ values resulting from different external loads can be found with equation (2.4). The results can be consulted in Appendix D.

The experimental data, following the work made in Meneghetti, Campagnolo, Babini [33], are then entered inside the PSM design curve proposed by Meneghetti Guzzella and Atzori:

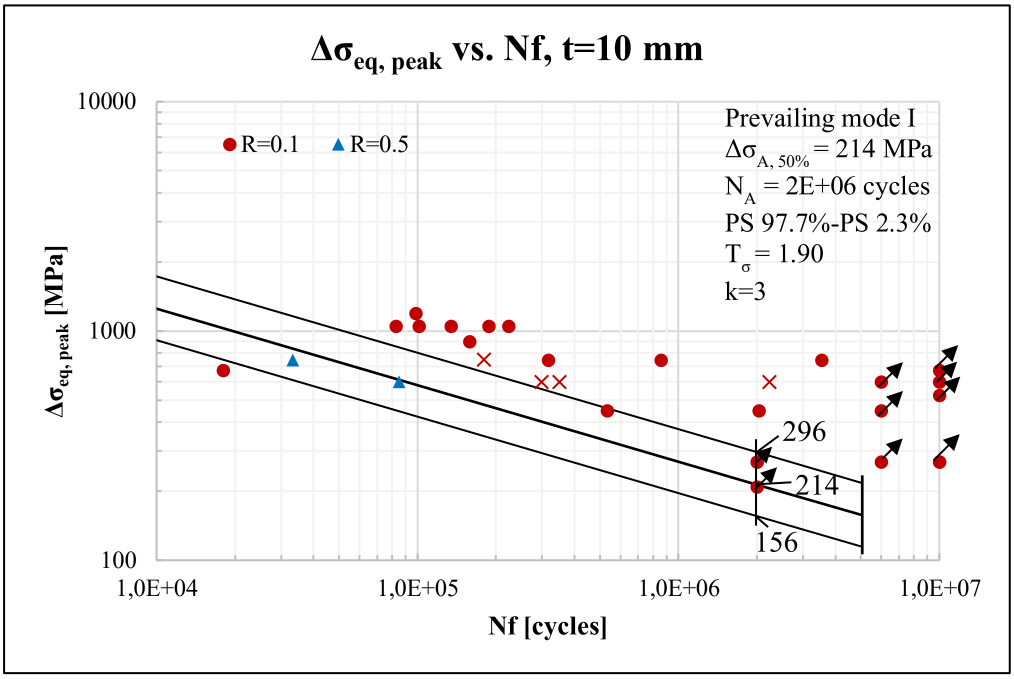

Figure 5. 17: data entry inside the PSM design curve, t=10 mm. The crossed data refer to ruptures at the parent material PM [28].

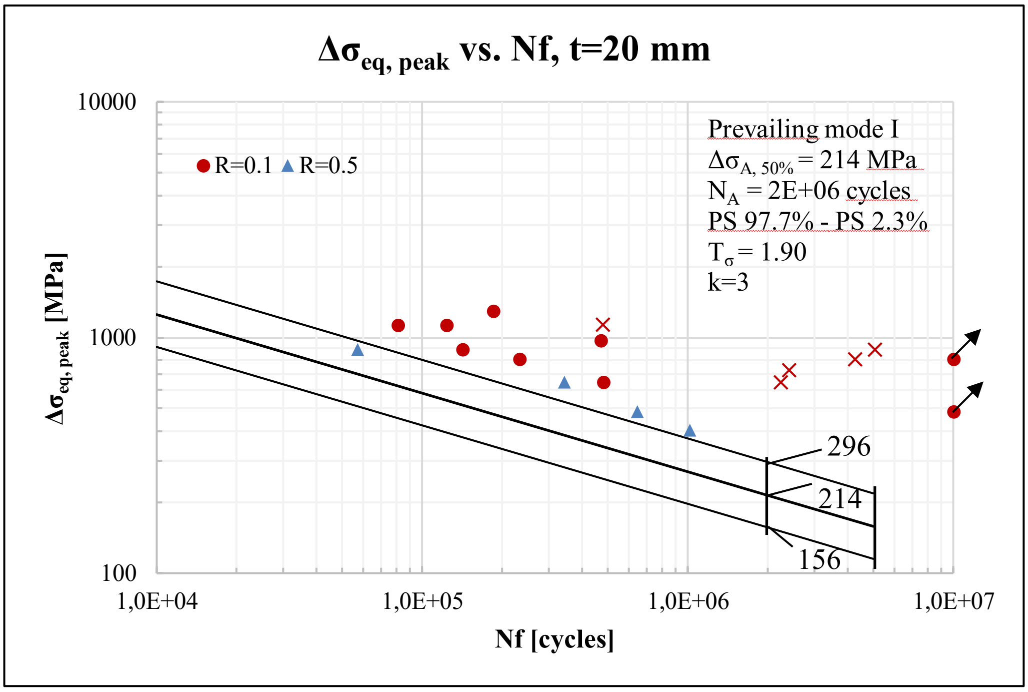

Figure 5. 18: data entry inside the PSM design curve, t=20 mm. The crossed data refer to ruptures at the parent material PM [28].

The following conclusions can be drawn:

1. The PSM in combination with the SED approach for blunt notches has correctly foreseen the experimental crack initiation point at weld toe;
2. Since the experimental data falls above the PS 2.3% line, the PSM design curve has proven to be effective and very conservative. However, this result is expected since the two methods have only been calibrated for as-welded and stress-relieved welded joints, in which the beneficial effects of compressive residual stresses are not present;
3. Regarding the R=0.5 data, they result to be lower than the R=0.1 ones, confirming the fatigue strength reduction caused by high stress ratios.

5.2.3 Data entry in the IIW curve

With reference to Chapter 3, paragraph 3.2.6, for an external applied load $\Delta\sigma_{nom}$=1 MPa, the related SHSS was $\Delta\sigma_{hs}$=1.35 MPa for the 10-mm specimen and $\Delta\sigma_{hs}$=1.18 MPa for the 20-mm specimen. In linear elasticity hypotheses, the effective SHSS related to a specific $\Delta\sigma_{nom}$ can be detected with (3.6). The experimental results can be consulted in Appendix D.

In agreement with the IIW recommendations on HFMI-treated welded joints [9], the hot-spot FAT class for 550 < f_y < 750, non-load carrying fillet welds, minimum $k_{S,min}$=1.15, corresponds to FAT 200. In case of stress ratio R=0.5, a three FAT class reduction is requested.

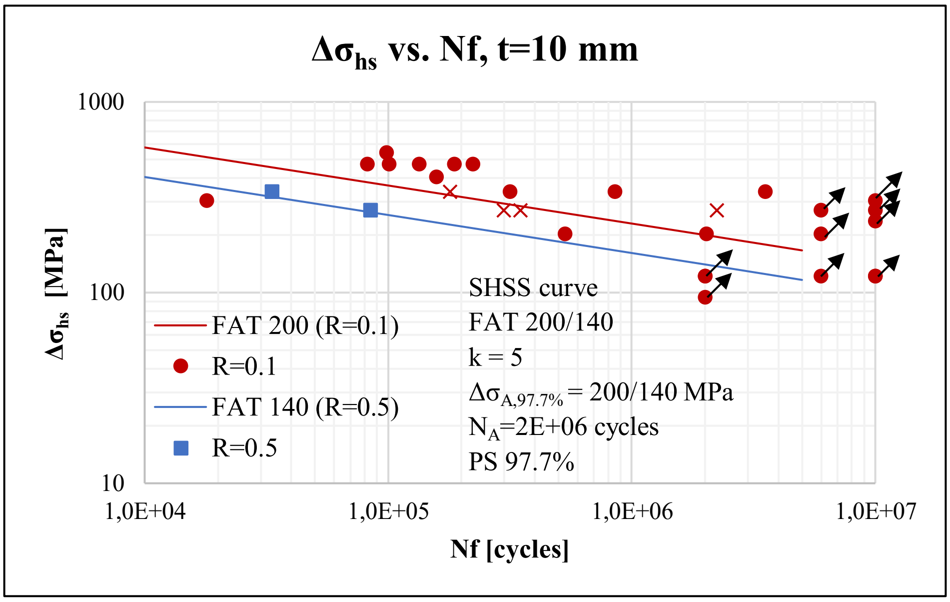

Figure 5. 19: data entry inside the FAT 200 and FAT 140 design curves, hot-spot approach, t=10 mm. The crossed data refer to ruptures at the parent material PM [9].

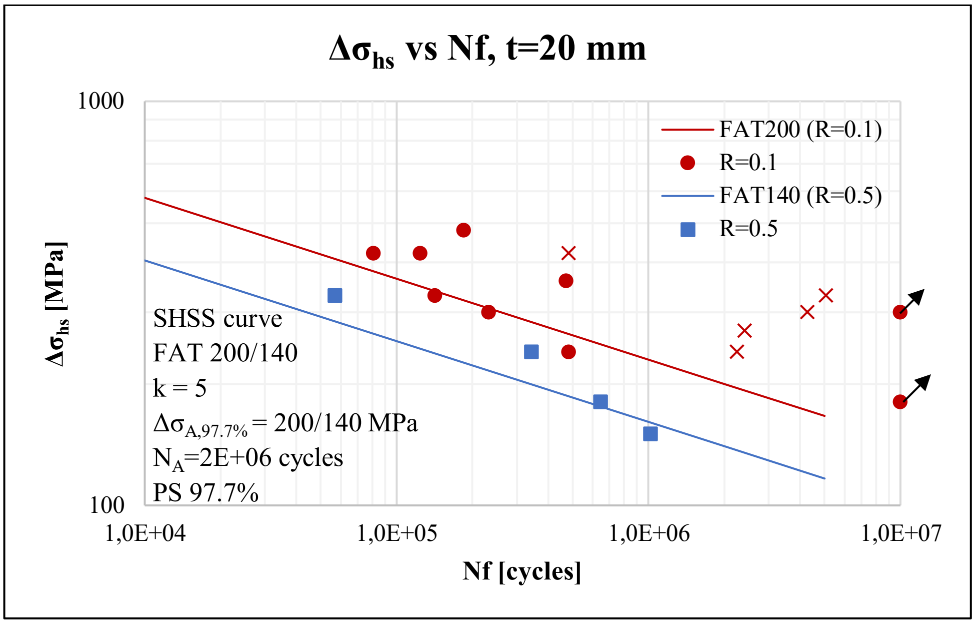

Figure 5. 20: data entry inside the FAT 200 and FAT 140 design curves, hot-spot approach, t=20 mm. The crossed data refer to ruptures at the parent material PM [9].

The following conclusions can be drawn:

1. The method has correctly been applied to weld toe fractures;
2. Even though misalignments have not been considered, since several R=0.1 experimental data fall below the PS 97.7% line, the hot-spot design curves have proven to be partially effective and conservative. This is also due to the fact that the hot-spot stress does not consider the size effect, since the outcoming values depend on the main plate thickness.

5.3 Transverse attachment, FAT 80 (Yildirim et al.)

Two non-load carrying FAT 80 transverse NLC joints, recently analysed by Yildirim et al, presented in HFMI conditions, have also been assessed in terms of hot-spot stress and equivalent peak stress. At the moment, the experimental data are classified, therefore no additional information on the material, the geometries, the experimental data and the re-elaborated results can be given. However, some general conclusions are worth to be reported:

1. Important assumptions were made with regard to the HFMI groove geometry;
2. By modelling the transverse attachment in two or three dimensions, the results in terms of strain energy density and equivalent peak stress generally differ depending on where to locate the structural volume along the weld toe profile of the transverse attachments;
3. The hot-spot detection still presents the issues abovementioned in Chapter 3.

5.4 Transverse attachment, FAT 80 (Okawa)

The fourth typology of welded joint to be investigated is a transverse NLC joint, fatigue class FAT 80, tested by Okawa in 2011 [36] under constant amplitude loading CAL.

Specific information on the component is reported below:

Weld condition	Fracture location	Load application	Main plate/gusset thickness
HFMI, non-load carrying, full penetration	*Weld toe*	*Axial, main plate, parent material*	*Main plate: 20 mm Gusset: 10 mm*

The mechanical properties are described below:

Material	Yield strength f_y	Young modulus	Poisson's ratio ν
AH36, HSS, linear elastic, isotropic	*392 MPa*	*206000 MPa*	*0.3*

The geometry of the specimen can be referred to *Figure 3.65*, Chapter 3, along with the weld profile parameters.

In regard of the HFMI groove geometry, since no information can be inferred relevant assumptions must be made: according to Okawa's article [36], the used HFMI indenter has a 3-mm diameter pin. Therefore, the weld toe groove radius is assumed to be equal to the pin radius, ρ_{HFMI}=1.5 mm. Always referring to the article [38] and *Figure 5.1*, a value of 0.16 mm is chosen as penetration depth. In regard of the indenter inclination angle, the latter is assumed along the V-notch bisector, i.e. 67.5° in this case.

Hence, the HFMI region is summed up in the table below, and displayed in *Figure 5.21*:

ρ_{HFMI} [mm]	Depth [mm]	Width [mm]
≅ *1.5*	*0.16*	*2.3*

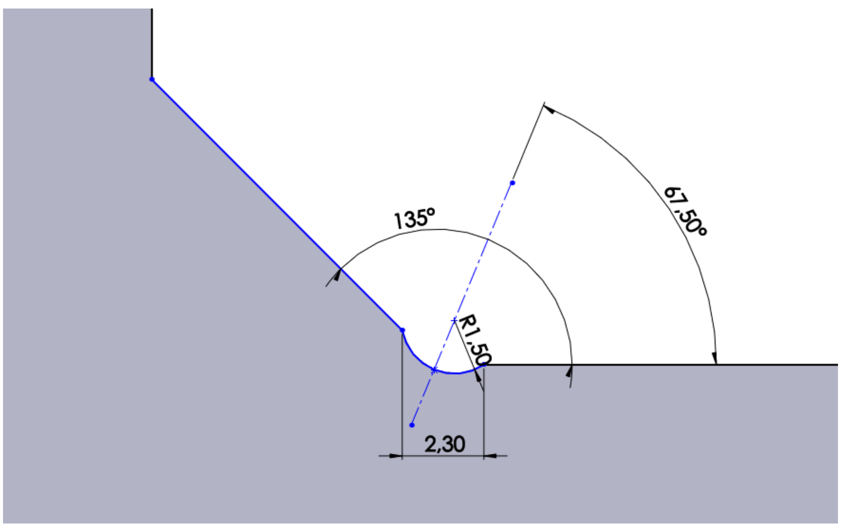

Figure 5. 21: representation of the HFMI treatment, with geometrical references.

The experimental data are reported in terms of nominal stress $\Delta\sigma_{nom}$. In barred, the runouts.

R	$\Delta\sigma_{nom}$ [MPa]	N_f [cycles]
0.1	~~250~~	~~5 000 000~~
	270	818 000
	260	1 067 000
	300	304 000
-1	420	378 000
	400	990 000
	380	2 295 000
0.5	175	346 000
	150	503 000
	~~125~~	~~5 000 000~~
	135	3 450 000

Since the compressive residual stresses at the weld toe are thought to be one of the main reasons for the improvement of fatigue endurance, their values, measured with X-ray diffraction, are reported in *Figure 5.22*:

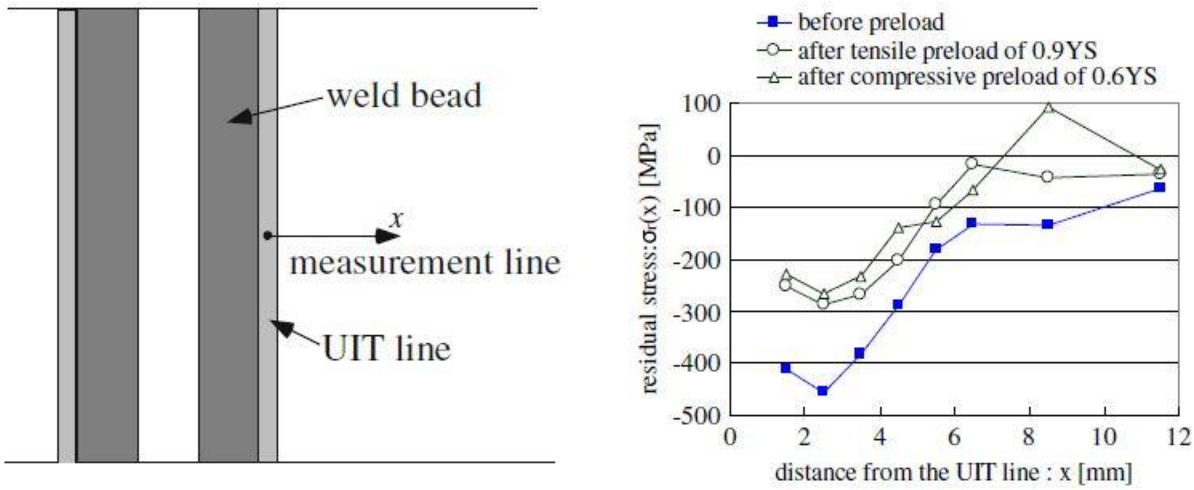

Figure 5. 22: referring to the blue line (before preload), residual stress distributions along the surface [36].

5.4.1 SED and PSM for blunt notches

In Ansys® APDL element library, Plane 182 element is chosen; the Key Option K1 is switched to *Simple Enhanced Strain*, while the Key Option K3 is set to *Plane Strain*.

As shown in *Figure 5.4*, the SED method for blunt notches is based on the creation of a rounded cylindrical sector, i.e. the structural volume, at the radiused weld toe, which can be rigidly rotated so as to capture the whole maximum principal stress (thus related to the highest strain energy density).

The first step consists in detecting the inclination with respect to the blunt notch bisector of the most stressed area (highlighted in red in Ansys®): after meshing the structure with an arbitrary global element size, an external nominal stress $\Delta\sigma_{nom}$=1 MPa is applied on the main plate, the system is solved, and the first principal stress $\Delta\sigma_{11}$ is plotted. The highest stress is not located exactly around the blunt notch bisector; thus, it is a matter of quantifying the grades of rotation.

The circular sector is created according to equations (4.4) and (4.5):

$$q = \frac{2\pi - 2\alpha}{\pi} = 2 - \frac{135}{180} = 1.25$$

$$r_0 = \frac{q-1}{1} \cdot \rho_{HFMI} = \frac{0.25}{1.25} \cdot 1.5 = 0.3\ mm$$

$$R_0 + r_0 = 0.28 + 0.3 = 0.58\ mm$$

As seen is *Figure 5.23*, the rounded circular sector has to be rigidly rotated by 10° anticlockwise about the global z-axis in order to capture the highest stress:

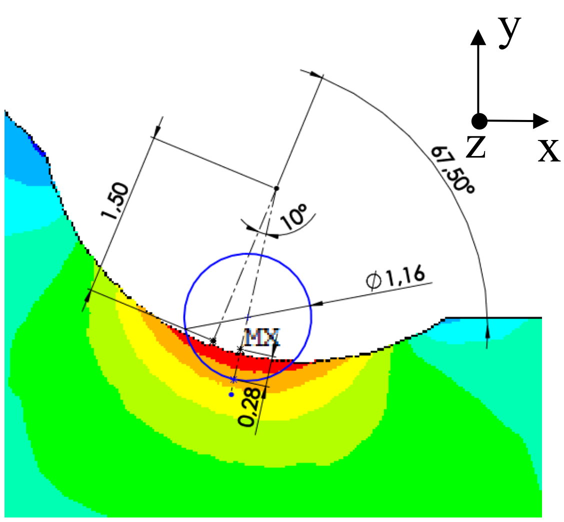

Figure 5. 23: structural volume, inclination and geometrical quantities. In black, the global coordinate system.

Inside Ansys® APDL environment, the following meshing procedures are followed:

a) The circular sector lines size is set to 0.06 mm:

Figure 5. 24: on the left, meshed structural volume. On the right, the proof that the highest stress is contained inside it.

b) The main plate and weld lines size is set to 0.05 mm, with a spacing ratio of 15, to guarantee a smooth element transition towards the circular sector. The resulting mesh conformation can be appreciated in *Figure 5.25*:

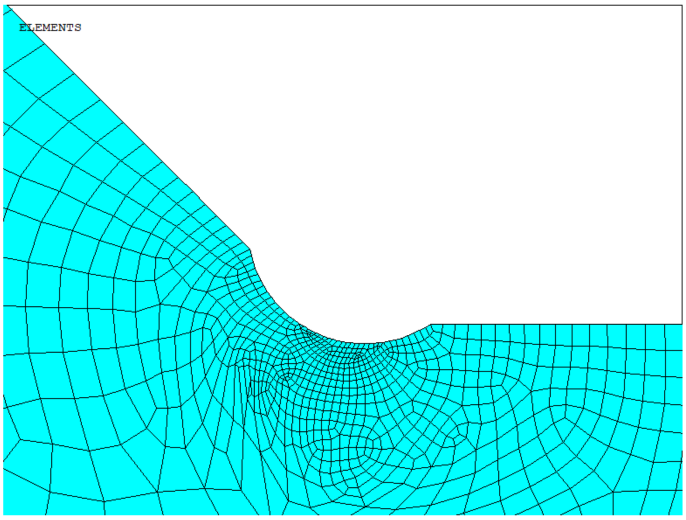

Figure 5. 25: resulting mesh conformation.

c) The remaining geometry is free meshed, with a global element size equal to 1 mm.

The system can now be solved:

Main Menu > Solution > Solve > Current LS

The averaged SED parameter is defined as the energy contained inside the structural volume. To obtain the average SED value, only the elements belonging to the circular sector must be selected. In Ansys® APDL, the following commands have to be used:

Utility Menu > Select > Entities > Areas > From Full

Utility Menu > Select > Everything Below > Selected Areas

At this moment, a table containing both the energy (SENE) and volume (VOLU) of the selected elements has to be created:

Main Menu > General Postproc > Element Table

Each single element SENE and VOLU values have now to be summed:

Main Menu > General Postproc > Element Table > Sum of Each Item

Finally, the SED value ($\Delta\overline{W}_{FEM}$ referring to FE software [33]) is calculated with equation (5.1):

$$\overline{W}_{FEM} = \frac{\sum_{V(R_0)} W_{FEM,i}}{V(R_0)} = \frac{SENE}{VOLU} = \left[\frac{MJ}{m^3}\right]$$

For an external applied load equal to $\Delta\sigma_{nom}$ = 175 MPa, the resultant strain energy density is then equal to:

$$SENE = 7.74 \cdot 10^{-2}\, J$$

$$VOLU = 0.22832\, mm^3$$

$$SED = \frac{7.74 \cdot 10^{-2}}{0.22832} = 0.339\, \frac{MJ}{m^3}$$

Finally, the equivalent peak stress is calculated with equation (4.7):

$$\Delta\sigma_{eq,peak} = \sqrt{c_w \cdot \frac{2E \cdot \Delta\overline{W}_{FEM}}{1-\nu^2}} = 392\, MPa$$

5.4.2 Data entry in the PSM curve

In linear elasticity hypothesis, the $\Delta\sigma_{eq,peak}$ values resulting from different external loads can be found with equation (2.4). The results can be consulted in Appendix E.

The experimental data, are then entered inside the PSM design curve proposed by Meneghetti and Lazzarin:

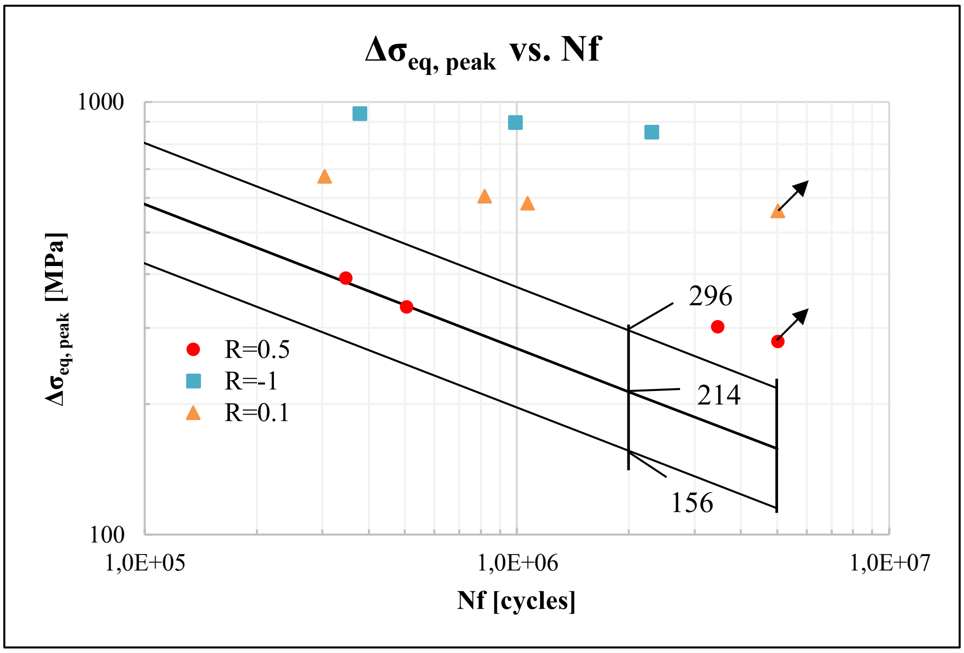

Figure 5. 26: data entry inside the PSM design curve [7].

The following conclusions can be drawn:

1. The PSM in combination with the SED approach for blunt notches has correctly foreseen the experimental crack initiation point at weld toe;
2. Since the experimental data falls above the PS 2.3% line, the PSM design curve has proven to be effective and very conservative. However, this result is expected since the two methods

have only been calibrated for as-welded and stress-relieved welded joints, in which the beneficial effects of compressive residual stresses are not present;

3. Regarding the R=0.5 data, they result to be lower than the R=0.1 ones, confirming the fatigue strength reduction caused by high stress ratios.

5.4.3 Data entry in the IIW curve

With reference to Chapter 3, paragraph 3.4.4, for an external applied load $\Delta\sigma_{nom}$=1 MPa, the related SHSS was $\Delta\sigma_{hs}$=1.02 MPa, very close to the nominal stress. In linear elasticity hypotheses, the effective SHSS related to a specific $\Delta\sigma_{nom}$ can be detected with (3.6). The experimental results can be consulted in Appendix E.

In agreement with the IIW recommendations on HFMI-treated welded joints [9], the hot-spot FAT class for 355 < f_y < 550, non-load carrying fillet welds, no $k_{S,min}$ indications , corresponds to FAT 180. In case of stress ratio R=0.5, a three FAT class reduction is requested.

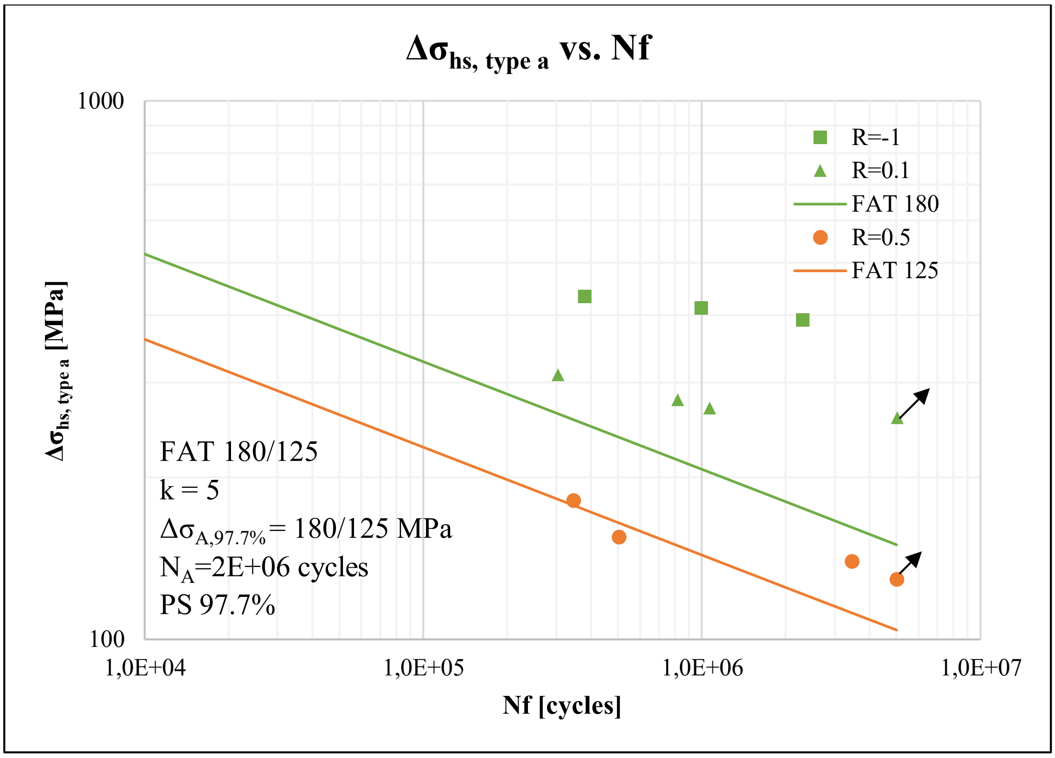

Figure 5. 27: data entry inside the FAT 180 and FAT 125 design curves, hot-spot approach [9].

The following conclusions can be drawn:

1. The method has correctly been applied to weld toe fractures;
2. Concerning R=0.1 and R=-1 data, even though misalignments have not been considered, since the totality of them falls above the PS 97.7% lines, the hot-spot design curves have proven to be very effective and conservative;
3. In case of R=0.5, however, one data falls below the PS 97.7% curve.

5.5 Transverse attachment FAT 80 (Kuhlmann 2009)

The fifth welded joint to be investigated is a transverse NLC joint, fatigue class FAT 80, tested by Kuhlmann in 2009 [37] under constant amplitude loading CAL.

Specific information on the component is reported below:

Weld condition	Fracture location	Load application	Main plate/gusset thickness
HFMI, non-load carrying, full penetration	*Weld toe + parent material*	*Axial, main plate, parent material*	*Main plate: 12 mm Gusset: 12 mm*

The mechanical properties of the specimens are described below. In brackets, the measured f_y.

Materials	Yield strength f_y	Young modulus	Poisson's ratio ν
S355J2, linear elastic, isotropic	*355 (422) MPa*	*206000 MPa*	*0.3*
S690QL, linear elastic, isotropic	*690 (781) MPa*		

The geometry of the specimen can be referred to *Figure 3.78*, Chapter 3, along with the weld profile parameters.

In regard of the HFMI groove geometry, since no information can be inferred relevant assumptions must be made: according to Kuhlmann's article [37], the used HFMI indenter has a 4-mm diameter pin. Therefore, the weld toe groove radius is assumed to be equal to the pin radius, ρ_{HFMI}=2 mm. Concerning the groove depth, it is affirmed that the value for S355J2 is nearly 0.17 mm, while for S690QL it is around 0.12 mm. In regard of the indenter inclination angle, the latter is assumed along the V-notch bisector, i.e. 67.5° in this case.

Hence, the HFMI region are summed up in the table below, and displayed in *Figure 5.28*:

Steel grade	ρ_{HFMI} [mm]	Depth [mm]	Width [mm]
S355J2	≅ *2*	*0.17*	*3*
S690QL	≅ *2*	*0.12*	*3*

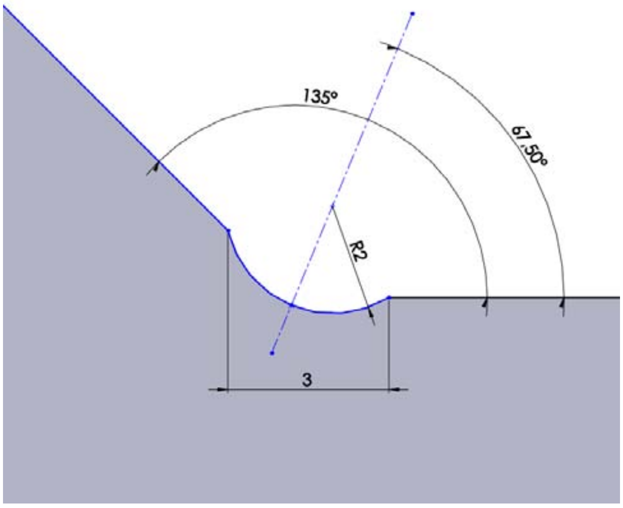

Figure 5. 28: representation of the HFMI treatment, with geometrical references. The penetration depth is 0.17 mm for the S355J2 specimen, and 0.12 mm for the S690QL.

The experimental data are reported in terms of nominal stress $\Delta\sigma_{nom}$. In barred, the runouts.

Steel grade	R	$\Delta\sigma_{nom}$ [MPa]	N_f [cycles]	Failure
S355J2	0.1	300	1 426 998	Weld toe
		300	762 972	PM
		340	137 721	Weld toe
		340	116 159	Weld toe
		315	711 012	Weld toe
		315	298 866	Weld toe
		280	799 250	Weld toe
		280	2 287 011	PM
		315	337 639	PM
S690QL	0.1	340	768 457	Weld toe
		340	478 283	Weld toe
		315	759 450	Weld toe
		315	1 270 270	Weld toe
		400	193 512	Weld toe
		400	228 100	Weld toe
		280	3 277 551	PM
		280	2 119 665	Weld toe
		~~280~~	~~5 000 000~~	Runout

Since the compressive residual stresses at the weld toe are thought to be one of the main reasons for the improvement of fatigue endurance, their values, measured with the hole drilling method, are reported in *Figure 5.29* for the S690QL specimen:

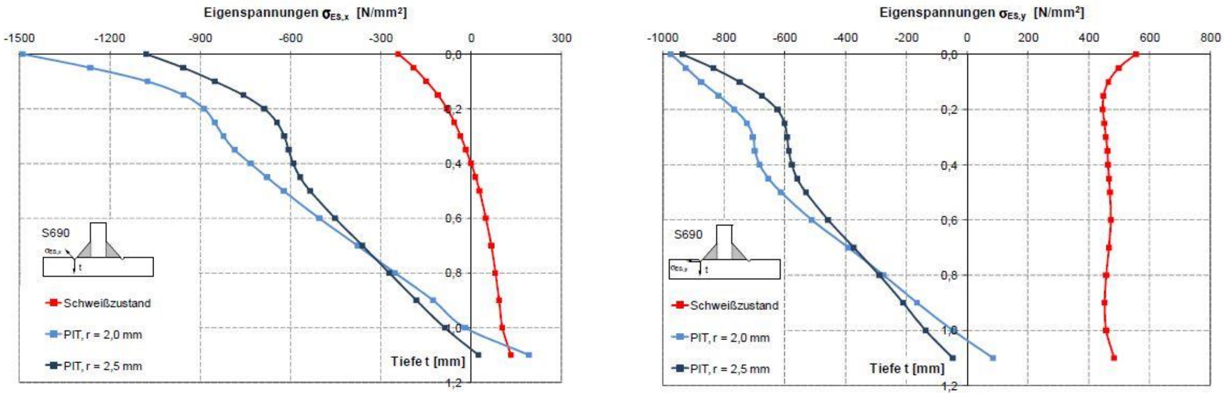

Figure 5. 29: residual stress distributions along the surface, both along x and y directions [37].

5.5.1 SED and PSM for blunt notches

Before proceeding, it is noted that since the results in terms of strain energy density between the penetration depth of 0.12 mm and 0.17 mm differ 1% with each other, the following simulation only refers to the S355J2 specimen. However, the results can be extended to the S690QL specimen.

In Ansys® APDL element library, Plane 182 element is chosen; the Key Option K1 is switched to *Simple Enhanced Strain*, while the Key Option K3 is set to *Plane Strain*.

The first step consists in detecting the inclination with respect to the blunt notch bisector of the most stressed area (highlighted in red in Ansys®): after meshing the structure with an arbitrary global element size, an external nominal stress $\Delta\sigma_{nom}$=1 MPa is applied on the main plate, the system is solved, and the first principal stress $\Delta\sigma_{11}$ is plotted. This time, the highest stress is not located exactly around the blunt notch bisector, thus it is a matter of quantifying the grades of rotation. The circular sector is created according to equations (4.4) and (4.5):

$$q = \frac{2\pi - 2\alpha}{\pi} = 2 - \frac{135}{180} = 1.25$$

$$r_0 = \frac{q-1}{1} \cdot \rho_{HFMI} = \frac{0.25}{1.25} \cdot 2 = 0.4\ mm$$

$$R_0 + r_0 = 0.28 + 0.4 = 0.68\ mm$$

As seen is *Figure 5.30*, the rounded circular sector has to be rigidly rotated by 7° anticlockwise about the global z-axis in order to capture the highest stress:

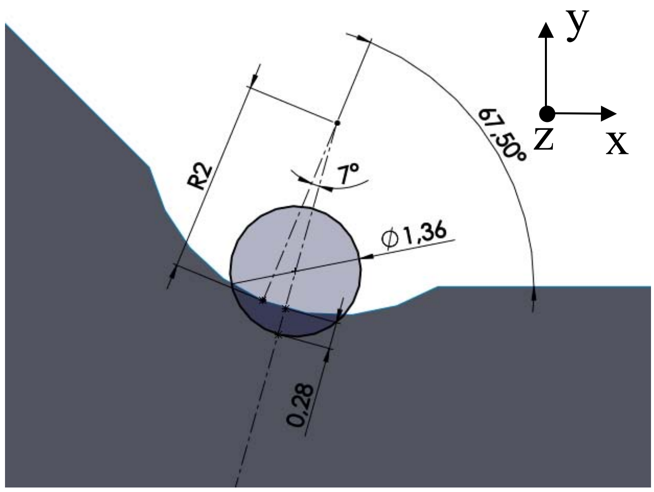

Figure 5. 30: structural volume, inclination and geometrical quantities. In black, the global coordinate system.

The meshing procedure follows the same dispositions previously mentioned for the FAT 80 (Okawa) longitudinal stiffener.

For an external applied load equal to $\Delta\sigma_{nom}$ = 300 MPa, the resultant strain energy density is equal to:

$$SENE = 1.93 \cdot 10^{-1}\, J$$

$$VOLU = 0.249068\, mm^3$$

$$SED = \frac{1.93 \cdot 10^{-1}}{0.249068} = 0.774\, \frac{MJ}{m^3}$$

Finally, the equivalent peak stress is calculated with equation (4.7):

$$\Delta\sigma_{eq,peak} = \sqrt{c_w \cdot \frac{2E \cdot \Delta\overline{W}_{FEM}}{1-\nu^2}} = 592\, MPa$$

5.5.2 Data entry in the PSM curve

In linear elasticity hypothesis, the $\Delta\sigma_{eq,peak}$ values resulting from different external loads can be found with equation (2.4). The results can be consulted in Appendix F.

The experimental data, are then entered inside the PSM design curve proposed by Meneghetti and Lazzarin:

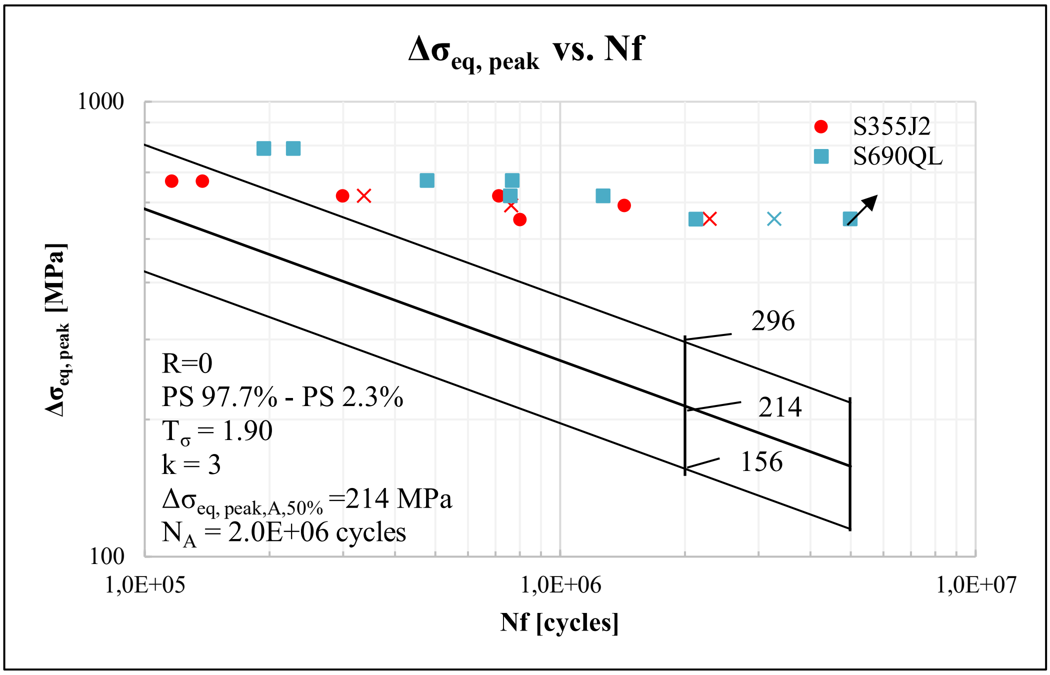

Figure 5. 31: data entry inside the PSM design curve. The crossed data refer to ruptures at the parent material PM [7].

The following conclusions can be drawn:

1. The PSM in combination with the SED approach for blunt notches has correctly foreseen the experimental crack initiation point at weld toe;
2. Since the experimental data falls above the PS 2.3% line, the PSM design curve has proven to be effective and very conservative. However, this result is expected since the two methods have only been calibrated for as-welded and stress-relieved welded joints, in which the beneficial effects of compressive residual stresses are not present;
3. Despite the improvement should theoretically be greater for higher strength steels, it seems that the benefit equally applies to both S355J2 and S690QL materials.

5.5.3 Data entry in the IIW curve

With reference to Chapter 3, paragraph 3.5.4, for an external applied load $\Delta\sigma_{nom}$=1 MPa, the related SHSS was $\Delta\sigma_{hs}$=1.01 MPa, very close to the nominal stress. In linear elasticity hypotheses, the effective SHSS related to a specific $\Delta\sigma_{nom}$ can be detected with (3.6). The experimental results can be consulted in Appendix F.

In agreement with the IIW recommendations on HFMI-treated welded joints [9], the hot-spot FAT class for 355 < f_y < 550, non-load carrying fillet welds, no $k_{S,min}$ restrictions, corresponds to FAT 180. On the other hand, the hot-spot FAT class for 750 < f_y < 950, non-load carrying fillet welds, $k_{S,min}$=1.25, corresponds to FAT 225. However, even though the calculated k_S=1.01 MPa is lower than the minimum $k_{S,min}$ = 1.25, the FAT 225 class proves to be conservative as well.

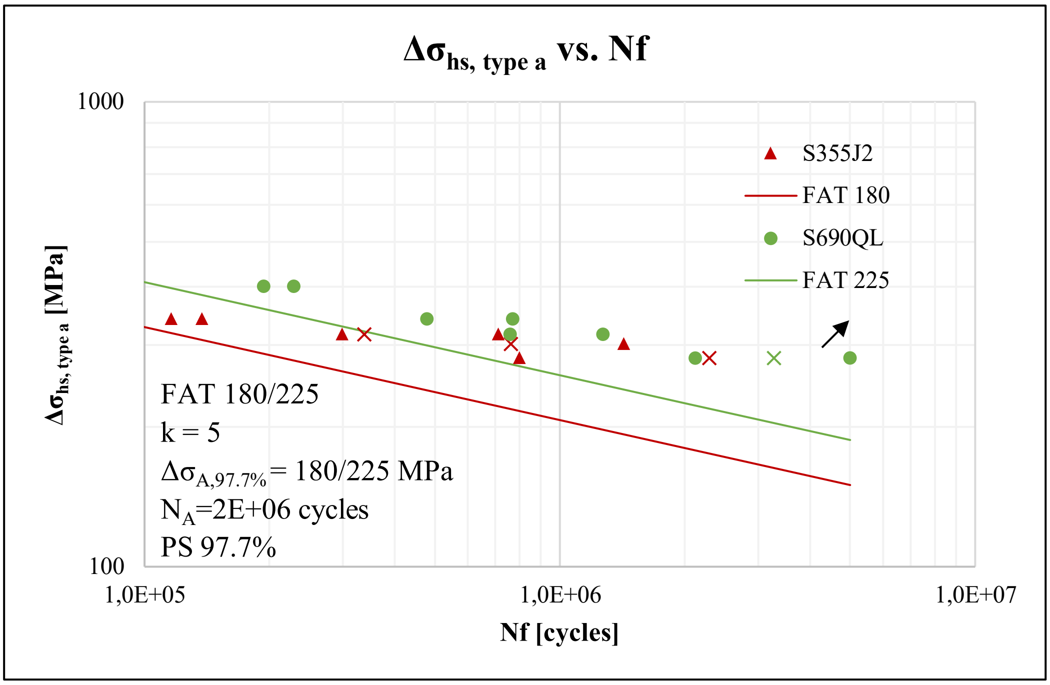

Figure 5. 32: data entry inside the FAT 180 design curve, hot-spot approach. The crossed data refer to ruptures at the parent material PM [9].

The following conclusions can be drawn:

1. The method has correctly been applied to weld toe fractures;
2. Even though misalignments have not been considered, since the totality of the experimental data falls above the PS 97.7% line, the hot-spot design curve has proven to be effective and conservative.

5.6 Transverse attachment FAT 80 (Kuhlmann 2006)

The fifth welded joint to be investigated is a transverse NLC joint, fatigue class FAT 80, tested by Kuhlmann in 2006 [46] under constant amplitude loading CAL. Since this kind of joint was not analysed in Chapter 3, indications on the geometry are given in the following pages.

Specific information on the component is reported below:

Weld condition	**Fracture location**	**Load application**	**Main plate/gusset thickness**
HFMI, non-load carrying, full penetration	*Weld toe*	*Axial, main plate, parent material*	*Main plate: 12 mm Gusset: 12 mm*

The mechanical properties of the specimens are described below.

Materials	**Yield strength f_y**	**Young modulus**	**Poisson's ratio ν**
S355, linear elastic, isotropic	*355 MPa*	*206000 MPa*	*0.3*
S460, linear elastic, isotropic	*460 MPa*		

Prüfkörper	Einflussfaktor	Stahl	Nachbehandlung	Dicke	Spannungs-verhältnis
Klein- und Großprüfkörper	Nachbehandlung Stahlsorte Größe	S355 S460 S690	im Schweißzustand WIG-Aufschmelzen UIT-Verfahren	12mm	R = 0,1
	Nachbehandlung	S690	Reinigungsstrahlung	12mm	R = 0,1
	Mittelspannung	S690	im Schweißzustand UIT-Verfahren	12mm	R = -1 R = 0,5
	Blechdicke	S690	im Schweißzustand UIT-Verfahren	25mm	R = 0,1
	Schweißnaht-ansatzstellen	S690	UIT-Verfahren	12mm	R = 0,1
	Nachbehandlung unter Last	S690	UIT-Verfahren	12mm	R = 0,5

Figure 5. 33: highlighted in red, the re-elaborated dataset [46].

In regard of the main geometrical quantities, *Figure 5.34* shows the most relevant information:

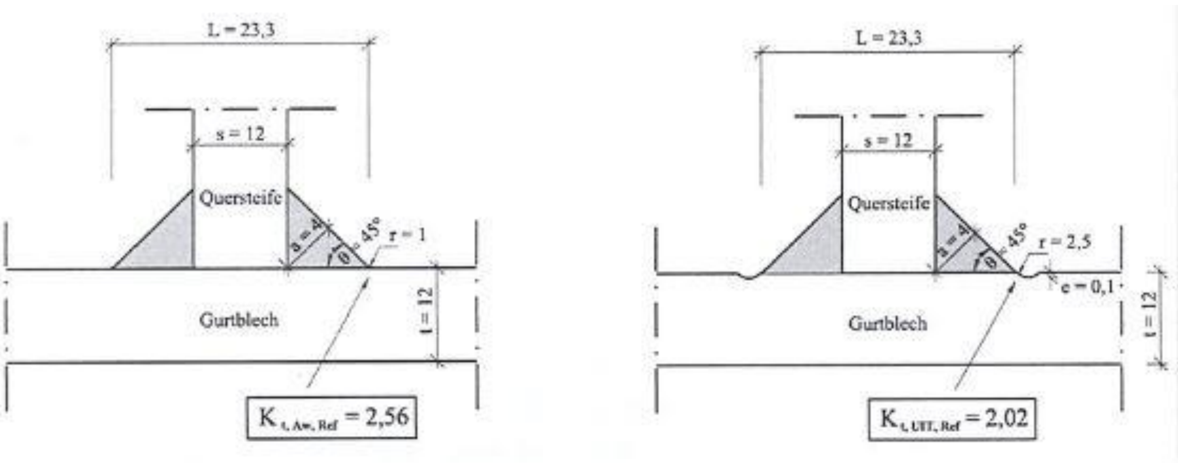

Figure 5. 34: on the left, schematic representation of the as-welded geometry; on the right, instead, of the HFMI geometry [46].

The weld profile parameters, in the AW condition, are described in the table below:

ρ weld toe tip [mm]	**Weld leg [mm]**	**Weld flank angle**	**2α**
≅ 1	*5.6*	*45°*	*Main plate: 135°* *Gusset: 135°*

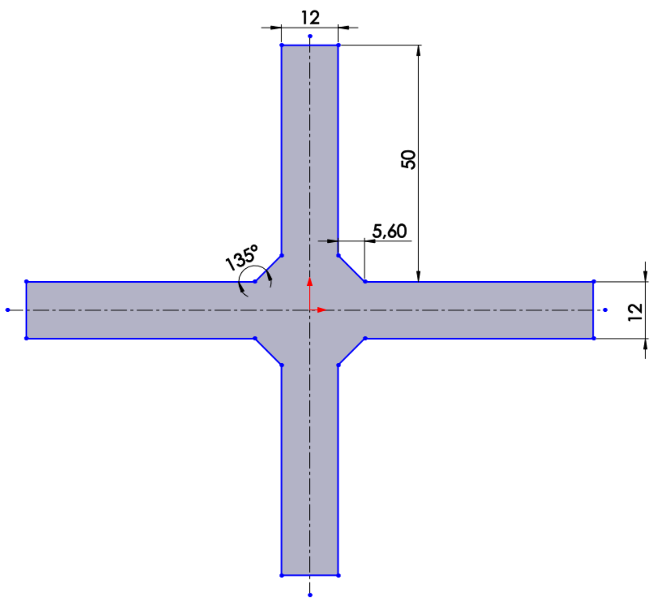

Figure 5. 35: Kuhlmann (2006), geometry. The quotes are expressed in [mm].

Modelling the total main plate length of the welded joint is not necessary: in fact, the latter shall be sufficient to represent the stress flowing from the "infinite".

Inside Ansys® APDL environment, the modelling procedure is briefly described and shown in *Figure 5.36*.

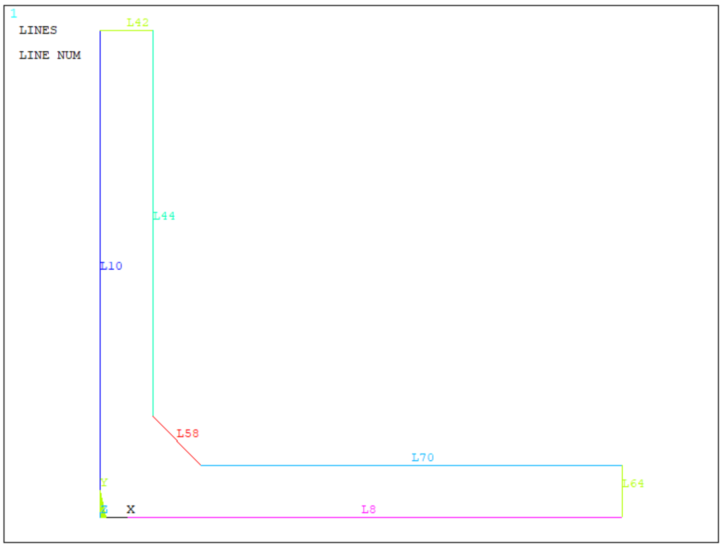

Figure 5. 36: loads and constraints application to Kuhlmann (2006).

- Symmetries: due to the double symmetry of the transverse NLC joint, only ¼ of the geometry is created, allowing to consistently speed up the computational time;
- Loading: the specimen is axially loaded, and the load is applied on the main plate as a constant pressure equal to $p = -\Delta\sigma_{nom}$, on Line 64;
- Constraints: symmetry boundary conditions are applied on Lines 8 and 10.

In regard of the HFMI groove geometry, *Figure 5.34* gives all the needed information: the measured weld toe groove radius is equal to ρ_{HFMI}=2.5 mm. Concerning the groove depth, it is affirmed that the value is equal to 0.1 mm, In regard of the indenter inclination angle, the latter is assumed along the V-notch bisector, i.e. 67.5°.

Hence, the HFMI region is summed up in the table below and displayed in *Figure 5.37*.

ρ_{HFMI} [mm]	Depth [mm]	Width [mm]
2.5	*0.1*	*3*

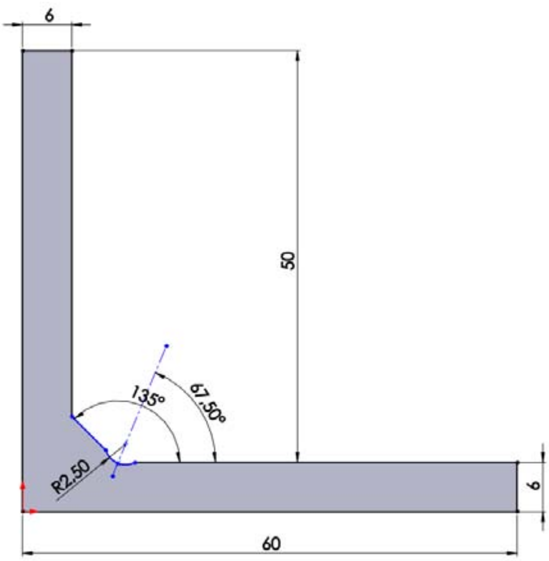

Figure 5. 37: representation of the HFMI treatment, with geometrical references.

The experimental fatigue data are reported in terms of nominal stress $\Delta\sigma_{nom}$:

Material	R	$\Delta\sigma_{nom}$ [MPa]	N_f [cycles]
		306	108 489
		278	363 274
		253	455 624
		230	977 946
		261	349 432
S355	0.1	264	315 592
		217	1 146 656
		260	845 460
		320	89 949
		250	1 365 764
		294	200 637

S460	0.1	290	595 040
		320	174 924
		287	346 406
		250	992 769
		240	1 077 822
		387	51 593
		294	221 726
		332	260 850
		356	162 744
		271	522 654

Since the compressive residual stresses at the weld toe are thought to be one of the main reasons for the improvement of fatigue endurance, their values are reported in *Figure 5.38* for the S355 and S460 specimens:

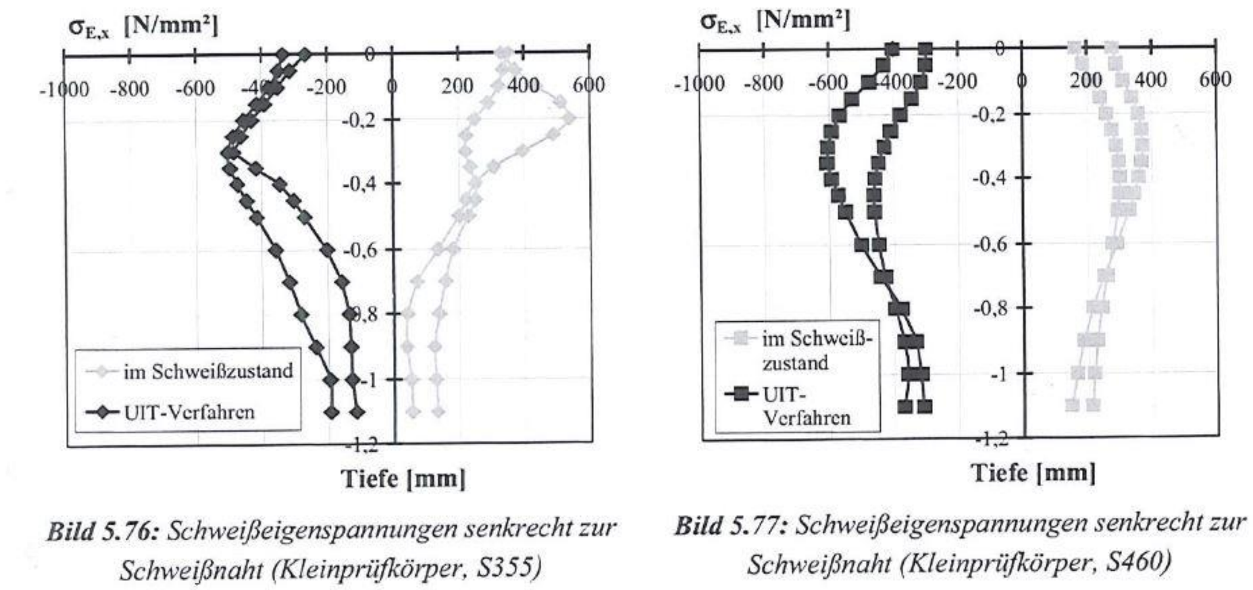

Figure 5. 38: residual stress distributions along the surface, both in AW and HFMI conditions [46].

5.6.1 SED and PSM for blunt notches

In Ansys® APDL element library, Plane 182 element is chosen; the Key Option K1 is switched to *Simple Enhanced Strain*, while the Key Option K3 is set to *Plane Strain*.

The first step consists in detecting the inclination with respect to the blunt notch bisector of the most stressed area (highlighted in red in Ansys®): after meshing the structure with an arbitrary global element size, an external nominal stress $\Delta\sigma_{nom}$=1 MPa is applied on the main plate, the system is solved, and the first principal stress $\Delta\sigma_{11}$ is plotted. The highest stress is not located exactly around the blunt notch bisector; thus, it is a matter of quantifying the grades of rotation.

The circular sector is created according to equations (4.4) and (4.5):

$$q = \frac{2\pi - 2\alpha}{\pi} = 2 - \frac{135}{180} = 1.25$$

$$r_0 = \frac{q-1}{1} \cdot \rho_{HFMI} = \frac{0.25}{1.25} \cdot 2.5 = 0.5\ mm$$

$$R_0 + r_0 = 0.28 + 0.5 = 0.78\ mm$$

As seen is *Figure 5.38*, the rounded circular sector has to be rigidly rotated by 15° anticlockwise about the global z-axis in order to capture the highest stress:

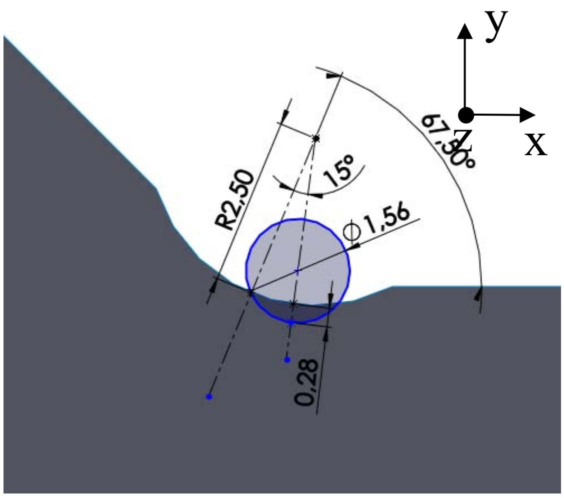

Figure 5. 39: structural volume, inclination and geometrical quantities. In black, the global coordinate system.

The meshing procedure follows the same dispositions previously mentioned for the FAT 80 (Okawa) longitudinal stiffener.

For an external applied load equal to $\Delta\sigma_{nom}$=306 MPa, the resultant strain energy density is equal to:

$$SENE = 1.87 \cdot 10^{-1}\ J$$

$$VOLU = 0.266373\ mm^3$$

$$SED = \frac{1.87 \cdot 10^{-1}}{0.266373} = 0.703\ \frac{MJ}{m^3}$$

Finally, the equivalent peak stress is calculated with equation (4.7):

$$\Delta\sigma_{eq,peak} = \sqrt{c_w \cdot \frac{2E \cdot \Delta\overline{W}_{FEM}}{1 - \nu^2}} = 564\ MPa$$

5.6.2 Data entry in the PSM curve

In linear elasticity hypothesis, the $\Delta\sigma_{eq,peak}$ values resulting from different external loads can be found with equation (2.4). The results can be consulted in Appendix G.

The experimental data, are then entered inside the PSM design curve proposed by Meneghetti and Lazzarin:

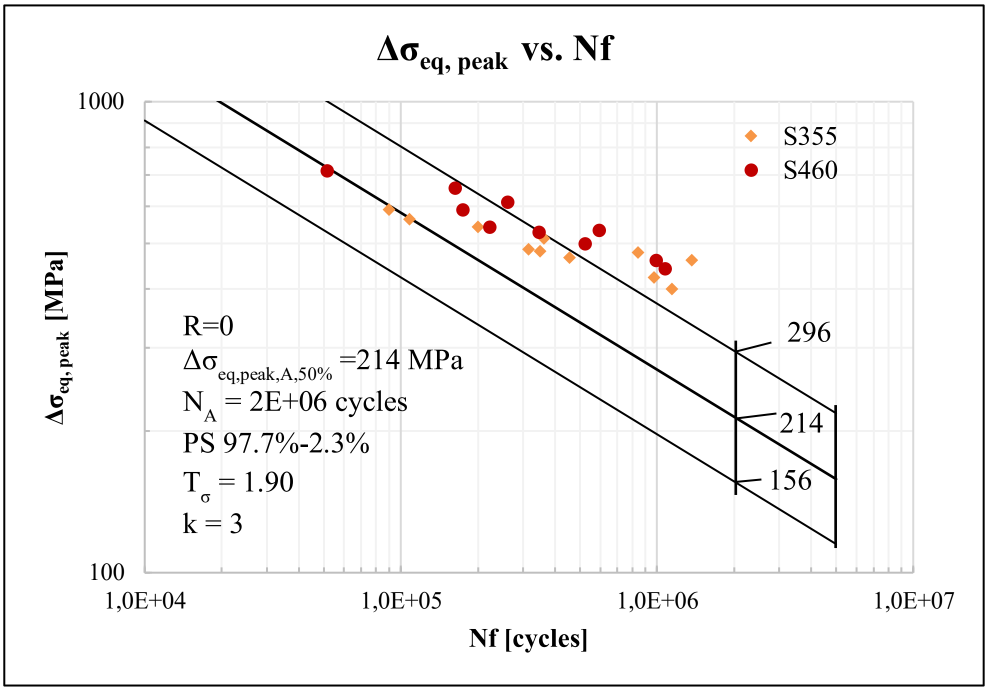

Figure 5. 40: data entry inside the PSM design curve [7].

The following conclusions can be drawn:

1. The PSM in combination with the SED approach for blunt notches has correctly foreseen the experimental crack initiation point at weld toe;
2. Since the experimental data falls above the PS 50% line, the PSM design curve has proven to be effective and very conservative. However, this result is expected since the two methods have only been calibrated for as-welded and stress-relieved welded joints, in which the beneficial effects of compressive residual stresses are not present;
3. Since the steel grades are in the same range, i.e. 355 MPa < f_y < 550 MPa, the improvement equally applies to both S355 and S430 materials.

5.6.3 Data entry in the IIW curve

In this paragraph, the fatigue assessment of the Kuhlmann 2006 FAT 80 welded joint is performed following the IIW recommendations [9] for the hot-spot stress extrapolation, with particular reference to the type "a" hot-spot, fine mesh, illustrated in *Figure 1.6*.

Proper mesh indications, concerning the stress extrapolation region, are given in the table below.

Element Type	Mesh algorithm	Main plate thickness t	Max element size	Adopted el. size
Plane 182 *KOs: Simple Enhanced Strain + Plane Strain*	Mapped	12 mm (6 mm modelled)	0.4*(t/2) = 2.4 mm	0.6 mm

The mesh pattern can be seen in *Figure 5.40*:

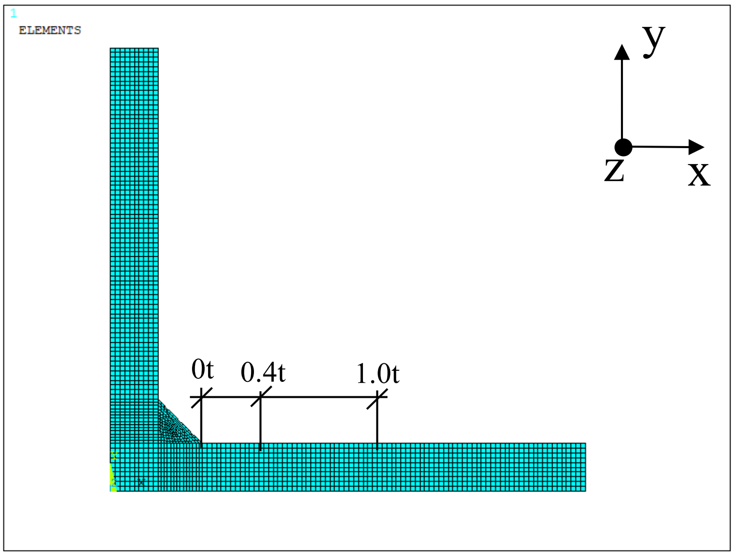

Figure 5. 41: mapped mesh for the hot-spot stress detection. In black, the global coordinate system.

According to [1], the structural hot-spot stress has to be extrapolated at two reference points located at 0.4t and 1.0t distance from the weld toe tip, it is to say 4.8 mm and 12 mm. In regard of the type of extrapolated stress, in Chapter 3 it was stated that σ_{11} and σ_{xx} are coincident, therefore the choice is indifferent.

For an external applied pressure equal to $\Delta\sigma_{nom}$=1 MPa, the resultant extrapolated stresses at the reference points are:

$$\Delta\sigma_{0.4t} = 1.00\ MPa$$

$$\Delta\sigma_{1.0t} = 0.99\ MPa$$

The structural hot-spot stress SHSS is finally detected with equation (3.5):

$$\Delta\sigma_{hs} = 1.67 \cdot \Delta\sigma_{0.4t} - 0.67 \cdot \Delta\sigma_{1.0t} = 1.01\ MPa$$

Again, the hot-spot approach shows that the resulting value has the tendency of being equal to the nominal stress. In linear elasticity hypotheses, the effective SHSS related to a specific $\Delta\sigma_{nom}$ can be detected with (3.6). The experimental results can be consulted in Appendix G.

In agreement with the IIW recommendations on HFMI-treated welded joints [9], the hot-spot FAT class for $355 < f_y < 550$, non-load carrying fillet welds, no $k_{S,min}$ restrictions, corresponds to FAT 180.

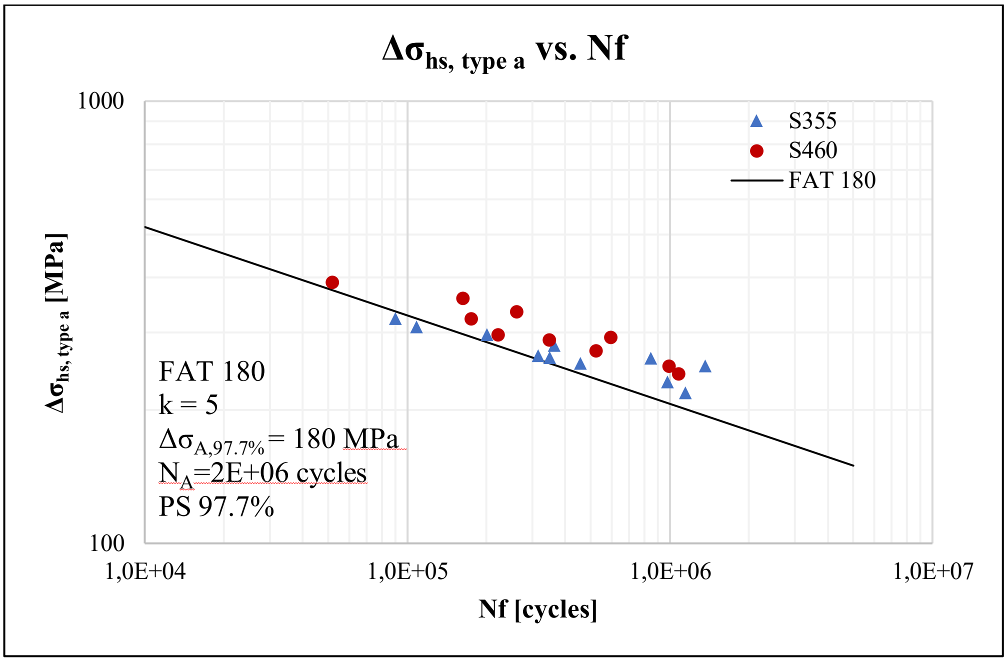

Figure 5. 42: data entry inside the FAT 180 design curve, hot-spot approach [9].

The following conclusions can be drawn:

1. The method has correctly been applied to weld toe fractures;
2. Even though misalignments have not been considered, since two experimental data fall below the PS 97.7% lines, the hot-spot design curves have proven to be partially effective and conservative.

Chapter 6: conclusions and proposal of two design curves for the fatigue assessment of HFMI-treated joints according to the Peak Stress Method

6.1 Fatigue assessment, overall conclusions

In this elaborate, several fatigue assessments have been performed on two particular typologies of welded joints: five transverse NLC attachments and three longitudinal stiffeners. The nominal fatigue classes range between FAT 63, FAT 71 and FAT 80; the main plate thicknesses range from 8 to 20 mm. The specimens have been presented in as-welded and HFMI-treated conditions.

As far as the as-welded joints analysis is concerned, the local approaches of the type "a" structural hot-spot stress and 1-mm stress, recommended by the IIW guideline, as well as the Peak Stress Method, the Strain Energy Density and the Notch Stress Intensity Factors, developed at the University of Padova, have been employed and compared to verify their grade of effectiveness and conservativeness, along with the fatigue life Nf prevision, in the analysis of each specimen. The influence of misalignments has not been considered, and sometimes assumptions on the weld profile geometry have been made. Overall, it can be said that:

1. All the methods have predicted the exact fracture location at the weld toe, with the exception of the PSM for V-notch opening angles higher than 135°, for which the calibration constants K_{FE} are not available. In this case, the PSM has foreseen the wrong rupture point;
2. The PSM, SED, and 1-mm stress, accounting of the size and thickness influence, have always proved to be effective and conservative because the greatest totality of the experimental data have fallen above the PS 97.7% curve. Tendentially, the PSM appears to be the most conservative one, exception made for V-notch opening angles greater than 135°, for which K_{FE} are not calibrated, giving several results falling slightly below the PS 97.7% curve;
3. The type "a" hot-spot stress does not predict the thickness effect. Along with this, the analyses on the transverse attachments provided a hot-spot stress value very similar to the nominal stress. As a consequence, the hot-spot stress has overall revealed to be partially effective and conservative. This behaviour could mainly be due to the misalignment neglection.

As far as the HFMI-treated joints are concerned, the local approaches of the structural hot-spot stress, recommended by the IIW guideline, and the PSM in combination with the SED approach for blunt notches have been employed. The investigation focused on how the SED and the PSM, never adopted before in case of high compressive residual stresses in the weld region, would behave in such cases. The influence of misalignments has not been considered, and sometimes assumptions on the HFMI geometry have been made. Overall, it can be said that:

1. The two methods have predicted the exact fracture location at the weld toe;
2. For each analysed specimen, the PSM curve has revealed to be very conservative. This result is consistent with the fact that the method has only been calibrated for as-welded and stress-relieved welded joints, in which the beneficial effects of compressive residual stresses are not present;

3. The HFMI hot-spot stress does not account of the thickness effect, and this especially affects the transverse attachments for which the hot-spot stress is very similar to the nominal stress. In cases like this, the hot-spot does not always reveal to be conservative, especially for the R=0.5 data.

6.2 Global data collection

The final objective of this elaborate is that of trying and propose a new methodology for the synthesis of data coming from different HFMI geometries, tested under constant amplitude loading CAL, into a unique $\Delta\sigma_{eq,peak}$ - N_f design curve, able to reliably account of the size and thickness effect, as well as the post-weld HFMI fatigue-life-affecting parameters of stress ratio and steel grade.

It is noted that FAT 80 (Yildirim et al.) data have not been entered because they could have altered the outcoming curve.

Exclusively considering fractures at the weld toe, all the 79 HFMI data re-elaborated in Chapter 5 in terms of equivalent peak stress are collected together to perform a first-tentative statistical analysis, with probability of survival covering the 2.3% - 97.7% percentages. The specimens consist of transverse NLC joints, as well as longitudinal NLC stiffeners, axially loaded on the main plate, FP; the stress ratio ranges between -1 < R < 0.5, the steel grade between 355 < f_y < 750 MPa; the inverse slope, in agreement with the theory [9], is set to 5. The resulting curve is displayed below:

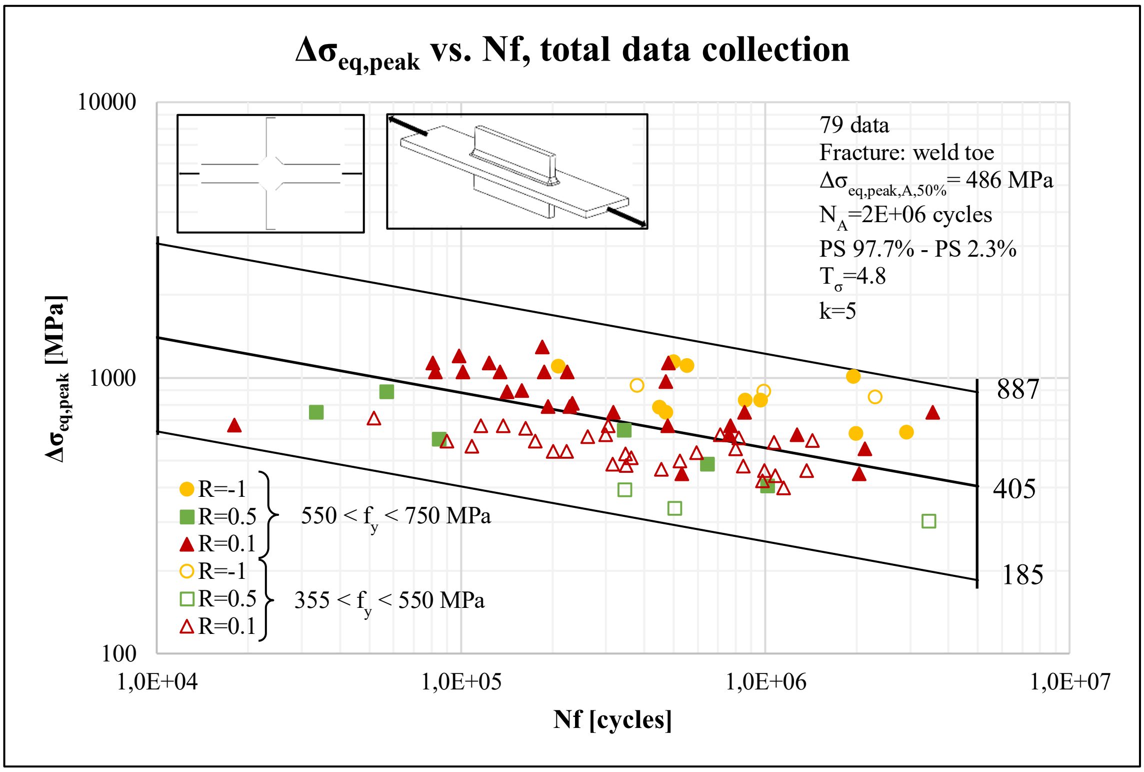

Figure 6. 1: total data collection and re-elaboration in terms of equivalent peak stress.

The outcoming T_σ=4.8 is very large, meaning that the feasibility of adopting one curve is not possible. However, a result like this could have been expected for several reasons:

1. A three FAT class reduction is recommended for stress ratios R=0.5. As evidence, all the R=0.5 data are under the PS 50% line, enlarging the scatter band;
2. Different steel grade range corresponds to different improvements: in fact, the lower strength steel data (i.e. the hollow points) are below the higher strength steel data (i.e. the full points);
3. Due to lack of information on them, misalignments for transverse attachments have not been taken into account;
4. c_w is incorrectly left to 1;
5. Assumptions have been made concerning the HFMI groove of the longitudinal stiffeners, potentially altering the final equivalent peak stress values.

6.3 Cluster of data points

From the previous considerations, a cluster of the experimental data is effectuated in agreement with the indications of the IIW guideline for HFMI-treated welded joints [9], so that to separate them according to the steel grade and the stress ratio ranges. However, important considerations are here described:

- Since R=0.5 data are associated with three FAT class reduction, and in the industry R=0.5 loadings are very rare, they are removed from the analysis;
- Concerning R=-1 data, showing the tendency of being higher than the R=0.1 ones, in first place they are also chosen to be excluded from the statistical analysis;
- The outlier with coordinates (18010; 674) is excluded from the analysis, but anyway inserted in the respective curve;
- Even though the Kuhlmann 2009 S690QL measured f_y is 781 MPa, since it does not largely exceed the $550 < f_y < 750$ MPa steel grade range, since the nominal f_y is 690 MPa, and since the improvement appears to be lower than weaker steels, it is left in the aforementioned range.

Conclusively, in parallel with the initial development of the PSM for as-welded joints, only R=0.1 data are statistically elaborated, then the R=-1 and R=0.5 data are entered in the found curves to investigate the overall trend.

6.3.1 PSM design curve proposal (R=0.1, 355 < f_y < 550 MPa)

The first data cluster is effectuated in terms of nominal and equivalent peak stress:

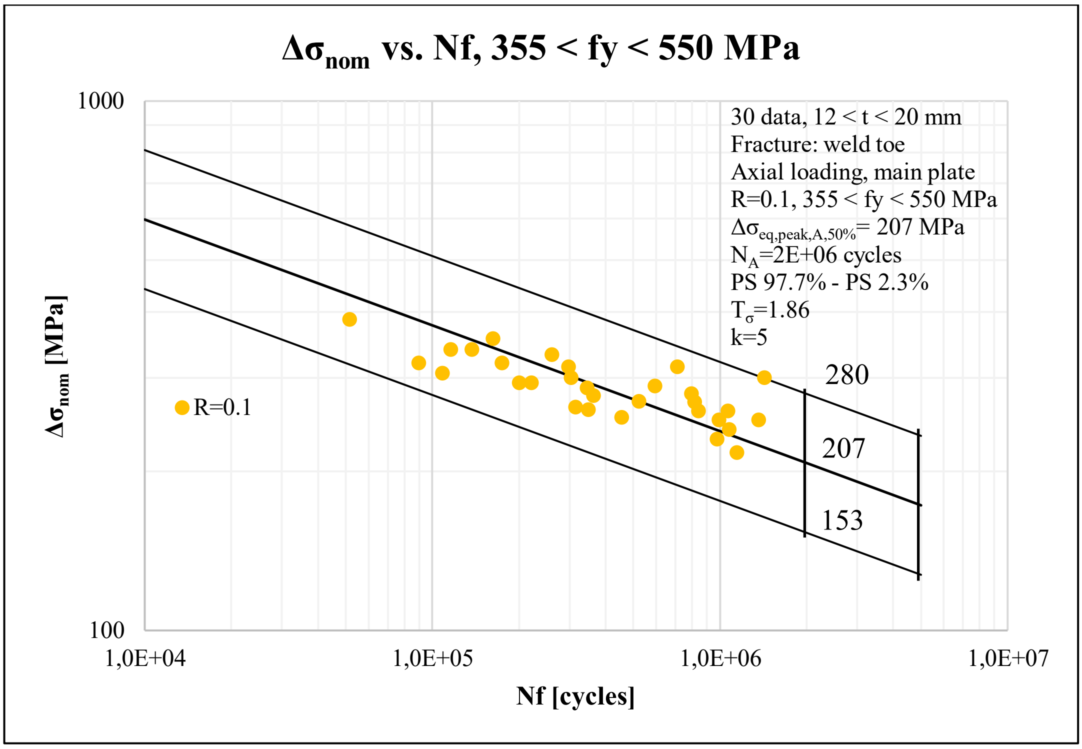

Figure 6. 2: HFMI data collection in terms of nominal stress, 355 < f_y < 550 MPa, R=0.1.

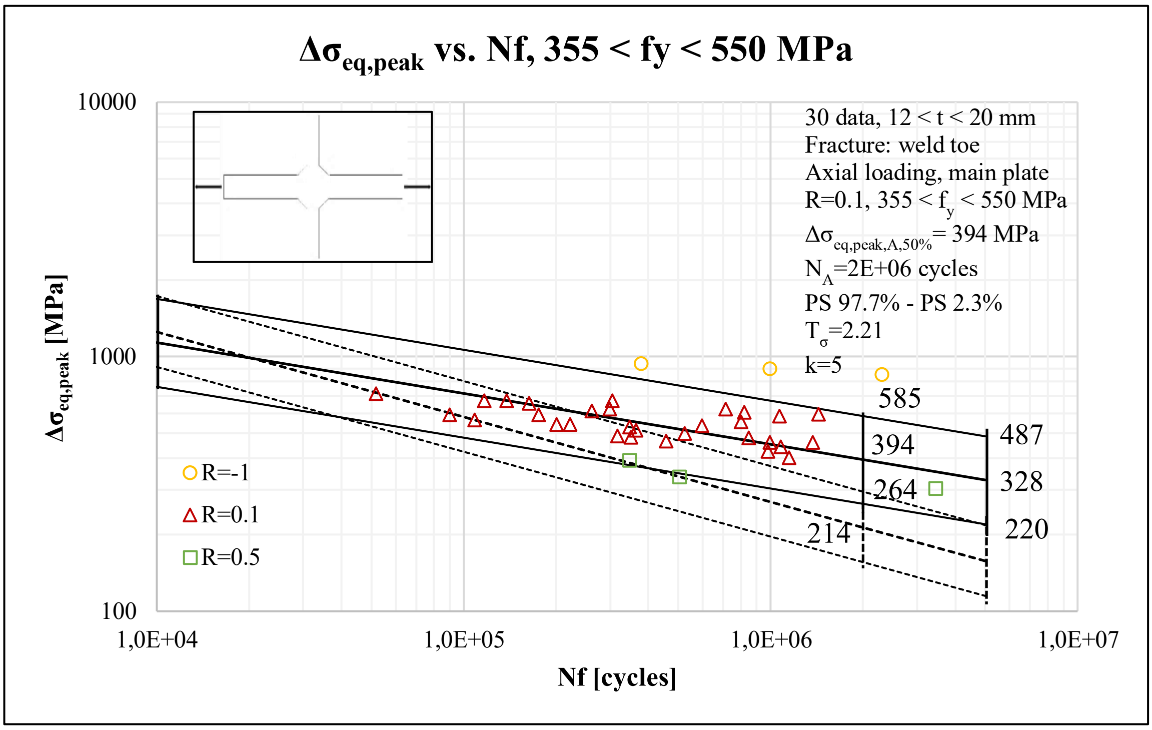

Figure 6. 3: proposed PSM design curve for HFMI-treated joints, 355 < f_y < 550 MPa, R=0.1. The dashed lines refer to the PSM curve calibrated for as-welded and stress relieved joints [7].

The proposed PSM curve presents the following characteristics:

1. The scatter band amplitude is equal to T_σ=2.21, higher than the nominal T_σ=1.86. The fact that the nominal scatter band is lower can be justified by the fact that all the considered joints present fatigue class FAT 80 and same geometry, being all double transverse stiffeners; therefore, since the provided grade of the HFMI improvement is the same, the fact that they arrange along the same trend line may be expected. When it comes to local approaches, since the value of the compressive residual stresses varies with the treatment, and since they are responsible of the improvement of the joint, probably a linear elastic analysis is not sufficient to summarize all the data in one single curve, because the scatter band reveals to be too high;
2. The curve is calibrated for R=0.1 data. If the R=-1 and R=0.5 are separately entered, the proposed curve proves to be conservative for the R=-1 data, and at the same time it is able to include the R=0.5 ones;
3. With respect to the dashed PSM curve for as-welded joints [7], the benefit of the HFMI treatment is evident: the respective reference value at 2 million cycles, PS 50%, is 394 MPa, against 214 MPa; the inverse slope is k=5; N_{int}, previously defined in Paragraph 4.2.1, is located at 40000 cycles.

6.3.2 PSM design curve proposal (R=0.1, 550 < f_y < 750 MPa)

The second data cluster is both effectuated in terms of nominal and equivalent peak stress:

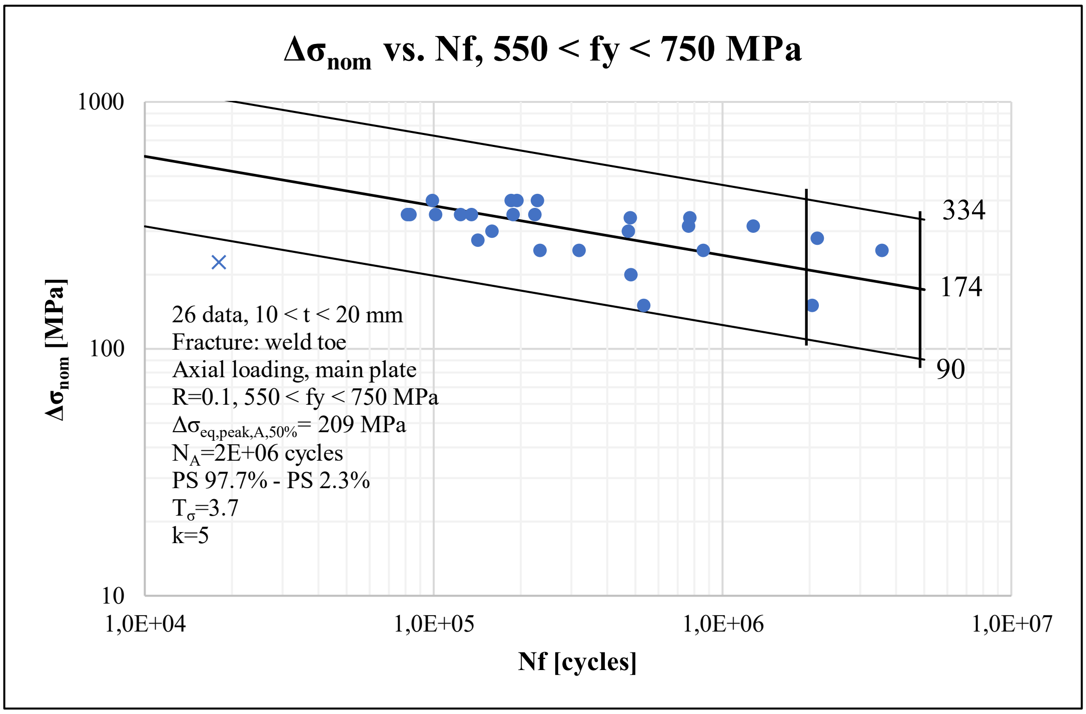

Figure 6. 4: HFMI data collection in terms of nominal stress, 550 < f_y < 750 MPa, R=0.1.

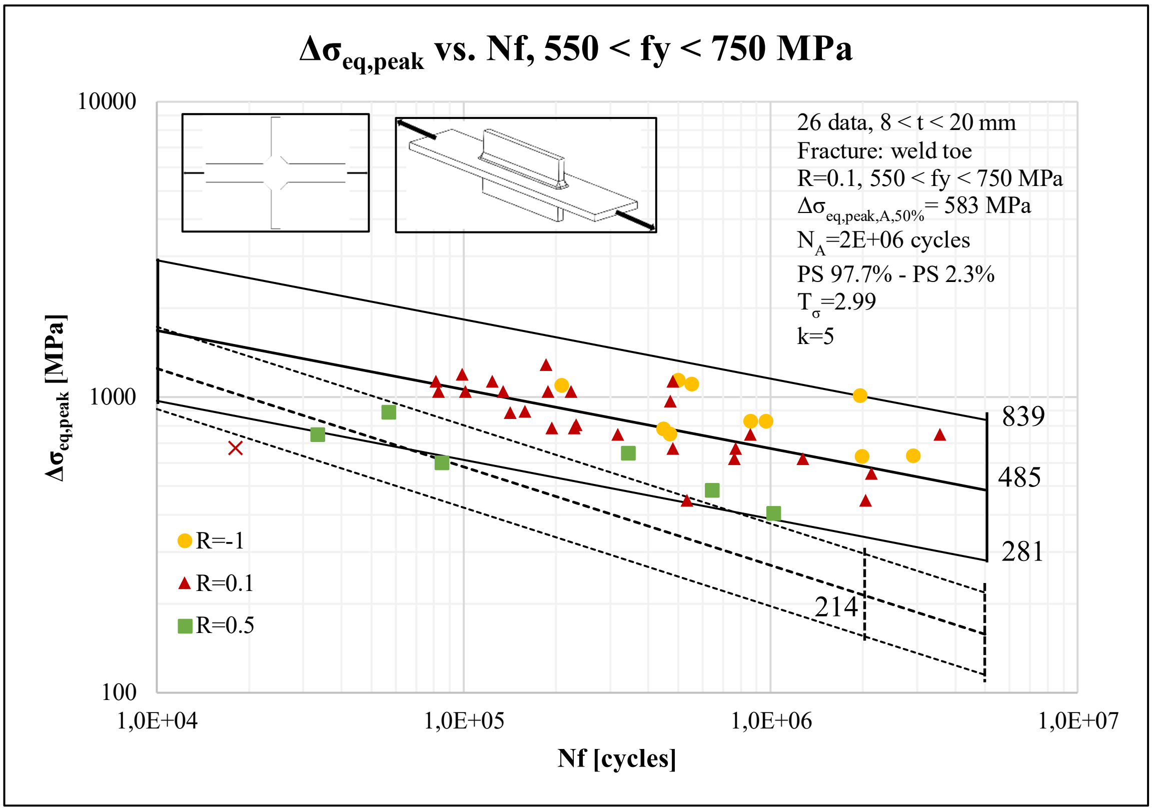

Figure 6. 5: proposed PSM design curve for HFMI-treated joints, 550 < f_y < 750 MPa, R=0.1. The dashed lines refer to the PSM curve calibrated for as-welded and stress relieved joints [7].

The proposed PSM curve presents the following characteristics:

1. The scatter band amplitude is equal to T_σ=2.99, lower than the nominal T_σ=3.7. The fact that this time the nominal scatter band is higher can be justified by the fact that the considered joints present different fatigue class (FAT 63, 71, 80) and geometry, being both transverse and longitudinal stiffeners; therefore, even their HFMI improvement is expected to be different. When it comes to local approaches, since the value of the compressive residual stresses varies with the treatment, and since they are responsible of the improvement of the joint, probably a linear elastic analysis is not sufficient to summarize all the data in one single curve, because the scatter band, even though lower than the nominal, appears to be too high;
2. The curve is calibrated for R=0.1 data. If the R=-1 and R=0.5 are separately entered, the proposed curve proves to be conservative for the R=-1 data, and at the same time it is able to include the R=0.5 ones;
3. With respect to the dashed PSM curve for as-welded joints [7], the benefit of the HFMI treatment is much more evident: the respective reference values at 2 million cycles, PS 50%, are 583 MPa against 214 MPa; the inverse slope is k=5; N_{int}, previously defined in Paragraph 4.2.1, is located before 10000 cycles, in the high-stress region, confirming the fact that higher strength steels benefit of greater improvements.

6.4 Further developments

As further developments:

1. The PSM calibration constants K_{FE} for V-notch opening angles higher than 135° should be validated in order to have more reliable results and predict the correct fracture location;
2. The c_w term should be found for a more reliable detection of the equivalent peak stress for HFMI-treated joints;
3. The focus on misalignment of transverse attachments should be deepened;
4. The analysis should also be extended to the $750 < f_y < 950$ MPa steel grade range;
5. Experimental data collection of HFMI specimens should be performed at the University of Padova;
6. Since the PSM curves for HFMI joints have a large scatter band, this may be due to the fact that the value of the compressive residual stresses consistently affect the fatigue endurance of the HFMI-treated joints along with the HFMI groove geometry. Henceforth, research should further with the involving of an elastoplastic analysis in the post-treated region.

Acknowledgments

This elaborate was written in a very challenging period for the human history, scraped by the COVID-19 outbreak. Despite all the difficulties we and I are still going through, it seems necessary to express my heartfelt thanks to the people who contributed to this important accomplishment of mine: the Master's in Mechanical Engineering.

First, I would like to sincerely thank Professor Giovanni Meneghetti, from University of Padova, and Professor Halid Can Yildirim, from Aarhus University, whose acquaintance gave me the chance of doing my thesis abroad, allowing me to live in a foreign country for the first time; even though for a small period, the time I spent at Aarhus allowed me to draw relevant guidance for my future career. I would also like to thank you for your strong passion in your job, letting me deepen my knowledge on the research of the fatigue on welded joints; thanks to your careful supervision and your precious advices I will always treasure.

Special thanks also to Professor Alberto Campagnolo, who had been tutoring me during these months, being always available to help me with scientific papers, as well as important suggestions and tips worthy of note, without which my troubles in FE analyses would have surely been worse. Thank you for your dedication to my activity.

Appendix A

APDL codes for the modelling of Gandhi geometry (Chapter 2)

Ten-node quadratic elements (Tetra 187), 1 volume model, PSM

```
/CLEAR,NOSTART
/PREP7

!* Variables
B=200
L=360
H=900
d=51
T=10

!* Element selection
ET,1,PLANE182
KEYOPT,1,1,3
KEYOPT,1,3,2
KEYOPT,1,6,0
ET,2,SOLID187
KEYOPT,2,6,0

!* Material properties
MPTEMP,,,,,,,,
MPTEMP,1,0
MPDATA,EX,1,,206000
MPDATA,PRXY,1,,0.3

!* Isometric view
/VIEW,1,1,1,1
/ANG,1
/REP,FAST

!* Keypoints half-SHS
K,14,0,0,0,
K,1,B/2,0,0,
K,2,B/2,-B,0,
K,3,0,-B,0,
K,4,0,-B+T,0,
K,5,B/2-T,-B+T,0,
K,6,B/2-T,-T,0,
K,7,0,-T,0,

!* Keypoints weld profile
K,8,d/2,0,0,
K,9,d/2+6.3,0,0,
K,10,d/2,6.3,0,

!* Keypoints CHS
K,11,d/2,H,
K,12,d/2-6.3,H,0,
K,13,d/2-6.3,0,0,

!*Keypoints for volume elimination
K,204,0,-T,0,
K,205,d/2-6.3,-T,0,
K,206,d/2,-T,0,
K,207,d/2+6.3,-T,0,

!* Lines half-SHS
LSTR,     14,     13
LSTR,     13,      8
LSTR,      8,      9
LSTR,      9,      1
LSTR,      1,      2
LSTR,      2,      3
LSTR,      3,      4
LSTR,      4,      5
LSTR,      5,      6
LSTR,      7,     14
LSTR,      7,    205
LSTR,    205,    206
LSTR,    206,    207
LSTR,    207,      6
LSTR,    205,     13
LSTR,    206,      8
LSTR,    207,      9

!* Lines weld profile
LSTR,      9,     10
LSTR,      8,     10

!* Lines CHS
LSTR,     10,     11
LSTR,     11,     12
LSTR,     12,     13

!* Merge items
NUMMRG,ALL,0.1, , ,LOW

!* Area half SHS
FLST,2,4,4
FITEM,2,1
FITEM,2,10
FITEM,2,11
FITEM,2,15
AL,P51X
FLST,2,4,4
FITEM,2,2
FITEM,2,15
FITEM,2,12
FITEM,2,16
AL,P51X
FLST,2,4,4
FITEM,2,3
FITEM,2,16
FITEM,2,17
FITEM,2,13
AL,P51X
FLST,2,8,4
FITEM,2,4
FITEM,2,17
FITEM,2,14
FITEM,2,9
FITEM,2,5
FITEM,2,6
FITEM,2,8
FITEM,2,7
AL,P51X

!* Area weld profile
FLST,2,3,4
FITEM,2,3
FITEM,2,19
FITEM,2,18
AL,P51X

!* Area CHS
FLST,2,5,4
FITEM,2,19
FITEM,2,2
FITEM,2,22
FITEM,2,20
FITEM,2,21
```

```
AL,P51X

!* Numbering and plotting of areas
/PNUM,AREA,1
/PNUM,LINE,0
APLOT

!* Element Extrusion Options
TYPE,   1
EXTOPT,ESIZE,0,0,
EXTOPT,ACLEAR,0
EXTOPT,ATTR,0,0,0
MAT,_Z2
REAL,_Z4
ESYS,0

!* Half-SHS extrusion
FLST,2,4,5,ORDE,2
FITEM,2,1
FITEM,2,-4
VEXT,P51X, , ,0,0,L,,,,

!* Add volumes
FLST,2,4,6,ORDE,2
FITEM,2,1
FITEM,2,-4
VADD,P51X

!* CHS areas add
VSEL,S, , ,       5
ALLSEL,BELOW,VOLU
APLOT

FLST,2,4,5,ORDE,4
FITEM,2,8
FITEM,2,13
FITEM,2,17
FITEM,2,21
AADD,P51X

FLST,2,4,5,ORDE,4
FITEM,2,7
FITEM,2,12
FITEM,2,16
FITEM,2,20
AADD,P51X

FLST,2,4,5,ORDE,4
FITEM,2,10
FITEM,2,15
FITEM,2,19
FITEM,2,27
AADD,P51X

ALLSEL,ALL
/AUTO,1
/REP,FAST

!* Half SHS lines add
FLST,2,4,4,ORDE,4
FITEM,2,25
FITEM,2,33
FITEM,2,38
FITEM,2,47
LCOMB,P51X, ,0
FLST,2,4,4,ORDE,4
FITEM,2,23
FITEM,2,31
FITEM,2,36
FITEM,2,41
LCOMB,P51X, ,0


!* Axis of revolution creation
K,260,0,6.5,0,
!* Weld profile and CHS revolution
K,14,0,0,0,
FLST,2,2,5,ORDE,2
FITEM,2,5
FITEM,2,-6
FLST,8,2,3
FITEM,8,14
FITEM,8,260
VROTAT,P51X, , , , , ,P51X, ,-90, ,

!* Volumes add
FLST,2,3,6,ORDE,3
FITEM,2,1
FITEM,2,-2
FITEM,2,5
VADD,P51X

!* Lateral areas add
FLST,2,4,5,ORDE,2
FITEM,2,1
FITEM,2,-4
AADD,P51X

!* Lines of lateral areas add
FLST,2,4,4,ORDE,2
FITEM,2,11
FITEM,2,-14
LCOMB,P51X, ,0

NUMMRG,ALL,0.1, , ,LOW

!* Meshing properties
ESIZE,5,0,
MSHKEY,0
MSHAPE,1,3d
CM,_Y,VOLU
VSEL, , , ,       3
CM,_Y1,VOLU
CHKMSH,'VOLU'
CMSEL,S,_Y
!*
VMESH,_Y1

!* Loads and constraints
FLST,2,1,5,ORDE,1
FITEM,2,16
SFA,P51X,1,PRES,-33.22

FLST,2,4,5,ORDE,4
FITEM,2,14
FITEM,2,19
FITEM,2,24
FITEM,2,27
DA,P51X,SYMM

FLST,2,3,5,ORDE,3
FITEM,2,5
FITEM,2,-6
FITEM,2,9
DA,P51X,SYMM

FLST,2,1,5,ORDE,1
FITEM,2,8
DA,P51X,ALL,

!* Solution of the system
/SOL
/STATUS,SOLU
SOLVE

!* Power graphics OFF
/GRAPHICS,FULL
```

Eight-node linear elements (Brick 185), 1 volume main model, PSM

```
/CLEAR,NOSTART
/PREP7

!* Variables
B=200
L=360
H=900
d=51
T=10

!* Element selection
ET,1,PLANE182
KEYOPT,1,1,3
KEYOPT,1,3,2
KEYOPT,1,6,0
ET,2,SOLID187
KEYOPT,2,6,0

!* Material properties
MPTEMP,,,,,,,,
MPTEMP,1,0
MPDATA,EX,1,,206000
MPDATA,PRXY,1,,0.3

!* Isometric view
/VIEW,1,1,1,1
/ANG,1
/REP,FAST

!* Keypoints half-SHS
K,14,0,0,0,
K,1,B/2,0,0,
K,2,B/2,-B,0,
K,3,0,-B,0,
K,4,0,-B+T,0,
K,5,B/2-T,-B+T,0,
K,6,B/2-T,-T,0,
K,7,0,-T,0,

!* Keypoints weld profile
K,8,d/2,0,0,
K,9,d/2+6.3,0,0,
K,10,d/2,6.3,0,

!* Keypoints CHS
K,11,d/2,H,
K,12,d/2-6.3,H,0,
K,13,d/2-6.3,0,0,

!*Keypoints for volume elimination
K,204,0,-T,0,
K,205,d/2-6.3,-T,0,
K,206,d/2,-T,0,
K,207,d/2+6.3,-T,0,

!* Lines half-SHS
LSTR,     14,     13
LSTR,     13,      8
LSTR,      8,      9
LSTR,      9,      1
LSTR,      1,      2
LSTR,      2,      3
LSTR,      3,      4
LSTR,      4,      5
LSTR,      5,      6
LSTR,      7,     14
LSTR,      7,    205
LSTR,    205,    206
LSTR,    206,    207
LSTR,    207,      6
LSTR,    205,     13
LSTR,    206,      8
LSTR,    207,      9

!* Lines weld profile
LSTR,      9,     10
LSTR,      8,     10

!* Lines CHS
LSTR,     10,     11
LSTR,     11,     12
LSTR,     12,     13

!* Merge items
NUMMRG,ALL,0.1, , ,LOW

!* Area half SHS
FLST,2,4,4
FITEM,2,1
FITEM,2,10
FITEM,2,11
FITEM,2,15
AL,P51X
FLST,2,4,4
FITEM,2,2
FITEM,2,15
FITEM,2,12
FITEM,2,16
AL,P51X
FLST,2,4,4
FITEM,2,3
FITEM,2,16
FITEM,2,17
FITEM,2,13
AL,P51X
FLST,2,8,4
FITEM,2,4
FITEM,2,17
FITEM,2,14
FITEM,2,9
FITEM,2,5
FITEM,2,6
FITEM,2,8
FITEM,2,7
AL,P51X

!* Area weld profile
FLST,2,3,4
FITEM,2,3
FITEM,2,19
FITEM,2,18
AL,P51X

!* Area CHS
FLST,2,5,4
FITEM,2,19
FITEM,2,2
FITEM,2,22
FITEM,2,20
FITEM,2,21
AL,P51X

!* Numbering and plotting of areas
/PNUM,AREA,1
/PNUM,LINE,0
APLOT

!* Element Extrusion Options
TYPE,   1
EXTOPT,ESIZE,0,0,
EXTOPT,ACLEAR,0
EXTOPT,ATTR,0,0,0
MAT,_Z2
REAL,_Z4
```

```
ESYS,0

!* Half-SHS extrusion
FLST,2,4,5,ORDE,2
FITEM,2,1
FITEM,2,-4
VEXT,P51X, , ,0,0,L,,,,

!* Add volumes
FLST,2,4,6,ORDE,2
FITEM,2,1
FITEM,2,-4
VADD,P51X

!* CHS areas add
VSEL,S, , ,       5
ALLSEL,BELOW,VOLU
APLOT

FLST,2,4,5,ORDE,4
FITEM,2,8
FITEM,2,13
FITEM,2,17
FITEM,2,21
AADD,P51X

FLST,2,4,5,ORDE,4
FITEM,2,7
FITEM,2,12
FITEM,2,16
FITEM,2,20
AADD,P51X

FLST,2,4,5,ORDE,4
FITEM,2,10
FITEM,2,15
FITEM,2,19
FITEM,2,27
AADD,P51X

ALLSEL,ALL
/AUTO,1
/REP,FAST

!* Half SHS lines add
FLST,2,4,4,ORDE,4
FITEM,2,25
FITEM,2,33
FITEM,2,38
FITEM,2,47
LCOMB,P51X, ,0
FLST,2,4,4,ORDE,4
FITEM,2,23
FITEM,2,31
FITEM,2,36
FITEM,2,41
LCOMB,P51X, ,0

!* Axis of revolution creation
K,260,0,6.5,0,

!* Weld profile and CHS revolution
K,14,0,0,0,
FLST,2,2,5,ORDE,2
FITEM,2,5
FITEM,2,-6
FLST,8,2,3
FITEM,8,14
FITEM,8,260
VROTAT,P51X, , , , , ,P51X, ,-90, ,

!* Volumes add
FLST,2,3,6,ORDE,3
FITEM,2,1
FITEM,2,-2
FITEM,2,5
VADD,P51X

!* Lateral areas add
FLST,2,4,5,ORDE,2
FITEM,2,1
FITEM,2,-4
AADD,P51X

!* Lines of lateral areas add
FLST,2,4,4,ORDE,2
FITEM,2,11
FITEM,2,-14
LCOMB,P51X, ,0

NUMMRG,ALL,0.1, , ,LOW

!* Meshing properties
ESIZE,5,0,
MSHKEY,0
MSHAPE,1,3d
CM,_Y,VOLU
VSEL, , , ,       3
CM,_Y1,VOLU
CHKMSH,'VOLU'
CMSEL,S,_Y
!*
VMESH,_Y1

!* Loads and constraints
FLST,2,1,5,ORDE,1
FITEM,2,16
SFA,P51X,1,PRES,-33.22

FLST,2,4,5,ORDE,4
FITEM,2,14
FITEM,2,19
FITEM,2,24
FITEM,2,27
DA,P51X,SYMM

FLST,2,3,5,ORDE,3
FITEM,2,5
FITEM,2,-6
FITEM,2,9
DA,P51X,SYMM

FLST,2,1,5,ORDE,1
FITEM,2,8
DA,P51X,ALL,

SAVE,'Select directory'

FINISH

!* SUBMODEL

/CLEAR,NOSTART
/PREP7

!* Element selection
ET,1,PLANE182
KEYOPT,1,1,3
KEYOPT,1,3,2
KEYOPT,1,6,0

ET,2,SOLID185
KEYOPT,2,2,3
KEYOPT,2,3,0
KEYOPT,2,6,0
KEYOPT,2,8,0

!* Material properties
MPTEMP,,,,,,,,
MPTEMP,1,0
MPDATA,EX,1,,206000
MPDATA,PRXY,1,,0.3

!* 2D submodel
K,14,0,0,0
```

```
K,13,19.2,0,0
K,107,19.2,20,0
K,106,19.2+6.3,20,0
K,10,19.2+6.3,6.3,0
K,9,19.2+6.3+6.3,0,0
K,103,50,0,0
K,102,50,-10,0
K,7,0,-10,0

LSTR,     14,     13
LSTR,     13,    107
LSTR,    107,    106
LSTR,    106,     10
LSTR,      9,     10
LSTR,      9,    103
LSTR,    103,    102
LSTR,      7,    102
LSTR,      7,     14

AL,1,2,3,4,5,6,7,8,9

!* Area meshing properties
ESIZE,1,0,
TYPE,   2
MSHKEY,0
AMESH,1

!* Isometric view
/VIEW,1,1,1,1

!* Area extrusion
EXTOPT,ESIZE,50,0,
VROTAT, 1, , , , , , 7, 14, -90,
ACLEAR,1

EPLOT
/PNUM,AREA,1

!* Constraints
FLST,2,2,5,ORDE,2
FITEM,2,1
FITEM,2,10
DA,P51X,SYMM

!* Cutboundary definition
FLST,5,2,5,ORDE,2
FITEM,5,4
FITEM,5,8
ASEL,S, , ,P51X

APLOT
/REPLOT,RESIZE
NSLA,S,1
NPLOT

NWRITE,'submodel','node',' ',0
ALLSEL,ALL
SAVE, 'Select directory'

!* MAIN MODEL SOLUTION

RESUME,'MainModel' ,0,0

/SOL
/STATUS,SOLU
SOLVE

!* INTERPOLATE DOF

/POST1
CBDOF,'submodel','node',' ','submodel','cbdo',' ',0, ,0

!* RESUME SUBMODEL

RESUME, 'Submodel',0,0/
/PREP7
GRAPHICS,FULL
```

At this moment, manually utlity menu → file → read input from → submodel.cbdo, and solve the system.

Appendix B

APDL codes for the modelling of longitudinal stiffener FAT 71, AW (Chapter 3)

Ten-node quadratic elements (Tetra 187), 1 volume model, straight junction, PSM

```
/CLEAR,NOSTART
/PREP7

!* Elements
ET,1,PLANE182
KEYOPT,1,1,3
KEYOPT,1,3,2
KEYOPT,1,6,0

ET,2,SOLID187
KEYOPT,2,6,0

!* Material models
MPTEMP,,,,,,,,
MPTEMP,1,0
MPDATA,EX,1,,206000
MPDATA,PRXY,1,,0.3

!*Variables
a=8
b=100
c=350
h=40
l=150
z=10.4
y=6
u=30
p=15

!* Keypoints main plate and gusset
K,1,0,0,0,
K,2,0,0,b/2
K,3,0,-a/2,0
K,4,0,-a/2,b/2
K,5,0,0,a/2
K,6,0,h,a/2
K,7,0,h,0
K,8,0,0,a/2+z
K,9,0,y,a/2

NUMMRG,ALL,0.1, , ,LOW


!* Lines main plate and gusset
LSTR,      1,      5
LSTR,      5,      8
LSTR,      8,      2
LSTR,      2,      4
LSTR,      3,      4
LSTR,      3,      1
LSTR,      5,      9
LSTR,      9,      6
LSTR,      7,      6
LSTR,      1,      7
LSTR,      8,      9

!* Merge items
NUMMRG,ALL,0.1, , ,LOW

!* Plot lines
LPLOT
/PNUM,LINE,1
```

```
!* Areas main plate ad gusset
AL,1,2,3,4,5,6
AL,1,7,8,9,10
AL,2,7,11

NUMMRG,ALL,0.1, , ,LOW

!* Isometric view
/VIEW,1,1,1,1

!* Main plate and gusset area extrusion
VEXT,1, , ,c/2,0,0,,,,
AADD,5,6,7
VEXT,2, , ,l/2,0,0,,,,
AADD,12,7

!* Double lines deletion
FLST,2,3,4,ORDE,2
FITEM,2,12
FITEM,2,-14
LCOMB,P51X, ,0

FLST,2,1,4,ORDE,1
FITEM,2,18
LSBL,      18,      26

LDELE,      18, , ,1

NUMMRG,ALL,0.1, , ,LOW

!* Anterior weld profile
K,101,l/2+z,0,0,
K,102,l/2,y,0,
K,103,l/2+z,0,a/2

LSTR,      18,      102

BOPTN,KEEP,1
LSBL,      26,      14
BOPTN,KEEP,0

LDEL,26

NUMMRG,ALL,0.1, , ,LOW

LSTR,      17,     103
LSTR,     101,     103
LSBL,      13,      32
LSTR,     101,     103
LSTR,     102,     101
LSTR,      18,     103

NUMMRG,ALL,0.1, , ,LOW

AL,34,18,32
AL,34,13,26,19
AL,19,18,14,20
AL,26,35,20
AL,13,35,14,32

ASBL,      5,      14

VA,7,12,16,17,18
```

```
!* Longitudinal weld profile
VEXT,3, , ,l/2,0,0,,,,

ASBL,     15,     41


!* Straight junction
LSTR,     103,     12

NUMMRG,ALL,0.1, , ,LOW

AL,43,26,36
AL,43,37,35

VA,23,5,17,15

!* Volumes and lateral area add
VADD,1,2,3,4,5
AADD,14,10,7
AADD,1,2,3


!* Gusset bevel
K,104,l/2-u,h,0
K,105,l/2-u,h,a/2
K,106,l/2,h-u,a/2
K,107,l/2,h-u,0

LSTR,     105,     104
LSTR,     106,     107
LSTR,     106,     105
LSTR,     107,     104

FLST,2,4,4
FITEM,2,7
FITEM,2,18
FITEM,2,1
FITEM,2,2
AL,P51X
VSBA,     6,     1
FLST,2,4,4
FITEM,2,7
FITEM,2,18
FITEM,2,1
FITEM,2,2
AL,P51X
VDELE,     1, , ,1

ADELE,     5, , ,1

!* Lines and keypoint numbering
/PNUM,LINE,1
/PNUM,KP,1
LPLOT

NUMMRG,ALL,0.1, , ,LOW

!* Lines add
FLST,2,2,4,ORDE,2
FITEM,2,6
FITEM,2,10
LCOMB,P51X, ,0

NUMMRG,ALL,0.1, , ,LOW

!* Mesh properties
ESIZE,2,0,
VMESH,2
DA,9,SYMM
DA,15,SYMM
DA,6,SYMM
SFA,4,1,PRES,-1

NUMMRG,ALL,0.1, , ,LOW

!* Solution of the system
/SOL
/STATUS,SOLU
SOLVE

/GRAPHICS,FULL
```

Eight-node linear elements (Brick 185), 2 volumes main model, straight junction, PSM

```
/CLEAR,NOSTART
/PREP7

!* MAIN MODEL

!* Elements
ET,1,PLANE182
KEYOPT,1,1,3
KEYOPT,1,3,2
KEYOPT,1,6,0

ET,2,SOLID187
KEYOPT,2,6,0

!* Material models
MPTEMP,,,,,,,,
MPTEMP,1,0
MPDATA,EX,1,,206000
MPDATA,PRXY,1,,0.3

!*Variables
a=8
b=100
c=350
h=40
l=150
z=10.4
y=6
u=30
p=15

!* Keypoints main plate and gusset
K,1,0,0,0,
K,2,0,0,b/2
K,3,0,-a/2,0
K,4,0,-a/2,b/2
K,5,0,0,a/2
K,6,0,h,a/2
K,7,0,h,0
K,8,0,0,a/2+z
K,9,0,y,a/2

NUMMRG,ALL,0.1, , ,LOW

LSTR,      1,      5
LSTR,      5,      8
LSTR,      8,      2
LSTR,      2,      4
LSTR,      3,      4
LSTR,      3,      1
LSTR,      5,      9
LSTR,      9,      6
LSTR,      7,      6
LSTR,      1,      7
LSTR,      8,      9

NUMMRG,ALL,0.1, , ,LOW

LPLOT
/PNUM,LINE,1

!* Area main plate and gusset
AL,1,2,3,4,5,6
AL,1,7,8,9,10
AL,2,7,11

NUMMRG,ALL,0.1, , ,LOW

/VIEW,1,1,1,1
!* Main plate and gusset area extrusion
VEXT,1, , ,c/2,0,0,,,,
AADD,5,6,7
VEXT,2, , ,l/2,0,0,,,,
AADD,12,7

!* Boolean operations on double lines
FLST,2,3,4,ORDE,2
FITEM,2,12
FITEM,2,-14
LCOMB,P51X, ,0

FLST,2,1,4,ORDE,1
FITEM,2,18
LSBL,      18,      26

LDELE,      18, , ,1

NUMMRG,ALL,0.1, , ,LOW

!* Anterior weld toe
K,101,l/2+z,0,0,
K,102,l/2,y,0,
K,103,l/2+z,0,a/2

LSTR,      18,     102

BOPTN,KEEP,1
LSBL,      26,      14
BOPTN,KEEP,0

LDEL,26

NUMMRG,ALL,0.1, , ,LOW

LSTR,      17,     103
LSTR,     101,     103
LSBL,      13,      32
LSTR,     101,     103
LSTR,     102,     101
LSTR,      18,     103

NUMMRG,ALL,0.1, , ,LOW

AL,34,18,32
AL,34,13,26,19
AL,19,18,14,20
AL,26,35,20
AL,13,35,14,32

ASBL,       5,      14

VA,7,12,16,17,18


!* Longitudinal weld toe
VEXT,3, , ,l/2,0,0,,,,

ASBL,      15,      41


!* Straight junction
LSTR,     103,      12

NUMMRG,ALL,0.1, , ,LOW

AL,43,26,36
AL,43,37,35

VA,23,5,17,15

!* Volumes and lateral areas add
VADD,1,2,3,4,5
```

```
AADD,14,10,7
AADD,1,2,3


!* Gusset bevel
K,104,l/2-u,h,0
K,105,l/2-u,h,a/2
K,106,l/2,h-u,a/2
K,107,l/2,h-u,0

LSTR,     105,     104
LSTR,     106,     107
LSTR,     106,     105
LSTR,     107,     104

FLST,2,4,4
FITEM,2,7
FITEM,2,18
FITEM,2,1
FITEM,2,2
AL,P51X
VSBA,       6,       1

FLST,2,4,4
FITEM,2,7
FITEM,2,18
FITEM,2,1
FITEM,2,2
AL,P51X
VDELE,       1, , ,1

ADELE,       5, , ,1

!* Lines and keypoint numbering
/PNUM,LINE,1
/PNUM,KP,1
LPLOT

NUMMRG,ALL,0.1, , ,LOW

!* Cutboundary volume inside the main model
K,201,l/2+z+p,-a/2,0
K,202,l/2+z+p,0,0
K,205,l/2+z+p,0,a/2
K,206,l/2+z+p,-a/2,a/2
K,208,l/2-6,-a/2,a/2
K,204,l/2-6,-a/2,0
K,203,l/2-6,y+30,0
K,207,l/2-6,y+30,a/2

LSTR,     201,     202
LSTR,     202,     205
LSTR,     205,     206
LSTR,     206,     201
LSTR,     206,     208
LSTR,     208,     204
LSTR,     204,     201
LSTR,     204,     203
LSTR,     207,     208
LSTR,     205,     103
LSTR,     202,     101

LSBL,      31,       7
LSBL,      30,      18
LSBL,       7,      44
LSBL,      18,      31

LSTR,       5,      11

AL,2,47,18,44
AL,18,46,45,27
AL,27,29,25,26
AL,24,25,19,20
AL,20,42,13,39
AL,26,24,39,35,36,47,45
AL,44,46,29,19,42,32,38

FLST,2,9,5,ORDE,9
FITEM,2,2
FITEM,2,-3
FITEM,2,5
FITEM,2,7
FITEM,2,10
FITEM,2,12
FITEM,2,-13
FITEM,2,16
FITEM,2,18
VA,P51X

ASBL,      13,      41
ASBL,      14,      31
ASBL,       1,      18

!* Eliminate area in excess
!FLST,2,2,5,ORDE,2
!FITEM,2,2
!FITEM,2,17
!ADELE,P51X, , ,1

NUMMRG,ALL,0.1, , ,LOW

/PNUM,LINE,0
/PNUM,KP,0
/PNUM,AREA,1
APLOT

!* Volume split in two parts
FLST,3,5,5,ORDE,5
FITEM,3,3
FITEM,3,5
FITEM,3,7
FITEM,3,17
FITEM,3,19
VSBA,       2,P51X

/PNUM,VOLU,1

!* Glue volumes
FLST,2,2,6,ORDE,2
FITEM,2,1
FITEM,2,3
VGLUE,P51X

NUMMRG,ALL,0.1, , ,LOW

!* Mesh properties
ESIZE,2,0,
TYPE,2
VMESH,1
VMESH,3
DA,24,SYMM
DA,5,SYMM
DA,20,SYMM
DA,16,SYMM
DA,1,SYMM
DA,6,SYMM
SFA,4,1,PRES,-1

NUMMRG,ALL,0.1, , ,LOW

SAVE,'Select directory'

!* SUBMODEL

/CLEAR,NOSTART
/PREP7

!* Element selection
ET,1,PLANE182
KEYOPT,1,1,3
KEYOPT,1,3,2
KEYOPT,1,6,0

ET,3,SOLID185
```

```
KEYOPT,3,2,3

!* Material models
MPTEMP,,,,,,,,
MPTEMP,1,0
MPDATA,EX,1,,206000
MPDATA,PRXY,1,,0.3

/VIEW,1,1,1,1

!*Variables
a=8
b=100
c=350
h=40
l=150
z=10.4
y=6
u=30
p=15

!* 2D submodel area
K,101,l/2+z,0,0
K,102,l/2,y,0
K,107,l/2,h-u,0
K,201,l/2+z+p,-a/2,0
K,202,l/2+z+p,0,0
K,203,l/2-6,y+10,0
K,204,l/2-6,-a/2,0

LSTR,    204,    201
LSTR,    201,    202
LSTR,    202,    101
LSTR,    101,    202
LSTR,    101,    102
LSTR,    102,    107
LSTR,    107,    203
LSTR,    203,    204

AL,1,2,3,4,5,6,7

!* Area mesh properties
ESIZE,0.5
MSHKEY,0
TYPE,3
AMESH,1

FLST,2,1,5,ORDE,1
FITEM,2,1
TYPE,   1
EXTOPT,ESIZE,8,0,
FLST,2,1,5,ORDE,1
FITEM,2,1
VEXT,P51X, , ,0,0,4,,,,

ACLEAR,      1

!* Constraints
FLST,2,2,5,ORDE,2
FITEM,2,1
FITEM,2,3
DA,P51X,SYMM

!* Cutboundary definition
FLST,5,2,5,ORDE,2
FITEM,5,4
FITEM,5,9
ASEL,S, , ,P51X
NSLA,S,1
NPLOT

NWRITE,'submodel','node',' ',0
ALLSEL,ALL
SAVE,'Select directory'

!* MAIN MODEL SOLUTION

RESUME,'MainModel',0,0

/SOL
/STATUS,SOLU
SOLVE

/GRAPHICS,FULL

!* INTERPOLATE DOF

/POST1
CBDOF,'submodel','node',' ','submodel','cbdo',' ',0, ,0

!* RESUME SUBMODEL

RESUME, 'Submodel',0,0
/PREP7

/GRAPHICS,FULL
```

At this moment, manually utility menu → file → read input from → submodel.cbdo and solve the system.

Ten-node quadratic elements (Tetra 187), 1 volume model, curve junction, PSM

```
/CLEAR,NOSTART
/PREP7

!* Elements
ET,1,PLANE182
KEYOPT,1,1,3
KEYOPT,1,3,2
KEYOPT,1,6,0

ET,2,SOLID187
KEYOPT,2,6,0

!* Material models
MPTEMP,,,,,,,,
MPTEMP,1,0
MPDATA,EX,1,,206000
MPDATA,PRXY,1,,0.3

!*Variables
a=8
b=100
c=350
h=40
l=150
z=10.4
y=6
u=30
p=15

!* Keypoints and lines main plate and gusset
K,1,0,0,0,
K,2,0,0,b/2
K,3,0,-a/2,0
K,4,0,-a/2,b/2
K,5,0,0,a/2
K,6,0,h,a/2
K,7,0,h,0
K,8,0,0,a/2+z
K,9,0,y,a/2

NUMMRG,ALL,0.1, , ,LOW

LSTR,       1,       5
LSTR,       5,       8
LSTR,       8,       2
LSTR,       2,       4
LSTR,       3,       4
LSTR,       3,       1
LSTR,       5,       9
LSTR,       9,       6
LSTR,       7,       6
LSTR,       1,       7
LSTR,       8,       9

NUMMRG,ALL,0.1, , ,LOW

LPLOT
/PNUM,LINE,1

!* Areas main plate and gusset
AL,1,2,3,4,5,6
AL,1,7,8,9,10
AL,2,7,11

NUMMRG,ALL,0.1, , ,LOW

/VIEW,1,1,1,1

!* Main plate and gusset extrusion
VEXT,1, , ,c/2,0,0,,,,

AADD,5,6,7

VEXT,2, , ,l/2,0,0,,,,
AADD,12,7

!* Boolean operations on lines
FLST,2,3,4,ORDE,2
FITEM,2,12
FITEM,2,-14
LCOMB,P51X, ,0

FLST,2,1,4,ORDE,1
FITEM,2,18
LSBL,      18,      26

LDELE,      18, , ,1

NUMMRG,ALL,0.1, , ,LOW

!* Anterior weld profile
K,101,l/2+z,0,0,
K,102,l/2,y,0,
K,103,l/2+z,0,a/2

LSTR,      18,     102

BOPTN,KEEP,1
LSBL,      26,      14
BOPTN,KEEP,0

LDEL,26

NUMMRG,ALL,0.1, , ,LOW

LSTR,      17,     103
LSTR,     101,     103
LSBL,      13,      32
LSTR,     101,     103
LSTR,     102,     101
LSTR,      18,     103

NUMMRG,ALL,0.1, , ,LOW

AL,34,18,32
AL,34,13,26,19
AL,19,18,14,20
AL,26,35,20
AL,13,35,14,32

ASBL,       5,      14

VA,7,12,16,17,18


!* Longitudinal weld profile
VEXT,3, , ,l/2,0,0,,,,

ASBL,      15,      41


!* Straight junction
LSTR,     103,      12

NUMMRG,ALL,0.1, , ,LOW

AL,43,26,36
AL,43,37,35

VA,23,5,17,15
```

```
!* Volumes and lateral area add
VADD,1,2,3,4,5
AADD,14,10,7
AADD,1,2,3

 !* Gusset bevel
K,104,l/2-u,h,0
K,105,l/2-u,h,a/2
K,106,l/2,h-u,a/2
K,107,l/2,h-u,0

LSTR,     105,     104
LSTR,     106,     107
LSTR,     106,     105
LSTR,     107,     104

FLST,2,4,4
FITEM,2,7
FITEM,2,18
FITEM,2,1
FITEM,2,2
AL,P51X
VSBA,       6,       1

FLST,2,4,4
FITEM,2,7
FITEM,2,18
FITEM,2,1
FITEM,2,2
AL,P51X
VDELE,       1, , ,1

ADELE,       5, , ,1

!* Keypoint and lines numbering
/PNUM,LINE,1
/PNUM,KP,1
LPLOT

NUMMRG,ALL,0.1, , ,LOW

!* Curve junction
VDELE,       2

FLST,2,2,5,ORDE,2
FITEM,2,23
FITEM,2,25
ADELE,P51X
LDELE,      43, , ,1
K,1000,l/2,0,a/2,

LARC,12,103,1000,10.4,

FLST,2,3,4
FITEM,2,19
FITEM,2,37
FITEM,2,35
AL,P51X

NUMMRG,ALL,0.1, , ,LOW

FLST,2,7,4
FITEM,2,3
FITEM,2,40
FITEM,2,19
FITEM,2,13
FITEM,2,33
FITEM,2,12
FITEM,2,21
AL,P51X
FLST,2,13,5,ORDE,11
FITEM,2,1
FITEM,2,-4
FITEM,2,6
FITEM,2,8
FITEM,2,-9
FITEM,2,11
FITEM,2,-12
FITEM,2,14
FITEM,2,-15
FITEM,2,18
FITEM,2,21
VA,P51X

!* Mesh properties
ESIZE,2,0,
VMESH,1
DA,9,SYMM
DA,15,SYMM
DA,6,SYMM
SFA,4,1,PRES,-1

!* Solution of the system
/SOL
/STATUS,SOLU
SOLVE
FINISH
```

Eight-node linear elements (Brick 185), 2 volumes main model, curve junction, PSM

```
/CLEAR,NOSTART
/PREP7

!* MAIN MODEL

!* Elements
ET,1,PLANE182
KEYOPT,1,1,3
KEYOPT,1,3,2
KEYOPT,1,6,0

ET,2,SOLID187
KEYOPT,2,6,0

!* Material models
MPTEMP,,,,,,,,
MPTEMP,1,0
MPDATA,EX,1,,206000
MPDATA,PRXY,1,,0.3

!*Variables
a=8
b=100
c=350
h=40
l=150
z=10.4
y=6
u=30
p=15

!* Keypoints and lines main plate and gusset
K,1,0,0,0,
K,2,0,0,b/2
K,3,0,-a/2,0
K,4,0,-a/2,b/2
K,5,0,0,a/2
K,6,0,h,a/2
K,7,0,h,0
K,8,0,0,a/2+z
K,9,0,y,a/2

NUMMRG,ALL,0.1, , ,LOW

LSTR,      1,      5
LSTR,      5,      8
LSTR,      8,      2
LSTR,      2,      4
LSTR,      3,      4
LSTR,      3,      1
LSTR,      5,      9
LSTR,      9,      6
LSTR,      7,      6
LSTR,      1,      7
LSTR,      8,      9

NUMMRG,ALL,0.1, , ,LOW

LPLOT
/PNUM,LINE,1

!* Main plate and gusset areas
AL,1,2,3,4,5,6
AL,1,7,8,9,10
AL,2,7,11

NUMMRG,ALL,0.1, , ,LOW

/VIEW,1,1,1,1

!* Main plate and gusset extrusion
VEXT,1, , ,c/2,0,0,,,,


AADD,5,6,7

VEXT,2, , ,l/2,0,0,,,,
AADD,12,7

!* Boolean operation on lines
FLST,2,3,4,ORDE,2
FITEM,2,12
FITEM,2,-14
LCOMB,P51X, ,0

FLST,2,1,4,ORDE,1
FITEM,2,18
LSBL,     18,     26

LDELE,     18, , ,1

NUMMRG,ALL,0.1, , ,LOW

!* Anterior weld profile
K,101,l/2+z,0,0,
K,102,l/2,y,0,
K,103,l/2+z,0,a/2

LSTR,     18,     102

BOPTN,KEEP,1
LSBL,     26,     14
BOPTN,KEEP,0

LDEL,26

NUMMRG,ALL,0.1, , ,LOW

LSTR,     17,     103
LSTR,    101,     103
LSBL,     13,     32
LSTR,    101,     103
LSTR,    102,     101
LSTR,     18,     103

NUMMRG,ALL,0.1, , ,LOW

AL,34,18,32
AL,34,13,26,19
AL,19,18,14,20
AL,26,35,20
AL,13,35,14,32

ASBL,      5,     14

VA,7,12,16,17,18


!* Longitudinal weld profile
VEXT,3, , ,l/2,0,0,,,,

ASBL,     15,     41


!* Straight junction
LSTR,    103,     12

NUMMRG,ALL,0.1, , ,LOW

AL,43,26,36
```

```
AL,43,37,35

VA,23,5,17,15

!* Volume and lateral area add
VADD,1,2,3,4,5
AADD,14,10,7
AADD,1,2,3


!* Gusset bevel
K,104,l/2-u,h,0
K,105,l/2-u,h,a/2
K,106,l/2,h-u,a/2
K,107,l/2,h-u,0

LSTR,     105,     104
LSTR,     106,     107
LSTR,     106,     105
LSTR,     107,     104

FLST,2,4,4
FITEM,2,7
FITEM,2,18
FITEM,2,1
FITEM,2,2
AL,P51X
VSBA,       6,       1

FLST,2,4,4
FITEM,2,7
FITEM,2,18
FITEM,2,1
FITEM,2,2
AL,P51X
VDELE,       1, , ,1

ADELE,       5, , ,1

!* Lines and Keypoints number
/PNUM,LINE,1
/PNUM,KP,1
LPLOT

NUMMRG,ALL,0.1, , ,LOW

!* Curve junction
VDELE,       2

FLST,2,2,5,ORDE,2
FITEM,2,23
FITEM,2,25
ADELE,P51X
LDELE,      43, , ,1
K,1000,l/2,0,a/2,
!*
LARC,12,103,1000,10.4,

KDELE,1000

FLST,2,3,4
FITEM,2,19
FITEM,2,37
FITEM,2,35
AL,P51X

NUMMRG,ALL,0.1, , ,LOW

FLST,2,7,4
FITEM,2,3
FITEM,2,40
FITEM,2,19
FITEM,2,13
FITEM,2,33
FITEM,2,12
FITEM,2,21
AL,P51X
```

```
FLST,2,13,5,ORDE,11
FITEM,2,1
FITEM,2,-4
FITEM,2,6
FITEM,2,8
FITEM,2,-9
FITEM,2,11
FITEM,2,-12
FITEM,2,14
FITEM,2,-15
FITEM,2,18
FITEM,2,21
VA,P51X

!* Submodel inside the main model
K,202,l/2+z+p,0,0
K,203,l/2+z+p,0,a/2
K,204,l/2+z+p,-a/2,0
K,205,l/2+z+p,-a/2,a/2
K,206,l/2-6,-a/2,0
K,207,l/2-6,-a/2,a/2
K,208,l/2-6,30,0
K,209,l/2-6,30,a/2

LSTR,     203,     202
LSTR,     202,     204
LSTR,     204,     205
LSTR,     205,     203
LSTR,     205,     207
LSTR,     207,     206
LSTR,     206,     204
LSTR,     207,     209
LSTR,     206,     208
LSBL,       7,      31
LSBL,      18,      39
LSTR,     207,       5
LSTR,       5,      11
LSTR,     206,      11
LSTR,     202,     101
LSTR,     103,     203

AL,43,31,39,2
AL,38,36,2,14
AL,13,32,14,35
AL,46,20,45,13
AL,20,24,25,26
AL,29,30,25,27
AL,30,24,45,32,38,31,44
AL,18,43,36,35,46,26,27
AL,39,18,29,44
AL,13,46,45,20

VA,5,7,18,13,16,20,22,17,19

NUMMRG,ALL,0.1, , ,LOW

!* Two volumes creation and glue
FLST,3,4,5,ORDE,4
FITEM,3,16
FITEM,3,-17
FITEM,3,20
FITEM,3,22
VSBA,       1,P51X

NUMMRG,ALL,0.1, , ,LOW

VDELE,       3, , ,1

!* Glue volumes
FLST,2,2,6,ORDE,2
FITEM,2,2
FITEM,2,4
VGLUE,P51X

NUMMRG,ALL,0.1, , ,LOW

!* Mesh properties
```

```
ESIZE,2,0,
TYPE,2
VMESH,1
VMESH,3
DA,6,SYMM
DA,32,SYMM
DA,17,SYMM
DA,27,SYMM
DA,19,SYMM
DA,30,SYMM
SFA,4,1,PRES,-1

!* Save model
SAVE,'MainModel'
FINISH

!* SUBMODEL

/CLEAR,NOSTART
/PREP7

!* Elements
ET,1,PLANE182
KEYOPT,1,1,3
KEYOPT,1,3,2
KEYOPT,1,6,0

ET,3,SOLID185
KEYOPT,3,2,3

!* Material models
MPTEMP,,,,,,,,
MPTEMP,1,0
MPDATA,EX,1,,206000
MPDATA,PRXY,1,,0.3

/VIEW,1,1,1,1

!*Variables
a=8
b=100
c=350
h=40
l=150
z=10.4
y=6
u=30
p=15

!* 2D area submodel
K,101,l/2+z,0,0
K,102,l/2,y,0
K,107,l/2,h-u,0
K,201,l/2+z+p,-a/2,0
K,202,l/2+z+p,0,0
K,203,l/2-6,y+10,0
K,204,l/2-6,-a/2,0

LSTR,    204,    201
LSTR,    201,    202
LSTR,    202,    101
LSTR,    101,    202
LSTR,    101,    102
LSTR,    102,    107
LSTR,    107,    203
LSTR,    203,    204

AL,1,2,3,4,5,6,7

!* Mesh properties
ESIZE,0.5
TYPE,3
MSHKEY,0
AMESH,1

FLST,2,1,5,ORDE,1
FITEM,2,1
TYPE,   1
EXTOPT,ESIZE,8,0,
FLST,2,1,5,ORDE,1
FITEM,2,1
VEXT,P51X, , ,0,0,4,,,,

ACLEAR,      1

!* Constraints
FLST,2,2,5,ORDE,2
FITEM,2,1
FITEM,2,3
DA,P51X,SYMM

!* Cutboundary definition
FLST,5,2,5,ORDE,2
FITEM,5,4
FITEM,5,9
ASEL,S, , ,P51X
NSLA,S,1
NPLOT

/PREP7
NWRITE,'submodel','node',' ',0
ALLSEL,ALL

SAVE,'SubModel',0,0

/SOL
/STATUS,SOLU
SOLVE

!* INTERPOLATE DOF

/POST1
CBDOF,'submodel','node',' ','submodel','cbdo',' ',0, ,0

!* RESUME SUBMODEL

RESUME,'SubModel\' ,0,0
GRAPHICS,FULL
 /PREP7
```

At this moment, manually utility menu → file → read input from → submodel.cbdo and solve the system

Appendix C

Longitudinal stiffener FAT 71, AW experimental results

NB: all the experimental failures occurred at the weld toe. The barred data refer to runouts.

Straight fillet

		Tetra 187	Brick 185	
	Nf	$\Delta\sigma_{eq,peak}$ [MPa]	$\Delta\sigma_{eq,peak}$ [MPa]	SED [MJ/m^3]
R=-1	229,600	327	316	3.00E-01
	265,500	326	314	2.97E-01
	679,800	325	314	2.95E-01
	402,100	306	296	2.63E-01
	2,808,000	280	270	2.20E-01
	564,900	239	231	1.60E-01
	844,100	214	207	1.28E-01
	~~6,403,000~~	~~206~~	~~199~~	~~1.19E-01~~

Curve fillet

		Tetra 187	Brick 185		
	Nf	$\Delta\sigma_{eq,peak}$ [MPa]	$\Delta\sigma_{eq,peak}$ [MPa]	$\Delta\sigma_{hs}$ [MPa]	1-mm stress [MPa]
R=-1	229,600	322	301	223	227
	265,500	320	300	222	226
	679,800	319	299	221	225
	402,100	301	282	209	212
	2,808,000	276	258	191	194
	564,900	235	220	163	166
	844,100	210	197	146	148
	~~6,403,000~~	~~203~~	~~190~~	~~140~~	~~143~~

Longitudinal stiffener FAT 71, HFMI experimental results

	Nf	SED [MJ/m^3]	$\Delta\sigma_{eq,peak}$ [MPa]	$\Delta\sigma_{hs}$ [MPa]
R=-1	499,700	2.90	1145	648
	552,400	2.72	1109	627
	208,600	2.67	1100	622
	1,949,000	2.26	1012	572
	964,800	1.53	831	470
	858,400	1.53	831	470
	447,500	1.35	781	442
	469,700	1.25	751	425
	2,907,000	0.89	634	359
	1,980,000	0.88	630	356

Appendix D

Longitudinal stiffener FAT 63, t=10 mm, AW experimental results

NB: all the experimental failures occurred at the weld toe. The barred data refer to runouts.

		Tetra 187	Brick 185		
	Nf	**$\Delta\sigma_{eq,peak}$ [MPa]**	**$\Delta\sigma_{eq,peak}$ [MPa]**	**$\Delta\sigma_{hs}$ [MPa]**	**1-mm stress [MPa]**
R=0.1	~~10,000,000~~	~~161~~	~~183~~	~~67~~	~~74~~
	~~10,000,000~~	~~225~~	~~256~~	~~94~~	~~104~~
	3,466,968	289	330	121	133
	204,202	642	732	270	296
	112,546	803	915	337	370
	47,716	1124	1281	472	518
R=0.5	~~10,000,000~~	~~161~~	~~183~~	~~67~~	~~74~~
	2,333,651	225	256	94	104
	893,070	289	330	121	133
	88,800	642	732	270	296
	49,800	803	915	337	370
	33,700	963	1098	405	444

Longitudinal stiffener FAT 63, t=20 mm, AW experimental results

NB: all the experimental failures occurred at the weld toe. The barred data refer to runouts.

		Tetra 187	Brick 185		
	Nf	**$\Delta\sigma_{eq,peak}$ [MPa]**	**$\Delta\sigma_{eq,peak}$ [MPa]**	**$\Delta\sigma_{hs}$ [MPa]**	**1-mm stress [MPa]**
R=0.1	3,600,954	243	285	84	115
	1,513,276	312	367	108	148
	125,887	694	814	240	330
	113,433	868	1018	301	412
	41,521	1215	1425	421	577
R=0.5	~~10,000,000~~	~~243~~	~~285~~	~~84~~	~~115~~
	1,612,500	312	367	108	148
	828,000	434	509	150	206
	136,936	694	814	240	330
	85,459	868	1018	301	412
	49,546	1042	1222	361	495

Longitudinal stiffener FAT 63, t=10 mm, HFMI experimental results

NB: the barred data refer to runouts.

	Nf	SED [MJ/m^3]	$\Delta\sigma_{eq,peak}$ [MPa]	$\Delta\sigma_{hs}$ [MPa]
R=0.1	158,200	1.78	899	405
	2,031,700	0.45	449	202
	~~10,000,000~~	~~0.16~~	~~270~~	~~121~~
	2,235,000	0.79	599	270
	3,547,800	1.24	749	337
	101,200	2.43	1049	472
	~~10,000,000~~	~~0.61~~	~~524~~	~~236~~
	532,122	0.45	449	202
	~~6,000,000~~	~~0.16~~	~~270~~	~~121~~
	350,000	0.79	599	270
	187,828	2.43	1049	472
	855,162	1.24	749	337
	~~6,000,000~~	~~0.45~~	~~449~~	~~202~~
	~~2,000,000~~	~~0.16~~	~~270~~	~~121~~
	~~6,000,000~~	~~0.79~~	~~599~~	~~270~~
	82,506	2.43	1049	472
	98,500	3.17	1198	539
	~~10,000,000~~	~~1.00~~	~~674~~	~~303~~
	~~10,000,000~~	~~0.16~~	~~270~~	~~121~~
	~~10,000,000~~	~~0.79~~	~~599~~	~~270~~
	317,200	1.24	749	337
	223,100	2.43	1049	472
	18,010	1.00	674	303
	~~2,000,000~~	~~0.10~~	~~210~~	~~94~~
	~~2,000,000~~	~~0.16~~	~~270~~	~~121~~
	299,234	0.79	599	270
	179,511	1.24	749	337
	134,300	2.43	1049	472
R=0.5	33,391	1.24	749	337
	84,895	0.79	599	270

Longitudinal stiffener FAT 63, t=20 mm, HFMI experimental results

NB: the barred data refer to runouts.

	Nf	SED [MJ/m^3]	$\Delta\sigma_{eq,peak}$ [MPa]	$\Delta\sigma_{hs}$ [MPa]
R=0.1	141,700	1.75	890	331
	~~10,000,000~~	~~0.52~~	~~485~~	~~180~~
	2,411,800	1.17	728	270
	4,267,720	1.45	809	301
	480,227	2.83	1133	421
	480,200	0.93	647	240
	2,241,008	0.93	647	240
	232,323	1.45	809	301
	80,830	2.83	1133	421
	184,642	3.70	1295	481
	5,068,136	1.75	890	331
	470,640	2.08	971	361
	~~10,000,000~~	~~1.45~~	~~809~~	~~301~~
	123,655	2.83	1133	421
R=0.5	343,210	0.93	647	240
	1,019,256	0.36	405	150
	644,530	0.52	485	180
	56,926	1.75	890	331

Appendix E

Transverse stiffener FAT 80, Okawa, AW experimental results

NB: all the experimental failures occurred at the weld toe; the barred data refer to runouts.

		Plane 182		
	Nf	$\Delta\sigma_{eq,peak}$ [MPa]	$\Delta\sigma_{hs}$ [MPa]	1-mm stress [MPa]
R=0.1	164,000	433	207	236
	354,000	325	155	177
	1,320,000	216	103	118
	~~5,000,000~~	~~173~~	~~83~~	~~94~~

Transverse stiffener FAT 80, Okawa, HFMI experimental results

NB: the barred data refer to runouts.

	Nf	SED [MJ/m^3]	$\Delta\sigma_{eq,peak}$ [MPa]	$\Delta\sigma_{hs}$ [MPa]
R=0.5	346,000	3.39E-01	392	181
	503,000	2.49E-01	336	155
	~~5,000,000~~	~~1.73E-01~~	~~280~~	~~129~~
	3,450,000	2.02E-01	302	139
R=-1	378,000	1.95E+00	941	434
	990,000	1.77E+00	896	413
	2,295,000	1.60E+00	851	392
R=0.1	~~5,000,000~~	~~6.92E-01~~	~~560~~	~~258~~
	818,000	8.07E-01	605	279
	1,067,000	7.49E-01	582	269
	304,000	9.97E-01	672	310

Appendix F

Transverse stiffener FAT 80, Kuhlmann (2009), AW experimental results

NB: all the experimental failures occurred at the weld toe.

	Nf	$\Delta\sigma_{eq,peak}$ [MPa]	$\Delta\sigma_{hs}$ [MPa]	1-mm stress [MPa]
f_y =422 MPa R=0.1	67,921	591	332	324
	64,159	591	332	324
	574,631	335	188	184
	456,289	335	188	184
	1,400,261	246	138	135
	3,712,215	246	138	135
	185,219	443	249	243
	160,863	443	249	243
	1,933,751	246	138	135
f_y =781 MPa R=0.1	106,797	591	332	324
	123,652	591	332	324
	537,534	443	249	243
	415,846	443	249	243
	1,028,720	374	210	205
	575,000	374	210	205
	1,034,355	374	210	205
	3,517,443	295	166	162
	1,833,757	295	166	162

Transverse stiffener FAT 80, Kuhlmann (2009), HFMI experimental results

NB: the barred data refer to runouts.

	Nf	SED [MJ/m^3]	$\Delta\sigma_{eq,peak}$ [MPa]	$\Delta\sigma_{hs}$ [MPa]
fy=441 MPa R=0.1	1,426,998	7.74E-01	592	301
	762,972	7.74E-01	592	301
	137,721	9.94E-01	671	342
	116,159	9.94E-01	671	342
	711,012	8.53E-01	622	317
	298,866	8.53E-01	622	317
	799,250	6.74E-01	553	281
	337,639	8.53E-01	622	317
fy=781 MPa R=0.1	768,457	9.94E-01	671	342
	478,283	9.94E-01	671	342
	759,450	8.53E-01	622	317
	1,270,270	8.53E-01	622	317
	193,512	1.38E+00	789	402
	228,100	1.38E+00	789	402
	3,277,551	6.74E-01	553	281
	2,119,665	6.74E-01	553	281
	~~5,000,000~~	~~6.74E-01~~	~~553~~	~~281~~

Appendix G

Transverse stiffener FAT 80, Kuhlmann (2006), HFMI experimental results

	Nf	SED [MJ/m^3]	$\Delta\sigma_{eq,peak}$ [MPa]	$\Delta\sigma_{hs}$ [MPa]
fy=355 MPa R=0.1	108,489	7.03E-01	564	309
	363,274	5.80E-01	512	280
	455,624	4.80E-01	466	255
	977,946	3.97E-01	424	232
	349,432	5.11E-01	481	263
	315,592	5.23E-01	487	266
	1,146,656	3.53E-01	400	219
	845,460	5.07E-01	479	262
	89,949	7.69E-01	590	323
	1,365,764	4.69E-01	461	252
	200,637	6.49E-01	542	297
fy=460 MPa R=0.1	595,040	6.31E-01	535	293
	174,924	7.69E-01	590	323
	346,406	6.18E-01	529	290
	992,769	4.69E-01	461	252
	1,077,822	4.32E-01	442	242
	51,593	1.12E+00	713	390
	221,726	6.49E-01	542	297
	260,850	8.27E-01	612	335
	162,744	9.51E-01	656	359
	522,654	5.51E-01	500	273

Bibliography

[1] Hobbacher A. IIW recommendations for fatigue design of welded joints and components, WRC Bulletin 520. New York: The Welding Research Council; 2009.

[2] European Committee for Standardization (1992) Eurocode 3. Design of steel structures. Part 1-1: General rules and rules for buildings, ENV 1993–1-1:1992.

[3] Xiao, Z.-G., Yamada, K. (2004). A method of determining geometric stress for fatigue strength evaluation of steel welded joints, Int. J. of Fatigue, vol. 26, pp. 1277–1293.

[4] S. Kihara and A. Yoshii. A Strength Evaluation Method of a Sharply Notched Structure by a New Parameter, "The Equivalent Stress Intensity Factor". *JSME international journal. Ser. 1, Solid mechanics, strength of materials*, 34(1):70-75, Jan 1991.

[5] P. Lazzarin and R. Tovo. A notch intensity factor approach to the stress analysis of welds. *Fatigue Fract. Eng. Mater. Struct.*, pages 1089-1104, 1998.

[6] P. Lazzarin and R. Zambardi. A finite-volume-energy based approach to predict the static and fatigue behaviour of components with sharp V-shaped notches. *International Journal of Fracture*, 112(3):275-298, Dec 2001.

[7] G. Meneghetti and P. Lazzarin. Significance of the elastic peak stress evaluated by FE analyses at the point of singularity of sharp V-notched components. Fatigue Fract. Eng. Mater. Struct., pages 95-106, 2007.

[8] G. Meneghetti, A. Campagnolo, M. Avalle, D. Castagnetti, M. Colussi, P. Corigliano, M. De Agostinis, E. Dragoni, V. Fontanari, F. Frendo, L. Goglio, G. Marannano, G. Marulo, F. Moroni, A. Pantano, A. Rebora, A. Scattina, A. Spaggiari, and B. Zuccarello. Rapid evaluation of notch stress intensity factors using the peak stress method: comparison of commercial finite element codes for a range of mesh patterns. *Fatigue and Fracture of Engineering Materials and Structures*, 41(5), 2018.

[9] Marquis GB, Barsoum Z. IIW recommendations for the HFMI treatment – for improving the fatigue strength of welded joints. *Singapore: Springer Singapore*; 2016.

[10] P. Lazzarin and F. Berto. Some expressions for the strain energy in a finite volume surrounding the root of blunt V-notches. *International Journal of Fracture* (2005) 135:161-185.

[11] D. Radaj, C. M. Sonsino, and W. Fricke. Fatigue Assessment of Welded Joints by Local Approaches: Second Edition. *Elsevier Ltd*, 2006.

[12] Poutiainen I, Tanskanen P and Marquis G. Finite element methods for structural hot spot determination – a comparison of procedures. *Int J Fatigue*, 2004, 26, 1147–1157.

[13] R. Gross and A. Mendelson. Plane elastostatic analysis of V-notched plates. *Int. J. Fract. Mech.*, pages 267-276, 1972.

[14] D. S. Kammer. Slip Fronts at Frictional Interfaces: A Numerical and Theoretical Study. *EPFL Thesis*, 2014-12.

[15] G. Meneghetti, A. Campagnolo. Fatica dei giunti saldati. Approcci locali basati sugli NSIF: SED e PSM. Corso di Costruzione di Macchine 2.

[16] M. L. Williams. Stress singularities resulting from various boundary conditions in angular corners of plates in tension. *J Appl Mech*, 19:526-528, 1952.

[17] J. Qian and N. Hasebe. Property of eigenvalues and eigenfunctions for an interface V-notch in anti-plane elasticity. *Engineering Fracture Mechanics*, 56(6):729-734, Apr 1997.

[18] A. Campagnolo and G. Meneghetti. Rapid estimation of notch stress intensity factors in 3D large scale welded structures using the peak stress method. *MATEC Web Conf*, page 165, 2018.

[19] B. Atzori and G. Meneghetti. Fatigue strength of fillet welded structural steels: finite elements, strain gauges and reality. *International Journal of Fatigue*, 23(8):713-721, Sep 2001.

[20] P. Lazzarin, C. M. Sonsino, and R. Zambardi. A notch stress intensity approach to assess the multiaxial fatigue strength of welded tube-to-flange joints subjected to combined loadings. *Fatigue & Fracture of Engineering Materials & Structures*, 27(2):127-140, Feb 2004.

[21] P. Lazzarin, P. Livieri, F. Berto, M. Zappalorto. Local strain energy density and fatigue strength of welded joints under uniaxial and multiaxial loading. *Engineering Fracture Mechanics*, 75 (2008) 1875–1889.

[22] P. Lazzarin, F. Berto, and M. Zappalorto. Rapid calculations of notch stress intensity factors based on averaged strain energy density from coarse meshes: Theoretical bases and applications. *International Journal of Fatigue*, 32(10):1559-1567, Oct 2010.

[23] Fischer C, Fricke W, Rizzo CM. Review of the fatigue strength of welded joints based on the notch stress intensity factor and SED approaches. *Int. J. Fatigue*, 2016;84:59–66.

[24] Fischer C, Fricke W, Rizzo CM. Fatigue tests of notched specimens made from butt joints at steel. *Fatigue Fract. Eng. Mater Struct*, 2016;39:1526–41.

[25] A. Campagnolo, I. Roveda, and G. Meneghetti. The Peak Stress Method combined with 3D finite element models to assess the fatigue strength of complex welded structures. *Structural Integrity Procedia*, 2019.

[26] G. Meneghetti. The use of peak stresses for fatigue strength assessments of welded lap joints and cover plates with toe and root failures. *Engineering Fracture Mechanics*, 89 (2012) 40-51.

[27] G. Meneghetti. The peak stress method for fatigue strength assessment of tube-to-flange welded joints under torsion loading. *Welding in the World*, 57(2):265-275, Feb 2013.

[28] G. Meneghetti, C. Guzzella, and B. Atzori. The peak stress method combined with 3D finite element models for fatigue assessment of toe and root cracking in steel welded joints subjected to axial or bending loading. *Fatigue Fract. Eng. Mater. Struct.*, 37:722-739, 2014.

[29] ANSYS Inc. Ansys guide 19, 2019.

[30] Maddox, S. J. The Effect of Plate Thickness on the Fatigue Strength of Fillet Welded Joints. *Abington Publishing, Abington, Cambridge*, 1987.

[31] Gurney, T. R. The Fatigue Strength of Transverse Fillet Welded Joints. *Abington Publishing, Abington, Cambridge*, 1991.

[32] P. Gandhi and S. Berge. Fatigue behaviour of T-joints: square chords and circular braces. *J. Struct. Eng.,* 124:399-404, 1998.

[33] G. Meneghetti, A. Campagnolo, V. Babini, M. Riboli, and A. Spagnoli. Multiaxial fatigue assessment of welded steel details according to the peak stress method: Industrial case studies. *International Journal of Fatigue*, 125(April):362-380, 2019.

[34] H.C. Yildirim, G. Marquis, C.M. Sonsino. Lightweight design with welded high-frequency mechanical impact (HFMI) treated high-strength steel joints from S700 under constant and variable amplitude loadings. *International Journal of Fatigue*, 91 (2016) 466–474.

[35] FATWELDHSS, Technical report n°3 - 2013.

[36] Okawa T, Shimanuki H, Funatsu Y, Nose T, Sumi Y. Effect of preload and stress ratio on fatigue strength of welded joints improved by ultrasonic impact treatment. *Weld World* (2013) 57:235–241.

[37] Kuhlmann U, Gunther H. Experimental investigations of the fatigue-enhancing effect of the PIT process (Experimentelle Untersuchungen zur ermüdungssteigernden Wirkung des PITVerfahrens). *Versuchsbericht, Universität Stuttgart, Institut für Konstruktion und Entwurf*, Sep 2009.

[38] Yildirim H., Marquis G. A Round Robin study of high frequency mechanical impact treated welded joints subjected to variable amplitude loading. *Welding in the World*, vol. 57, nr. 3, pp. 437-447, 2013.

[39] Pedersen M, Mouritsen OØ, Hansen M, Andersen JG, Wenderby J. Comparison of post weld treatment of high strength steel welded joints in medium cycle fatigue. *Weld World* 2009; 54(7/8):208–17.

[40] A. Nussbaumer, V. Grigoriou. Round Robin on Local stress evaluation for fatigue by various FEM software. *IIW-doc*. XIII-2650-16.

[41] Haagensen PJ, Maddox SJ. IIW recommendations on post weld fatigue life improvement of steel and aluminium structures. *Paris: International Institute of Welding*; 2011.

[42] Statnikov E, Trufyakov V, Mikheev P, Kudryavtsev Y. Specification for weld toe improvement by ultrasonic impact treatment. *Paris: International Institute of Welding*; 1996. Document XIII-1617-96.

[43] Yildirim H., Marquis G. Fatigue strength improvement factors for high strength steel welded joints treated by high frequency mechanical impact. *International Journal of Fatigue* 44 (2012) 168 176.

[44] H.C. Yildirim, G. Marquis. Fatigue data of High-Frequency Mechanical Impact (HFMI) improved welded joints subjected to overloads. *Analysis and Design of Marine Structures – Guedes Soares & Shenoi (Eds)*, 2015.

[45] Neuber, H. Theory of Notch Stresses. Springer-Verlag, Berlin, 1958.

[46] Kuhlmann U, Dürr A, Bergmann J, Thumser R. Fatigue strength improvement for welded high strength steel connections due to the application of post-weld treatment methods (Effizienter Stahlbau aus höherfesten Stählen unter Ermüdungsbeanspruchung). *Forschungsvorhaben P620 FOSTA, Verlag und Vertriebsgesellschaft GmbH*, Düsseldorf; 2006.

[47] Morgan MR, Lee MMK. Stress concentration factors in tubular K-joints under in-plane moment loading. *Journal of Structural Engineering*, ASCE 1998;124(4):382–90.

[48] Van Wingerde AM, Packer JA, Wardenier J. Criteria for the fatigue assessment of hollow structural section connections. *Journal of Construction and Steel Research* 1995;35:71–115.